



NATIONAL AND KAPODISTRIAN UNIVERSITY OF ATHENS

SCHOOL OF SCIENCE

DEPARTMENT OF CHEMISTRY

PhD THESIS

**Catalytic Polymerization of Olefins and Cycloolefins
with Transition Metal Complexes**

**GRIGORIOS RAPTOPOULOS
CHEMIST, M.Sc.**

ATHENS

OCTOBER 2016

PhD THESIS

Catalytic Polymerization of Olefins and Cycloolefins with Transition Metal Complexes

GRIGORIOS RAPTOPOULOS

R.N.: 001220

THESIS SUPERVISOR:

Patrina Paraskevopoulou, Assistant Professor, N.K.U.A.

SUPERVISING COMMITTEE:

Marinos Pitsikalis, Professor, N.K.U.A.

Panayotis Kyritsis, Associate Professor, N.K.U.A.

Patrina Paraskevopoulou, Assistant Professor, N.K.U.A.

THESIS COMMITTEE

Christiana Mitsopoulou, Professor, N.K.U.A.

Marinos Pitsikalis, Professor, N.K.U.A.

Pericles Stavropoulos, Associate Professor, MS&T

Spyros Koinis, Associate Professor, N.K.U.A.

Panayotis Kyritsis, Associate Professor, N.K.U.A.

Constantinos Methenitis, Associate Professor, N.K.U.A.

Patrina Paraskevopoulou, Assistant Professor, N.K.U.A.

DATE OF THESIS DEFENSE 13/10/2016

ABSTRACT

In this thesis we study two types of metal-mediated polymerization reactions: Controlled Radical Polymerization (**CRP**) and Ring Opening Metathesis Polymerization (**ROMP**).

CRP. We studied the catalytic activity of a family of tripodal Co^{II} and Mn^{II} complexes bearing trianionic triphenylamido-amine ligands towards **CRP** of styrene and methyl methacrylate. Co^{II} complexes were more reactive than Mn^{II} complexes, with the steric factor playing an essential role in their reactivity and control over the polymerization. In many cases polymers featured bimodal molecular weight distributions, which indicate that two parallel mechanisms may be in operation.

ROMP. We used the bimetallic compound $\text{Na}[\text{W}_2(\mu\text{-Cl})_3\text{Cl}_4(\text{THF})_2]\cdot(\text{THF})_3$ (**{W₂}**, $\{\text{W}^3\text{W}\}^{6+}, a^{-2}e^{-4}$) for the synthesis of new polymeric materials. **{W₂}** is a highly efficient room-temperature initiator for the **ROMP** of norbornene (**NBE**) and some of its derivatives. We synthesized statistical **NBE/NBD** (**NBD**: norbornadiene) copolymers, which combine the properties of linear and crosslinked polymers. The catalytic activity of **{W₂}** can be improved by addition of small amounts of phenylacetylene (**PA**) as co-initiator. Both catalytic systems (**{W₂}** and **{W₂}/PA**) provided polymers with high-*cis* content. We investigated the reactivity of **{W₂}/PA** and we used this system for the synthesis of highly crosslinked poly(dicyclopentadiene) (**PDCPD**) gels via **ROMP** of dicyclopentadiene (**DCPD**); their structure and properties were compared to those of **PDCPD** gels obtained using the commercially available WCl_6 and the well-established 1st and 2nd generation Ru-based Grubbs' catalysts. The configuration of the polymeric chain plays a key role in the swelling behavior of those **PDCPD** dry-gels in organic solvents, which was studied extensively and exploited for the estimation of Hansen Solubility Parameters (HSP) of mostly-*cis* **PDCPD** and for the separation of chlorinated solvents from water. Therefore, it is concluded that **{W₂}/PA** shows unique advantages in terms of stereochemistry, properties and potential applications of **PDCPD** gels over the mononuclear W- and Ru-based catalytic systems.

SUBJECT AREA: Catalysis

KEYWORDS: controlled radical polymerization, ring opening metathesis polymerization, metal-metal bonds, crosslinked polymers, gel swelling

ΠΕΡΙΛΗΨΗ

Καταλυτικός Πολυμερισμός Ολεφινών και Κυκλοολεφινών με Σύμπλοκα των Στοιχείων Μεταπτώσεως.

Στην παρούσα διατριβή μελετάμε δύο είδη πολυμερισμού που προάγονται από μεταλλικά σύμπλοκα: τον ελεγχόμενο ριζικό πολυμερισμό (**CRP**) και το μεταθετικό πολυμερισμό με διάνοιξη δακτυλίου (**ROMP**).

CRP. Μελετήσαμε την καταλυτική δραστηριότητα μιας οικογένειας συμπλόκων των Co^{II} και Mn^{II} που φέρουν τριφαινυλαμιδο-αμινικούς υποκαταστάτες ως προς τη **CRP** του στυρενίου και του μεθακρυλικού μεθυλεστέρα. Τα σύμπλοκα του Co^{II} είναι πιο δραστήρια, με τη στερεοχημεία τους να παίζει κύριο ρόλο στη δραστηριότητα και τον έλεγχο του πολυμερισμού. Σε πολλές περιπτώσεις τα λαμβανόμενα πολυμερή εμφανίζουν διμοριακές κατανομές μοριακών βαρών, υποδεικνύοντας τη δράση δύο παράλληλων μηχανισμών.

ROMP. Χρησιμοποιήσαμε το διμεταλλικό σύμπλοκο $\text{Na}[\text{W}_2(\mu\text{-Cl})_3\text{Cl}_4(\text{THF})_2] \cdot (\text{THF})_3$ (**{W₂}**, $\{\text{W}^3\text{-W}\}^{6+}$, a^2e^4) για τη σύνθεση νέων πολυμερικών υλικών. Το **{W₂}** είναι ένας δραστήριος ενεργοποιητής της **ROMP** του νορβορνενίου (**NBE**) και παραγώγων του. Συνθέσαμε στατιστικά συμπολυμερή **NBE/NBD** (**NBD**: νορβορναδιένιο), που συνδυάζουν ιδιότητες γραμμικών και δικτυωμένων πολυμερών. Η καταλυτική δραστηριότητα του **{W₂}** μπορεί να βελτιωθεί με προσθήκη μικρής ποσότητας φαινυλακετυλενίου (**PA**) ως συγκαταλύτη. Το **{W₂}** και το **{W₂}/PA** παρέχουν πολυμερή με υψηλή *cis* στερεοεκλεκτικότητα. Μελετήσαμε τη δραστηριότητα του **{W₂}/PA** και το χρησιμοποιήσαμε για τη σύνθεση μέσω **ROMP** πηκτωμάτων πολυ(δικυκλοπενταδιενίου) (**PDCPD**) με υψηλό βαθμό δικτύωσης. Η δομή και οι ιδιότητές τους συγκρίθηκαν με εκείνες πηκτωμάτων **PDCPD** που ελήφθησαν με χρήση του εμπορικά διαθέσιμου WCl_6 και των καταλυτών Grubbs 1^{ης} και 2^{ης} γενιάς. Η διαμόρφωση της αλυσίδας παίζει σημαντικό ρόλο στη διόγκωση των πηκτωμάτων **PDCPD** σε οργανικούς διαλύτες, η οποία μελετήθηκε διεξοδικά και οδήγησε στην εκτίμηση των παραμέτρων διαλυτότητας Hansen (HSP) του **PDCPD** με υψηλό ποσοστό *cis* και της δυνατότητας διαχωρισμού χλωριωμένων διαλυτών από το νερό. Συμπερασματικά, το **{W₂}/PA** διαθέτει μοναδικά πλεονεκτήματα ως προς τη στερεοχημεία, τις ιδιότητες και τις πιθανές εφαρμογές των πηκτωμάτων **PDCPD** σε σχέση με μονοπυρηνικά συστήματα βασισμένα σε W ή Ru.

ΘΕΜΑΤΙΚΗ ΠΕΡΙΟΧΗ: Κατάλυση

ΛΕΞΕΙΣ-ΚΛΕΙΔΙΑ: ελεγχόμενος ριζικός πολυμερισμός, μεταθετικός πολυμερισμός με διάνοιξη δακτυλίου, δεσμοί μετάλλου-μετάλλου, δικτυωμένα πολυμερή, διόγκωση πηκτωμάτων.

To my family and friends

To everyone too stubborn to ever give up.

ACKNOWLEDGEMENTS

The present study was conducted at the Laboratory of Inorganic Chemistry of National and Kapodistrian University of Athens (November 2011 – September 2016). I would like to thank everyone who contributed in its fulfillment, specifically:

My supervisor, Assistant Professor Patrina Paraskevopoulou for the assignment of the subject and her guidance through all these years.

Professor Marinós Pitsikalis and Associate Professor Panayotis Kyritsis for participating in my supervising committee and for their valuable advice.

Emeritus Professor Konstantinos Mertis for his contagious love for Chemistry.

Associate Professor Pericles Stavropoulos (Missouri University of Science & Technology, Rolla MO, USA) for his integral role in the Controlled Radical Polymerization part of this work.

Professor Christiana Mitsopoulou, Associate Professor Spyros Koinis and Associate Professor Constantinos Methenitis for participating in my thesis committee.

Professor Thomas Mavromoustakos (Department of Chemistry, N.K.U.A., Athens, Greece) and Professor Gragor Mali (National Institute of Chemistry, Ljubljana, Slovenia) for their help with the solid state NMR spectra.

Dr. Georgios D. Chryssikos and Dr. Constantinos Tsiantos (National Hellenic Research Foundation, Athens, Greece) for their help with the FT-IR and FT-Raman spectra.

Alice Scarpellini (Istituto Italiano di Tecnologia, Genova, Italy) for her help with the SEM studies.

All faculty and staff members of the Laboratory of Inorganic Chemistry for providing any help needed.

All my past and present lab co-workers, namely Dr. Alexios Grigoropoulos, Dr. George C. Anyfantis, Katerina Kyriakou, Despoina Chriti and Aspasia Kanellou, along with Christiana Nikovia and Georgios Theodosopoulos from the Laboratory of Industrial Chemistry.

Most importantly, my mother for tolerating and supporting my never-ending studies.

Funding from two research projects is acknowledged:

1. *Synthesis of Novel Advanced Materials by New Generation Catalysts via ROMP (Ring Opening Metathesis Polymerization) Reactions*

Operational Program “Education and Lifelong Learning” of the National Strategic Reference Framework (NSRF), co-financed by the European Union (European Social Fund) and Greek national funds - Research Funding Program: THALES. Investing in knowledge society through the ESF – MIS 377252.



2. *NanoHybrids: New generation of nanoporous organic and hybrid aerogels for industrial applications: from laboratory to pilot scale production*

This project has received funding from the European Union’s Horizon 2020 research and innovation programme under grant agreement No 685648. This publication reflects the views only of the author, and the Commission cannot be held responsible for any use, which may be made of the information contained therein.



CONTENTS

| | |
|---|-----------|
| 1. CHAPTER 1 CONTROLLED RADICAL POLYMERIZATION | 27 |
| 1.1 Introduction..... | 27 |
| 1.2 Cobalt in controlled radical polymerization reactions..... | 28 |
| 1.3 Manganese in controlled radical polymerization reactions..... | 30 |
| 2. CHAPTER 2 RING OPENING METATHESIS POLYMERIZATION..... | 32 |
| 2.1 Introduction..... | 32 |
| 2.2 Draw-backs of known ROMP catalysts..... | 33 |
| 2.3 Binuclear complexes as ROMP catalysts | 33 |
| 2.3.1 Molybdenum complexes | 34 |
| 2.3.2 Tungsten complexes | 35 |
| 2.3.3 Ruthenium and osmium complexes | 36 |
| 2.3.4 Heterometallic complexes | 37 |
| 3. CHAPTER 3 PURPOSE OF THIS STUDY..... | 40 |
| 4. CHAPTER 4 EXPERIMENTAL | 42 |
| 4.1 Materials and physical measurements..... | 42 |
| 4.2 CRP reactions | 44 |
| 4.2.1 Typical experimental procedure | 44 |
| 4.2.2 Reinitiation experiment 1..... | 45 |
| 4.2.3 Reinitiation experiment 2..... | 45 |
| 4.3 ROMP reactions | 46 |
| 4.3.1 Copolymerization reactions..... | 46 |
| 4.3.2 Use of PA as co-initiator..... | 46 |
| 4.3.3 Catalytic reactions in NMR tubes | 47 |
| 4.4 PDCPD gels | 47 |

| | | |
|-----------|--|-----------|
| 4.4.1 | Catalytic system $\{W_2\}/PA$ | 47 |
| 4.4.2 | Catalytic system WCl_6/PA | 47 |
| 4.4.3 | Swelling measurements | 48 |
| 4.4.4 | Separation of organic solvents from water | 48 |
| 5. | CHAPTER 5 CATALYTIC ACTIVITY OF Co AND Mn TRIPHENYLAMIDO-AMINE COMPLEXES IN CONTROLLED RADICAL POLYMERIZATION OF OLEFINS | 49 |
| 5.1 | Co^{II} complexes..... | 49 |
| 5.1.1 | Cyclic voltammetry | 49 |
| 5.1.2 | Polymerization results | 52 |
| 5.1.3 | Reinitiation experiments..... | 58 |
| 5.1.4 | Tacticity of PMMA | 60 |
| 5.2 | Mn^{II} complexes | 63 |
| 5.2.1 | Cyclic voltammetry | 65 |
| 5.2.2 | Polymerization results | 66 |
| 5.2.3 | Tacticity of PMMA | 69 |
| 5.3 | Conclusions | 70 |
| 6. | CHAPTER 6 COPOLYMERIZATION OF NORBORNENE AND NORBORNADIENE VIA RING OPENING METATHESIS POLYMERIZATION USING A DITUNGSTEN-BASED CATALYTIC SYSTEM | 71 |
| 6.1 | General..... | 71 |
| 6.2 | Catalyst and polymerization reactions | 71 |
| 6.3 | Morphology..... | 74 |
| 6.4 | NMR spectroscopy | 77 |
| 6.5 | Thermal analysis | 82 |
| 6.6 | Conclusions..... | 85 |
| 7. | CHAPTER 7 EXPANDING AND IMPROVING THE CATALYTIC ACTIVITY OF $Na[W_2(\mu-Cl)_3Cl_4(THF)_2]\cdot(THF)_3$ | 86 |

| | | |
|------------|---|------------|
| 7.1 | General..... | 86 |
| 7.2 | Polymerization reactions..... | 86 |
| 7.3 | Results and discussion..... | 89 |
| 7.4 | Mechanistic considerations..... | 96 |
| 7.5 | Conclusions..... | 98 |
| 8. | CHAPTER 8 SOLUBILITY PARAMETERS AND POTENTIAL APPLICATIONS OF POLYDICYCLOPENTADIENE GELS OBTAINED USING A DITUNGSTEN-BASED CATALYTIC SYSTEM..... | 99 |
| 8.1 | General..... | 99 |
| 8.2 | Synthesis of PDCPD gels..... | 99 |
| 8.3 | Vibrational spectroscopy..... | 102 |
| 8.4 | NMR spectroscopy..... | 106 |
| 8.5 | Thermal analysis..... | 109 |
| 8.6 | Swelling of PDCPD gels in toluene..... | 110 |
| 8.7 | Conclusions..... | 112 |
| 9. | CHAPTER 9 HANSEN SOLUBILITY PARAMETERS AND POTENTIAL APPLICATIONS OF MOSTLY-CIS POLYDICYCLOPENTADIENE GELS..... | 114 |
| 9.1 | General..... | 114 |
| 9.2 | Swelling of W ₂ -PDCPD gels in organic solvents..... | 114 |
| 9.3 | Hansen Solubility Parameters..... | 124 |
| 9.4 | Separation of organic solvents from water..... | 139 |
| 9.5 | Conclusions..... | 141 |
| 10. | CONCLUSIONS..... | 143 |
| 11. | ΣΥΜΠΕΡΑΣΜΑΤΑ..... | 147 |
| 12. | ABBREVIATIONS-ACRONYMS..... | 151 |
| 13. | REFERENCES..... | 152 |

LIST OF SCHEMES

| | |
|---|-----|
| Scheme 1: Mechanisms of ATRA and ATRP reactions. | 29 |
| Scheme 2: Mechanisms of (a) OMRP and (b) CCTP reactions. | 29 |
| Scheme 3: Ring Opening Metathesis Polymerization (ROMP) reaction and mechanism. . | 32 |
| Scheme 4: Binuclear Mo complexes that have been employed as ROMP catalysts. | 34 |
| Scheme 5: Binuclear W complexes that have been employed as ROMP catalysts. | 36 |
| Scheme 6: Binuclear Ru and Os complexes that have been employed as ROMP catalysts. | 37 |
| Scheme 7: Binuclear heterometallic complexes that have been employed as ROMP catalysts. | 38 |
| Scheme 8: General structure of triphenylamido-amine complexes. | 40 |
| Scheme 9: Schematic representation of all metal compounds employed in this study for ROMP reactions. | 41 |
| Scheme 10: Structures of Co ^{II} complexes studied in CRP reactions. | 50 |
| Scheme 11: Structures of Mn ^{II} complexes studied in CRP reactions. | 64 |
| Scheme 12: Schematic representation of the equilibrium between {W ₂ } and {W ₂ }'. | 72 |
| Scheme 13: Possible products of NBE and NBD polymerization <i>via</i> ROMP. | 73 |
| Scheme 14: Possible reaction pathways and products for VNBE and DCPD polymerization. | 88 |
| Scheme 15: Synthesis of W ₂ -PDCPD and W-PDCPD gels. | 101 |

LIST OF FIGURES

- Figure 1: Cyclic voltammograms (Co^{II}/Co^{III} redox couple) of compounds [K(L³)Co^{II}-NCMe]_n (Co-1) and [K(NCMe)₃(L¹³)Co^{II}-NCMe] (Co-6) in MeCN/[(*n*-Bu)₄N]PF₆, [K(THF)₆][(L⁵)Co^{II}]_n•1.5THF (Co-2), [K(THF)₂(L⁸)Co^{II}]_n (Co-3) and [K₂(L⁹)₂Co^{II}]_n (Co-4) in DMF/[(*n*-Bu)₄N]PF₆, and {[K₂(DMA)₃(L¹⁰)₂Co^{II}]_n•0.5Et₂O} (Co-5) in DMA/[(*n*-Bu)₄N]PF₆, as indicated, with a Au disk electrode (1.6 mm in diameter); scan rate 0.1 V/s.....51
- Figure 2: SEC traces for PS obtained from the reaction of (Co-5) (0.01 mmol) with St (10 mmol) and ethyl-2-bromo-isobutyrate (0.05 mmol) in toluene (1.0 mL) under reflux at 110°C.....56
- Figure 3: SEC traces for PS obtained from the reaction of (Co-3) (0.01 mmol) with St (10 mmol) and ethyl-2-bromo-isobutyrate (0.05 mmol) in toluene (1.0 mL) under reflux at 110°C.....56
- Figure 4: SEC traces for PS obtained from the reaction of (Co-4) (0.01 mmol) with St (10 mmol) and ethyl-2-bromo-isobutyrate (0.05 mmol) in toluene (1.0 mL) under reflux at 110°C.....56
- Figure 5: SEC traces for PMMA obtained from the reaction of (Co-4) (0.01 mmol) with MMA (10 mmol) and ethyl-2-bromo-isobutyrate (0.05 mmol) in toluene (1.0 mL) under reflux at 110°C.....57
- Figure 6: SEC traces for PMMA obtained from the reaction of (Co-5) (0.01 mmol) with MMA (10 mmol) and ethyl-2-bromo-isobutyrate (0.10 mmol) in toluene (1.0 mL) under reflux at 110°C.....57
- Figure 7: SEC traces for PMMA obtained from the reaction of (Co-2) (0.01 mmol) with MMA (10.0 mmol) and ethyl-2-bromo-isobutyrate (0.05 mmol, top; 0.10 mmol, middle; 0.15 mmol, bottom) in toluene (1.0 mL) under reflux at 110 °C.58
- Figure 8: SEC traces for PS obtained from the reaction of (Co-4) (0.01 mmol) with St (9.6 mmol) and ethyl-2-bromo-isobutyrate (0.05 mmol) in toluene (2.0 mL) under reflux at 110 °C (top) and PS obtained after the second addition of St (9.6 mmol, bottom).....59
- Figure 9: SEC traces for PMMA obtained from the reaction of (Co-2) (0.01 mmol) with MMA (10.0 mmol) and ethyl-2-bromo-isobutyrate (0.05 mmol) in toluene (2.0 mL) under

| | |
|--|----|
| reflux at 110 °C (top) and PMMA-b-PS obtained after the reaction of 2 (0.01 mmol) with St (9.6 mmol) and PMMA (0.05 mmol) in toluene (2.0 mL) under reflux at 110 °C (bottom). .60 | |
| Figure 10: ¹ H NMR spectrum of PMMA-b-PS from the reaction of (Co-2) with MMA and St, in CDCl ₃ | 61 |
| Figure 11: ¹ H NMR spectrum of PMMA from the reaction of [K ₂ (DMA) ₃ (L ¹⁰)Co ^{II}] \cdot 0.5Et ₂ O (Co-5) with MMA, in CDCl ₃ | 63 |
| Figure 12: Cyclic voltammograms (Mn ^{II} /Mn ^{III} redox couple) of compounds [K ₂ (DMA) ₃ (L ⁴) ₂ Mn ^{II}] ₂ (Mn-1), [K(L ⁹)Mn ^{II}] _n (Mn-5) and [K(THF) ₃][(L ¹³)Mn ^{II} -THF] (Mn-7) in DMA/[(<i>n</i> -Bu) ₄ N]PF ₆ , [K(THF) ₄][(L ⁵)Mn ^{II} -THF] (Mn-2) and [K ₂ (THF) ₃][(L ¹⁰)Mn ^{II}] ₂ \cdot 2THF (Mn-6) in DMF/[(<i>n</i> -Bu) ₄ N]PF ₆ , [K(NCMe)][(L ⁶)Mn ^{II} -NCMe] \cdot MeCN (Mn-3) and [K(DMA)][(L ⁸)Mn ^{II} -DMA] (Mn-4) in MeCN/[(<i>n</i> -Bu) ₄ N]PF ₆ , as indicated, with a Au disk electrode (1.6 mm in diameter); scan rate 0.1 V/s..... | 66 |
| Figure 13: SEM image of the PNBE homopolymer..... | 75 |
| Figure 14: SEM image of the PNBE/PNBD 400/100 copolymer. | 75 |
| Figure 15: SEM image of the PNBE/PNBD 700/700 copolymer. | 76 |
| Figure 16: SEM image of the PNBE/PNBD 100/400 copolymer. | 76 |
| Figure 17: SEM image of the PNBD homopolymer..... | 77 |
| Figure 18: ¹³ C CPMAS NMR spectrum of PNBE. | 78 |
| Figure 19: ¹³ C CPMAS NMR spectrum of PNBD..... | 79 |
| Figure 20: ¹³ C CPMAS NMR spectrum of PNBE/PNBD 100/400 copolymer..... | 79 |
| Figure 21: ¹³ C CPMAS NMR spectrum of PNBE/PNBD 400/100 copolymer..... | 80 |
| Figure 22: ¹³ C CPMAS NMR spectrum of PNBE/PNBD 1100/300 copolymer..... | 80 |
| Figure 23: ¹³ C CPMAS NMR spectrum of PNBE/PNBD 700/700 copolymer..... | 81 |
| Figure 24: ¹³ C CPMAS NMR spectrum of PNBE/PNBD 300/1100 copolymer..... | 81 |
| Figure 25: Weight loss (%/°C) with temperature (°C) for all samples, as indicated..... | 83 |
| Figure 26: Derivative weight loss (%/°C) with temperature (°C) for all samples, as indicated. | 84 |

| | |
|---|-----|
| Figure 27: (a) ^1H and (b) $^{13}\text{C}\{^1\text{H}\}$ NMR spectra (CDCl_3) of PNBE obtained from the reaction of $\{W_2\}/\text{PA}/\text{NBE}$ in CH_2Cl_2 | 92 |
| Figure 28: (a) ^1H and (b) $^{13}\text{C}\{^1\text{H}\}$ NMR spectra (CDCl_3) of PVNBE obtained from the reaction of $\{W_2\}/\text{PA}/\text{VNBE}$ in CH_2Cl_2 | 93 |
| Figure 29: Derivative weight loss with temperature and weight loss ($\%/^\circ\text{C}$) with temperature ($^\circ\text{C}$; inset) of PNBD obtained from the ROMP of NBD with catalytic systems $\{W_2\}/\text{PA}$ (black line) and $\{W_2\}$ (red line). | 94 |
| Figure 30: Derivative weight change with temperature of insoluble PDCPD obtained from the reaction of $\{W_2\}/\text{PA}/\text{DCPD}$ in CH_2Cl_2 | 95 |
| Figure 31: ^1H NMR spectra (up: region 8.5–0.5 ppm; bottom: region 14.0-10.0 ppm) of: $\{W_2\}$ (a), from the reaction of $\{W_2\}$ (8.0 mg, 0.008 mmol) with PA (5 μL , 4.6 mg, 0.05 mmol) (b), and from the reaction of $\{W_2\}/\text{PA}$ with NBE (5 mg, 0.05 mmol) in d^8 -THF at various time intervals, as indicated (c–g). Signals denoted by “*” are due to coordinated THF of $\{W_2\}$, “S” to residual solvent, “M” to NBE, “P” to PNBE, and “A” to PA and/or PPA. | 97 |
| Figure 32: ^1H NMR spectrum (CDCl_3) of the residue remaining after evaporation of toluene from the first wash of a W_2 -PDCPD wet-gel. Peaks at 5.60 and 5.47 ppm are characteristic of linear PDCPD. ³⁴ Peaks at 7.02 (sh.), 6.88 and 5.89 ppm are characteristic of PPA. ⁹⁰ | 101 |
| Figure 33: Swelling data for W_2 -PDCPD wet-gels in toluene and de-swelling in pentane. | 102 |
| Figure 34: FTIR-ATR spectra (top: 1700-1590 cm^{-1} ; bottom: 1500-600 cm^{-1}) of PDCPD dry-gels obtained from the ROMP of DCPD by the following catalytic systems: $\{W_2\}/\text{PA}$ (black line), WCl_6/PA (green line), Ru-II (blue line) and Ru-I (red line). | 104 |
| Figure 35: FT-Raman spectra (1700-1580 cm^{-1}) of PDCPD dry-gels obtained from the ROMP of DCPD by the following catalytic systems: $\{W_2\}/\text{PA}$ (black line), WCl_6/PA (green line), Ru-II (blue line) and Ru-I (red line)..... | 105 |
| Figure 36: ^{13}C CPMAS spectra of PDCPD dry-gels and aerogels obtained from four different catalytic systems, as indicated. Spectra of Ru-I-PDCPD and Ru-II-PDCPD aerogels were taken from ref. 111. | 107 |
| Figure 37: HC LG-HETCOR NMR spectrum of a W_2 -PDCPD gel. | 107 |

| | |
|--|-----|
| Figure 38: Derivative weight loss with temperature ($^{\circ}\text{C}$) and weight loss ($\%/^{\circ}\text{C}$) with temperature ($^{\circ}\text{C}$; inset) for PDCPD dry-gels obtained from the polymerization of DCPD by the following catalytic systems: $\{W_2\}/\text{PA}$ (black line), WCl_6/PA (green line), Ru-I (red line) and Ru-II (blue line). | 110 |
| Figure 39: Swelling of PDCPD gels in toluene as a function of the catalytic system: $\{W_2\}/\text{PA}$ (black squares), WCl_6/PA (green diamonds), Ru-II (blue triangles) and Ru-I (red dots). Inset: Swelling of a W_2 -PDCPD dry-gel in toluene with time..... | 111 |
| Figure 40: Swelling of a W_2 -PDCPD gel in toluene..... | 112 |
| Figure 41: Swelling of a W_2 -PDCPD gel in toluene with time..... | 117 |
| Figure 42: Swelling of a W_2 -PDCPD gel in CHCl_3 with time. | 117 |
| Figure 43: Swelling of a W_2 -PDCPD gel in THF with time. | 118 |
| Figure 44: Swelling of a W_2 -DCPD gel in THF..... | 118 |
| Figure 45: Swelling of a W_2 -PDCPD gel in 1,3-dichlorobenzene with time..... | 119 |
| Figure 46: Swelling of a W_2 -PDCPD gel in CS_2 with time. | 119 |
| Figure 47: Swelling of a W_2 -PDCPD gel in chlorobenzene with time..... | 120 |
| Figure 48: Swelling of a W_2 -PDCPD gel in CCl_4 with time. | 120 |
| Figure 49: Swelling of a W_2 -PDCPD gel in benzene with time..... | 121 |
| Figure 50: Swelling of a W_2 -PDCPD gel in CH_2Cl_2 with time. | 121 |
| Figure 51: Swelling of a W_2 -PDCPD gel in 1,3,5-trimethylbenzene with time. | 122 |
| Figure 52: Swelling of a W_2 -PDCPD gel in 1,4-dimethylbenzene with time. | 122 |
| Figure 53: Swelling of a W_2 -PDCPD gel in 1,3-dimethylbenzene with time. | 123 |
| Figure 54: Swelling of a W_2 -PDCPD dry-gel in 1,2-dichlorobenzene with time..... | 123 |
| Figure 55: Swelling of a W_2 -PDCPD dry-gel in benzyl chloride with time. | 124 |
| Figure 56: Swelling of a W_2 -DCPD gel in benzyl chloride..... | 124 |
| Figure 57: Relation between the maximum volume degree of swelling (q_{max}) of W_2 -PDCPD gels and the total solubility parameter (δ_T) of the respective solvents..... | 128 |

| | |
|---|-----|
| Figure 58: Relation between the maximum volume degree of swelling (q_{\max}) of W_2 -PDCPD gels and the Hansen H-component (δ_H) of the respective solvents. | 128 |
| Figure 59: Relation between the maximum volume degree of swelling (q_{\max}) of W_2 -PDCPD gels and the Hansen P-component (δ_P) of the respective solvents..... | 129 |
| Figure 60: Relation between the maximum volume degree of swelling (q_{\max}) of W_2 -PDCPD gels and the Hansen D-component (δ_D) of the respective solvents. | 129 |
| Figure 61: 3D plot of the individual Hansen Solubility Parameters (HSP) for each solvent tested. Blue dots represent solvents in which W_2 -PDCPD gels swelled (“good” solvents). Red squares represent solvents in which no swelling was observed (“bad” solvents). The green dot represents W_2 -PDCPD. The green sphere contains all “good” solvents; the center of the sphere is a reasonable estimate of the HSP of W_2 -PDCPD. | 132 |
| Figure 62: 2D plots of the individual Hansen Solubility Parameters (HSP) for each solvent tested, as indicated. Blue dots represent solvents in which W_2 -PDCPD gels swelled (“good” solvents). Red squares represent solvents in which no swelling was observed (“bad” solvents). The green dot represents W_2 -PDCPD. The green circle contains all “good” solvents. | 132 |
| Figure 63: 3D plot of the individual Hansen Solubility Parameters (HSP) for each solvent tested. Blue dots represent solvents in which W_2 -PDCPD gels swelled (“good” solvents). Red squares represent solvents in which no swelling was observed (“bad” solvents). The green dot represents W_2 -PDCPD. The green sphere contains all “good” solvents; the center of the sphere is a reasonable estimate the HSP of W_2 -PDCPD. | 135 |
| Figure 64: 2D plots of the individual Hansen Solubility Parameters (HSP) for each solvent tested, as indicated. Blue dots represent solvents in which W_2 -PDCPD gels swelled (“good” solvents). Red squares represent solvents in which no swelling was observed (“bad” solvents). The green dot represents W_2 -PDCPD. The green circle contains all “good” solvents. | 135 |
| Figure 65: Same as Figure 63 showing also the location of DCPD (orange dot)..... | 136 |
| Figure 66: Separation of CH_2Cl_2 (dyed with Sudan blue) from water..... | 140 |
| Figure 67: Separation of $CHCl_3$ (dyed with Sudan blue) from water. | 140 |
| Figure 68: Separation of chlorobenzene (dyed with Sudan blue) from water. | 140 |

| | |
|---|-----|
| Figure 69: Separation of 1,3-dichlorobenzene (dyed with Sudan blue) from water..... | 141 |
| Figure 70: Separation of benzyl chloride (dyed with Sudan blue) from water. | 141 |

LIST OF TABLES

| | |
|--|-----|
| Table 1: Electrochemical data for compounds Co-1-6. | 51 |
| Table 2: Reactions of compounds Co-1-6 with styrene (St). ^a | 54 |
| Table 3: Reactions of compounds Co-1-6 with methyl methacrylate (MMA). ^a | 55 |
| Table 4: Tacticity of PMMA obtained from reactions with Co ^{II} complexes. ^{a,b} | 62 |
| Table 5: Electrochemical data for compounds Mn-1-7..... | 65 |
| Table 6: Reactions of compounds Mn-1-4 and Mn-6 with styrene (St) in toluene. ^a | 67 |
| Table 7: Reactions of compounds Mn-1-4 with styrene (St) in THF. ^a | 68 |
| Table 8: Reactions of compounds Mn-1-7 with methyl methacrylate (MMA) in toluene. ^a .. | 68 |
| Table 9: Reactions of compounds Mn-1, Mn-3 and Mn-4 with methyl methacrylate (MMA) in THF. ^a | 69 |
| Table 10: Tacticity of poly(methyl methacrylate) (PMMA) obtained from reactions with Mn ^{II} complexes in toluene. ^{a,b} | 69 |
| Table 11: Tacticity of poly(methyl methacrylate) (PMMA) obtained from reactions with Mn ^{II} complexes in THF. ^{a,b} | 69 |
| Table 12: Reactions of {W ₂ } with NBE and NBD. ^a | 73 |
| Table 13: TGA results at the heating rate of 10 ⁰ C/min..... | 82 |
| Table 14: Experimental Tg values. | 85 |
| Table 15: Polymerization of cycloolefins with catalytic systems {W ₂ } and {W ₂ }/PA..... | 87 |
| Table 16: Formulation of W ₂ -PDCPD, W-PDCPD, Ru-I-PDCPD and Ru-II-PDCPD..... | 100 |
| Table 17: IR characterization of W ₂ -PDCPD, W-PDCPD, Ru-I-PDCPD and Ru-II-PDCPD. | 105 |
| Table 18: IR characterization of W ₂ -PDCPD, W-PDCPD, Ru-I-PDCPD and Ru-II-PDCPD; the relative absorbance values. | 105 |
| Table 19: Calculation of the fraction of PDCPD double bonds that participate in crosslinking <i>via</i> olefin coupling, based on ¹³ C CPMAS spectroscopic data. | 108 |
| Table 20: Swelling of W ₂ -PDCPD gels in various organic solvents. | 116 |

| | |
|---|-----|
| Table 21: Hansen Solubility Parameters (HSP) of solvents used in this study and experimentally measured maximum degree of swelling (q_{\max}) of swollen W_2 -PDCPD gels. | 126 |
| Table 22: Hansen Solubility Parameters (HSP) of the solvents used in this study, scoring according to whether they are good solvents (1) or non-solvents (0), and calculated Relative Energy Differences (RED). | 131 |
| Table 23: Hansen Solubility Parameters (HSP) of the solvents used in this study, scoring according to their swelling capacity from 1 (maximum swelling observed) to 6 (no swelling observed), and calculated Relative Energy Differences (RED)..... | 134 |
| Table 24: Hansen Solubility Parameters (HSP) of solvents used in this study, experimentally measured maximum normalized volumes ($V_{\text{norm,max}}$) of swollen W_2 -PDCPD gels and calculated Ra values. | 138 |
| Table 25: Uptake for each solvent when separated from a 1:1 v/v mixture with water. ... | 141 |

CHAPTER 1

CONTROLLED RADICAL POLYMERIZATION

1.1 Introduction

Controlled Radical Polymerization (**CRP**) is one of the most important subjects in polymer chemistry and synthesis of macromolecules. For many years, there has been pessimism regarding its prospects, due to the nature of free radicals, which are sensitive towards intermolecular termination reactions, while their reactions have low chemo- and regioselectivity. But since the 1980s and mainly 1990s, several methods began developing, which have led to achievement of control over radical polymerization reactions.¹⁻³

All **CRP** reactions are based on a common principle, the reversible dynamic equilibrium between a propagating radical and a dormant species. The dormant species is stable enough to avoid undergoing side reactions, thus being unable to propagate the polymerization, but capable of creating a growth-active intermediate through chemical (catalytic) or physical (by heat or light) removal of an appropriate group.

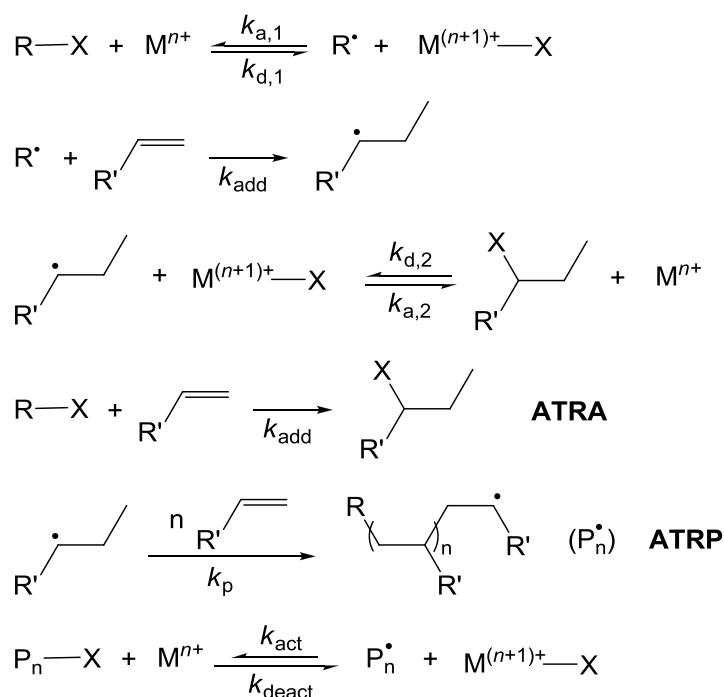
Common dormant species are alkyl halides bearing α -substituents which can stabilize a radical, e.g. bromoisobutyrate $[(\text{CH}_3)_2\text{C}(\text{Br})\text{CO}_2\text{R}$ (R = alkyl, etc)]. Under suitable conditions, the bromine becomes a leaving atom, creating a radical that starts the polymerization. To achieve control over the polymerization, radical intermediates must be “capped” by bromine, through a reversible process, to recreate the dormant species. The equilibrium between the dormant and active species must be shifted towards the dormant one, while the exchange between the two has to be faster than the concurrent propagation of the polymer chain. Combination of all those factors leads to a good control over the radical polymerization, giving polymers with well-defined molecular weights and main chain structure, and narrow molecular weight distributions.

1.2 Cobalt in controlled radical polymerization reactions

Radical polymerization reactions mediated by cobalt reagents⁴ have played a historic role in the development of **CRP** processes, owing to the early, seminal contributions of Wayland⁵ and Harwood.⁶ More recent work has shown that cobalt reagents can be intriguingly more complex in their mode of operation, and can induce **CRP** reactions *via* both atom-transfer radical polymerization (**ATRP**) mechanisms and organometallic-mediated radical polymerization (**OMRP**) pathways that rely on the well-known propensity of the Co–C bond towards cleavage and generation of carbon-centered radicals.

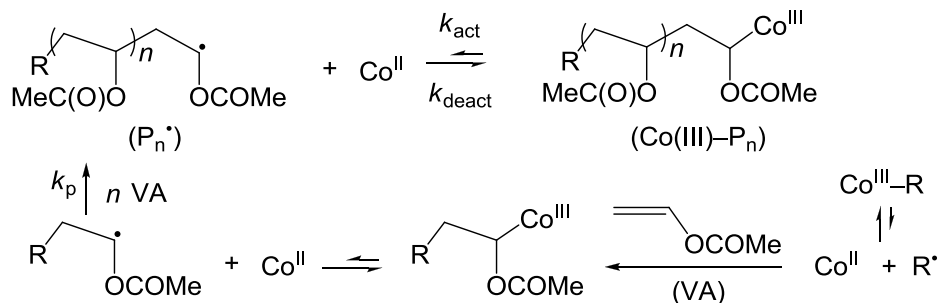
For the mechanistically related atom-transfer radical addition (**ATRA**) and polymerization (**ATRP**) reactions, the key step is a reversible halogen-atom transfer between an organohalide (RX) and the cobalt site, shuttling between two oxidation states (Co^{II}/Co^{III}) (Scheme 1).^{7,8} The resulting R[•] radical could then add to an olefin to generate a new organic radical, which would either be halogenated to provide the monomeric product (**ATRA**)⁹ or continue adding olefin to afford a living polymer (**ATRP**). Its success relies on the control exercised by the dynamic equilibrium ($K_{\text{ATRP}} = k_{\text{act}}/k_{\text{deact}}$) established between the halide-capped dormant species (P_n–X) and the propagating radical (P_n[•]), which is very sensitive to the catalyst, olefin monomer, and RX (initiator) used, and depend on the solvent and the reaction conditions.¹⁰

On the other hand, the **OMRP** process (or **CMRP**, for cobalt-mediated radical polymerization) relies on an equilibrium (Scheme 2, (a), demonstrated by vinyl acetate) heavily favoring a cobalt-capped dormant form of the polymer radical (Co^{III}–P_n). An alternative, albeit related, process, known as catalytic chain transfer polymerization (**CCTP**), applies to substrates that are prone to β-H elimination (methacrylates, α-methylstyrene, methacrylonitrile), inasmuch as the Co^{III}–P_n species may induce β-H atom abstraction to generate a Co^{III}–H and a polymer chain with an unsaturated terminal group (Scheme 2, (b), demonstrated for methyl methacrylate (**MMA**)). The Co^{III}–H is a key ingredient of the catalytic cycle, because it can generate the primary radical species *via* insertion of the hydride into the monomer (for instance **MMA**).

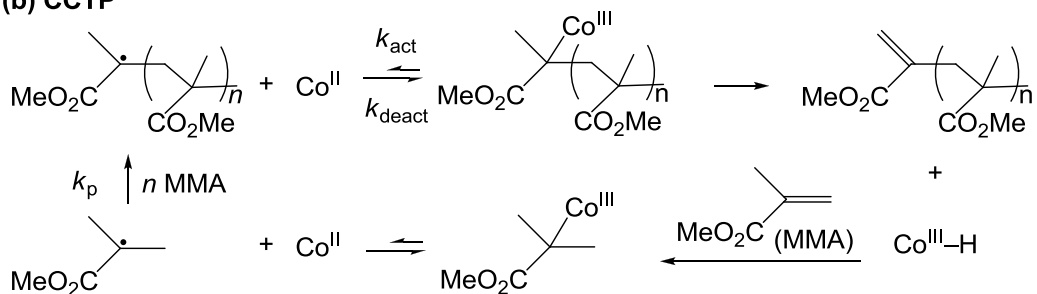


Scheme 1: Mechanisms of ATRA and ATRP reactions.

(a) OMRP



(b) CCTP



Scheme 2: Mechanisms of (a) OMRP and (b) CCTP reactions.

The **ATRP** mechanism is apparently followed by cobaltocene, acting as a precatalyst in the polymerization of styrene (**St**) and **MMA**.¹¹ Other common Co^{II} species, such as cobalt carboxylates are also known to induce **ATRP** reactions of **MMA** and **St** (oligomerization).^{12–14} In particular, cobalt acetate polymerizes **MMA** in good yields (82%) and narrow polydispersity ($M_w/M_n = 1.26$). Addition of small amounts of CoCl₂, Cu(OAc)₂ or tris(2-(dimethyl amino) ethyl)amine (Me₆TREN), improves the rate of the reaction, but the control over the polymerization is reduced ($M_w/M_n = 1.49-1.74$).¹² The CoCl₂/Me₆TREN system has been reported as catalyst for the ATRP of MMA, exerting modest control over the polymerization and molecular weight distribution of **PMMA** ($M_w/M_n = 1.63-1.80$),¹⁵ which can be improved by addition of a small amount of hybrid deactivators (FeBr₃/Me₆TREN or CuBr₂/Me₆TREN; $M_w/M_n = 1.15-1.46$). Heterogeneous versions have also been developed, such as a Co^{II}/Cu^{II} bimetallic catalyst immobilized on a crosslinked poly(acrylic acid) resin¹⁶ or a “hybrid” catalyst, consisting of Co^{II} immobilized on an ion exchange resin along with a small amount of soluble catalyst (CuCl₂/Me₆TREN).¹⁷ Among Co^I systems, [CoX(PPh₃)₃] (X = Cl, Br, I) are the first compounds reported to mediate **ATRP** reactions,¹⁸ with the iodide being the most reactive. On the other hand, the **OMRP** mechanism is reportedly obeyed by [Co(acac)₂] in the polymerization of vinyl acetate, and copolymerization of vinyl acetate and vinyl chloroacetate,^{19–22} as well as by Co^{II} porphyrin complexes in the polymerization of acrylate monomers.^{22–25} Finally, low-spin Co^{II} complexes, such as cobaloximes,²⁶ Co^{II}-5,10,15,20-tetraphenyl-21*H*,23*H*-porphine,²⁷ and Co^{II}-glyoximato species^{28–31} operate *via* the **CCTP** mechanism in the (co)polymerization of (meth)acrylates, α -methylstyrene and styrenes, yielding low molecular weight macromolecules in organic and aqueous media.

1.3 Manganese in controlled radical polymerization reactions

Although manganese can be found in several oxidative states (from -3 to 7), which renders it attractive to use in ATRP reactions, few examples have been reported so far. Most characteristic is [Mn(acac)₃] (acac = CH₃COCH₂COCH₃), which polymerizes styrene,³² but with wide molecular weight distribution, and binuclear •[Mn(CO)₅], which successfully polymerizes

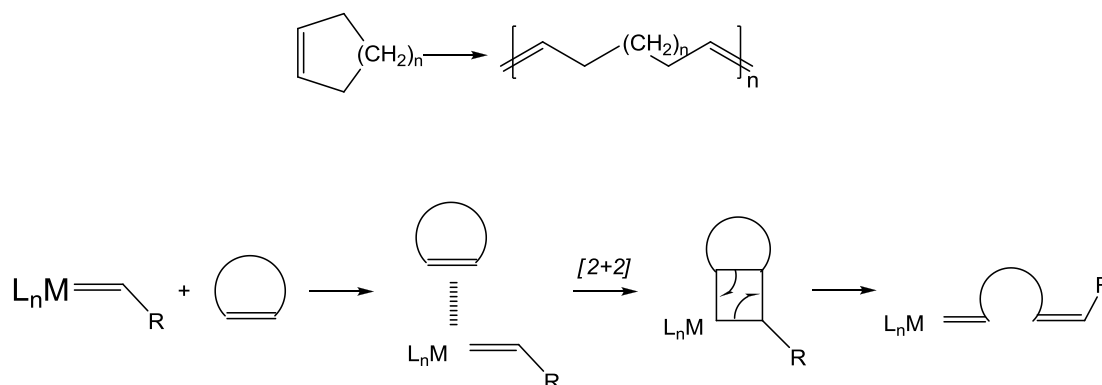
vinyl acetate with $M_w/M_n = 1.40-1.95$.³³ In the latter case, the binuclear complex decomposes to its monomer after being exposed to visible light, creating a radical manganese complex, which is the actual catalyst.

CHAPTER 2

RING OPENING METATHESIS POLYMERIZATION

2.1 Introduction

Olefin metathesis reactions are metal-mediated carbon-carbon (C–C) double bond exchange processes and have found several important applications. Olefin metathesis polymerization is an application of metathesis reactions to polymer synthesis, which includes, among others, the Ring Opening Metathesis Polymerization (**ROMP**) process (Scheme 3). The latter provides a wide range of unsaturated polymers of unique architectures and useful functions (e.g., outstanding elastomeric or thermoplastic engineering materials), the physicochemical properties of which strongly depend on their structure. The reaction can be catalyzed by a broad range of uni-, bi- or multicomponent systems based on transition metal complexes (Ti, Nb, Ta, Cr, Mo, W, Re, Co, Ru, Os),^{34–39} with those of Mo, W and Ru playing a major role. They can be classified in two major categories:^{34–42} (i) ill-defined systems, where the active metallocarbenes are generated *in situ*, i.e., the classical high-valent halides of Mo and W (e.g., WCl_6 and derivatives thereof), which become very effective when activated by organometallic co-catalysts (e.g., SnMe_4 , AlEt_3), as well as the industrially used $\text{RuCl}_3/\text{alcohol}$ ⁴³ catalytic system; (ii) well-defined metallocarbenes, such as the Grubbs⁴⁴ and Schrock⁴⁵ catalysts and their numerous variations.



Scheme 3: Ring Opening Metathesis Polymerization (ROMP) reaction and mechanism.

2.2 Draw-backs of known ROMP catalysts

Although the **ROMP** reaction was discovered in the mid 1950's and has been the subject of intensive research ever since, many difficulties are still encountered. For example, the widely employed in industry Mo and W halides present a number of draw-backs: (a) the halides themselves are hydrolytically unstable; (b) in some cases high activity is achieved with the use of organometallic initiators; (c) the polymerization is not "living", preventing precise control over the reaction(s); (d) they are not stereoselective; and (e) the exact nature of the active species remains a cloudy landscape.

In contrast, precision catalysts guarantee a high degree of reaction control over a diverse range of cyclo-olefins. Considerable progress has been made with Grubbs catalysts in terms of stability and design, but they are very expensive and difficult to remove them from the product. On the other hand, Schrock catalysts are highly reactive (especially the Mo-alkylidenes), but also highly sensitive to oxygen and moisture, and their synthesis is elaborate. Those issues present themselves as limitations for the utilization of those systems in large scale.

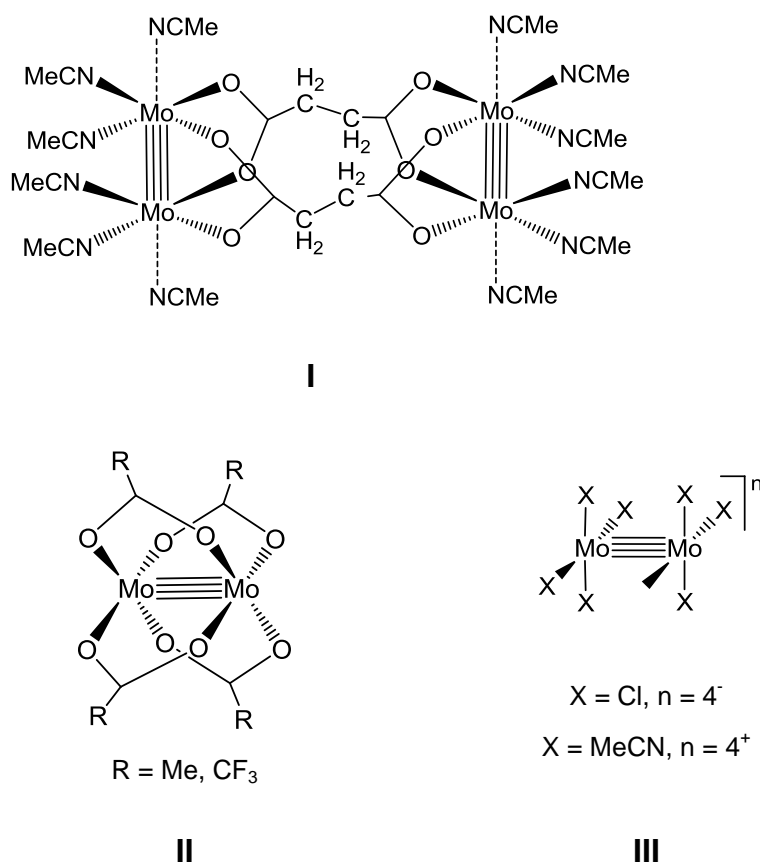
Additionally, another long-standing problem is controlling the stereochemistry of the reaction (*cis/trans*). This issue has been overcome up to now by serendipity, empirically (additives affecting the stereochemistry of the reaction), or by elaborate catalyst design. Thus, improving known catalytic systems or finding new ones, which are robust, cost-effective, highly active and stereoselective, is still a challenge.

2.3 Binuclear complexes as ROMP catalysts

The majority of the existing catalytic systems consists of mononuclear complexes. Bimetallic complexes with metal-metal bonds have been scarcely employed,⁴⁶ even though they provide more precise control over stereoselectivity, *via* the involvement of both metal centers in the reaction.

2.3.1 Molybdenum complexes

Neutral or ionic complexes of the general formulas $[\text{Mo}_2\text{L}_4]$, $[\text{Mo}_2\text{X}_8]^n$ and $[\text{Mo}_2\text{L}_2\text{X}_4]^n$, all containing the $\{\text{Mo}^4\text{-Mo}\}^{4+}$ core, with a variety of ligands (acetates, halides, allyl, acetonitrile), have been employed for the **ROMP** of norbornene (**NBE**) at ambient temperature.⁴⁷ Most of these complexes require activation with AlEtCl_2 . The same behavior is encountered with the tetrameric compound $[\{\text{Mo}_2(\mu\text{-O}_2\text{C}(\text{CH}_2)_2\text{CO}_2)(\text{NCMe})_6\}_2](\text{BF}_4)_4 \cdot 3\text{MeCN}$ ⁴⁸ (Scheme 4-I). When activated with AlEtCl_2 , complexes $[\text{Mo}_2(\mu\text{-O}_2\text{CR})_4]$ (R = Me, CF_3 ; Scheme 4-II) and $\text{K}_4[\text{Mo}_2\text{Cl}_8]$ (Scheme 4-III) also induce the **ROMP** of 1-methylnorbornene.⁴⁹ The reaction is immediate and exothermic. In all cases, the different ligands exert little or no influence on the stereoselectivity of the reaction.⁴⁷



Scheme 4: Binuclear Mo complexes that have been employed as ROMP catalysts.

However, noteworthy are the changes in the stereochemistry of poly(norbornene) (**PNBE**) observed, when the $[\text{Mo}_2(\text{NCMe})_8](\text{BF}_4)_4/\text{AlEtCl}_2$

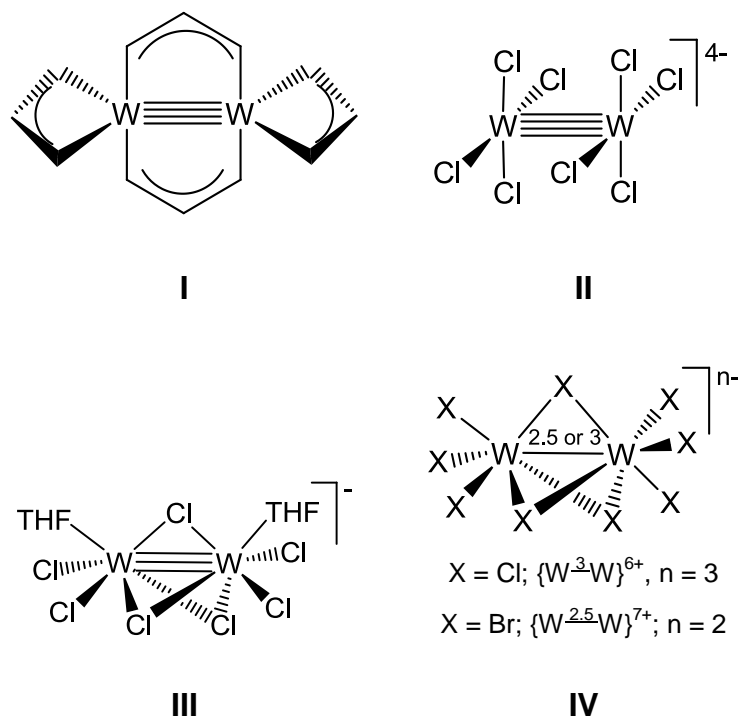
(Scheme 4-III) system is employed homogeneously or heterogeneously (supported on SiO₂). In the first case, the *cis*-content is almost 30%, whereas in the latter it increases to 70%.⁴⁷ This has been attributed to the greater steric hindrance (wall-effect), due to the coordination of the metal to silica, which obliges the monomer molecule (**NBE**) to approach the metals, minimizing repulsions that favor the formation of *cis*- rather than *trans*-junctions in the polymer chain. Such an effect has been considered responsible for the formation of an *all-cis*-**PNBE** polymer from the *in situ* reaction of [WCl₆]/PSLi/NBE [PS = poly(styrene)].⁵⁰

2.3.2 Tungsten complexes

The first report on a **ROMP** reaction catalyzed by a metal-metal bonded catalyst precursor was published in 1970. A bicomponent system consisting of [W₂(π -C₃H₅)₄] ($\{W^4-W\}^{4+}$; Scheme 5-I) and [WCl₆] was found to be active in the **ROMP** of cyclopentene, providing in low yields (18%) poly(pentenamer) with a *trans*-content of 60%.⁵¹ The ditungsten halide Na₄[W₂Cl₈](THF)_x ($\{W^4-W\}^{4+}$; Scheme 5-II) polymerizes **NBE** and norbornadiene (**NBD**) within a few minutes in almost quantitative yields, providing polymers of high molecular weight and high *cis*-stereoselectivity (>80% *cis* for **PNBE**).⁵² A major drawback of this system is its high sensitivity towards oxidation (oxygen, moisture) and its thermal instability.

The ditungsten complex Na[W₂(μ -Cl)₃Cl₄(THF)₂](THF)₃ (**{W₂}**, $\{W^3-W\}^{6+}$, a^2e^4 , Scheme 5-III) is a highly efficient unicomponent room temperature homogeneous and/or heterogeneous initiator for the **ROMP** of norbornene (**NBE**) and some of its derivatives.⁵³ **{W₂}** distinctly differs from its mononuclear counterparts, offering significant advantages over them, such as: (a) high reactivity similar to that of the bi- or multicomponent analogues (e.g., WCl₆/AlR₃); (b) high *cis*-stereoselectivity; (c) tolerance to olefinic side groups, providing polymeric materials suitable for post-polymer functionalization. The catalytic activity of the all-bromo-derivative (Ph₄P)₂[W₂(μ -Br)₃Br₆] ($\{W^{2.5}-W\}^{7+}$; Scheme 5-IV) towards the **ROMP** of **NBE** and derivatives has been also investigated.⁵⁴ Despite the fact that bromide

ligands are more labile than the chloride ones, addition of AgBF_4 is necessary in order to activate the ditungsten complex. The reactions are more efficient in CH_2Cl_2 , providing high yields of polymers, in the presence of four AgBF_4 equivalents. The reactions are stereoselective and the polymers obtained features high *cis*-content (87%).

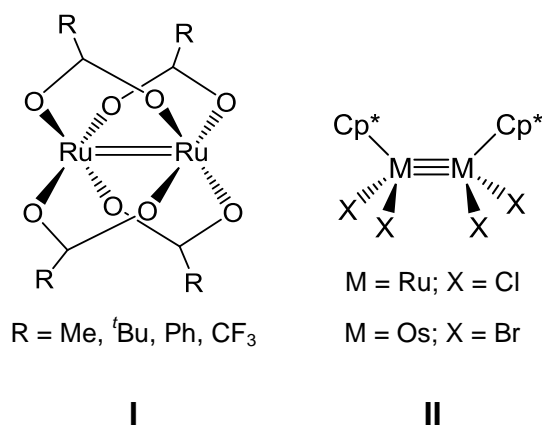


Scheme 5: Binuclear W complexes that have been employed as ROMP catalysts.

2.3.3 Ruthenium and osmium complexes

Despite the abundance of the mononuclear Ru-based catalytic systems, there are only few examples of binuclear one reported so far. Diruthenium tetracarboxylates, $[\text{Ru}_2\text{L}_4]$ ($\{\text{Ru}^2\text{Ru}\}^{4+}$; L = acetate, pivalate, benzoate, trifluoroacetate; Scheme 6-I) are inactive for initiating **ROMP** reactions in nonalcoholic media, even in the presence of various Lewis acids. However, upon addition of ethyldiazoacetate in a chlorobenzene solution of $[\text{Ru}_2(\text{OOCF}_3)_4]$, highly-*cis*-PNBE can be obtained in moderate yields, but with broad molecular weight distribution ($M_w/M_n = 5.1$).⁵⁵ Complex $[\text{Cp}^*\text{Ru}_2\text{Cl}_4]$ ($\{\text{Ru}^3\text{Ru}\}^{6+}$; $\text{Cp}^* = \eta^5\text{-C}_5\text{Me}_5$; Scheme 6-II) polymerizes **NBE** and **NBD** in refluxing ethanol, in low yields.⁵⁶ Higher reactivity is observed with the

analogous compound $[\text{Cp}^*_2\text{Os}_2\text{Br}_4]$ ($\{\text{Os}^3\text{-Os}\}^{6+}$; Scheme 6-II), which upon activation by MAO (MAO = methylaluminoxane) polymerizes **NBE** to 40-60% *cis*-PNBE, insoluble to organic solvents.⁵⁷ For **NBE**, the activity of this system is higher than that of the respective chloride salts OsCl_3 and RuCl_3 .⁵⁸ This complex also operates without cocatalysts. The addition of AlMe_3 or MAO, as well as the solvents used, do not affect significantly the nature of **PNBE** formed, but considerably increase the polymerization rates and yields.

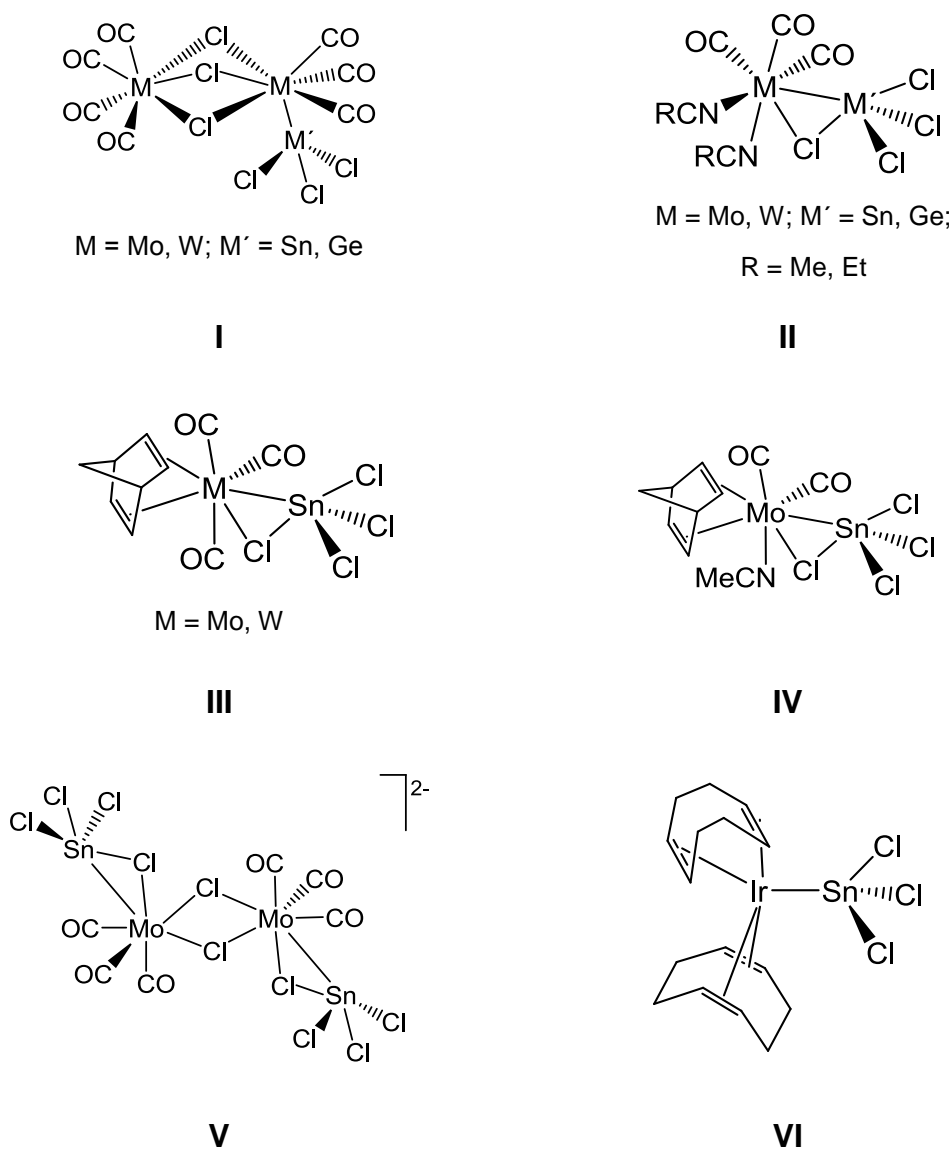


Scheme 6: Binuclear Ru and Os complexes that have been employed as ROMP catalysts.

2.3.4 Heterometallic complexes

Compounds $[\text{M}_2(\mu\text{-Cl})_3(\text{CO})_7(\text{M}'\text{Cl}_3)]$ (Scheme 7-I), $[\text{M}(\mu\text{-Cl})(\text{CO})_3(\text{NCR})_2(\text{M}'\text{Cl}_3)]$ (Scheme 7-II), ($\text{M} = \text{Mo}, \text{W}$; $\text{M}' = \text{Sn}, \text{Ge}$; $\text{R} = \text{Me}, \text{Et}$) act as catalytic precursors for the **ROMP** of **NBE** and **NBD**.⁵⁹ The polymerization of **NBE** is chemoselective, but slow, when $[\text{M}(\mu\text{-Cl})(\text{CO})_3(\text{NCMe})_2(\text{M}'\text{Cl}_3)]$ ($\text{M} = \text{Mo}, \text{W}$; $\text{M}' = \text{Sn}, \text{Ge}$) is used as initiator; it is faster with $[\text{M}_2(\mu\text{-Cl})_3(\text{CO})_7(\text{SnCl}_3)]$ ($\text{M} = \text{Mo}, \text{W}$), but of low selectivity. The polymers obtained have high molecular weights ($M_w > 10^4$), but rather broad molecular weight distributions (M_w/M_n 1.8-3.6). Upon reaction with stoichiometric amounts of **NBD**, the above mentioned compounds provide the corresponding **NBD**-adducts, $[\text{M}(\mu\text{-Cl})(\text{CO})_3(\eta^4\text{-NBD})(\text{SnCl}_3)]$ ($\text{M} = \text{Mo}, \text{W}$; Scheme 7-III) and $[\text{Mo}(\mu\text{-Cl})(\text{CO})_2(\text{NCMe})(\eta^4\text{-NBD})(\text{SnCl}_3)]$ (Scheme 7-IV), which, in the presence of excess **NBD**, have been found to initiate the **ROMP** of **NBD**.^{60,61} The polymerization is slow and not selective. The molecular

characteristics of PNBD formed have not been reported, due to their insolubility; however the *cis*-content has been determined by *in-situ* NMR experiments and provided valuable mechanistic insight.



Scheme 7: Binuclear heterometallic complexes that have been employed as ROMP catalysts.

Substituted cycloolefins have also been polymerized. Compounds $[M(\mu\text{-Cl})(\text{CO})_3(\text{NCMe})_2(\text{M}'\text{Cl}_3)]$ ($M = \text{Mo}, \text{W}$; $M' = \text{Sn}, \text{Ge}$) catalyze the **ROMP** of *endo,endo*-5,6-bis(chloromethyl)norbornene to soluble polymers of high molecular weight ($M_w > 5 \times 10^5$) and moderate molecular weight distribution

(M_w/M_n 1.4-2.0).⁶² The choice of transition metal determines the stereochemistry of the polymer formed, as W-initiators give predominately *cis*-polymers (84-95% *cis*), while with Mo-analogues the % *cis* content is in the range of 20-50%. In addition, $[W_2(\mu-Cl)_3(CO)_7(GeCl_3)]$, polymerizes 5-vinyl-2-norbornene (**VNBE**) with high yields of polymers of low molecular weight (less than 3,000), along with small amounts of side products (~10%), and bimodal peaks of broad molecular weight distribution ($M_w/M_n > 2$).⁶³ The pendant double bonds remain intact.

The anionic complex $[(\mu-Cl)_2\{Mo(\mu-Cl)(CO)_3(SnCl_3)\}_2]^{2-}$ (Scheme 7-V) also promotes the **ROMP** of **NBE** at r.t. and under strictly anhydrous conditions, providing **PNBE** in high yields (89%).⁶⁴

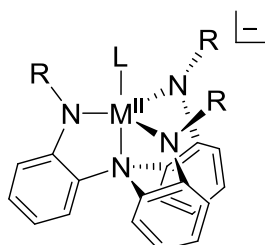
Another bimetallic metal-tin catalyst, $[Ir(COD)_2SnCl_3]$ (COD = 1,5-cyclooctadiene; Scheme 7-VI), bearing an Ir–Sn bond has been reported for the **ROMP** of **NBE** in toluene at elevated temperatures and sealed vials, providing clear films of **PNBE** at low yields (<10%).⁶⁵

CHAPTER 3

PURPOSE OF THIS STUDY

The purpose of this study was to develop new catalytic systems for two types of metal-mediated polymerization reactions and to employ the best of those systems for the synthesis of new polymeric products. The polymerization reactions studied are: Controlled Radical Polymerization (**CRP**) and Ring Opening Metathesis Polymerization (**ROMP**).

CRP. Recently, the synthesis and reactivity of a series of tripodal transition metal compounds (M = Fe, Mn, Co) with rigid triphenylamido-amine cores and a variety of pendant arms (R = aryl, acyl, alkyl) (Scheme 8) has been explored.⁶⁶⁻⁷⁵ Many members of this family of reagents have been recognized as active in oxo- and nitrene-transfer chemistry, as well as in Controlled Radical Polymerization (**CRP**) catalysis, enabled by a reversible or semi-reversible $M^{n+}/M^{(n+1)+}$ couple at easily accessible, and frequently highly reducing potentials. In this work, we examined the **CRP** activity of a series of tripodal Co^{II} and Mn^{II} triphenylamido-amine complexes bearing a selection of aryl, acyl and alkyl arms.



M = Mn, Fe, Co
R = aryl, acyl, alkyl
L = solvent or vacant

Scheme 8: General structure of triphenylamido-amine complexes.

ROMP. In view of the properties of the catalytic system based on $Na[W_2(\mu-Cl)_3Cl_4(THF)_2] \cdot (THF)_3$ (**W₂**, Scheme 9), i.e., high efficiency and high-*cis* stereoselectivity, which may address some of the limitations of known **ROMP** catalysts, we used **W₂** for the copolymerization of norbornene (**NBE**) and norbornadiene (**NBD**). The addition of **NBE** moieties in the polymer chain was

CHAPTER 4

EXPERIMENTAL

4.1 Materials and physical measurements

All operations were performed under anaerobic conditions under a pure dinitrogen or argon atmosphere using Schlenk techniques on an inert gas/vacuum manifold or in a dry-box (O_2 , H_2O < 1 ppm). Starting materials were purchased from Sigma-Aldrich and are of the highest available purities. Dicyclopentadiene (**DCPD**, >91% *endo*-isomer) was purchased from Acros. WCl_6 was purchased from Alfa Aesar in sealed ampules. The L^xCo^{II} and L^xMn^{II} compounds were kindly provided by Prof. Pericles Stavropoulos (Missouri University of Science & Technology, Rolla MO, USA). Complex $Na[W_2(\mu-Cl)_3Cl_4(THF)_2] \cdot (THF)_3$ ($\{W_2\}$)⁷⁶ was prepared according to literature procedures. Norbornene (**NBE**) was dissolved in the solvent used for the reaction, was dried by stirring with CaH_2 under argon and was distilled under vacuum prior to use. Poly(dicyclopentadiene) (**PDCPD**) aerogels synthesized using 1st and 2nd generation Grubbs' catalysts were kindly provided by Prof. Nicholas Leventis.⁷⁷ Norbornadiene (**NBD**) was passed through an Al_2O_3 column. 5-vinyl-2-norbornene (**VNBE**), **DCPD** and phenylacetylene (**PA**) were dried by stirring with CaH_2 under argon, were distilled under vacuum and were stored in the dark under argon. THF and Et_2O were distilled over Na/Ph_2CO , toluene and hexanes over Na , CH_2Cl_2 over P_4O_{10} and methanol over sodium methoxide. All solvents were distilled in an inert atmosphere, and were degassed by three freeze-pump-thaw cycles, with the exception of methanol, which was degassed by bubbling nitrogen or argon for 0.5 h.

NMR spectra were recorded on a Varian Unity Plus 300 spectrometer. In all cases, chemical shifts are reported in ppm relative to the deuterated solvent resonances.

Solid-state NMR spectra were obtained at the National Institute of Chemistry, Ljubljana, Slovenia, with a 600 MHz Varian spectrometer (Palo Alto, CA) operating at 150.80 MHz for ^{13}C . For 1H - ^{13}C ramped CPMAS (Cross-

Polarization Magic Angle Spinning) and HC LG-HETCOR (HETeronuclear CORrelation) spectra the spinning rate used was 5 kHz and the temperature run the experiment was 25 °C.

Mid-IR spectra (525-4000 cm^{-1}) were measured at the National Hellenic Research Foundation, Athens, Greece, with a Fourier-transform instrument (Equinox 55 by Bruker Optics) equipped with a single-reflection diamond ATR accessory (DuraSamplIR II by SensIR Technologies). Contact between the powder samples and the diamond element was ensured by a suitable press. Each spectrum represents the average of 100 scans recorded at an optical resolution of 4 cm^{-1} . FT-Raman spectra were obtained at the National Hellenic Research Foundation, Athens, Greece, with a Fourier transform instrument (RFS 100 by Bruker Optics) employing for excitation ca. 300mW of the Nd:YAG 1064 nm line in a backscattering geometry. The spectra have been measured at a resolution of 4 cm^{-1} and represent averages of ca. 5,000–8,000 scans.

Size exclusion chromatography (SEC) experiments were carried out at the Laboratory of Industrial Chemistry, Department of Chemistry, N.K.U.A., Athens, Greece, with a modular instrument consisting of a Waters model 600 pump, a Waters model U6K sample injector, a Waters model 410 differential refractometer and a set of 4 μ -Styragel columns with a continuous porosity range of 10^6 - 10^3 Å. The columns were housed in an oven thermostated at 40 °C. THF was the carrier solvent at a flow rate of 1 mL/min. The instrument was calibrated with PS standards covering the molecular weight range of 4,000-900,000.

The thermal stability of the polymers was studied by thermogravimetric analysis (TGA) at the Laboratory of Industrial Chemistry, Department of Chemistry, N.K.U.A., Athens, Greece, employing a Q50 TGA model from TA instruments. Samples were placed in platinum crucibles. An empty platinum crucible was used as a reference. Samples were heated from ambient temperatures to 600 °C in a 60 mL/min flow of N_2 at a heating rate of 10 °C/min.

Cyclic voltammetry was carried out with an Eco Chemie Autolab PGSTAT100 electrochemical workstation fitted in a Dry Box and controlled with a General Purpose Electrochemical Software (GPES) or with a Bipotentiostat AFCBP1 from Pine Instrument Company fitted in a Dry Box and controlled with the PineChem 2.7.9 software. Experiments were performed using a gold disk working electrode (2 mm diameter) and a Ag/Ag⁺ (0.01 M AgNO₃ and 0.5 M [(*n*-Bu)₄N]PF₆ in MeCN or DMF) non-aqueous reference electrode (Bioanalytical Systems, Inc.) with a prolonged bridge (0.5 M [(*n*-Bu)₄N]PF₆ in MeCN or DMF). A thin Pt foil or gauge (8 cm², Sigma-Aldrich) was employed as counter electrode. The working electrode was polished using successively 6, 3, 1 μm diamond paste on a DP-Nap polishing cloth (Struers, Westlake, OH), washed with water, acetone and air-dried. The Pt foil and gauge electrodes were cleaned in a H₂O₂/H₂SO₄(conc) solution (1:4 v:v) and oven-dried. The concentrations of the samples were between 1 and 3 mM and that of [(*n*-Bu)₄N]PF₆ (supporting electrolyte) was 0.5 M. The potential sweep rate varied between 10–1000 mV/s. All potentials are reported versus the ferrocenium/ferrocene (*Fc*⁺/*Fc*) couple.

Scanning electron microscopy images were taken at Istituto Italiano di Tecnologia, Genova, Italy, using a field emission scanning electron microscope coupled with energy dispersive X-ray microanalysis (SEM/EDS, JEOL, JSM-7500F, Japan). The samples were fixed on aluminium stubs and coated with a 10 nm thick gold layer with an Emitech K950X. The measurements were realized in high vacuum with a pressure of 9.6×10⁻⁵ Pa by using a SEI detector at a tension of 5 kV.

4.2 CRP reactions

4.2.1 Typical experimental procedure

All operations were carried out under an inert atmosphere. The M^{II} (M = Co, Mn) compound (0.01 mmol; e.g. [K(L³)Co^{II}-NCMe]_{*n*} (**Co-1**): 10.6 mg) and the solvent (toluene, 1.0 mL) were added to a Schlenk flask, followed by the monomer (styrene (**St**), 1.0 g, 9.6 mmol; methyl methacrylate (**MMA**), 1.0 g, 10.0 mmol) and the initiator (ethyl-2-bromo-isobutyrate, 7.5 μL, 5.1×10⁻⁵ mol).

The flask was immediately immersed in the oil bath at 110 °C and kept for a given time. After heating was stopped, the reaction vessel was cooled to room temperature and a large excess of MeOH was added to precipitate the polymer formed. The resulting solids were filtered, washed with methanol and redissolved in toluene, where Dowex ion exchange resin was added to remove any metal compound before analysis. The colorless solution was then decanted and concentrated to a small volume (~ 1 mL). MeOH was added again to precipitate the polymers, which were then dried in vacuo for several hours. Polymers were characterized by SEC in CHCl₃ and by ¹H NMR in CDCl₃ at room temperature.

4.2.2 Reinitiation experiment 1

Compound [K₂(L⁹)₂Co^{II}]_n (**Co-4**) (10.2 mg, 0.01 mmol) and the solvent (toluene, 2.0 mL) were added to a Schlenk flask, followed by **St** (1.0 g, 9.6 mmol) and the initiator (ethyl-2-bromo-isobutyrate, 7.5 μL, 5.1×10⁻⁵ mol). The flask was immediately immersed in the oil bath at 110 °C and kept for 20 h. After heating was stopped, the reaction vessel was cooled to room temperature and an aliquot (0.5 mL) was taken. To this aliquot a large excess of MeOH was added to precipitate the polymer formed, which was purified and characterized as described above.

To the rest of the reaction mixture, **St** (1.0 g, 9.6 mmol) was added and was left to react for another 20 h at 110 °C. After heating was stopped, the reaction vessel was cooled to room temperature and a large excess of MeOH was added to precipitate the polymer formed, which was purified and characterized as described above.

4.2.3 Reinitiation experiment 2

Compound [K(THF)₆][(L⁵)Co^{II}]⁺•1.5THF (**Co-2**) (13.6 mg, 0.01 mmol) and the solvent (toluene, 2.0 mL) were added to a Schlenk flask, followed by **MMA** (1.0 g, 10.0 mmol) and the initiator (ethyl-2-bromo-isobutyrate, 7.5 μL, 5.1×10⁻⁵ mol). The flask was immediately immersed in the oil bath at 110 °C and kept for 16 h. After heating was stopped, the reaction vessel was cooled to room

temperature and a large excess of MeOH was added to precipitate the polymer formed, which was purified and characterized as described above.

The **PMMA** obtained was redissolved in toluene (2.0 mL), where the metal complex (13.6 mg, 0.01 mmol) and **St** (1.0 g, 9.6 mmol) were added and the mixture was left to react for another 20 h at 110 °C. After heating was stopped, the reaction vessel was cooled to room temperature and a large excess of MeOH was added to precipitate the polymer formed, which was purified and characterized as described above.

4.3 ROMP reactions

4.3.1 Copolymerization reactions

All operations were carried out under an inert atmosphere. In a typical experiment, the complex (9.0 mg, 0.009 mmol) and CH₂Cl₂ were added to a Schlenk flask, followed by the monomers (**NBE** or/and **NBD**). The mixture was left under stirring for a given time. After the end of the reaction, the mixture (if not gelled) was concentrated to approx. half the initial volume and a large excess of MeOH was added to precipitate the copolymer formed. The resulting solids were filtered and washed with methanol. The polymers were characterized by SEC (if soluble) and ¹³C CP-MAS NMR spectroscopy, their thermal degradation was studied with thermogravimetric analysis (TGA) and differential scanning calorimetry (DSC) and the morphology of the materials was studied with scanning electron microscopy (SEM).

4.3.2 Use of PA as co-initiator

All operations were carried out under an inert atmosphere. A typical procedure is described as follows. **PA** (e.g., 10 μL, 9.2 mg, 0.09 mmol) was added to a solution of **{W₂}** (9.0 mg, 0.009 mmol) in a solvent (2.0 mL), followed by the substrate (e.g., **NBE**, 423 mg, 4.5 mmol). When no **PA** was used, the substrate was added to the solution of **{W₂}**. The mixture was allowed to react at room temperature for a given time, after which it was concentrated to half volume and treated with excess of methanol to have the polymeric products precipitated. The resulting solids were filtered and washed

repeatedly with methanol. They were redissolved in THF and the above procedure was repeated at least three times. The products were dried *in vacuo*.

4.3.3 Catalytic reactions in NMR tubes

Complex **{W₂}** was dissolved in *d*⁸-THF (8.0 mg, 0.008 mmol) and the green solution was transferred in an NMR tube. The appropriate amounts of **PA** (5 μ L, 4.6 mg, 0.05 mmol) and **NBE** (5 mg, 0.05 mmol) were added using a microliter syringe.

4.4 PDCPD gels

4.4.1 Catalytic system **{W₂}/PA**

PA (225 μ L, 209 mg, 2.05 mmol) was added to a solution of **{W₂}** (105.0 mg, 0.105 mmol) in CH₂Cl₂ (15.0 mL), followed by **DCPD** (5.0 mL, 4.89 g, 37.0 mmol). The mixture was stirred vigorously at room temperature for 30 min and was poured into molds (Wheaton poly(propylene) OmniVials, 1.1 cm in diameter). All solutions gelled within 18 h. The resulting wet-gels were aged in their molds for 6 h at room temperature. Subsequently, wet-gels were transferred into toluene and were washed 4 \times 8 h per wash cycle, using 4 \times the volume of the gels. It is noted that during processing wet-gels swell in toluene. That was accounted for by adjusting the volume of the wash solutions to be always 4 \times the volume of the wet-gel. Next, pore-filling toluene was exchanged with pentane (4 washes, 8 h per wash cycle, 4 \times the volume of the gel per cycle), and wet-gels were air-dried in the oven at 50 °C. It is noted that wet-gels deswell in pentane almost to their original volume. The resulting gels are referred to as **W₂-PDCPD** (where **W₂** stands for the catalytic system **{W₂}/PA**).

4.4.2 Catalytic system **WCl₆/PA**

PA (50 μ L, 46.5 mg, 0.455 mmol) was added to a solution of WCl₆ (160.0 mg, 0.403 mmol) in toluene (15.0 mL), followed by **DCPD** (5.0 mL, 4.89 mg, 37.0 mmol). The mixture was stirred vigorously at room temperature for 1 min and

was poured into molds (Wheaton poly(propylene) OmniVials, 1.1 cm in diameter). All solutions gelled within 5 min. The resulting wet-gels were aged in their molds for 15 min at room temperature. Subsequently, wet-gels were transferred into THF and were washed 4×, 8 h per wash cycle, using 4× the volume of the gels. Next, pore-filling THF was exchanged with acetonitrile (4 washes, 8 h per wash cycle, 4× the volume of the gel per cycle) and pentane (4 washes, 8 h per wash cycle, 4× the volume of the gel per cycle). No change in the volume of the gels was observed during wash cycles. The wet-gels were air-dried in the oven at 50 °C. The resulting gels are referred to as **W-PDCPD** (where **W** stands for the catalytic system **WCl₆/PA**).

4.4.3 Swelling measurements

The ability of gels to absorb various solvents (toluene, CH₂Cl₂, CHCl₃, CCl₄, THF, CS₂, benzene, chlorobenzene, 1,2- and 1,3-dichlorobenzene, benzyl chloride, 1,3- and 1,4-dimethylbenzene, 1,3,5-trimethylbenzene, pentane, acetone, CH₃CN, CH₃OH, DMF, DMSO, water, 1,4-dioxane) has been evaluated. Dry cylindrical gels were immersed in selected solvents. At selected time intervals, gels were taken out of the solvents and their height and diameter were measured, to determine their volume. Gels were re-immersed in their respective solvents immediately to continue swelling. Their normalized volume was calculated as the ratio of the volume of swollen gels to the volume of dry gels.

4.4.4 Separation of organic solvents from water

To determine the ability of gels to separate chlorinated solvents from water, disks were cut from gels and they were immersed in mixtures of water and chlorinated solvents in equal volumes. Sudan blue dye was used to visualize the lowering of the organic phase and the solvent absorption from the gel. Gels were kept in the solvent mixture for a given time. The uptake for each solvent was determined by the weight difference of gels before and after solvent absorption.

CHAPTER 5

CATALYTIC ACTIVITY OF Co AND Mn TRIPHENYLAMIDO-AMINE COMPLEXES IN CONTROLLED RADICAL POLYMERIZATION OF OLEFINS

5.1 Co^{II} complexes

The structures of the Co^{II} compounds used in this study are presented in Scheme 10.⁷⁸ These complexes have been synthesized by the reaction of anhydrous CoCl₂ with the deprotonated ligands and exhibit stoichiometric and structural variation. Solid-state structures revealed that in all cases the four nitrogen-atom residues of the ligands are coordinated to the metal center in a distorted trigonal-pyramidal geometry. In two cases (**Co-1** and **Co-6**), the presence of a solvent molecule (CH₃CN) adds a fifth moiety to the coordination sphere.

5.1.1 Cyclic voltammetry

The electrochemical properties of compounds **Co-1-6** have been studied by cyclic voltammetry. Electrochemical data for the Co^{II}/Co^{III} couple are listed in Table 1 and the corresponding waves are shown in Figure 1. Compound [K(NCMe)₃][(L¹³)Co^{II}-NCMe] (**Co-6**), which bears the electron-donating aryl substituent 2,6-(CH₃)₂ was oxidized at the most negative potential. The presence of the electron-withdrawing aryl substituents 3,5-(CF₃)₂ and 3,5-Cl₂ in [K(L³)Co^{II}-NCMe]_n (**Co-1**) and [K(THF)₆][(L⁵)Co^{II}]_n•1.5THF (**Co-2**) respectively, shifted the oxidation redox potential to more positive values. Complex [K₂(L⁹)₂Co^{II}]_n (**Co-4**) showed two overlapping redox waves, which may reflect the two distinct Co^{II} ions observed in the repeating dinuclear unit of the solid-state structure. The potential values were close to that of **Co-6** and are in agreement with the electron-rich nature of the arylalkylamido-amine ligand. Finally, as expected, the electron-withdrawing COO^tBu and COCF₃ substituents of {[K₂(DMA)₃(L¹⁰)₂Co^{II}]_n•0.5Et₂O} (**Co-5**) and [K(THF)₂(L⁸)Co^{II}]_n (**Co-3**) caused significant anodic shift. The assignment of these irreversible waves to the Co^{II}/Co^{III} couple is tentative. Contributions from ligand-centered

Table 1: Electrochemical data for compounds Co-1-6.

| Compound | Solvent | $E_{1/2}$ (or $E_{p,a}$) (V vs. Fc^+/Fc) | ΔE (mV) |
|---|---------|---|--------------------|
| $[K(L^3)Co^{II}-NCMe]_n$ (Co-1) | MeCN | -0.090 | 72 |
| $[K(THF)_6][L^5Co^{II}] \cdot 1.5THF$ (Co-2) | DMF | -0.258 | 102 |
| $[K(THF)_2(L^8)Co^{II}]_n$ (Co-3) | DMF | 0.719 | |
| $[K_2(L^9)_2Co^{II}_2]_n$ (Co-4) | DMF | -0.654, -0.500 | 88, 75 |
| $\{[K_2(DMA)_3(L^{10})_2Co^{II}_2] \cdot 0.5Et_2O\}_n$ (Co-5) | DMA | 0.559 | |
| $[K(NCMe)_3(L^{13})Co^{II}-NCMe]$ (Co-6) | MeCN | -0.665 | 78 |

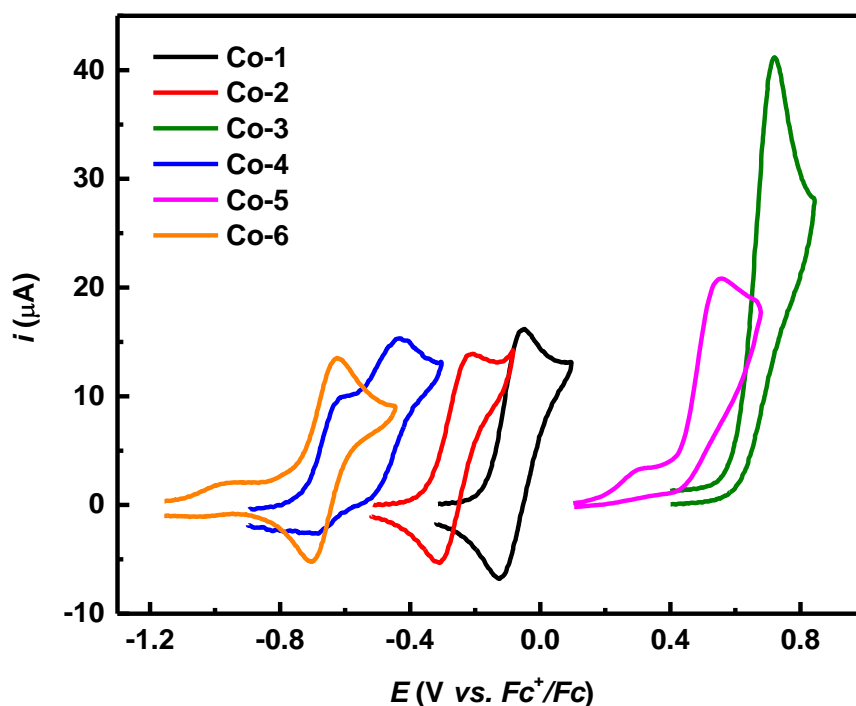


Figure 1: Cyclic voltammograms (Co^{II}/Co^{III} redox couple) of compounds $[K(L^3)Co^{II}-NCMe]_n$ (Co-1) and $[K(NCMe)_3(L^{13})Co^{II}-NCMe]$ (Co-6) in MeCN/ $[(n-Bu)_4N]PF_6$, $[K(THF)_6][L^5Co^{II}] \cdot 1.5THF$ (Co-2), $[K(THF)_2(L^8)Co^{II}]_n$ (Co-3) and $[K_2(L^9)_2Co^{II}_2]_n$ (Co-4) in DMF/ $[(n-Bu)_4N]PF_6$, and $\{[K_2(DMA)_3(L^{10})_2Co^{II}_2] \cdot 0.5Et_2O\}_n$ (Co-5) in DMA/ $[(n-Bu)_4N]PF_6$, as indicated, with a Au disk electrode (1.6 mm in diameter); scan rate 0.1 V/s.

5.1.2 Polymerization results

Compounds **Co-1**, **Co-2**, **Co-4**, and **Co-6** have properties that make them promising reagents for use as **ATRP** catalysts. They provide reversible or semi-reversible $\text{Co}^{\text{II}}/\text{Co}^{\text{III}}$ couples at easily accessible potentials, as shown by the electrochemical data. They have either a vacant coordination site, or a weakly bound ligand (solvent molecule), which makes it possible for a halide or (pseudohalide) ligand to enter the coordination sphere. **Co-3** and **Co-5**, which feature an irreversible $\text{Co}^{\text{II}}/\text{Co}^{\text{III}}$ couple, have also been studied, as the halidophilicity is in some cases a factor of equal or even higher importance. Indeed, it has been found that the activity of an **ATRP** catalyst mainly depends on the redox potential of the $\text{M}^{n+}/\text{M}^{(n+1)+}$ couple and the halidophilicity of the $\text{M}^{(n+1)+}$ complex. For Cu-based catalysts the key factor seems to be the redox potential, for Ru- and Os-complexes the halidophilicity, while for other metal catalysts the two factors have intermediate effects.⁷⁹ In addition, since **ATRP** is not the only possible pathway for Co-induced radical polymerizations, other parameters, such as the strength and reactivity of $\text{Co}^{\text{III}}-\text{C}$ or $\text{Co}^{\text{III}}-\text{H}$ bonds, can play a dominant role.

The catalytic activity of compounds **Co-1-6** towards the polymerization of styrene (**St**) and methyl methacrylate (**MMA**) was studied in toluene solutions at 110 °C using ethyl-2-bromo-isobutyrate as initiator. The results are summarized in Tables 2 and 3. Blank experiments are also included for comparison purposes. **Co-1**, **Co-5** and **Co-6** are readily soluble in toluene, **Co-2** is partially dissolved, whereas **Co-3** and **Co-4** are insoluble. However, the solutions became homogeneous after the addition of the monomer and the initiator, with the only exception of **Co-3**, which got partly dissolved during the reaction with **St** and remained insoluble during the reaction with **MMA**. The reaction mixtures were allowed to react for a given time. In some cases, high-viscosity mixtures had formed at that time. The catalyst/monomer/initiator molar ratio was 1/1000/5, unless otherwise stated. The polymers, poly(styrene) (**PS**) and poly(methyl methacrylate) (**PMMA**), were obtained after addition of MeOH and were purified by Dowex ion exchange resin in toluene solutions.

From the data shown in Table 2, higher yields of **PS** have been obtained with compounds **Co-3-5**. The reaction mixtures containing **Co-3** and **Co-5** gelled after 2 h (entries 4 and 7). For this reason, they were repeated with 2.0 mL of toluene instead of 1.0 mL. It is notable however that the reaction with **Co-5** gave high yields (51%) in a short period of time. When a larger amount of solvent (2.0 mL; entry 8) was used, the reaction proceeded in a more controlled fashion, giving a polymer with molecular weight closer to the theoretical value, although with a bimodal distribution (Figure 2), which caused broadening of the molecular weight distribution ($M_w/M_n = 2.00$). Among the three systems, **Co-4** and **Co-5** showed better control over the molecular weight of the **PS** obtained (entries 6 and 8), while **Co-3** and **Co-4** provided **PS** with bimodal distribution and yet relatively narrow (1.56 and 1.57, respectively; entries 5 and 6; Figures 3 and 4). The other three compounds showed low reactivity (entries 1-3 and 9), yielding polymers with broad molecular weight distributions.

Similar reactivity was observed in **MMA** polymerization in most cases, with **Co-4** and **Co-5** being the most reactive in terms of polymer yields. The only notable exception was **Co-3** (Table 3, entries 6 and 7), which was the most reactive compound for **St** polymerization, and one of the least reactive for **MMA** polymerization. In fact, the complex had no control over the reaction, as the molecular characteristics of the polymers formed did not differ from the blank experiment (entry 13). That result was not unexpected, since **Co-3** is totally insoluble in the reaction mixture. The molecular weight of **PMMA** obtained with **Co-4** showed the best agreement with the theoretical value, compared to the other samples, and the molecular weight distribution was not very broad ($M_w/M_n = 1.52$; entry 9; Figure 5). **Co-5** provided high yields of **PMMA**, although with higher molecular weights and bimodal molecular weight distributions (entries 9 and 10; Figure 6). With **Co-2** and **Co-6** lower yields were obtained (entries 3, 11 and 12). However, the metal complex seemed to have a better control over the reaction, giving **PMMA** with relatively narrow molecular weight distribution, especially with **Co-2** (1.40). Addition of 0.10 and 0.15 mmol of initiator (entries 4 and 5) did not significantly alter the

controllability of the reaction, although the GPC plots had different characteristics (Figure 7), which will be discussed below. In the latter case, the yield was reduced. Finally, **Co-1** was the least reactive of the compounds studied (entries 1 and 2).

Table 2: Reactions of compounds Co-1-6 with styrene (St).^a

| Entry | Compound | <i>t</i> (h) | Yield (%) | <i>M_n</i> (th) ^b | <i>M_n</i> (exp) ^c | <i>M_w</i> / <i>M_n</i> |
|-------|---|-----------------|-----------------|--|---|---|
| 1 | [K(L ³)Co ^{II} -NCMe] _{<i>n</i>} (Co-1) | 16 | 15 | 3,000 | ^d | ^d |
| 2 | [K(THF) ₆][(L ⁵)Co ^{II}] _{<i>n</i>} •1.5THF (Co-2) | 20 | 14 | 2,800 | 9,600 | 2.78 |
| 3 | | 20 | 12 ^e | 1,200 | 7,100 | 2.39 |
| 4 | [K(THF) ₂ (L ⁸)Co ^{II}] _{<i>n</i>} (Co-3) | 2 | 12 | 2,400 | 81,900 | 1.47 |
| 5 | | 18 | 90 ^f | 18,000 | 110,500 | 1.56 |
| 6 | [K ₂ (L ⁹) ₂ Co ^{II}] _{<i>n</i>} (Co-4) | 22 | 86 | 17,200 | 57,400 | 1.57 |
| 7 | {[K ₂ (DMA) ₃ (L ¹⁰) ₂ Co ^{II}] _{<i>n</i>} •0.5Et ₂ O} (Co-5) | 2 | 51 | 10,200 | 86,100 | 1.82 |
| 8 | | 16 | 86 ^f | 17,200 | 38,900 | 2.00 |
| 9 | [K(NCMe) ₃ (L ¹³)Co ^{II} -NCMe] (Co-6) | 22 | 16 | 3,200 | 5,700 | 1.97 |
| 10 | - | 16 | 21 | 4,200 | 326,500 | 1.54 |

^a Conditions: catalyst (0.01 mmol), **St** (9.6 mmol), ethyl-2-bromo-isobutyrate (0.05 mmol), 1.0 mL toluene, reflux at 110°C.

^b *M_n*(th) = (g of monomer / mol initiator) × % yield.

^c By SEC in CHCl₃ at r.t.

^d Very broad molecular weight distribution.

^e Ethyl-2-bromo-isobutyrate (0.10 mmol).

^f 2.0 mL of toluene.

Table 3: Reactions of compounds Co-1-6 with methyl methacrylate (MMA).^a

| Entry | Compound | t (h) | Yield (%) | M_n (th) ^b | M_n (exp) ^c | M_w/M_n |
|-------|---|-------|-----------------|-------------------------|--------------------------|-----------|
| 1 | [K(L ³)Co ^{II} -NCMe] _n (Co-1) | 20 | 5 | 1,000 | 14,500 | 1.26 |
| 2 | | 16 | 3 ^d | 600 | 16,700 | 1.16 |
| 3 | [K(THF) ₆][(L ⁵)Co ^{II}] _n •1.5THF (Co-2) | 15 | 30 | 6,000 | 37,900 | 1.43 |
| 4 | | 15 | 33 ^e | 3,300 | 24,500 | 1.40 |
| 5 | | 21 | 13 ^f | 870 | 20,700 | 1.26 |
| 6 | [K(THF) ₂ (L ⁸)Co ^{II}] _n (Co-3) | 16 | 6 | 1,200 | 439,800 | 1.24 |
| 7 | | 15 | 12 ^d | 2,400 | 300,800 | 1.29 |
| 8 | [K ₂ (L ⁹) ₂ Co ^{II}] _n (Co-4) | 17 | 70 | 14,000 | 51,400 | 1.52 |
| 9 | {[K ₂ (DMA) ₃ (L ¹⁰) ₂ Co ^{II}] _n •0.5Et ₂ O} (Co-5) | 15 | 72 | 14,400 | 67,000 | 2.00 |
| 10 | | 15 | 60 ^e | 6,000 | 57,300 | 1.91 |
| 11 | [K(NCMe) ₃ (L ¹³)Co ^{II} -NCMe] (Co-6) | 15 | 40 | 8,000 | 55,800 | 1.54 |
| 12 | | 21 | 45 ^d | 9,000 | 54,700 | 1.58 |
| 13 | - | 17 | 9 | 1,800 | 356,700 | 1.20 |

^a Conditions: catalyst (0.01 mmol), **MMA** (10 mmol), ethyl-2-bromo-isobutyrate (0.05 mmol), 1.0 mL toluene, reflux at 110°C.

^b M_n (th) = (g of monomer / mol initiator) × % yield.

^c By SEC in CHCl₃ at r.t.

^d 2.0 mL of toluene.

^e Ethyl-2-bromo-isobutyrate (0.10 mmol).

^f Ethyl-2-bromo-isobutyrate (0.15 mmol).

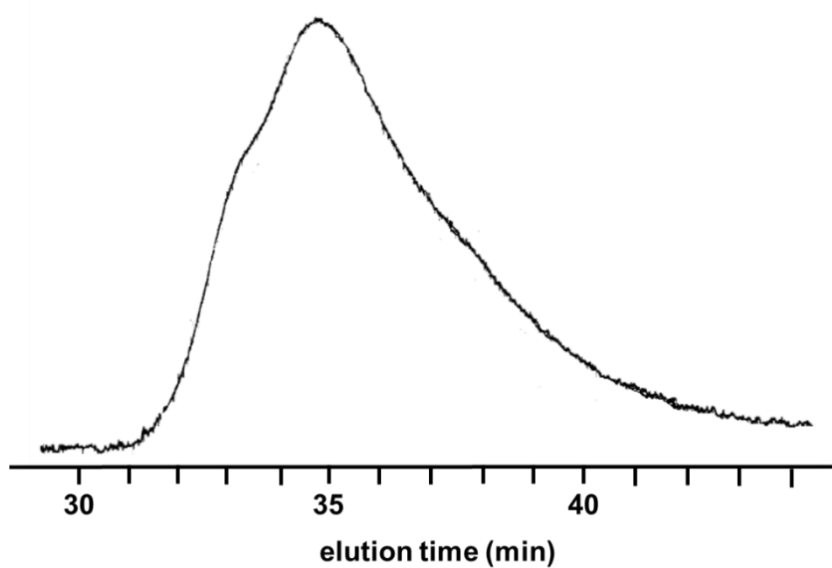


Figure 2: SEC traces for PS obtained from the reaction of (Co-5) (0.01 mmol) with St (10 mmol) and ethyl-2-bromo-isobutyrate (0.05 mmol) in toluene (1.0 mL) under reflux at 110°C.

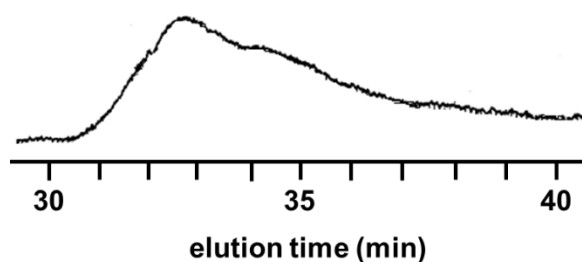


Figure 3: SEC traces for PS obtained from the reaction of (Co-3) (0.01 mmol) with St (10 mmol) and ethyl-2-bromo-isobutyrate (0.05 mmol) in toluene (1.0 mL) under reflux at 110°C.

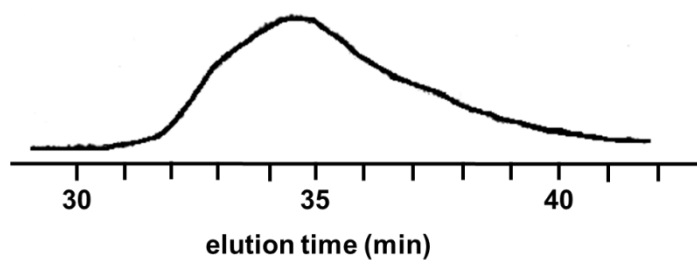


Figure 4: SEC traces for PS obtained from the reaction of (Co-4) (0.01 mmol) with St (10 mmol) and ethyl-2-bromo-isobutyrate (0.05 mmol) in toluene (1.0 mL) under reflux at 110°C.

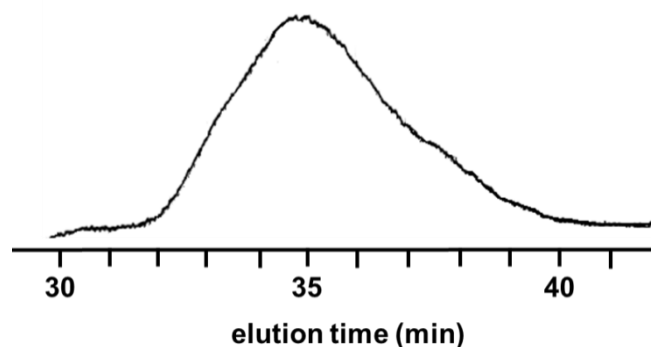


Figure 5: SEC traces for PMMA obtained from the reaction of (Co-4) (0.01 mmol) with MMA (10 mmol) and ethyl-2-bromo-isobutyrate (0.05 mmol) in toluene (1.0 mL) under reflux at 110°C.

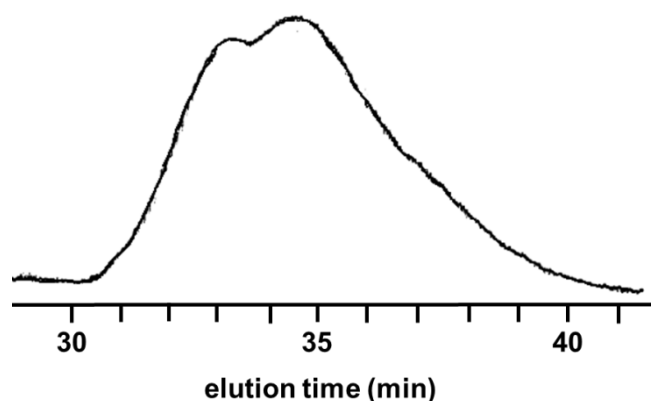


Figure 6: SEC traces for PMMA obtained from the reaction of (Co-5) (0.01 mmol) with MMA (10 mmol) and ethyl-2-bromo-isobutyrate (0.10 mmol) in toluene (1.0 mL) under reflux at 110°C.

A common characteristic of all experiments is that the experimental molecular weights were higher than the theoretical ones, which shows that termination reactions were taking place during the polymerization. Another interesting point was that in many cases a bimodal distribution was observed (**PS** and **PMMA** obtained with **Co-2-5**), resulting in the broadening of the molecular weight distribution. This is indicative of the presence of at least two reactive centers, and given that the molecular weight distributions were not very broad (1.40-2.00, except for the **Co-2/St** system), these results strongly indicate that two parallel mechanisms are in operation. The reactions of **Co-2** with **MMA** further supported this argument. Three experiments were carried out, with different quantities of initiator (0.05, 0.10 and 0.15 mmol). In all cases, GPC

plots showed bimodal distributions, but the ratio of the two peaks differed from one experiment to the other, as shown in Figure 7. These results show that the reaction proceeds with two distinct mechanisms, and that the amount of initiator used can favor one over the other.

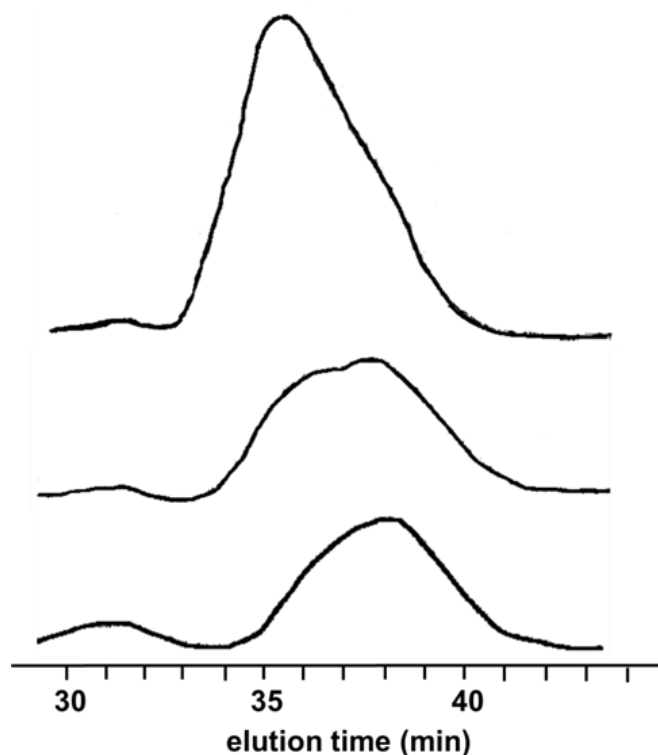


Figure 7: SEC traces for PMMA obtained from the reaction of (Co-2) (0.01 mmol) with MMA (10.0 mmol) and ethyl-2-bromo-isobutyrate (0.05 mmol, top; 0.10 mmol, middle; 0.15 mmol, bottom) in toluene (1.0 mL) under reflux at 110 °C.

5.1.3 Reinitiation experiments

In order to gain more evidence on the controlled nature of the polymerization and the operation of the **ATRP** mechanism, we examined the ability of the polymers formed to reinitiate the polymerization reaction.

In the first experiment, **St** was polymerized with compound $[K_2(L^9)_2Co^{II}]_n$ (**Co-4**) for 20 h. A small aliquot of the solution was taken and MeOH was added, yielding **PS** with $M_n = 50,200$ and $M_w/M_n = 1.80$ (Figure 8). To the rest of the reaction mixture, **St** was added and was left to react for another 20 h, providing **PS** with $M_n = 67,000$ and $M_w/M_n = 1.59$ (Figure 8). The fact that the molecular weight increased and the molecular weight distribution decreased is

a strong indication that the polymerization does not proceed through free radicals but in a rather controlled way, where the Co^{II} complex plays a crucial role.

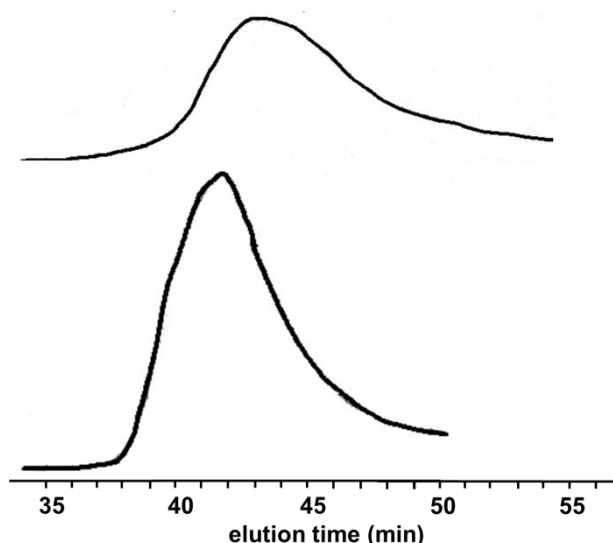


Figure 8: SEC traces for PS obtained from the reaction of (Co-4) (0.01 mmol) with St (9.6 mmol) and ethyl-2-bromo-isobutyrate (0.05 mmol) in toluene (2.0 mL) under reflux at 110 °C (top) and PS obtained after the second addition of St (9.6 mmol, bottom).

For the second experiment, **MMA** was polymerized with $[\text{K}(\text{THF})_6][(\text{L}^5)\text{Co}^{\text{II}}] \cdot 1.5\text{THF}$ (**Co-2**) and 0.05 mmol of the initiator, because under these conditions one mechanism seems to be dominant. After the end of the reaction (20 h), the **PMMA** formed was precipitated and characterized ($M_n = 23,700$ and $M_w/M_n = 1.33$). Then, it was redissolved in toluene, where the metal complex and St were added, and kept under reflux for 20 h) yielding a **PMMA-b-PS** block copolymer with $M_n = 72,400$ and $M_w/M_n = 1.60$. From the comparison of the chromatographic traces (Figure 9), it is obvious that the peak of **PMMA** at 36.9 min is absent in the GPC of the copolymer, which indicates that the end-Br groups of the **PMMA** chains were exclusively employed as initiation sites for the polymerization of **St** or in other words that **PMMA** served as macroinitiator for the synthesis of **PMMA-b-PS** block copolymers. The bimodality of the GPC trace of the final product can be attributed to possible termination reactions and/or the increase of viscosity of the reaction medium leading to polymerization under non-homogeneous conditions. The successful synthesis of the block copolymer was verified by

^1H NMR spectroscopy (Figure 10; **PMMA-b-PS** 20-80 % mol). This result confirms that the polymerization does not proceed through a coordination mechanism of the monomer to the metal center, since in this case the results would be a mixture of **PMMA** and **PS** homopolymers.

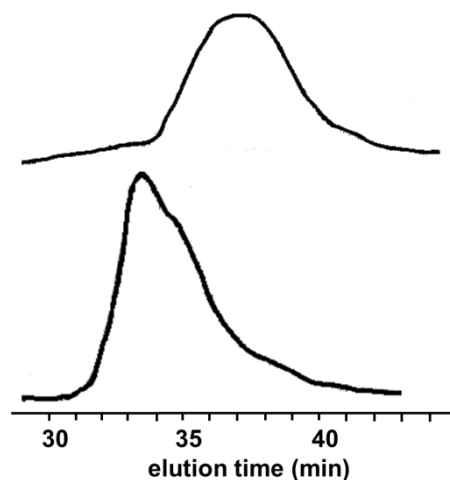


Figure 9: SEC traces for **PMMA** obtained from the reaction of **(Co-2)** (0.01 mmol) with **MMA** (10.0 mmol) and ethyl-2-bromo-isobutyrate (0.05 mmol) in toluene (2.0 mL) under reflux at 110 °C (top) and **PMMA-b-PS** obtained after the reaction of **2** (0.01 mmol) with **St** (9.6 mmol) and **PMMA** (0.05 mmol) in toluene (2.0 mL) under reflux at 110 °C (bottom).

5.1.4 Tacticity of **PMMA**

The tacticity of **PMMA** macromolecules formed in the present study was determined by ^1H NMR spectroscopy. The results are summarized in Table 4 and a representative spectrum is shown in Figure 11. Polymers obtained by conventional radical polymerization are mainly syndiotactic (rr:rm:mm = 64:32:4), due to the repulsion between the substituents of the chain end and less-controlled chain propagation.⁸⁰ The sequence distribution of the tacticity of **PMMA** was approximately Bernoullian. Similar microstructural results have been reported from **ATRP** of **MMA** using various catalytic species, such as those based on Rh,⁸¹ Fe,^{82,83} Ni,^{84,85} Cu⁸⁶ and Ru⁸⁷ complexes. The polymers obtained in this study were predominately syndiotactic, consistent with radical polymerization. **Co-1** and **Co-2** exhibit unusually high ratios of isotactic triads. It is known that several Co^{II} complexes act as efficient chain transfer agents during methacrylate polymerization. The Co^{II} radical may interact with the

propagating radical and induce single-handed helical structures in the polymerization of bulky methacrylates.⁸⁸ The polymerization proceeds with a different mechanism from typical catalytic chain transfer although the detailed mechanism is not clear.⁸⁹ It is possible that a similar situation exists, at least to some extent, with **Co-1** and **Co-2** leading to increased isotacticities. Further mechanistic studies are needed to clarify this finding.

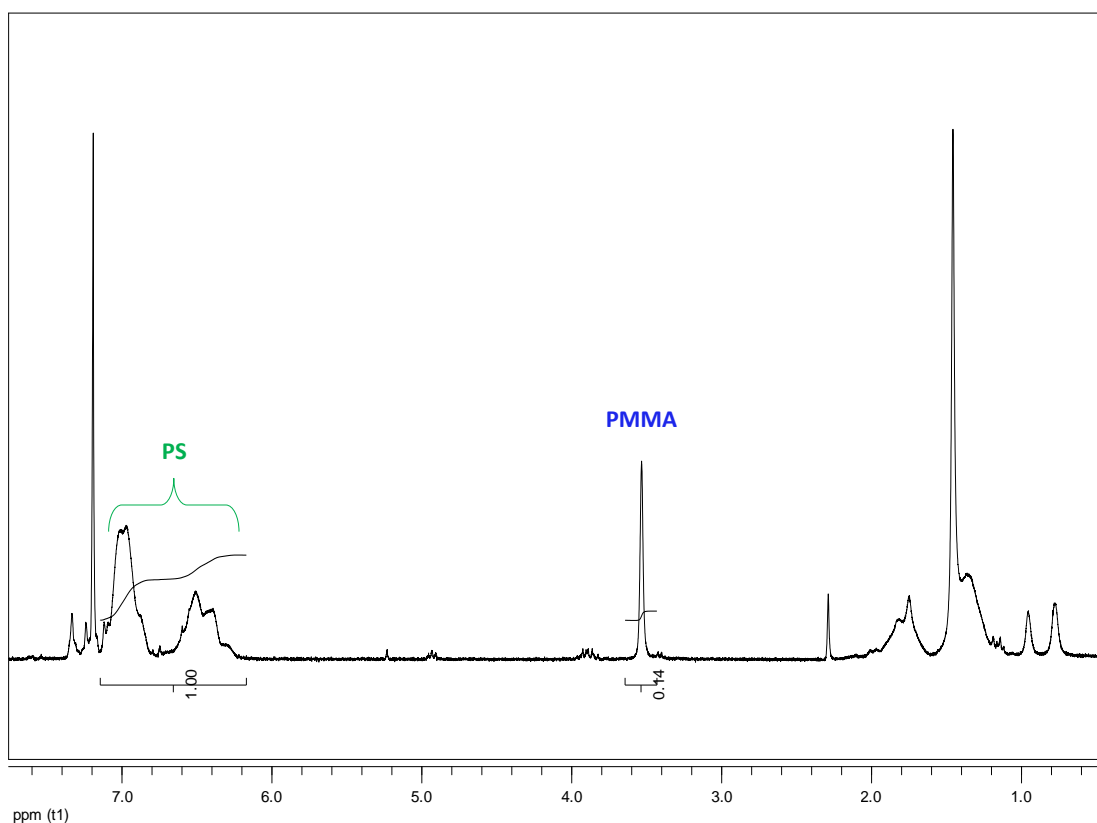


Figure 10: ¹H NMR spectrum of PMMA-b-PS from the reaction of (Co-2) with MMA and St, in CDCl₃.

Table 4: Tacticity of PMMA obtained from reactions with Co^{II} complexes. ^{a,b}

| Entry | Compound | mm (%) | mr (%) | rr (%) |
|-------|---|--------|--------|--------|
| 1 | [K(L ³)Co ^{II} -NCMe] _n (Co-1) | 28 | 31 | 41 |
| 2 | | 8 | 36 | 56 |
| 3 | [K(THF) ₆][(L ⁵)Co ^{II}] _n •1.5THF (Co-2) | 16 | 33 | 51 |
| 4 | | 10 | 37 | 53 |
| 5 | | 8 | 39 | 53 |
| 6 | [K(THF) ₂ (L ⁸)Co ^{II}] _n (Co-3) | 7 | 38 | 55 |
| 7 | | 5 | 35 | 60 |
| 8 | [K ₂ (L ⁹) ₂ Co ^{II}] _n (Co-4) | 10 | 38 | 52 |
| 9 | {[K ₂ (DMA) ₃ (L ¹⁰) ₂ Co ^{II}] _n •0.5Et ₂ O} (Co-5) | 6 | 40 | 54 |
| 10 | | 10 | 39 | 51 |
| 11 | [K(NCMe) ₃ (L ¹³)Co ^{II} -NCMe] (Co-6) | 7 | 39 | 54 |
| 12 | | 7 | 40 | 53 |
| 13 | - | 6 | 38 | 56 |

^a Calculated from ¹H NMR spectra.

^b Experiments are presented in the same order as in Table 3.

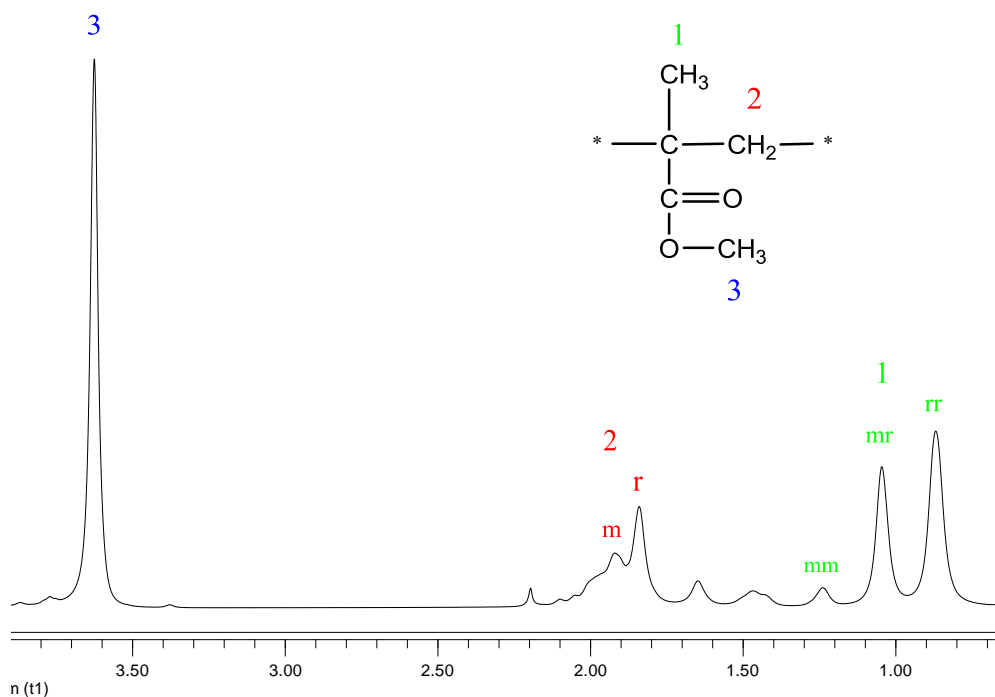
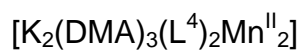
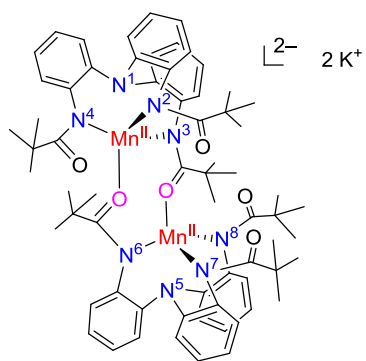


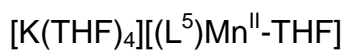
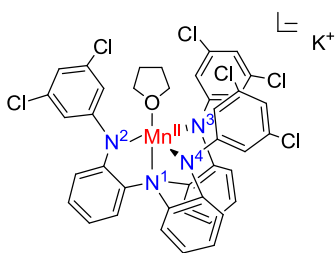
Figure 11: ^1H NMR spectrum of PMMA from the reaction of $[\text{K}_2(\text{DMA})_3(\text{L}^{10})\text{Co}^{\text{II}}]\cdot 0.5\text{Et}_2\text{O}$ (**Co-5**) with MMA, in CDCl_3 .

5.2 Mn^{II} complexes

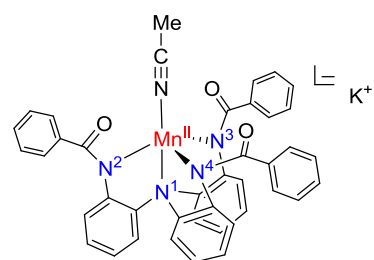
The structures of the Mn^{II} compounds used in this study are presented in Scheme 11. These complexes have been synthesized by the reaction of anhydrous MnCl_2 with the deprotonated ligands and exhibit stoichiometric and structural variation. Solid-state structures of compounds **Mn-2-4** and **Mn-7** revealed that the four nitrogen-atom residues of the ligands are coordinated to the metal center in a distorted trigonal-pyramidal geometry and a solvent molecule (THF, CH_3CN or DMA) occupies the fifth coordination site. **Mn-5** has a similar structure, but is four-coordinate (absence of coordinating solvent molecule). Compounds **Mn-1** and **Mn-6** feature a dimeric structure. The axial nitrogen-atom of the ligand is not coordinated to the metal center; the fourth coordination site is occupied by carbonyl moieties provided by an amidato residue of the partner monomer.



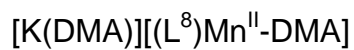
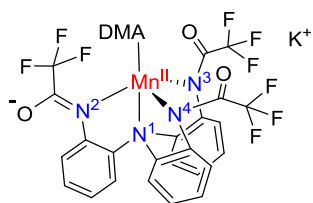
Mn-1



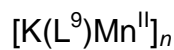
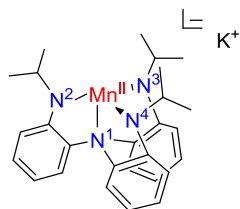
Mn-2



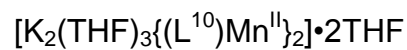
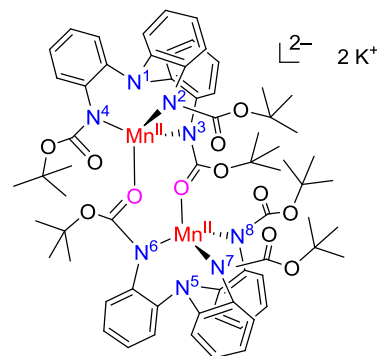
Mn-3



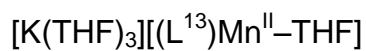
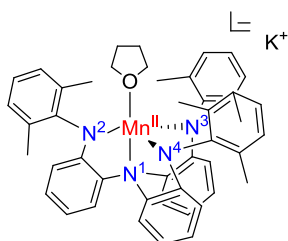
Mn-4



Mn-5



Mn-6



Mn-7

Scheme 11: Structures of Mn^{II} complexes studied in CRP reactions.

5.2.1 Cyclic voltammetry

The electrochemical properties of compounds **Mn-1-7** have been studied by cyclic voltammetry. Electrochemical data for the Mn^{II}/Mn^{III} couple are listed in Table 5 and the corresponding waves are shown in Figure 12. Compound [K(THF)₃][(L¹³)Mn^{II}-THF] (**Mn-7**), which bears the electron-donating aryl substituent 2,6-(CH₃)₂ was oxidized at the most negative potential, followed by complex [K(L⁹)Mn^{II}]_n (**Mn-5**), whose potential is in agreement with the electron-rich nature of the arylalkylamido-amine ligand. The presence of the electron-withdrawing aryl substituent 3,5-Cl₂ in [K(THF)₄][(L⁵)Mn^{II}-THF] (**Mn-2**) shifted the redox potential to more positive values. Complexes [K₂(DMA)₃(L⁴)₂Mn^{II}]₂ (**Mn-1**) and [K₂(THF)₃{(L¹⁰)Mn^{II}}]₂•2THF (**Mn-6**) exhibited potentials shifted to higher values, due to their electron-withdrawing substituents CO^tBu and COO^tBu. Finally, the electron-withdrawing COC₆H₅ and COCF₃ substituents of [K(NCMe)][(L⁶)Mn^{II}-NCMe]•MeCN (**Mn-3**) and [K(DMA)][(L⁸)Mn^{II}-DMA] (**Mn-4**) caused the most significant anodic shifts. The assignment of the irreversible waves to the Mn^{II}/Mn^{III} couple is tentative. Contributions from ligand-centered events cannot be excluded at the present time, especially for **Mn-4** and **Mn-6**, for which large *i*_{p,a} values were observed. These results were consistent with the electronic character of the ligands and prior electrochemical data obtained for the analogous Fe^{II} complexes,⁶⁹ although the potentials of the Mn^{II} compounds were shifted anodically, as expected, by a factor of 0.4-0.6 V.

Table 5: Electrochemical data for compounds Mn-1-7.

| Compound | Solvent | <i>E</i> _{1/2} (or <i>E</i> _{p,a}) (V vs. Fc ⁺ /Fc) | Δ <i>E</i> (mV) |
|---|---------|--|--------------------|
| [K ₂ (DMA) ₃ (L ⁴) ₂ Mn ^{II}] ₂ (Mn-1) | DMA | -0.078 | |
| [K(THF) ₄][(L ⁵)Mn ^{II} -THF] (Mn-2) | DMF | -0.442 | 71 |
| [K(NCMe)][(L ⁶)Mn ^{II} -NCMe]•MeCN (Mn-3) | MeCN | 0.062 | |
| [K(DMA)][(L ⁸)Mn ^{II} -DMA] (Mn-4) | MeCN | 0.526 | |
| [K(L ⁹)Mn ^{II}] _n (Mn-5) | DMA | -0.798 | |
| [K ₂ (THF) ₃ {(L ¹⁰)Mn ^{II} }] ₂ •2THF (Mn-6) | DMF | -0.110 | |
| [K(THF) ₃][(L ¹³)Mn ^{II} -THF] (Mn-7) | DMA | -1.260 | 6 |

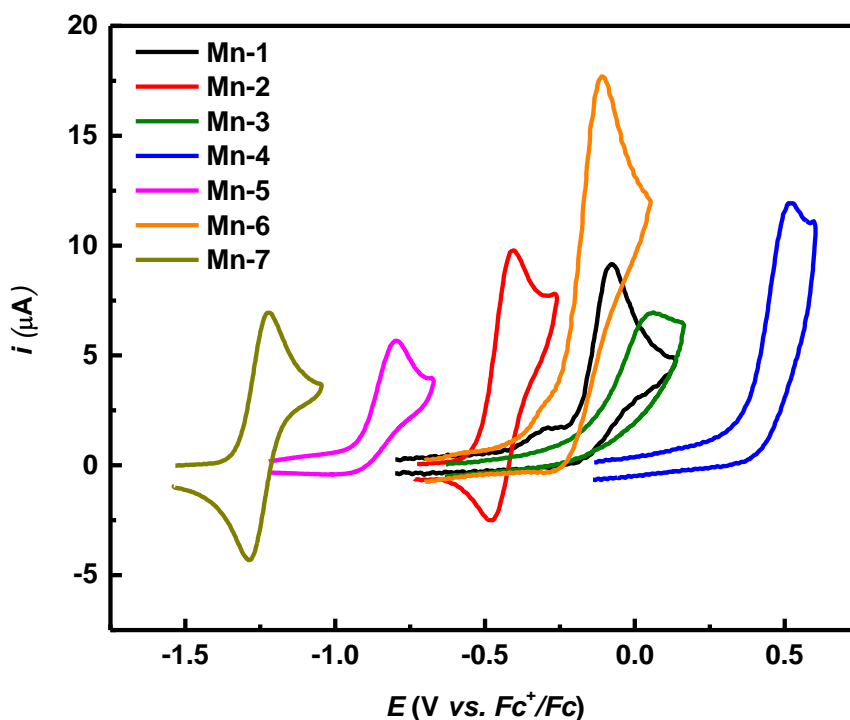


Figure 12: Cyclic voltammograms ($\text{Mn}^{\text{II}}/\text{Mn}^{\text{III}}$ redox couple) of compounds $[\text{K}_2(\text{DMA})_3(\text{L}^4)_2\text{Mn}^{\text{II}}_2]$ (Mn-1), $[\text{K}(\text{L}^9)\text{Mn}^{\text{II}}]_n$ (Mn-5) and $[\text{K}(\text{THF})_3][(\text{L}^{13})\text{Mn}^{\text{II}}\text{-THF}]$ (Mn-7) in DMA/ $[(n\text{-Bu})_4\text{N}]\text{PF}_6$, $[\text{K}(\text{THF})_4][(\text{L}^5)\text{Mn}^{\text{II}}\text{-THF}]$ (Mn-2) and $[\text{K}_2(\text{THF})_3\{(\text{L}^{10})\text{Mn}^{\text{II}}\}_2\cdot 2\text{THF}]$ (Mn-6) in DMF/ $[(n\text{-Bu})_4\text{N}]\text{PF}_6$, $[\text{K}(\text{NCMe})][(\text{L}^6)\text{Mn}^{\text{II}}\text{-NCMe}\cdot\text{MeCN}]$ (Mn-3) and $[\text{K}(\text{DMA})][(\text{L}^8)\text{Mn}^{\text{II}}\text{-DMA}]$ (Mn-4) in MeCN/ $[(n\text{-Bu})_4\text{N}]\text{PF}_6$, as indicated, with a Au disk electrode (1.6 mm in diameter); scan rate 0.1 V/s.

5.2.2 Polymerization results

The catalytic activity of compounds **Mn-1-7** towards the polymerization of styrene (**St**) and methyl methacrylate (**MMA**) was studied in toluene or THF solutions at 110 °C using ethyl-2-bromo-isobutyrate as initiator. The results are summarized in Tables 6-9. Blank experiments are also included for comparison purposes. **Mn-7** is readily soluble in toluene, **Mn-2** and **Mn-6** are partially soluble, whereas **Mn-1**, **Mn-4** and **Mn-5** are insoluble, with **Mn-5** being dissolved under heating. Compound **Mn-2** is readily soluble in THF, whereas **Mn-1**, **Mn-3** and **Mn-4** are insoluble. However, the solutions become homogeneous after the addition of the monomer and the initiator. The reaction mixtures were allowed to react for a given time. In some cases, high-viscosity

mixtures had formed at that time. The catalyst/monomer/initiator molar ratio was 1/1000/5, unless otherwise stated. The polymers, poly(styrene) (**PS**) and poly(methyl methacrylate) (**PMMA**), were obtained after addition of MeOH and were purified by Dowex ion exchange resin in toluene solutions.

In most cases, reaction yields were low and theoretical and experimental molecular weights were not in agreement. Molecular weight distributions were broad, which is partly due to them being bimodal, similarly to the Co^{II} complexes mentioned above. In general, better results were obtained from reactions in toluene than in THF and for **St** than for **MMA**. The most notable results were those of **St** polymerization using **Mn-6** in toluene (Table 6, entry 9) and **MMA** polymerization using **Mn-3** in THF (Table 9, entry 2), both of which gave relatively high yields (43 and 60%, respectively) and, in the first case, a relatively narrow molecular weight distribution.

Table 6: Reactions of compounds Mn-1-4 and Mn-6 with styrene (St) in toluene.^a

| Entry | Compound | <i>t</i> (h) | Yield (%) | <i>M_n</i> (th) ^b | <i>M_n</i> (exp) ^c | <i>M_w</i> / <i>M_n</i> |
|-------|---|--------------|-----------|--|---|---|
| 1 | [K ₂ (DMA) ₃ (L ⁴) ₂ Mn(II) ₂] (Mn-1) | 20 | 12 | 2,400 | 91,200 | 1.62 |
| 2 | [K(THF) ₄][(L ⁵)Mn(II)-THF] (Mn-2) | 17 | 18 | 3,600 | 64,700 | 1.59 |
| 3 | [K(NCMe)][(L ⁶)Mn(II)-NCMe]•MeCN (Mn-3) | 16 | 35 | 7,000 | 77,601 | 1.54 |
| 4 | [K(DMA)][(L ⁸)Mn(II)-DMA] (Mn-4) | 16 | 35 | 7,000 | 68,152 | 1.53 |
| 5 | [K ₂ (THF) ₃ [(L ¹⁰)Mn(II)] ₂]•2THF (Mn-6) | 16 | 43 | 8,600 | 91,146 | 1.37 |
| 6 | - | 16 | 21 | 4,200 | 326,500 | 1.54 |

^a Conditions: catalyst (0.01 mmol), **St** (9.6 mmol), ethyl-2-bromo-isobutyrate (0.05 mmol), 2.0 mL toluene, reflux at 110°C.

^b *M_n*(th) = (g of monomer / mol initiator) × % yield.

^c By SEC in CHCl₃ at r.t.

Table 7: Reactions of compounds Mn-1-4 with styrene (St) in THF. ^a

| Entry | Compound | <i>t</i> (h) | Yield (%) | <i>M_n</i> (th) ^b | <i>M_n</i> (exp) ^c | <i>M_w</i> / <i>M_n</i> |
|-------|---|--------------|-----------|--|---|---|
| 1 | [K ₂ (DMA) ₃ (L ⁴) ₂ Mn(II) ₂] (Mn-1) | 19 | 11 | 2,200 | 110,500 | 1.47 |
| 2 | [K(THF) ₄][(L ⁵)Mn(II)-THF] (Mn-2) | 17 | 7 | 1,400 | - | - |
| 3 | [K(NCMe)][(L ⁶)Mn(II)-NCMe]•MeCN (Mn-3) | 17 | 4 | 800 | - | - |
| 4 | [K(DMA)][(L ⁸)Mn(II)-DMA] (Mn-4) | 18 | - | - | - | - |

^a Conditions: catalyst (0.01 mmol), **St** (9.6 mmol), ethyl-2-bromo-isobutyrate (0.05 mmol), 2.0 mL THF, reflux at 65°C.

^b *M_n*(th) = (g of monomer / mol initiator) × % yield.

^c By SEC in CHCl₃ at r.t.

Table 8: Reactions of compounds Mn-1-7 with methyl methacrylate (MMA) in toluene. ^a

| Entry | Compound | <i>t</i> (h) | Yield (%) | <i>M_n</i> (th) ^b | <i>M_n</i> (exp) ^c | <i>M_w</i> / <i>M_n</i> |
|-------|---|--------------|----------------|--|---|---|
| 1 | [K ₂ (DMA) ₃ (L ⁴) ₂ Mn(II) ₂] (Mn-1) | 18 | 8 ^d | 1,600 | 210,900 | 1.26 |
| 2 | [K(THF) ₄][(L ⁵)Mn(II)-THF] (Mn-2) | 17 | 23 | 4,600 | 51,900 | 1.66 |
| 3 | [K(NCMe)][(L ⁶)Mn(II)-NCMe]•MeCN (Mn-3) | 16 | 11 | 2,200 | 185,800 | 1.60 |
| 4 | [K(DMA)][(L ⁸)Mn(II)-DMA] (Mn-4) | 16 | 3 | 600 | - | - |
| 5 | [K(L ⁹)Mn(II)] _{<i>n</i>} (Mn-5) | 17 | 2 ^d | 400 | - | - |
| 6 | [K ₂ (THF) ₃ {(L ¹⁰)Mn(II)} ₂]•2THF (Mn-6) | 17 | 32 | 6,400 | 134,400 | 1.48 |
| 7 | [K(THF) ₃][(L ¹³)Mn(II)-THF] (Mn-7) | 17 | 2 ^d | 400 | - | - |
| 8 | - | 17 | 9 | 1,800 | 356,700 | 1.20 |

^a Conditions: catalyst (0.01 mmol), **MMA** (10.0 mmol), ethyl-2-bromo-isobutyrate (0.05 mmol), 1.0 mL toluene, reflux at 110°C.

^b *M_n*(th) = (g of monomer / mol initiator) × % yield.

^c By SEC in CHCl₃ at r.t.

^d 2.0 mL of toluene.

Table 9: Reactions of compounds Mn-1, Mn-3 and Mn-4 with methyl methacrylate (MMA) in THF.^a

| Entry | Compound | t (h) | Yield (%) | M _n (th) ^b | M _n (exp) ^c | M _w /M _n |
|-------|---|-------|-----------|----------------------------------|-----------------------------------|--------------------------------|
| 1 | [K ₂ (DMA) ₃ (L ⁴) ₂ Mn(II) ₂] (Mn-1) | 19 | 9 | 1,800 | - | - |
| 2 | [K(NCMe)][(L ⁶)Mn(II)-NCMe]•MeCN (Mn-3) | 20 | 60 | 12,000 | 53,100 | 1.86 |
| 3 | [K(DMA)][(L ⁸)Mn(II)-DMA] (Mn-4) | 21 | 25 | 5,000 | 106,500 | 1.34 |

^a Conditions: catalyst (0.01 mmol), **MMA** (10.0 mmol), ethyl-2-bromo-isobutyrate (0.05 mmol), 1.0 mL THF, reflux at 65°C.

^b M_n(th) = (g of monomer / mol initiator) × % yield.

^c By SEC in CHCl₃ at r.t.

5.2.3 Tacticity of PMMA

The tacticity of the **PMMA** macromolecules formed in the present study was determined by ¹H NMR spectroscopy. The results are summarized in Tables 10 and 11. The polymers obtained in this study were predominately syndiotactic, consistent with radical polymerization. **Mn-2-4** exhibit unusually high ratios of isotactic triads.

Table 10: Tacticity of poly(methyl methacrylate) (PMMA) obtained from reactions with Mn^{II} complexes in toluene.^{a,b}

| Entry | Compound | mm (%) | mr (%) | rr (%) |
|-------|---|--------|--------|--------|
| 1 | [K ₂ (DMA) ₃ (L ⁴) ₂ Mn(II) ₂] (Mn-1) | 9 | 36 | 55 |
| 2 | [K(THF) ₄][(L ⁵)Mn(II)-THF] (Mn-2) | 20 | 32 | 48 |
| 6 | [K ₂ (THF) ₃ [(L ¹⁰)Mn(II)] ₂]•2THF (Mn-6) | 6 | 40 | 54 |

^a Calculated from ¹H NMR spectra.

^b Entry numbers correspond to those of Table 8.

Table 11: Tacticity of poly(methyl methacrylate) (PMMA) obtained from reactions with Mn^{II} complexes in THF.^{a,b}

| Entry | Compound | mm (%) | mr (%) | rr (%) |
|-------|--|--------|--------|--------|
| 2 | [K(NCMe)][(L ⁶)Mn(II)-NCMe]•MeCN (Mn-3) | 14 | 31 | 55 |
| 3 | [K(DMA)][(L ⁸)Mn(II)-DMA] (Mn-4) | 22 | 29 | 49 |

^a Calculated from ¹H NMR spectra.

^b Entry numbers correspond to those of Table 9.

5.3 Conclusions

Our preliminary results show that compounds **Co-2-6** can induce the **CRP** of **St** and **MMA**. Some compounds (**Co-3-5**) provided good yields (60-90%; **Co-3** was active only in **St** polymerization), whereas others (**Co-2** and **Co-6**) had better control over the polymerization reactions, albeit with lower yields (12-16% for **PS** and 30-45% for **PMMA**). Although a firm correlation between the reactivity and the structure or the redox potential cannot be made at this point, the steric factor seems to play an essential role, since compounds that feature a less hindered fifth coordination site showed the highest reactivity and better control over the polymerization reaction.

The polymers obtained were predominately syndiotactic, consistent with radical polymerization, with two exceptions that exhibited unusually high ratios of isotactic triads. In many cases bimodal distributions were observed, although the molecular weight distributions were not very broad (1.40-2.00), and this strongly indicates that two parallel mechanisms are in operation. Among the three predominant mechanisms (**ATRP**, **OMRP** and **CCTP**) that have been established for cobalt-mediated **CRP** reactions, the first two seem to be more likely for our systems. A detailed mechanistic study is under way.

The Mn^{II} complexes **Mn-1-7** were far less reactive towards the **CRP** of **St** and **MMA** and the control over the polymerization was not good. Polymers with broad molecular weight distributions were obtained in low yields. Molecular weight distributions were bimodal, indicating two mechanisms operating in parallel. Because of the low yields and the bad control over the polymerization the reactions were not further investigated.

CHAPTER 6

COPOLYMERIZATION OF NORBORNENE AND NORBORNADIENE VIA RING OPENING METATHESIS POLYMERIZATION USING A DITUNGSTEN-BASED CATALYTIC SYSTEM

6.1 General

Compound $\text{Na}[\text{W}_2(\mu\text{-Cl})_3\text{Cl}_4(\text{THF})_2]\cdot(\text{THF})_3$ ($\{\text{W}_2\}$) is a highly efficient initiator for metathesis polymerization of alkynes⁹⁰ and the **ROMP** of norbornene (**NBE**) and some of its derivatives.⁵³ The most important feature of its reactivity is its high-*cis* stereoselectivity. Norbornadiene (**NBD**) is a cycloolefin bearing two double bonds, which lead to insoluble, crosslinked **ROMP** polymers. Copolymerization of **NBE** and **NBD** could yield products with desired properties usually observed in crosslinked polymers (thermal stability, mechanical strength etc.), while being more soluble and easy to process than poly(norbornadiene) (**PNBD**) homopolymer. In this Chapter, we present the results of **NBE** and **NBD** copolymerization using $\{\text{W}_2\}$ as **ROMP** initiator and the characterization of the products.

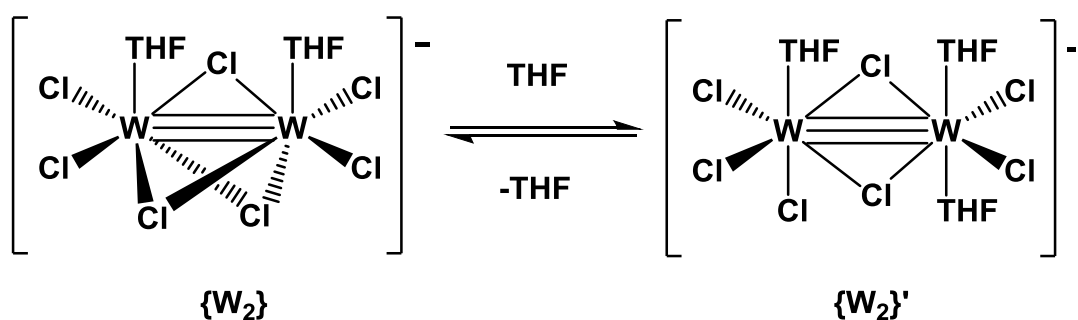
6.2 Catalyst and polymerization reactions

Compound $\text{Na}[\text{W}_2(\mu\text{-Cl})_3\text{Cl}_4(\text{THF})_2]\cdot(\text{THF})_3$ ($\{\text{W}_2\}$; Scheme 12) features fsbo geometry and contains a triple metal-metal bond. Structural characterization has revealed the presence of two THF ligands (one to each tungsten atom) in a *cis* arrangement along the dimetal axis,⁷⁶ which is the key for the reactivity of this compound towards metathesis polymerization reactions.^{53,90} Such species in solution, in the presence of donor ligands or coordinating solvents, may exist in an equilibrium between the highly symmetric confacial (D_{3h} , fsbo) structure $\{\text{W}_2\}$ and the edge-sharing (D_{2h} , esbo) bioctahedral one $\{\text{W}_2\}'$ (Scheme 12).⁹¹ $\{\text{W}_2\}$ is air-sensitive (oxygen, moisture), but in the solid state it is stable in air at room temperature for 1-2 hours. It is soluble in THF, CH_3CN and dme, less soluble in CH_2Cl_2 and CHCl_3 , and insoluble in toluene and

Et₂O. It was repeatedly recrystallized and checked carefully for purity (Vis-UV) before use.

Polymerization reactions were carried out at room temperature, under an inert atmosphere. The monomers were added to a solution of $\{W_2\}$ in CH₂Cl₂ and the mixture was stirred for a given time. The results are summarized in Table 12. The structures of polymers obtained from **ROMP** of norbornene (**NBE**) and norbornadiene (**NBD**) are shown in Scheme 13. In most cases, the products were insoluble, causing the reaction mixtures to gel, even at low yields, thus terminating the reactions in a short time. Reactions were generally faster when the **NBD/NBE** molar ratio was higher, which was expected, since we have shown that **NBD** polymerization by $\{W_2\}$ proceeds faster than **NBE** polymerization.⁵³

Molecular weights were measured only for soluble polymers. Copolymers were soluble when **NBE** was at a higher molar ratio than **NBD**. Higher **NBD** ratios compared to **NBE**, as well as equal ratios of the two monomers led to insoluble materials, which can be explained by the fact that **PNBD** forms crosslinked polymers (Scheme 13). **PNBE/PNBD** copolymers had lower molecular weights and broader molecular weight distributions than the **PNBE** homopolymer.



Scheme 12: Schematic representation of the equilibrium between $\{W_2\}$ and $\{W_2\}'$.

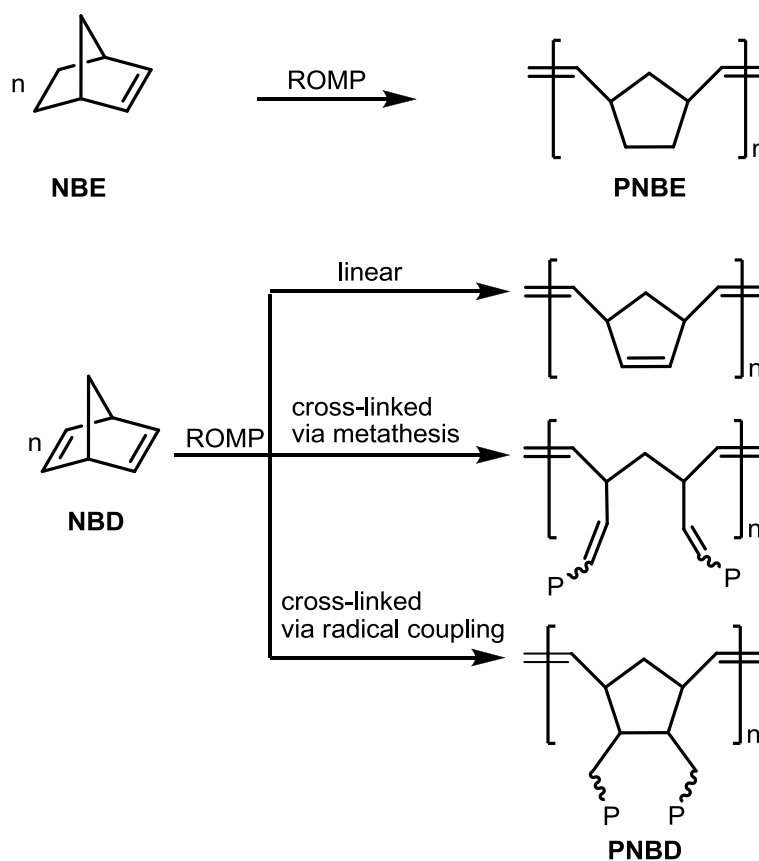
Table 12: Reactions of $\{W_2\}$ with NBE and NBD. ^a

| Sample | $\{W_2\}$ /NBE/NBD | t (min) | Yield (%) | $M_w \times 10^{-3}$ ^b | M_w/M_n |
|--------------------|--------------------|-----------|-----------|-----------------------------------|-----------|
| PNBE | 1/500/0 | 60 | 96 | 529 | 1,2 |
| PNBD | 1/0/500 | 6 | >99 | c | c |
| PNBE/PNBD 100/400 | 1/100/400 | 3 | 99 | c | c |
| PNBE/PNBD 400/100 | 1/400/100 | 10 | 61 | 129 | 2,0 |
| PNBE/PNBD 300/1100 | 1/300/1100 | 5 | 66 | c | c |
| PNBE/PNBD 700/700 | 1/700/700 | 7 | 18 | c | c |
| PNBE/PNBD 1100/300 | 1/1100/300 | 12 | 11 | 252 | 2,5 |

^a Conditions: $\{W_2\}$ (9.0 mg, 0.009 mmol), monomer(s), CH_2Cl_2 (homopolymerization, 2 mL; copolymerization, 15 mL).

^b By SEC in THF at 40 °C.

^c Insoluble polymer.



Scheme 13: Possible products of NBE and NBD polymerization *via* ROMP.

6.3 Morphology

SEM images (Figures 13-17) show the different morphologies of the materials. Homopolymers exhibited smooth, non-porous morphology. The morphology of the copolymers was wrinkled when the initial **NBE/NBD** molar ratio was >1. Increased **PNBD** content led to more even morphology.

The morphology of **PNBE/PNBD** copolymers synthesized with **{W₂}** differs significantly from the one reported by Lima-Neto *et al.*,⁹² who used Ru-based initiators to obtain **PNBE/PNBD** copolymers. In the latter case **PNBE** and all copolymers obtained were porous. Pore sizes decreased when the **NBD** content increased, with a compact surface for the copolymer obtained when the initiator/**NBE/NBD** molar ratio reached 1/5000/2000. This was attributed to the fact that crosslinking allowed polymer chains to approach each other, along with the fact that a higher amount of double bonds allowed polymer chains to be packed better through π -interactions. In our case the materials obtained (both the homopolymers and the copolymers) were not porous. This difference could be potentially attributed to the different configuration of the polymeric chains (polymers obtained using Ru initiators had ~50% *trans* double bond content, while **{W₂}** provided high-*cis* polymers) and/or the different degree of crosslinking.

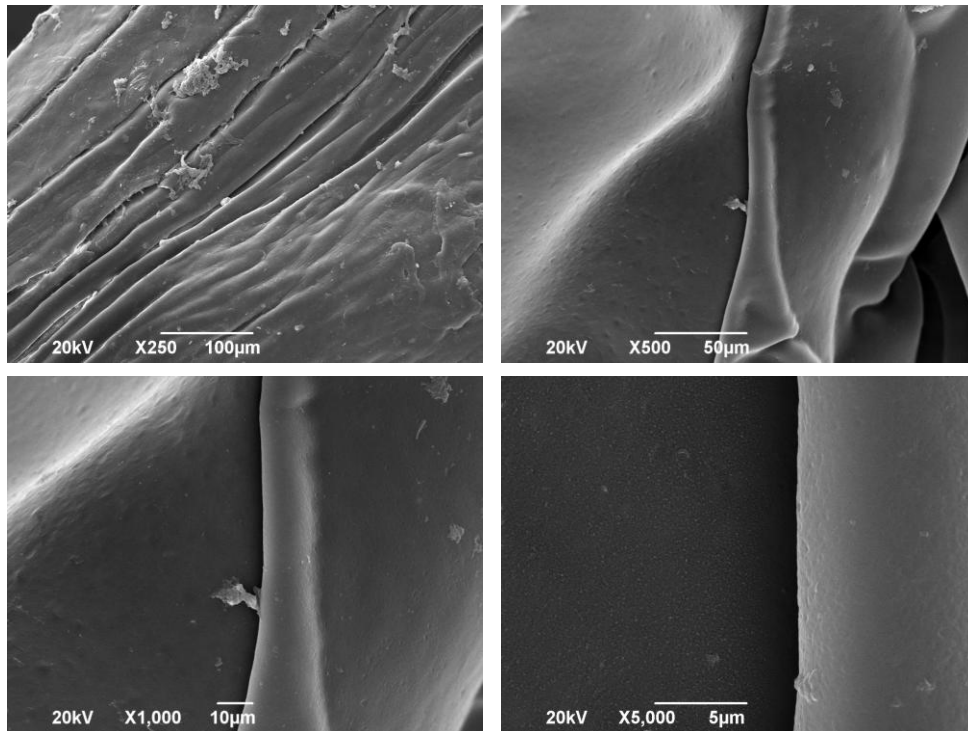


Figure 13: SEM image of the PNBE homopolymer.

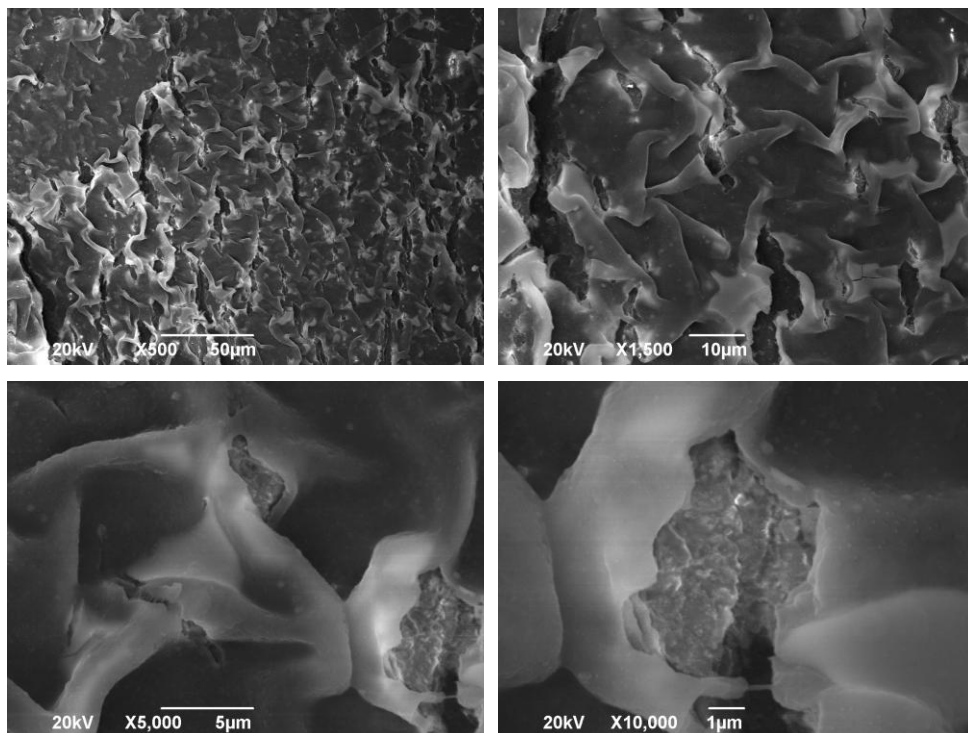


Figure 14: SEM image of the PNBE/PNBD 400/100 copolymer.

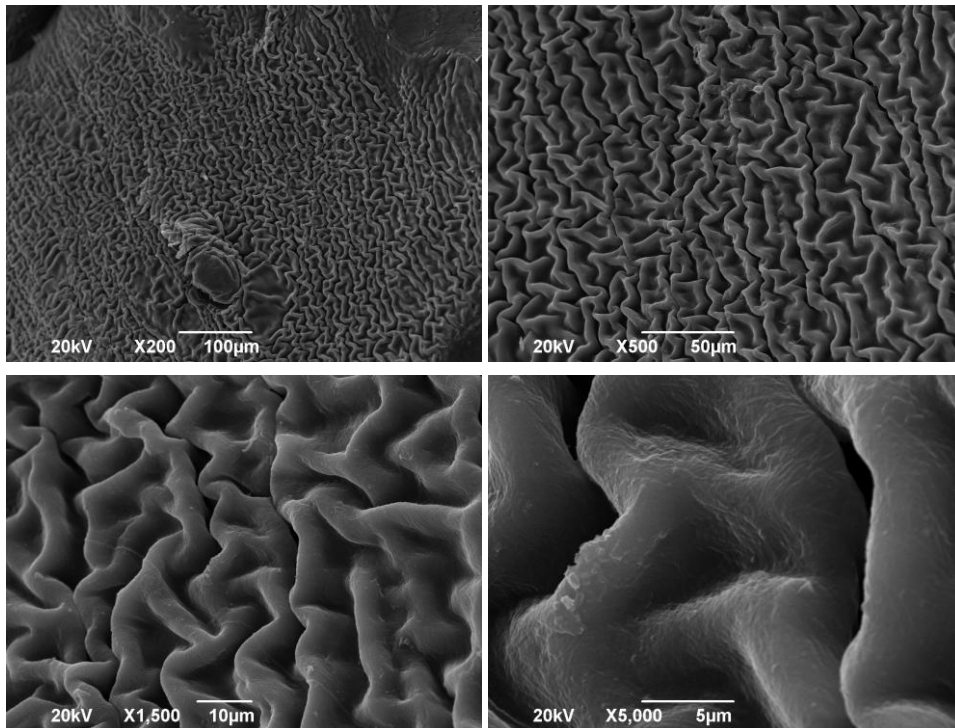


Figure 15: SEM image of the PNBE/PNBD 700/700 copolymer.

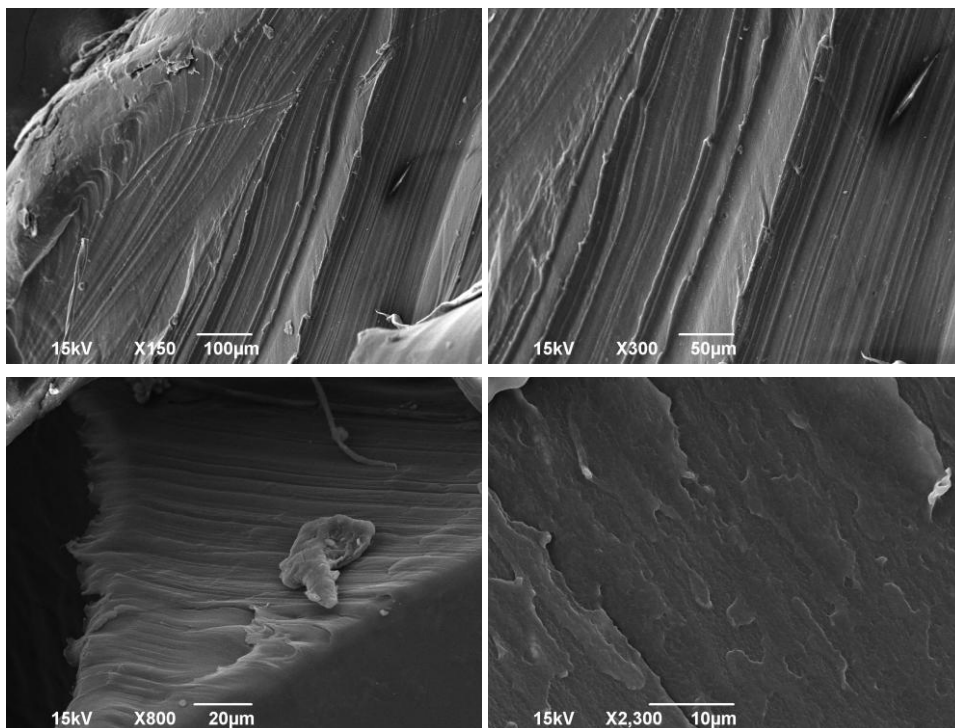


Figure 16: SEM image of the PNBE/PNBD 100/400 copolymer.

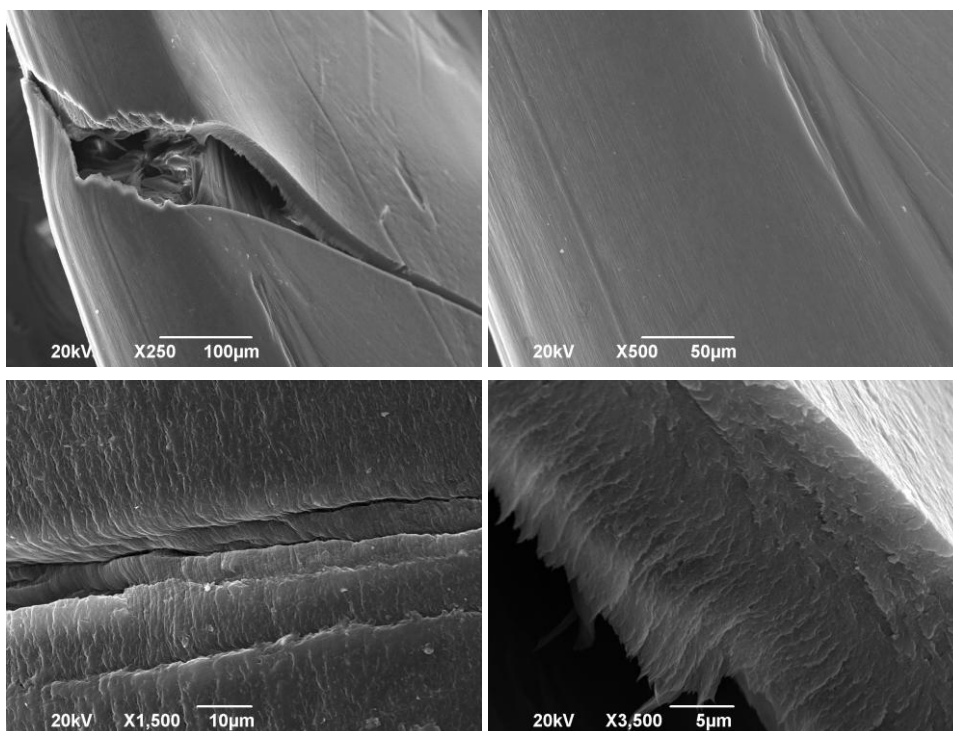


Figure 17: SEM image of the PNBD homopolymer.

6.4 NMR spectroscopy

Figures 18-24 show the ^{13}C CPMAS NMR spectra of homo- and copolymers. For **PNBE**, olefinic carbons appear at 134.0 ppm while aliphatic carbons give peaks at 43.3, 39.6 and 33.3 ppm, with those at 43.3 and 39.6 ppm being characteristic of *trans* and *cis* configurations, respectively.⁹³ For **PNBD**, olefinic carbons appear at 135.2 ppm while aliphatic carbons give peaks at 50.1, 43.8 and 39.2 ppm, with those at 50.1 and 43.8 ppm being characteristic of *trans* and *cis* configurations, respectively.⁹⁴

From the spectrum of **PNBD** homopolymer (Figure 19), it is possible to determine the olefin coupling contribution to the polymer's crosslinking (Scheme 13). Crosslinking can occur by either metathetic or olefin coupling reactions on the second double bond of **NBD**. The ratio of olefinic/aliphatic carbons depends on the mechanism of crosslinking and is equal to 4/3 (metathetic) and 2/5 (olefin coupling). Therefore, the olefin coupling contribution can be calculated via equation (1) that takes the ratio of the integrated areas of the corresponding ^{13}C CPMAS peaks as input.⁵⁴ Thus, C_{olefinic} refers to the total sp^2 carbons, $C_{\text{aliphatic}}$ to sp^3 carbons and x is the

fraction of polymer double bonds that participate in crosslinking *via* olefin coupling. Integration of **PNBD** spectra provided an olefinic/aliphatic carbons ratio equal to 1.36 (Figure 19), showing that no crosslinking *via* olefin coupling takes place ($x \approx 0$).

$$(4-2x) / (3+2x) = [C_{\text{olefinic}} / C_{\text{aliphatic}}]_{\text{experimental}} \quad (1)$$

In the spectra of **PNBE/PNBD** copolymers, the peaks at 33 and 50 ppm are characteristic of **PNBE** and **PNBD** moieties, respectively.^{93,94} Although it is not possible to determine the exact ratio of **NBE/NBD** units in the polymer chain, due to the peaks overlapping each other, it is evident that it is relative to the monomer molar ratio in the reaction mixture.

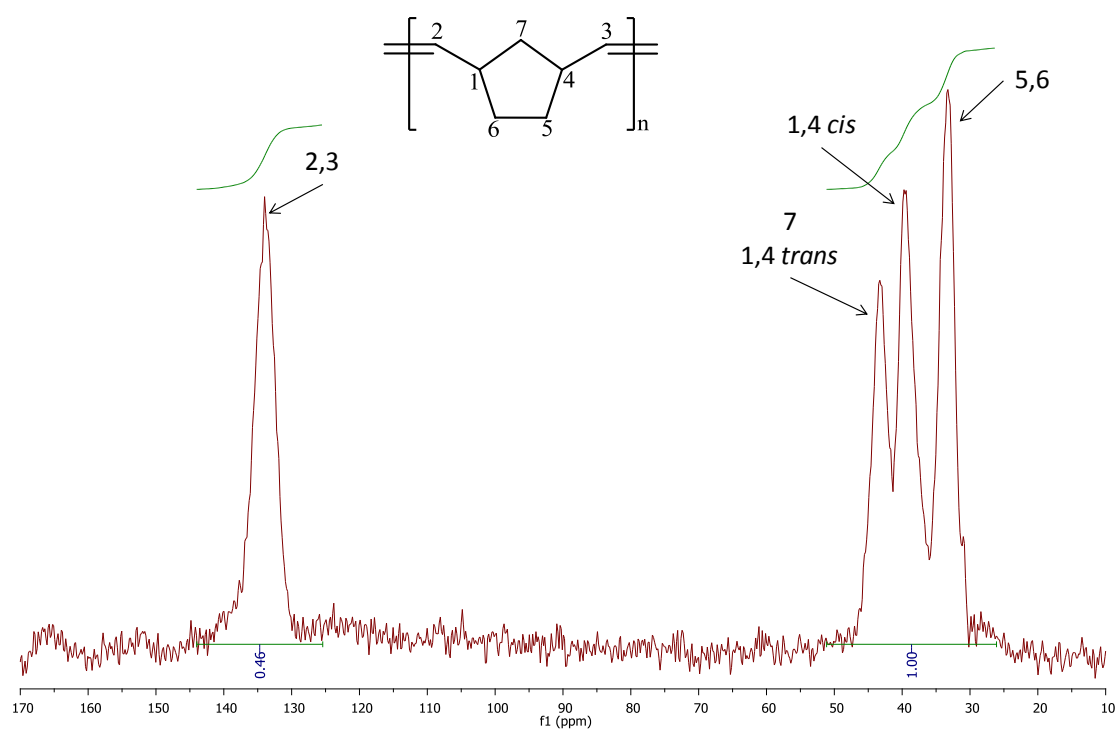


Figure 18: ¹³C CPMAS NMR spectrum of PNBE.

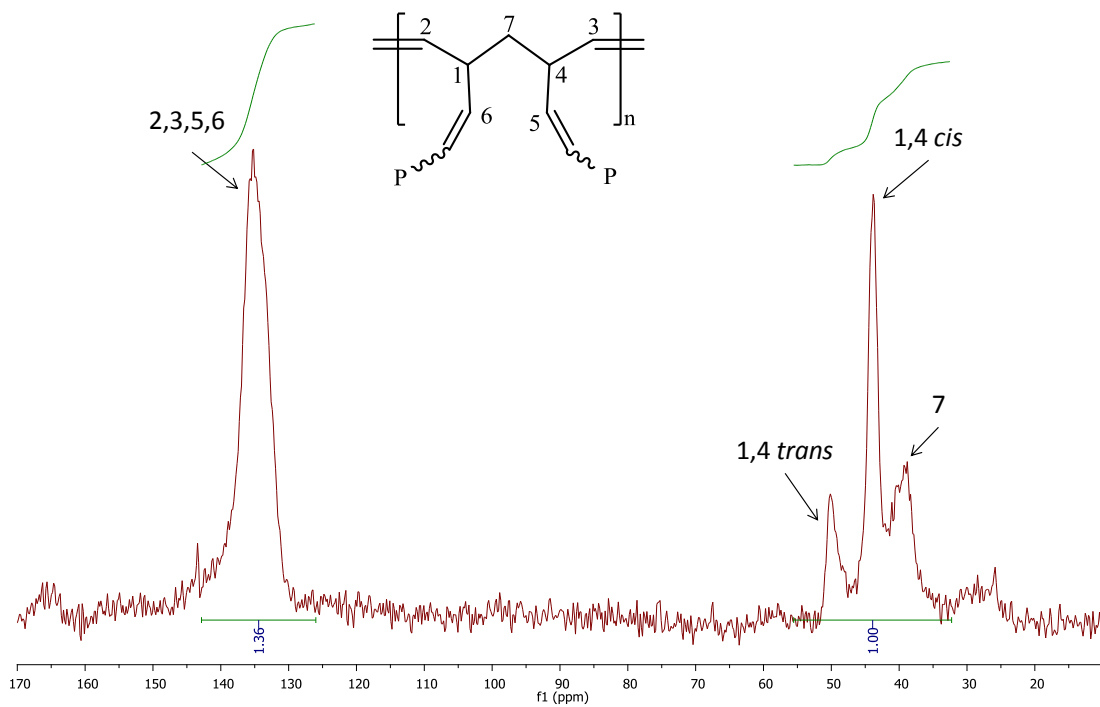


Figure 19: ^{13}C CPMAS NMR spectrum of PNBD.

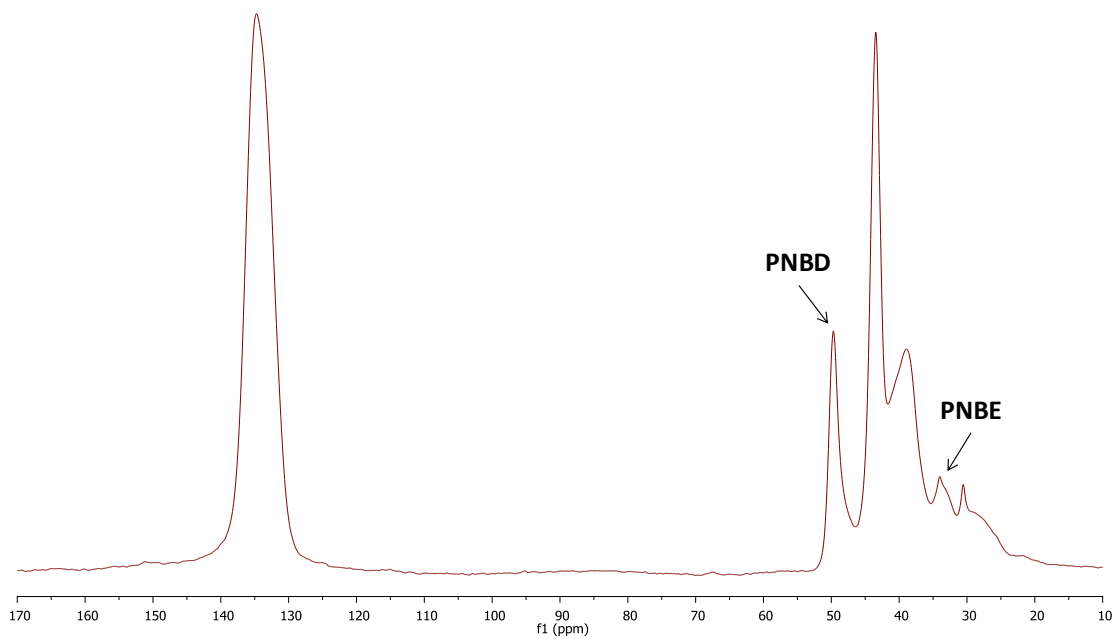


Figure 20: ^{13}C CPMAS NMR spectrum of PNBE/PNBD 100/400 copolymer.

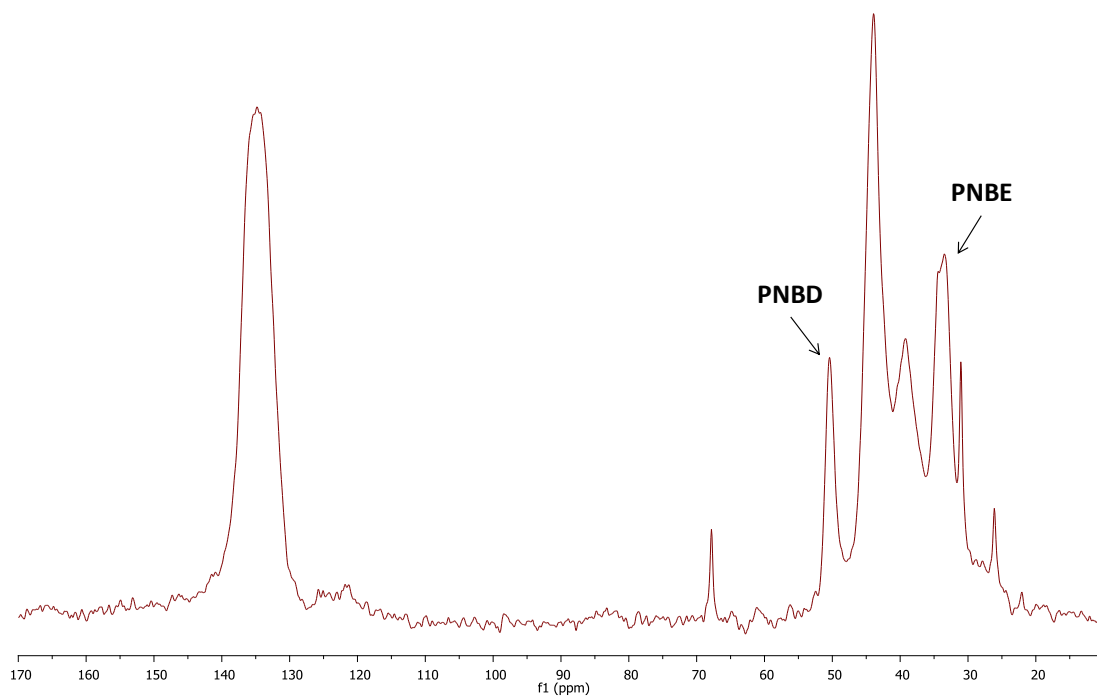


Figure 21: ^{13}C CPMAS NMR spectrum of PNBE/PNBD 400/100 copolymer.

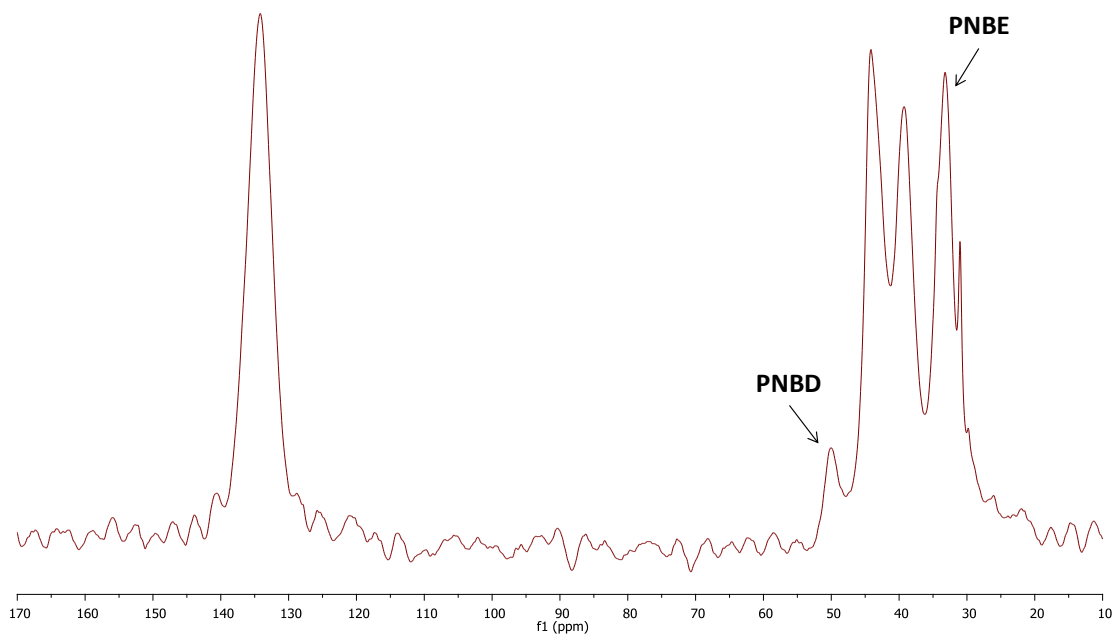


Figure 22: ^{13}C CPMAS NMR spectrum of PNBE/PNBD 1100/300 copolymer.

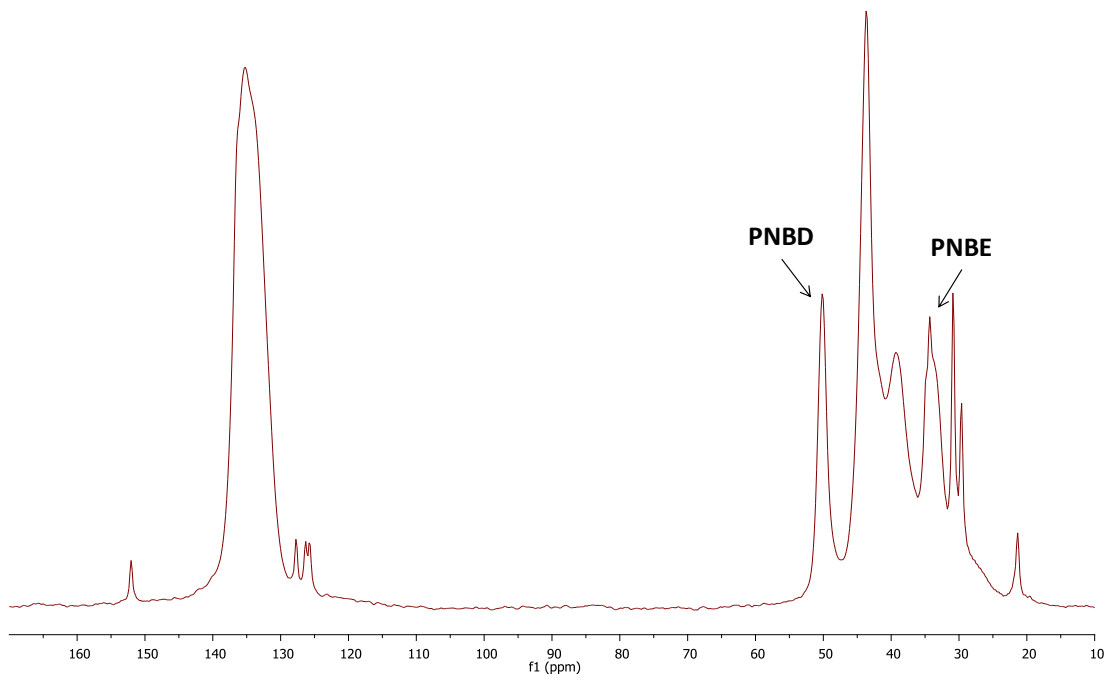


Figure 23: ^{13}C CPMAS NMR spectrum of PNBE/PNBD 700/700 copolymer.

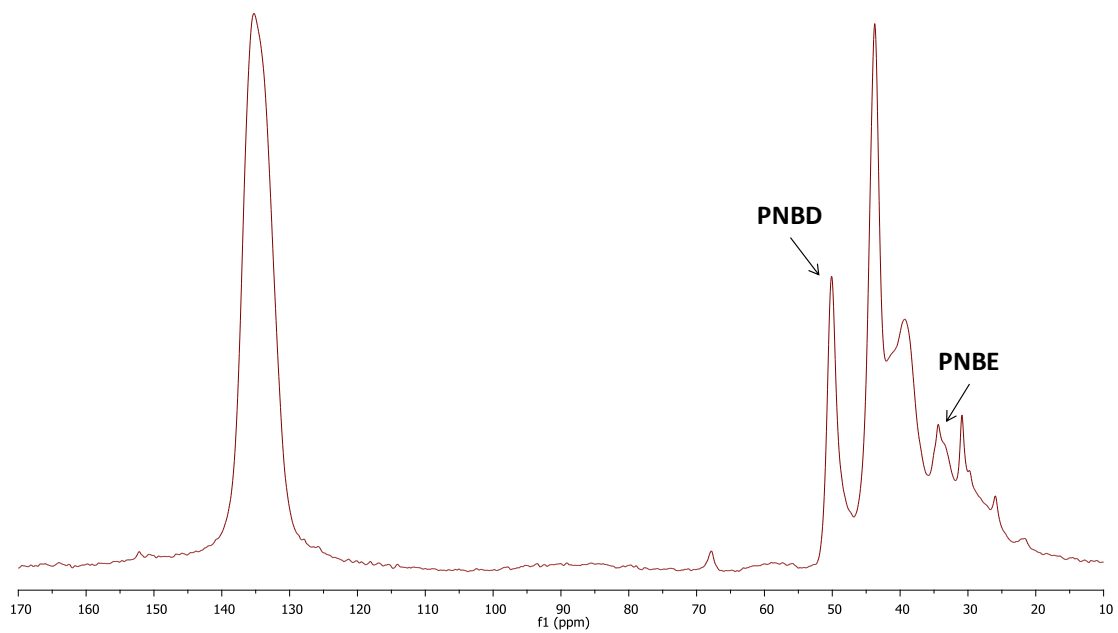


Figure 24: ^{13}C CPMAS NMR spectrum of PNBE/PNBD 300/1100 copolymer.

6.5 Thermal analysis

Thermal analysis results are recorded in Tables 13 and 14. Thermogravimetric analysis (TGA) curves for all samples showed a continuous weight loss up to almost 500 °C, which can be divided into three stages (Figure 25). The first stage from 100 to 250 °C corresponds to evaporation and decomposition of unreacted monomers, and is more prominent for the copolymers. In the second stage, from 250 to 400 °C, the weight remains constant for all samples, except for the **PNBD** homopolymer and the **NBE/NBD** 1/300/1100 copolymer. This stage has been attributed to the decomposition of small polymer chains⁹² in accordance with large molecular weight distribution values. In the final stage, starting after 400 °C, all curves show sharp drops in the weight loss indicating rapid degradation of the polymer backbones. The thermal stability of the copolymers practically does not change with their composition. This agrees with the fact that **PNBE** and **PNBD** units possess similar structures; therefore, the degradation of the polymeric chains involves the cleavage of similar bonds. It is noteworthy that the **PNBD** homopolymer, as well as the copolymers with high **PNBD** content in their chain leave a significant amount of residue (15-19%).

Table 13: TGA results at the heating rate of 10°C/min.

| Sample | Start (°C) | Finish (°C) | Peak (°C) | Residue (%) |
|---------------------------|------------|-------------|-----------|-------------|
| PNBE | 376.11 | 490.49 | 450.39 | 1.60 |
| PNBD | 377.69 | 561.96 | 433.42 | 18.89 |
| PNBE-PNBD 100-400 | 377.78 | 509.09 | 432.86 | 14.75 |
| PNBE-PNBD 400-100 | 353.54 | 495.96 | 443.78 | 7.35 |
| PNBE-PNBD 300-1100 | 389.90 | 539.39 | 435.51 | 18.46 |
| PNBE-PNBD 700-700 | 363.64 | 508.08 | 442.67 | 9.06 |
| PNBE-PNBD 1100-300 | 348.48 | 491.92 | 446.59 | 5.78 |

Differential thermogravimetry (DTG; Figure 26), showed a single decomposition peak for all samples, including the homopolymers, and a smaller one at lower temperatures, with the exception of **PNBE**, for which a small peak at higher temperatures appears. This is a manifestation that the

decomposition mechanism in **PNBD** homo- and copolymers is similar and not very complex involving mainly reactions in the main chain.

The thermal stability is similar for both homopolymers, although slightly higher decomposition temperatures and broader decomposition temperature range was obtained for **PNBE**. This seems unusual, since a higher decomposition temperature would be expected for **PNBD**, because of its crosslinked structure. However, the decomposition peak was significantly broader for **PNBD** than for **PNBE**, as shown in Table 13, indicating that the highly-crosslinked chains are decomposing at higher temps. Another explanation might be that structures containing rings decompose at higher temperatures. In either case, it is obvious from the results that the thermal stability was governed by the polymer backbone, which is very similar for both cases.

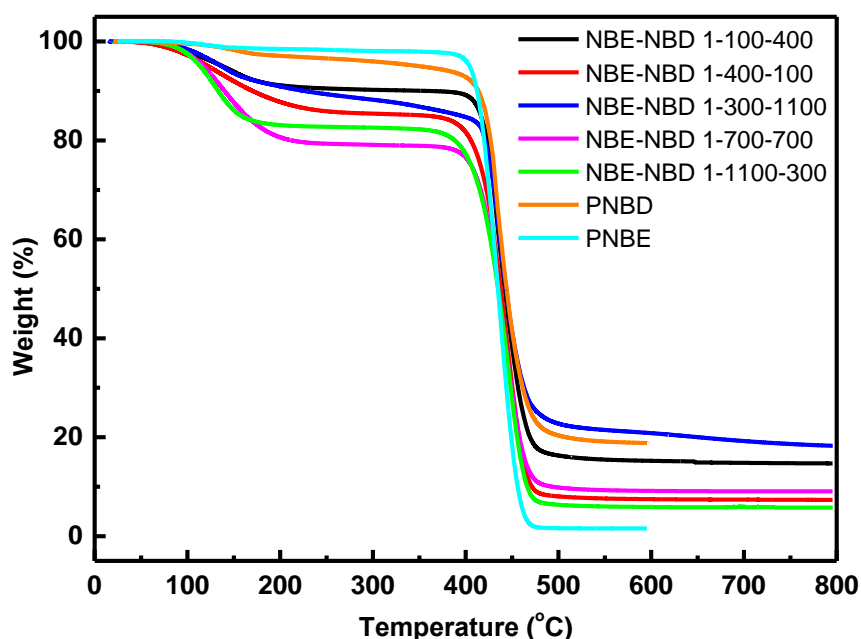


Figure 25: Weight loss (%/°C) with temperature (°C) for all samples, as indicated.

The decomposition temperature range of the copolymers and the decomposition temperature at the decomposition peak in DTG were similar to those of the corresponding **PNBD** homopolymer, or slightly higher when the **PNBE** content of the polymer backbone increased. This result indicates that

the presence of even a small amount of **PNBD** is sufficient to alter the thermal stability of the copolymers.

Differential scanning calorimetry (DSC) measurements showed that the glass transition (T_g) temperature for **PNBD** was lower than the that for **PNBE**, although **PNBD** copolymer is crosslinked (Table 14). The copolymers showed an increase in the T_g temperature, when the **PNBD** content increased, in agreement with an extended degree of crosslinking, with the exception of the 700-700 sample, for which the T_g temperature was significantly lower than any other sample. In any case, the T_g temperatures were lower for the copolymers than for the homopolymers. This is a strong indication that those materials are star-copolymers.

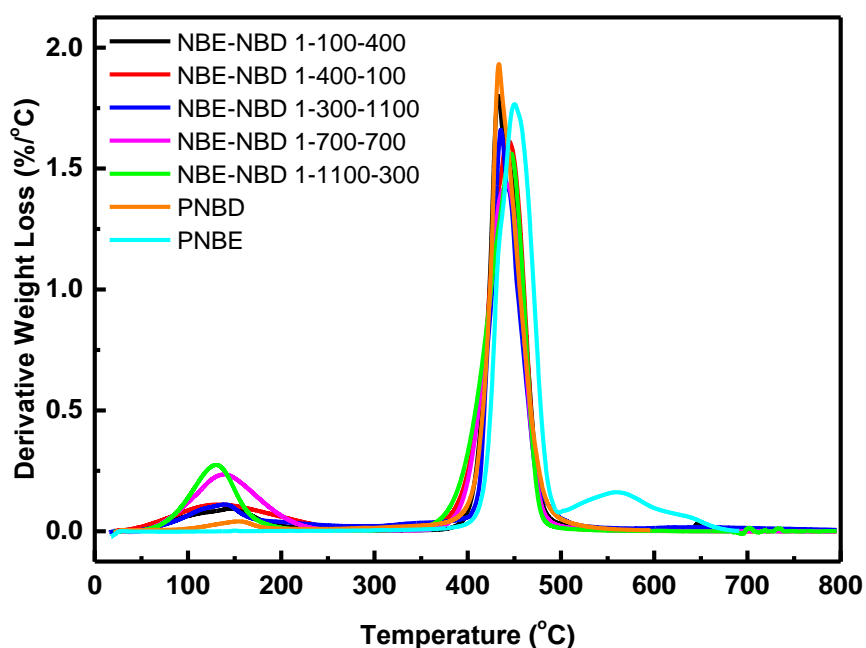


Figure 26: Derivative weight loss ($\%/^{\circ}\text{C}$) with temperature ($^{\circ}\text{C}$) for all samples, as indicated.

Table 14: Experimental Tg values.

| Sample | Tg, °C | Tg, °C Reverse |
|---------------------------|---------------|-----------------------|
| PNBE | 57.9 | |
| PNBD | 50.1 | 46.9 |
| PNBE-PNBD 100/400 | 39.5 | 36.3 |
| PNBE-PNBD 400/100 | 37.9 | 39.0 |
| PNBE-PNBD 300/1100 | 47.5 | 46.8 |
| PNBE-PNBD 700/700 | 29.1 | 34.2 |
| PNBE-PNBD 1100/300 | 39.4 | 42.9 |

6.6 Conclusions

Statistical poly(norbornene)/poly(norbornadiene) **PNBE/PNBD** copolymers have been synthesized *via* **ROMP** using compound $\text{Na}[\text{W}_2(\mu\text{-Cl})_3\text{Cl}_4(\text{THF})_2]\cdot(\text{THF})_3$ (**W₂**) as initiator. The composition of the polymeric chain was estimated, although not quantitatively, by solid state NMR data and it was found that the ratio of **NBE/NBD** units was relative to the monomer molar ratio in the reaction mixture. The morphology of the copolymers differed, according to the composition of the polymeric chain. Solid-state ¹³C CPMAS NMR spectroscopy of **PNBD** homopolymer revealed that the only crosslinking mechanism in operation was the metathetic one (no radical coupling). The thermal properties of all copolymers were similar, resembled the properties of **PNBD** homopolymer and indicated a high degree of crosslinking for both **PNBD** homopolymer and the copolymers. Glass transition (Tg) temperatures were lower for the copolymers than for the homopolymers, which is a strong indication that those materials are star-copolymers.

CHAPTER 7

EXPANDING AND IMPROVING THE CATALYTIC ACTIVITY OF $\text{Na}[\text{W}_2(\mu\text{-Cl})_3\text{Cl}_4(\text{THF})_2]\cdot(\text{THF})_3$

7.1 General

In order to improve the catalytic activity of $\text{Na}[\text{W}_2(\mu\text{-Cl})_3\text{Cl}_4(\text{THF})_2]\cdot(\text{THF})_3$ ($\{\text{W}_2\}$), we have utilized phenylacetylene (**PA**) as co-initiator and examined the reactivity of $\{\text{W}_2\}/\text{PA}$ towards the **ROMP** of a number of cycloolefins. A comparison of the two catalytic systems ($\{\text{W}_2\}$ and $\{\text{W}_2\}/\text{PA}$) between themselves and other systems reported in the literature is presented below, along with characterization of the polymers formed and an attempt to determine aspects of the reaction mechanism by ^1H NMR spectroscopy.

7.2 Polymerization reactions

Polymerization reactions were carried out at room temperature, for a given time. The results are summarized in Table 15. Results from the reactions of $\{\text{W}_2\}$ with cycloolefins that were previously published⁵³ are also presented on Table 15, for comparison purposes. All possible reaction pathways and products are shown in Scheme 13 Scheme 14.

Table 15: Polymerization of cycloolefins with catalytic systems $\{W_2\}$ and $\{W_2\}/PA$.

| Entry | Monomer | Solvent | $\{W_2\}/PA$ /monomer molar ratio | t (h) | Yield (%) | $M_w \times 10^{-3}$ ^e | M_w/M_n ^e |
|-------|-----------------------|---------------------------------|-----------------------------------|-------|----------------|-----------------------------------|------------------------|
| 1. | NBE ⁵³ | THF | 1/0/500 ^a | 19 | 12 | 86.2 | 1.2 |
| 2. | | CH ₂ Cl ₂ | | 1 | 96 | 529 | 1.2 |
| 3. | | dme | | 48 | - ^d | - | - |
| 4. | | CH ₃ CN | | 48 | - ^d | - | - |
| 5. | | toluene | | 24 | 37 | 296 | 2.9 |
| 6. | | Et ₂ O | | 20 | 94 | 422 | 1.4 |
| 7. | NBE/PA ⁹⁵ | THF | 1/20/500 ^b | 20 | >99 | 184 | 1.5 |
| 8. | | CH ₂ Cl ₂ | | 0.1 | >99 | 413 | 1.3 |
| 9. | | dme | | 20 | 18 | 3.2 | 1.5 |
| 10. | | CH ₃ CN | | 48 | - ^d | - | - |
| 11. | | toluene | | 20 | 34 | 11 | 1.5 |
| 12. | | Et ₂ O | | 20 | 72 | 392 | 1.4 |
| 13. | NBE/PA ⁹⁵ | THF | 1/20/1000 ^c | 1 | 95 | 22.3 | 2.5 |
| 14. | | CH ₂ Cl ₂ | | 0.1 | 97 | 300 | 1.2 |
| 15. | | toluene | | 0.3 | 95 | 62 | 4.5 |
| 16. | VNBE ⁵³ | CH ₂ Cl ₂ | 1/0/500 ^a | 8 | >99 | 974 | 2.6 |
| 17. | VNBE/PA ⁹⁵ | CH ₂ Cl ₂ | 1/20/500 ^b | 1 | >99 | 97 | 2.7 |
| 18. | NBD ⁵³ | THF | 1/0/500 ^a | 4 | >99 | - ^f | - |
| 19. | NBD/PA ⁹⁵ | THF | 1/20/500 ^b | 0.5 | 38 | - ^f | - |
| 20. | | | 1/20/1000 ^c | 21 | 61 | - ^f | - |
| 21. | DCPD ⁹⁵ | CH ₂ Cl ₂ | 1/0/500 ^a | 17 | 10 | - ^f | - |
| 22. | | toluene | | 17 | 20 | - ^f | - |
| 23. | | - | | 17 | 20 | - ^f | - |
| 24. | DCPD/PA ⁹⁵ | CH ₂ Cl ₂ | 1/20/500 ^b | 17 | >99 | - ^f | - |
| 25. | | toluene | | 17 | >99 | - ^f | - |
| 26. | | - | 1/20/1000 ^c | 20 | traces | - | - |

^a Conditions: $\{W_2\}$ (9.0 mg, 0.009 mmol), monomer (4.5 mmol) / 5.0 mL solvent.

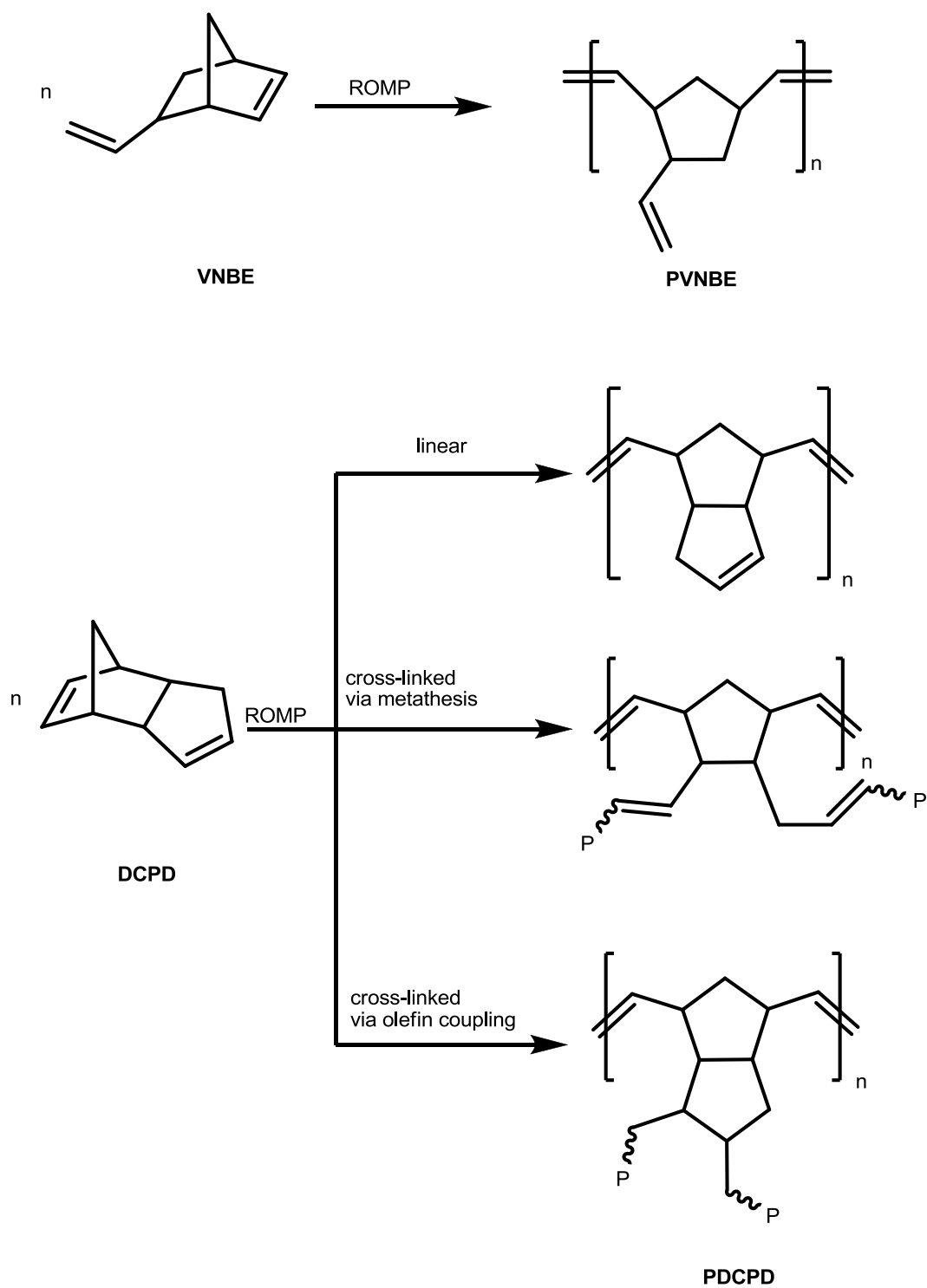
^b Conditions: $\{W_2\}$ (9.0 mg, 0.009 mmol), PA (20 μ L, 18.4 mg, 0.18 mmol), monomer (4.5 mmol) / 5.0 mL solvent.

^c Conditions: $\{W_2\}$ (9.0 mg, 0.009 mmol), PA (20 μ L, 18.4 mg, 0.18 mmol), monomer (9.0 mmol) / 5.0 mL solvent or bulk.

^d No polymerization.

^e By SEC in THF at 40 °C vs. poly(styrene) standards.

^f Polymer insoluble in THF.



Scheme 14: Possible reaction pathways and products for VNBE and DCPD polymerization.

7.3 Results and discussion

The polymerization of norbornene (**NBE**) induced by **{W₂}** was previously studied and it was found to proceed either homogeneously or heterogeneously in different solvent media (Table 15, entries 1-6).⁵³ In coordinating solvents the system was either inactive (dimethoxyethane (dme), CH₃CN), or afforded small yields of **PNBE** (THF, 12%, 19 h). In CH₂Cl₂ gelation was fast (1 h), and the polymer was obtained in high yield (96%) and had very good molecular characteristics ($M_w \approx 529,000$, $M_w/M_n = 1.2$). Suspension of **{W₂}** in toluene gave moderate yields of **PNBE** (37%, 24 h, $M_w \approx 296,000$, $M_w/M_n = 2.9$), while suspensions in Et₂O (94%, 20 h) gave high yields of high-molecular weight **PNBE** ($M_w \approx 422,000$, $M_w/M_n = 1.4$). The *cis*-stereoselectivity was high (86%) in all cases, and it was not affected by the reaction conditions.

Reactions with the catalytic system **{W₂}/PA** (Table 15, entries 7-12) were run at the same **{W₂}/NBE** molar ratio and under the same reaction conditions. **PA** (**{W₂}/PA/NBE** 1/20/500) was added to the system prior to the addition of **NBE**. Best results were obtained in THF and CH₂Cl₂ (entries 7-8). In both cases the reactions were quantitative providing polymers with high molecular weights and fairly narrow molecular weight distribution. By comparison to **{W₂}**, the catalytic system **{W₂}/PA** was significantly more active in those solvents. The rate of the reaction was significantly enhanced (in CH₂Cl₂ the reaction was completed within minutes), and yields were quantitative. The molecular weight of **PNBE** obtained in THF was doubled; this, in addition to the increase of the reaction yield, indicated good control over the polymerization reaction. In dme (entry 9) low molecular weight polymer was obtained in low yield, while in CH₃CN the catalytic system was unreactive even after long reaction times (entry 10). In toluene (entry 11) the rate of the reaction and the yield were not altered by the addition of **PA**, but the molecular weight of **PNBE** formed was significantly lower (by a factor of 27) and the molecular weight distribution was much narrower. This can be explained by considering the solubility of the active intermediate in toluene: **{W₂}/PA** in toluene turned very quickly homogeneous, and therefore the

concentration of the active sites for polymerization was higher (compared to $\{W_2\}$), leading to a better-controlled polymerization reaction. On the other hand, in Et₂O (entry 12), in which the catalytic system remained heterogeneous during the course of the reaction, the molecular characteristics of **PNBE** obtained by the two systems were similar, while the yield was somewhat lower. Addition of **PA** to the catalytic system did not affect the *cis*-stereoselectivity of the reactions, as high-*cis* (86-88%) polymers were obtained in all cases.

When higher molar ratios of **NBE**/ $\{W_2\}$ were employed (1000/1; entries 13-15) the reaction was accelerated, but polymers with lower molecular weights and broad molecular weight distributions were obtained, indicating that not only the main reaction, but also termination reactions were accelerated, and secondary metathesis reactions caused “chopping” of the polymeric chains, as was previously observed for catalytic system $\{W_2\}$.^{53,90} This effect was more obvious in THF and toluene, in which solvents the reaction times were higher.

All **PNBE** samples obtained were soluble in common organic solvents (CHCl₃, CH₂Cl₂, THF). The configuration of the polymer was determined by ¹H and ¹³C NMR spectra (Figure 27).⁹³ The relative proportions of double-bond pair sequences, represented as *trans-cis* (*tc*), *trans-trans* (*tt*), *cis-cis* (*cc*) and *cis-trans* (*ct*) units, were determined from the four methine carbon (C^{1,4}) signals of the ¹³C NMR spectrum of **PNBE** at δ_C 43.67 (*tc*), 43.44 (*tt*), 38.88 (*cc*) and 38.67 ppm (*ct*). The fraction of *cis* double bonds ($\sigma_c = 0.85$) estimated from this ¹³C NMR spectrum was in good agreement with that obtained from the ¹H NMR spectrum ($\sigma_c = 0.86$) by integration of the signals at δ_H 2.73 (HC^{1,4} *cis*-**PNBE**) and 2.37 ppm (HC^{1,4} *trans*-**PNBE**). The reactivity ratios $r_c = cc/ct = 7.4$, $r_t = tt/tc = 1.3$ and $r_c r_t = 9.6$ were calculated from the heights of the relevant signals in the ¹³C NMR spectra.

Other monomers that were activated by $\{W_2\}$ were also studied with the catalytic system $\{W_2\}$ /**PA**. These monomers include 5-vinyl-2-norbornene (**VNBE**), norbornadiene (**NBD**) and dicyclopentadiene (**DCPD**).

VNBE was polymerized quantitatively by $\{W_2\}^{53}$ yielding a very high molecular weight polymer (Table 15, entry 16). Addition of **PA** reduced the reaction time significantly, while the reaction remained quantitative (**VNBE**; entry 17). The most notable change in reactivity was, again, the molecular weight of the polymer formed, which was significantly lower (by a factor of 10). The 1H NMR spectrum of **PVNBE** (Figure 28) indicated that the ring-strained C=C bond was cleaved, while the vinylic one was left intact. The same reactivity had been observed with $\{W_2\}^{53}$. The overlapping signals of the olefinic protons of the polymeric chain with the vinylic ones prevented stereoregular assignment.

VNBE is a monomer of interest, as its polymers can be easily functionalized by the addition of new side groups via reactions with the pendant vinyl bonds. The pendant vinyl group of **VNBE** is usually involved in metathesis reactions, leading to crosslinked products, thus used for the synthesis of self-healing polymers.⁹⁶ There are only three more catalytic systems that polymerize **VNBE** in a manner similar to $\{W_2\}$ and $\{W_2\}/PA$: (a) $[(CO)_4W(\mu-Cl)_3W(GeCl_3)(CO)_3]^{63}$ yielding polymers of low molecular weight (<3,000) and bimodal peaks of broad molecular weight distribution (>2); (b) imidotungsten(VI) complexes bearing chelating phenol ligands, activated by EtMgBr, at room temperature, which provided polymers in moderate yields (up to 50%), but molecular characteristics of the samples have not been reported;⁹⁷ and (c) $[V(CHSiMe_3)(NAd)(OC_6F_5)(PMe_3)_2]$, giving quantitative yields at room temperature.⁹⁸

^1H NMR (CDCl_3 , 300 MHz): 5.25 (s, 2H, $\text{H}^{2,3}$ *t*), 5.10 (s, 2H, $\text{H}^{2,3}$ *c*), 2.73 (br, s, 2H, $\text{H}^{1,4}$ *c*), 2.37 (br, s, 2H, $\text{H}^{1,4}$ *t*), 1.95-1.60 (br, m, 3H, $\text{H}^{5a,6a,7a}$), 1.50-1.20 (br, m, 2H, $\text{H}^{5b,6b}$), 1.20-0.85 ppm (br, m, 1H, H^{7b}); ^{13}C NMR (CDCl_3 , 75.4 MHz): 133.99 (s, $\text{C}^{2,3}$ *ccc*), 133.21 (m, $\text{C}^{2,3}$ *ctt/ttt/ctc*), 133.08 (s, $\text{C}^{2,3}$ *ttc*), 43.67 (s, $\text{C}^{1,4}$ *tc*), 43.44 (s, $\text{C}^{1,4}$ *tt*), 42.88 (s, C^7 *cc*), 42.25 (s, C^7 *ct/tc*), 41.52 (s, C^7 *tt*), 38.88 (s, $\text{C}^{1,4}$ *cc*), 38.67 (s, $\text{C}^{1,4}$ *ct*), 33.39 (s, $\text{C}^{5,6}$ *cc*), 33.19 (s, $\text{C}^{5,6}$ *ct*), 32.61 (s, $\text{C}^{5,6}$ *tc*), 32.43 ppm (s, $\text{C}^{5,6}$ *tt*).

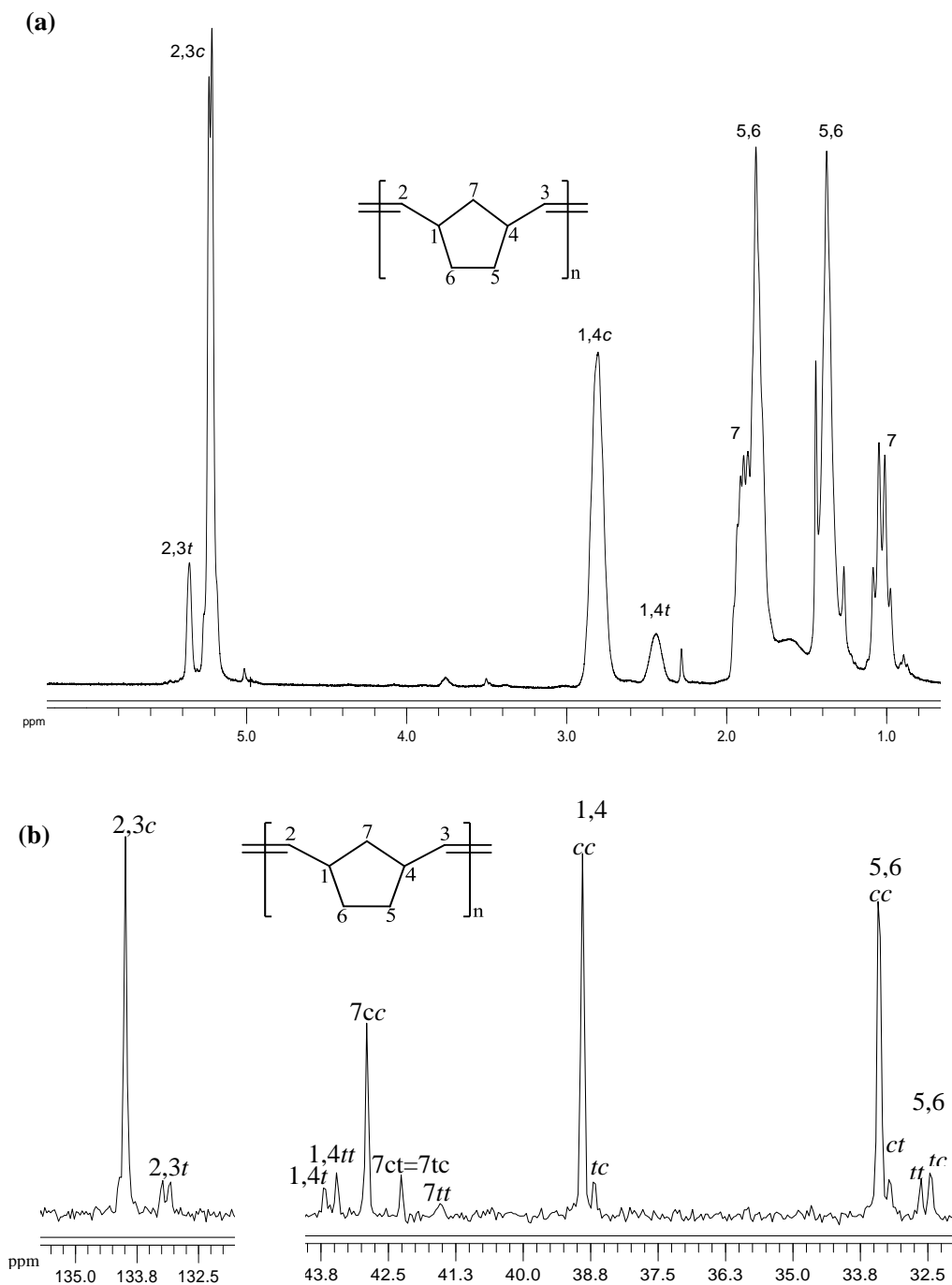


Figure 27: (a) ^1H and (b) $^{13}\text{C}\{^1\text{H}\}$ NMR spectra (CDCl_3) of PNBE obtained from the reaction of $\{\text{W}_2\}/\text{PA}/\text{NBE}$ in CH_2Cl_2 .

^1H NMR (CDCl_3 , 300 MHz): 5.76 (br, 1H, H^8), 5.30 (br, 2H, $\text{H}^{2,3}$), 4.89-4.96 (br, 2H, H^9), 2.19-3.10 (br, 3H, $\text{H}^{1,4,5}$), 1.10-2.10 ppm (br, m, 2H, $\text{H}^{6,7}$); ^{13}C NMR (CDCl_3 , 75.4 MHz): 141.7, 140.6 (s, C^8), 135.6-130.3 (m, $\text{C}^{2,3}$), 113.6, 113.1 (s, C^9), 50.1, 47.9 (s, C^5), 45.6, 37.5 (s, C^1), 45.6, 41.3 (s, C^4), 42.8, 41.3, 39.5 (s, C^7), 41.3 ppm (s, C^6).

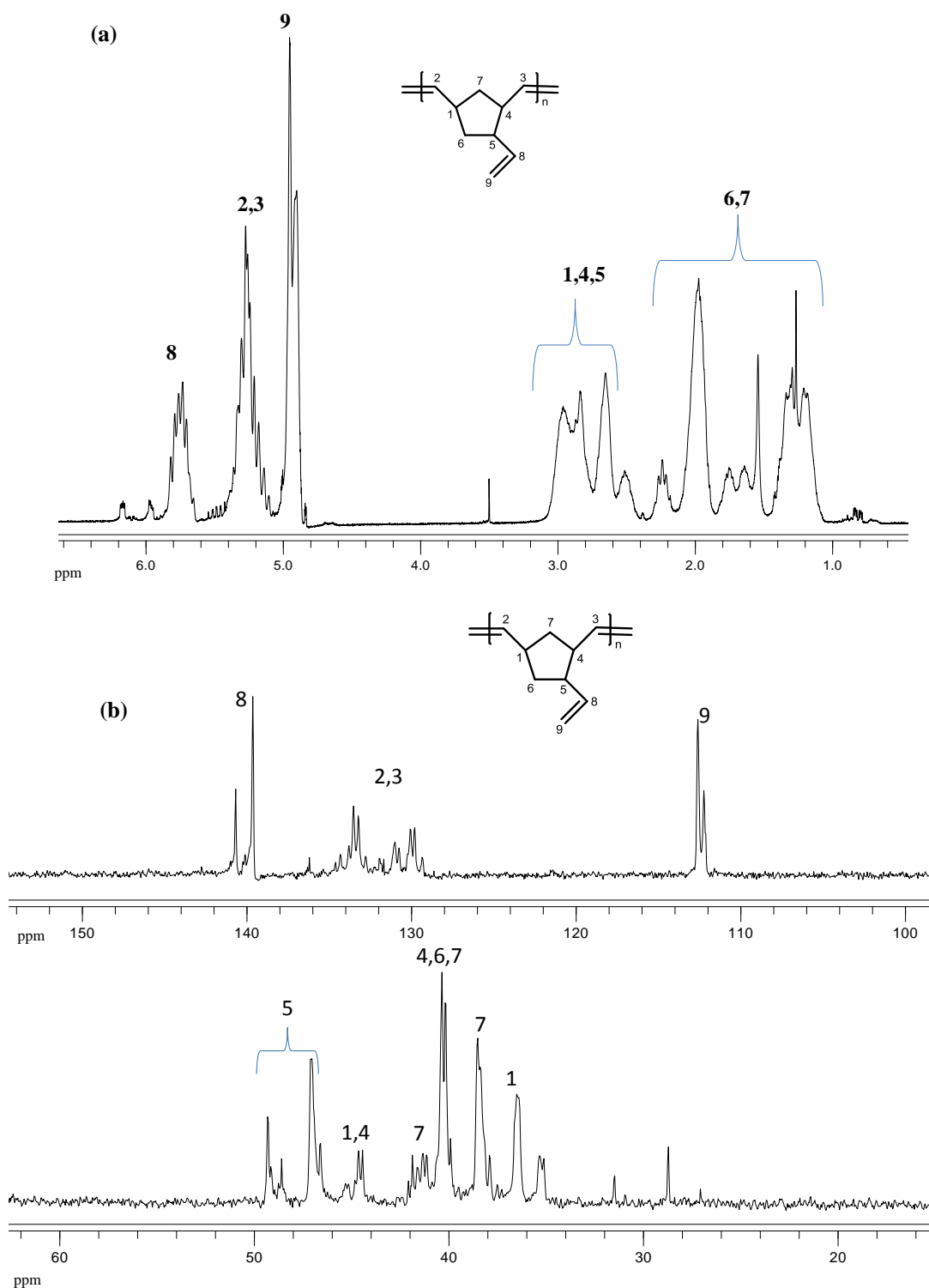


Figure 28: (a) ^1H and (b) $^{13}\text{C}\{^1\text{H}\}$ NMR spectra (CDCl_3) of PVNBE obtained from the reaction of $\{\text{W}_2\}/\text{PA}/\text{VNBE}$ in CH_2Cl_2 .

NBD was also polymerized quantitatively by $\{W_2\}^{53}$ in CH_2Cl_2 , THF and toluene as well as in bulk, yielding insoluble polymers. The reactions were completed within 5 min in all cases, except for THF, in which the rate of polymerization was much slower (Table 15, entry 18). Addition of **PA** yielded moderate yields of insoluble **PNBD** within minutes (entry 19). The reaction could not be kept longer, because of gelation of the reaction mixture. Thermogravimetric analysis of the polymer obtained showed a decomposition peak at high temperature (455 °C, slightly higher than **PNBD** obtained from the reaction with $\{W_2\}$, Figure 29), indicating high degree of crosslinking.

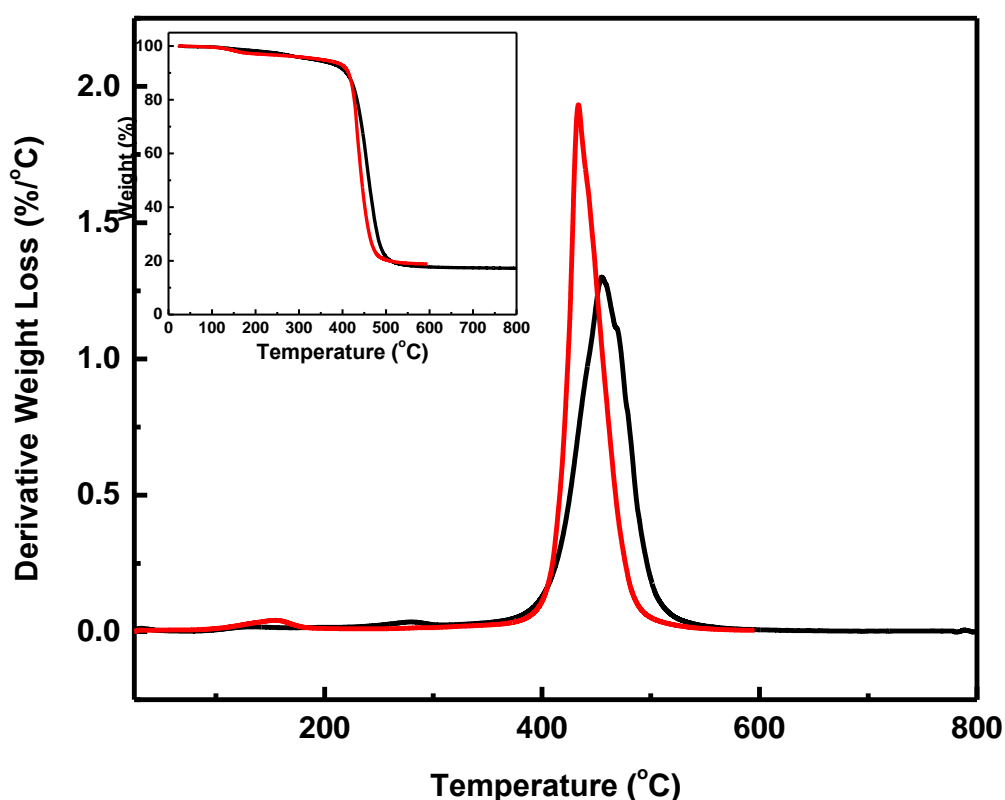


Figure 29: Derivative weight loss with temperature and weight loss (%/°C) with temperature (°C; inset) of **PNBD** obtained from the ROMP of **NBD** with catalytic systems $\{W_2\}/PA$ (black line) and $\{W_2\}$ (red line).

Finally, the **ROMP** of **DCPD** was studied under various reaction conditions, as this is a reaction of both academic and industrial interest. **DCPD** is an

inexpensive and readily available monomer and provides industrial polymers (**PDCPD**) of high mechanical strength.^{44,99} The reaction of **{W₂}** with **DCPD** in CH₂Cl₂ and toluene as well as in the absence of solvent provided low yields of insoluble **PDCPD** (Table 15, entries 21-23). Reaction in CH₂Cl₂ proceeded in a similar fashion at several **{W₂}/DCPD** molar ratios, ranging from 1/300 to 1/1000, in toluene ratios higher than 1/500 provided traces of polymer, while in the bulk ratios up to 1/500 gave optimum yields. Addition of **PA** turned the reaction quantitative in CH₂Cl₂ and toluene, yielding insoluble polymers (entries 24 and 25). In the bulk, traces of insoluble **PDCPD** were obtained (entry 26). **DCPD** is known to provide insoluble polymers, because of extensive crosslinking due to secondary metathesis or radical reactions on the double bond of the cyclopentene ring.¹⁰⁰ Thermogravimetric analysis of **PDCPD** samples obtained by the aforementioned systems showed a single decomposition peak at 470 °C (Figure 30), which confirms the high degree of crosslinking.⁹⁹

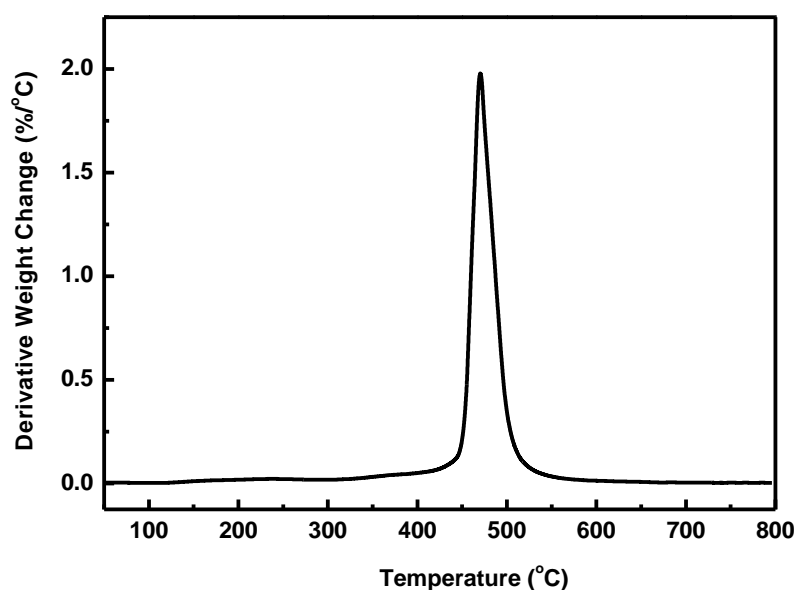


Figure 30: Derivative weight change with temperature of insoluble PDCPD obtained from the reaction of **{W₂}/PA/DCPD** in CH₂Cl₂.

7.4 Mechanistic considerations

The mechanistic study of non-well-defined catalytic systems has always been an intriguing problem, as isolation and characterization of the active intermediates (metallocyclobutanes or metallocarbenes) is in many cases not possible. The small initiation efficiencies of most catalytic systems and/or the high sensitivity of the active species are the most frequent limitations. However, several studies of Mo- or W-based catalytic systems have been published, based mostly on NMR spectroscopic data.^{53,59–61,90,101–105}

In our case, the first stages of **NBE** polymerization by **{W₂}/PA** were studied by ¹H NMR in *d*⁸-THF (Figure 31). The low rate of the reaction in THF allowed for better monitoring of the reaction course. The reaction was carried out at room temperature and with molar ratio of **{W₂}/PA/NBE** equal to 1/6/6. Upon addition of **PA** to a solution of **{W₂}** in *d*⁸-THF a number of peaks appeared in the W-carbene region (Figure 31; bottom), with those at 10.93 and 12.12 ppm predominating. The same peaks were observed in a previous study on the polymerization of **PA** by **{W₂}**,⁹⁰ in which the presence of at least two active alkylidene propagating centers was documented. In the present study, those peaks increased over time, even after the addition of **NBE**. However, after the initiation of **NBE** polymerization, the intensity of the aforementioned peaks decreased, and new peaks emerged, at 11.09 and 12.16 ppm, which represented the active propagating alkylidene species, in agreement with our previous studies on the polymerization of **NBE** by **{W₂}**.⁵³ Quenching the reaction mixture with benzaldehyde (**{W₂}/NBE/PhCHO**: 1/6/12, 10 μL) caused the disappearance of the high-field peaks. The formation of several alkylidenes and the complex multistage nature of the polymerization reactions induced by **{W₂}** render assignment of the peaks mentioned above very difficult; however, more detailed studies as well as theoretical calculations are in progress.

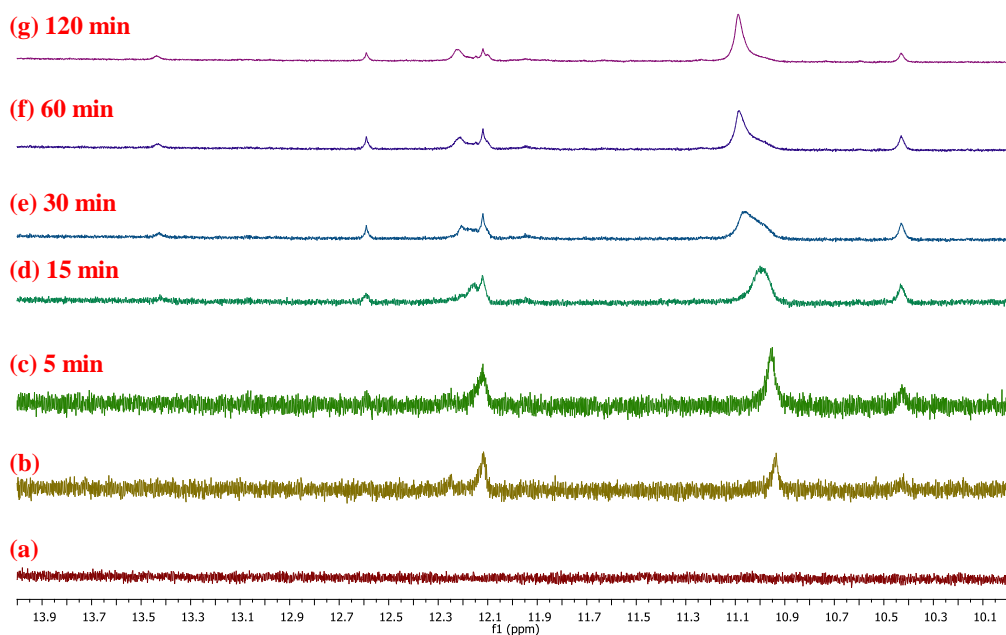
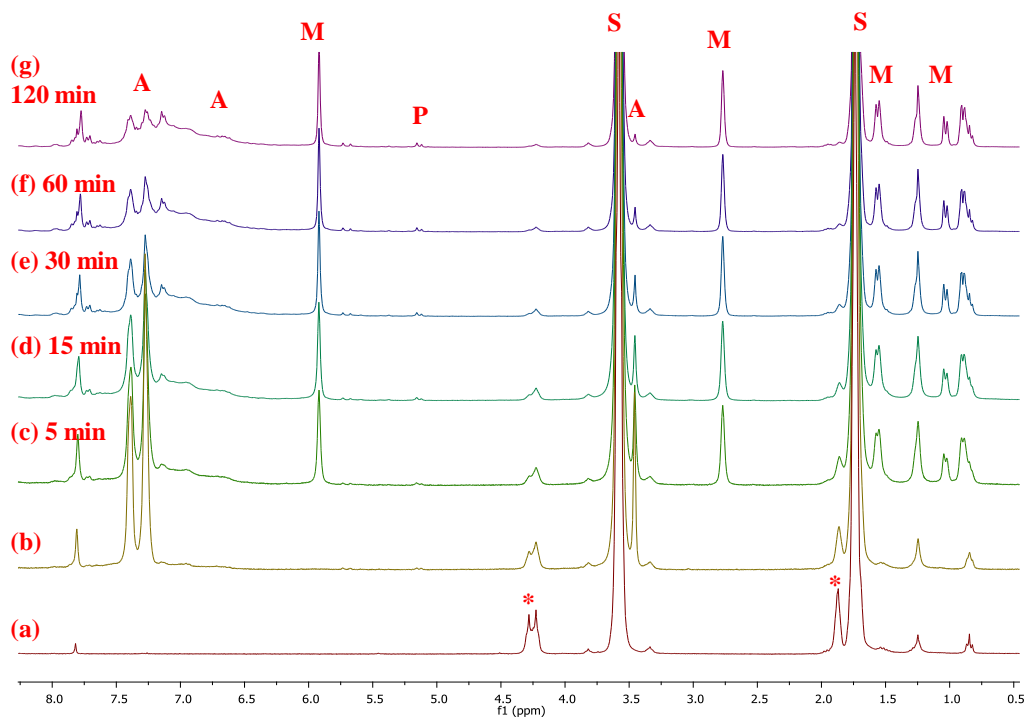


Figure 31: ^1H NMR spectra (up: region 8.5–0.5 ppm; bottom: region 14.0–10.0 ppm) of: $\{\text{W}_2\}$ (a), from the reaction of $\{\text{W}_2\}$ (8.0 mg, 0.008 mmol) with PA (5 μL , 4.6 mg, 0.05 mmol) (b), and from the reaction of $\{\text{W}_2\}$ /PA with NBE (5 mg, 0.05 mmol) in d^8 -THF at various time intervals, as indicated (c–g). Signals denoted by “*” are due to coordinated THF of $\{\text{W}_2\}$, “S” to residual solvent, “M” to NBE, “P” to PNBE, and “A” to PA and/or PPA.

7.5 Conclusions

Catalytic system **{W₂}/PA** (**{W₂}**: Na[W₂(μ-Cl)₃Cl₄(THF)₂](THF)₃ ; **PA**: phenylacetylene) promoted the **ROMP** of norbornene (**NBE**) and 5-vinyl-2-norbornene (**VNBE**) efficiently, providing high molecular weight polymers in high yields and with high stereoselectivity (86% *cis* for **PNBE**). It should be noted that less strained double bonds remained unaffected (–CH=CH₂). Norbornadiene (**NBD**) and dicyclopentadiene (**DCPD**) were also activated fast and quantitatively giving insoluble, highly crosslinked polymers.

Compared to **{W₂}**, **{W₂}/PA** was in general more active towards the **ROMP** of all monomers studied, in all solvents, as well as in bulk. The molecular weights of the polymers obtained were higher (with very few exceptions), while the molecular weight distributions were either retained or improved. The *cis*-specificity of **PNBE** was the same (86% *cis*) with either system.

In situ monitoring of the reaction (**{W₂}/PA/NBE**) by ¹H NMR spectroscopy revealed the formation of active alkylidenes of the propagating chains, in agreement with previous studies on the **W₂**-based catalytic system, but a detailed mechanistic study of the catalytic system is underway.

CHAPTER 8

SOLUBILITY PARAMETERS AND POTENTIAL APPLICATIONS OF POLYDICYCLOPENTADIENE GELS OBTAINED USING A DITUNGSTEN-BASED CATALYTIC SYSTEM

8.1 General

As mentioned previously, dicyclopentadiene (**DCPD**) is a monomer of interest because it provides polymers with good mechanical properties for industrial applications at a low cost.^{44,99} The $\text{Na}[\text{W}_2(\mu\text{-Cl})_3\text{Cl}_4(\text{THF})_2]\cdot(\text{THF})_3/\text{PA}$ ($\{\text{W}_2\}/\text{PA}$) catalytic system was found to catalyze efficiently and quantitatively the **ROMP** of **DCPD** (Section 7.3). Therefore, we proceeded by using the $\{\text{W}_2\}/\text{PA}$ catalytic system to synthesize poly(dicyclopentadiene) (**PDCPD**) gels. Among other catalytic systems, **ROMP** of **DCPD** can be induced by **WCl₆** (Scheme 9) alone,^{106,107} in the presence of organometallic alkylating reagents,³⁴ oxygen-containing compounds,¹⁰⁸ or **PA**.¹⁰⁹ Also, Ru-based 1st and 2nd generation Grubbs' catalysts (**Ru-I** and **Ru-II**; Scheme 9) have been recently utilized for the synthesis of **PDCPD** aerogels.^{77,110,111} In this Chapter, we describe the synthesis and characterization of **PDCPD** gels with catalytic systems $\{\text{W}_2\}/\text{PA}$ and **WCl₆**/**PA**, and we compare them to **PDCPD** aerogels synthesized using **Ru-I** and **Ru-II**.

8.2 Synthesis of PDCPD gels

The synthesis of **W₂-PDCPD** and **W-PDCPD** wet-gels (using the catalytic systems $\{\text{W}_2\}/\text{PA}$ and **WCl₆**/**PA**, respectively) was carried out at room temperature, as shown in Table 16 and Scheme 15. The process was analogous to the one previously reported for the **Ru-I-PDCPD** and **Ru-II-PDCPD** aerogels (using 1st and 2nd generation Grubbs' catalysts, respectively).⁷⁷ The weight percent of **DCPD** was the same for all samples (20% w/w). Attempts to work with lower concentration sols (e.g., 10 or 5% **DCPD**) gave gels (within 24 to 48 h), which were not very sturdy, and could not be handled easily during post-gelation solvent exchange. This behavior is

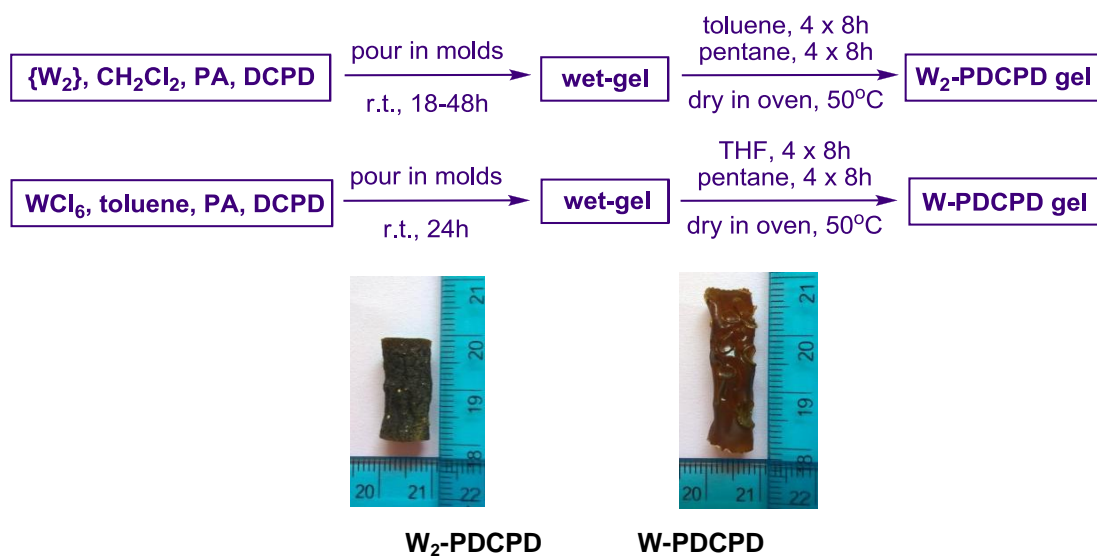
attributed to a higher amount of linear **PDCPD**, which is soluble in common organic solvents, and therefore is dissolved away in toluene during post-gelation washes as confirmed with ¹H NMR (Figure 32). Formation of linear **PDCPD** in low **DCPD** concentrations has been observed and reported previously by our group and others.^{100,112,113}

After aging, **PDCPD** wet-gels were removed from their molds and were washed with toluene or THF and acetonitrile (4×), then pentane (4×) and were air-dried at 50 °C. The reactions were quantitative (yields >98%). It is noted that gels were not aged for a long time, in order to prevent isomerization of *cis* double bonds. During washing with toluene, **W₂-PDCPD** wet-gels exhibited significant swelling as a function of time (Figure 33). This behavior is discussed further in Section 8.6 and Chapter 9. As soon as wet-gels were transferred to pentane, they deswelled rapidly without any noticeable deformation (Figure 33).

Insoluble **PDCPD** dry-gels were characterized using spectroscopic techniques (FTIR-ATR, FT-Raman and ¹³C CPMAS) and thermogravimetric analysis (TGA). All those techniques provided complementary information on the structure of the polymer and the configuration of the polymeric chain.

Table 16: Formulation of W₂-PDCPD, W-PDCPD, Ru-I-PDCPD and Ru-II-PDCPD.

| Catalytic system | Solvent | Solvent (mL) | Catalyst (mg) [mmol] | PA (μL) [mmol] | DCPD (mL) [mmol] | [DCPD] in sol (%w/w) | cat/PA/DCPD molar ratio | Gelation time |
|---------------------------|---------------------------------|--------------|----------------------|----------------|------------------|----------------------|-------------------------|---------------|
| {W₂}/PA | CH ₂ Cl ₂ | 15.0 | 105.0 [0.105] | 225 [2.05] | 5.0 [37.0] | 20.0 | 1/20/350 | 18 h |
| WCl₆/PA | toluene | 22.6 | 160.0 [0.403] | 50 [0.455] | 5.0 [37.0] | 20.0 | 1/1/90 | 5 min |
| Ru-II⁷⁷ | toluene | 18.48 | 6.53 [0.008] | - | 4.06 [30.3] | 20.0 | 1/-/4000 | 10 min |
| Ru-I⁷⁷ | toluene | 18.48 | 6.28 [0.008] | - | 4.06 [30.3] | 20.0 | 1/-/4000 | 5 min |



Scheme 15: Synthesis of W_2 -PDCPD and W-PDCPD gels.

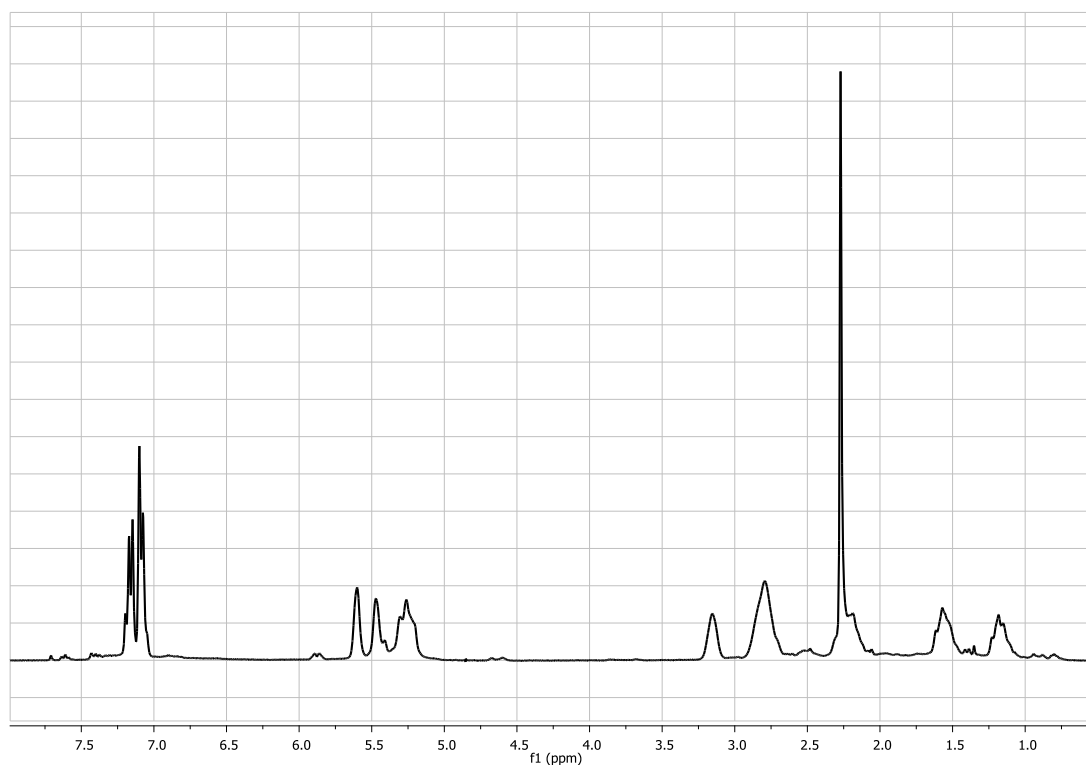


Figure 32: 1H NMR spectrum ($CDCl_3$) of the residue remaining after evaporation of toluene from the first wash of a W_2 -PDCPD wet-gel. Peaks at 5.60 and 5.47 ppm are characteristic of linear PDCPD.³⁴ Peaks at 7.02 (sh.), 6.88 and 5.89 ppm are characteristic of PPA.⁹⁰

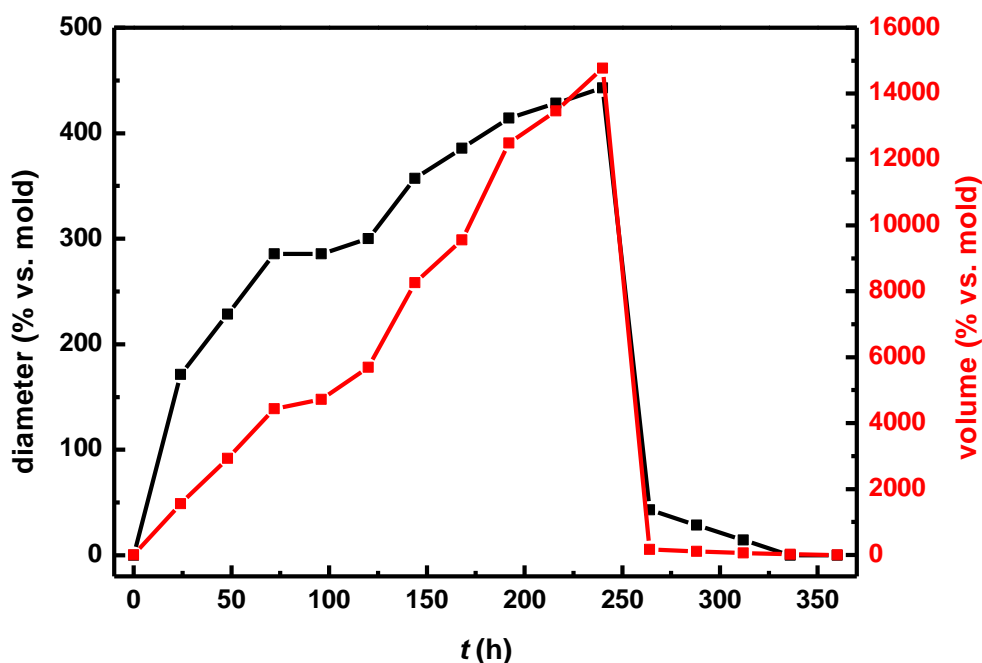


Figure 33: Swelling data for W_2 -PDCPD wet-gels in toluene and de-swelling in pentane.

8.3 Vibrational spectroscopy

Since *cis* and *trans* carbon-carbon double bonds provide distinct bands, vibrational spectroscopy is a useful tool for studying unsaturated systems. Characteristic bands of FTIR-ATR spectra of all **PDCPD** gels are shown in Figure 34. Assignments were made based on literature reports.^{77,112} Bands at 1660 and 1650 cm^{-1} were assigned to stretching vibrations of *trans* and *cis* C=C bonds, respectively, and bands at 972 and 752 cm^{-1} to deformation vibrations of C–H bonds on *trans* and *cis* double bonds, respectively. An estimation of the *cis/trans* ratio is possible from the relative absorbance values of the latter bands to the absorbance at 1450 cm^{-1} , which is assigned to deformation vibration of $-\text{CH}_2-$ groups of the polymeric chain.¹⁰⁸ From those values (Tables 17 and 18) it is clear that Ru catalysts favor formation of *trans* polymeric chains, while W-based catalytic systems show the opposite trend (although marginally in the case **W/PA**). The most extreme cases are **Ru-I**, for which bands related to *cis* configuration are almost invisible and the *cis/trans* ratio is very low, and **{W₂}/PA**, for which bands related to *trans* C=C

bonds are very weak and the *cis/trans* ratio is high. Bands at 1620 and 708 cm^{-1} , which are due to vibrations of the unreacted pendant cyclopentene ring, were present in all spectra showing that cyclopentene rings did not get involved in crosslinking quantitatively.

Those findings were further supported by FT-Raman spectroscopy (Figure 35), which is a very sensitive technique for non-polar groups, such as carbon-carbon double bonds. Raman bands at 1650 and 1664 cm^{-1} were assigned to stretching vibrations of the *cis* and *trans* double bonds of the polymeric chain.¹¹⁴ Although it is not possible to calculate accurately the *cis/trans* ratio along the polymeric chain, it is obvious that **Ru-I** yielded high-*trans* **PDCPD**, while **{W₂}/PA** provided high-*cis* **PDCPD** dry-gels; the remaining two catalytic systems gave mixtures of *cis* and *trans* double bonds, with the *trans* configuration prevailing when **Ru-II** is used, and the *cis* configuration when **W/PA** is employed. The Raman band at 1620 cm^{-1} is assigned to the stretching vibration of the double bond on the pendant cyclopentene ring, and is present in all four spectra, confirming that not all cyclopentene rings were involved in crosslinking.

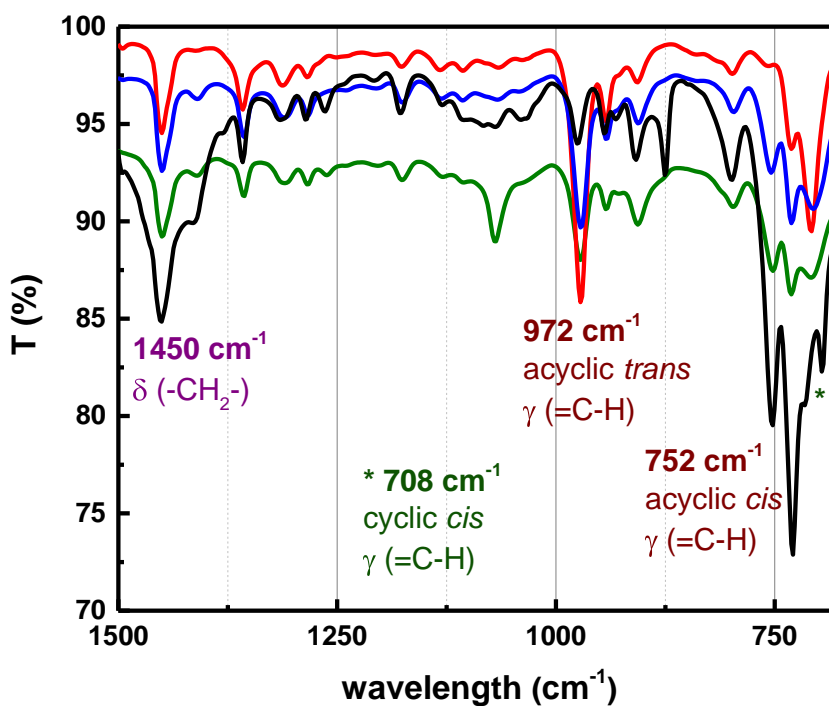
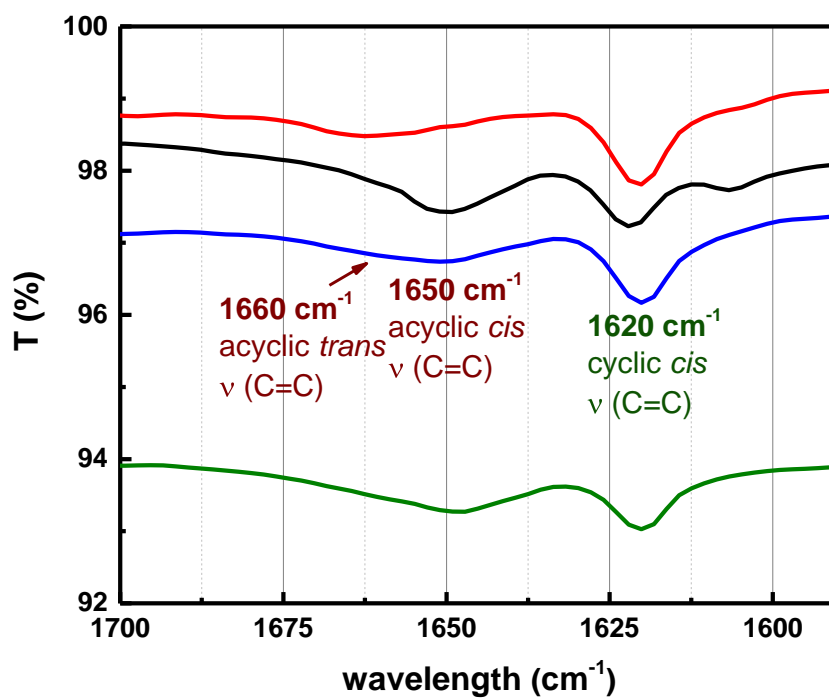


Figure 34: FTIR-ATR spectra (top: 1700-1590 cm^{-1} ; bottom: 1500-600 cm^{-1}) of PDCCPD dry-gels obtained from the ROMP of DCCPD by the following catalytic systems: $\{\text{W}_2\}/\text{PA}$ (black line), WCl_6/PA (green line), Ru-II (blue line) and Ru-I (red line).

Table 17: IR characterization of W₂-PDCPD, W-PDCPD, Ru-I-PDCPD and Ru-II-PDCPD.

| Catalytic system | % Transmittance | | | Absorbance | | |
|----------------------|----------------------|----------------------|-----------------------|----------------------|----------------------|-----------------------|
| | 752 cm ⁻¹ | 972 cm ⁻¹ | 1450 cm ⁻¹ | 752 cm ⁻¹ | 972 cm ⁻¹ | 1450 cm ⁻¹ |
| {W ₂ }/PA | 79.527 | 94.001 | 84.913 | 0.09949 | 0.02687 | 0.07103 |
| WCl ₆ /PA | 87.453 | 88.015 | 89.222 | 0.05823 | 0.05544 | 0.04953 |
| Ru-II | 92.495 | 89.687 | 92.589 | 0.03388 | 0.04727 | 0.03344 |
| Ru-I | 97.977 | 85.847 | 94.533 | 0.00888 | 0.06627 | 0.02442 |

Table 18: IR characterization of W₂-PDCPD, W-PDCPD, Ru-I-PDCPD and Ru-II-PDCPD; the relative absorbance values.

| Catalytic system | A ₇₅₂ / A ₉₇₂ / A ₁₄₅₀ |
|----------------------|---|
| {W ₂ }/PA | 1.40 / 0.38 / 1 |
| WCl ₆ /PA | 1.18 / 1.12 / 1 |
| Ru-II | 1.01 / 1.41 / 1 |
| Ru-I | 0.36 / 2.71 / 1 |

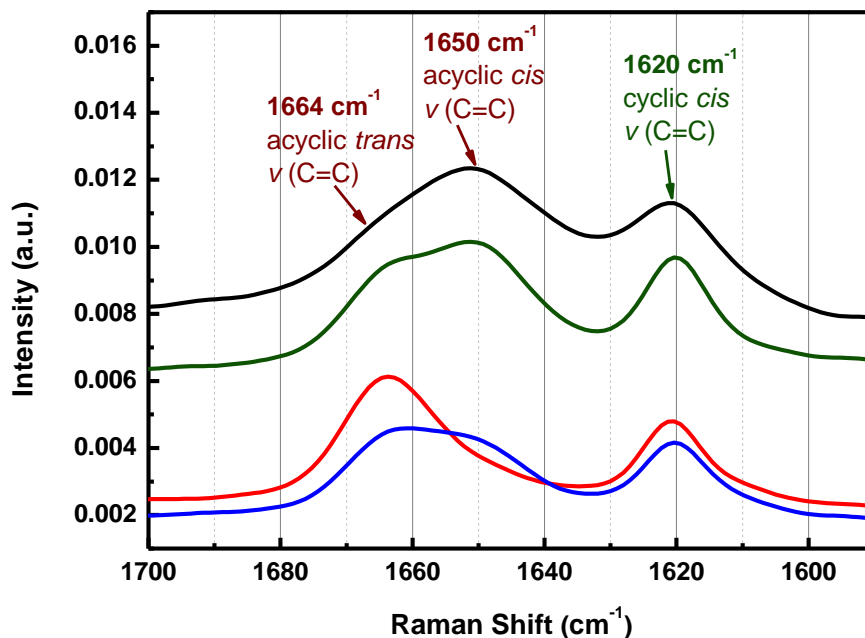


Figure 35: FT-Raman spectra (1700-1580 cm⁻¹) of PDCPD dry-gels obtained from the ROMP of DCPD by the following catalytic systems: {W₂}/PA (black line), WCl₆/PA (green line), Ru-II (blue line) and Ru-I (red line).

8.4 NMR spectroscopy

Further characterization of **PDCPD** dry-gels was carried out with solid-state ^{13}C CPMAS and HC LG-HETCOR, 1 and 2D experiments, respectively. The peak at 129 ppm in the ^{13}C NMR spectrum (Figure 36), was assigned to the olefinic carbons, and peaks in the 26–60 ppm region to aliphatic carbons. The HC LG-HETCOR experiment made assignment of the aliphatic carbons possible, as shown on Figure 37. That assignment is in accord with the APT spectrum of **DCPD** in CDCl_3 ,⁷⁷ which discriminates $-\text{CH}-$ from $-\text{CH}_2-$ groups. The key identifier of the *cis* versus the *trans* configuration was the chemical shift of carbons C5 and C7, which were different in the two configurations. The peak at 40 ppm, assigned to *cis*-polymeric chains,⁷⁷ predominates for **PDCPD** obtained from the W-based catalytic systems, while the peak at 44 ppm, assigned to *trans*-polymeric chains, predominates for **PDCPD** obtained from the Ru-based catalytic systems, as has been previously reported.⁷⁷ The two peaks are overlapping; therefore the exact determination of the *cis/trans* ratio was not feasible; however the stereoselectivity of each catalytic system is rather straightforward.

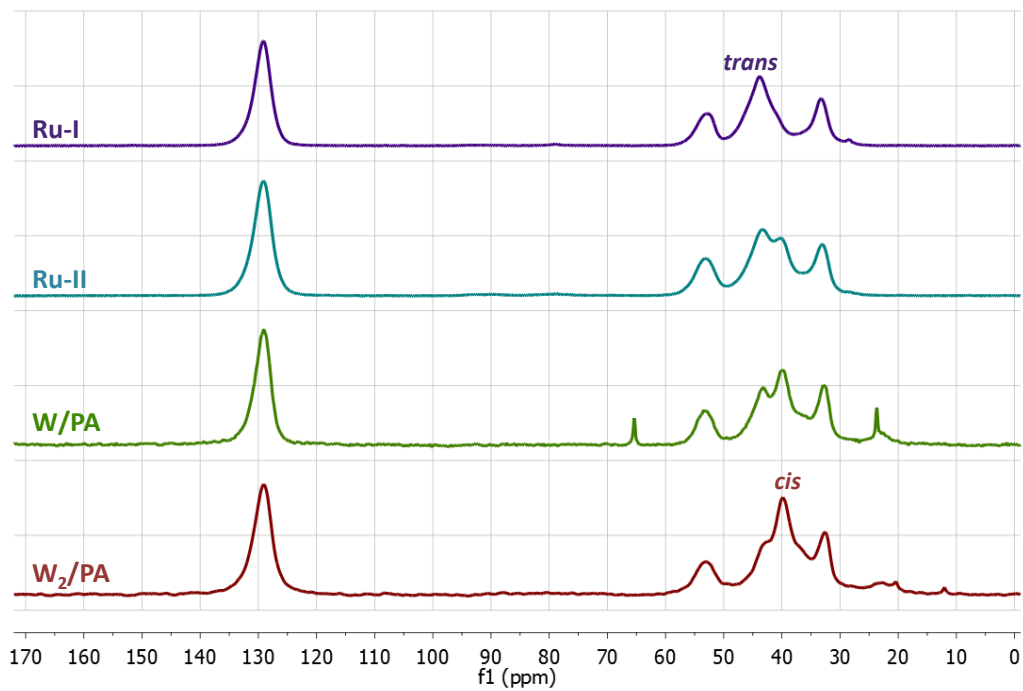


Figure 36: ^{13}C CPMAS spectra of PDCPD dry-gels and aerogels obtained from four different catalytic systems, as indicated. Spectra of Ru-I-PDCPD and Ru-II-PDCPD aerogels were taken from ref. 110.

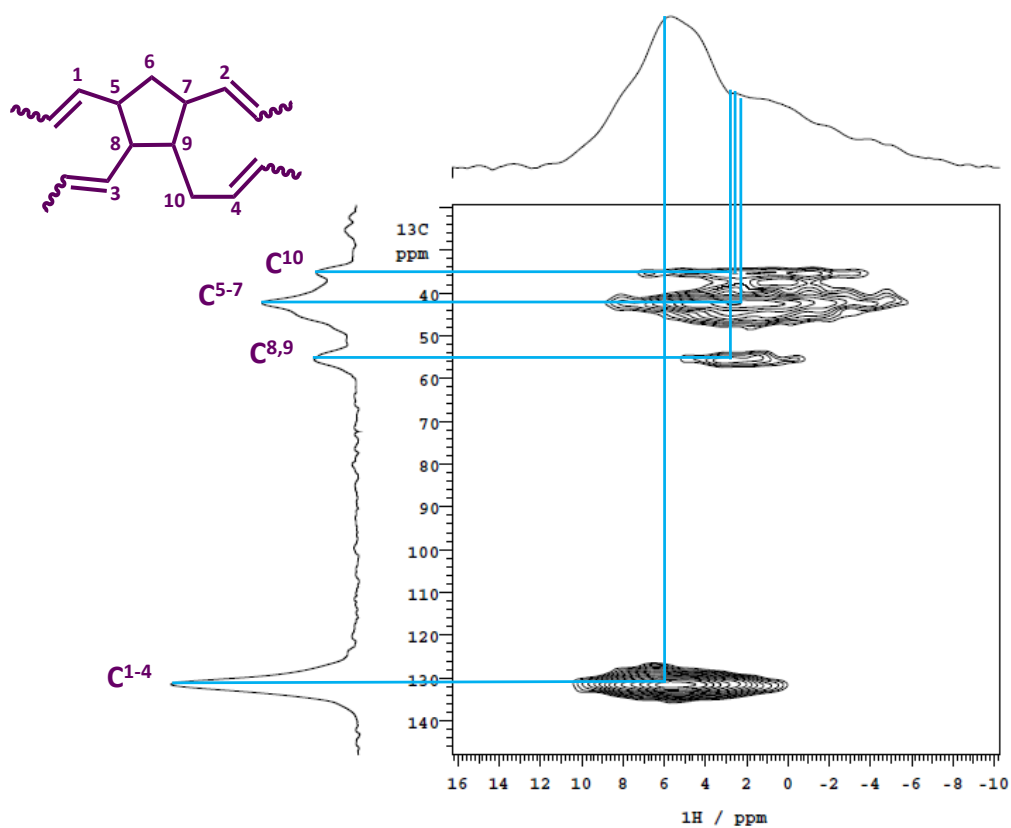


Figure 37: HC LG-HETCOR NMR spectrum of a W_2 -PDCPD gel.

¹³C CPMAS spectra also provide information on the mechanism of the **ROMP** of **DPCPD**. Scheme 14 shows all possible products of **PDCPD** polymerization *via* **ROMP**. Polymers obtained may be linear or crosslinked. Crosslinked polymers are formed by reactions taking place on the double bond of the cyclopentene ring. Those can be either metathetic or olefin coupling reactions and have been well-studied for **PDCPD**.¹⁰⁰ The ratio of olefinic/aliphatic carbons depends on the mechanism of crosslinking and is equal to 2/3 (metathetic) and 1/4 (olefin coupling). Therefore, the olefin coupling contribution can be calculated via equation (2) that takes the ratio of the integrated areas of the corresponding ¹³C CPMAS peaks as input.¹¹⁰ Thus, C_{olefinic} refers to the total sp^2 carbons, $C_{\text{aliphatic}}$ to sp^3 carbons and x is the fraction of polymer double bonds that participate in crosslinking *via* olefin coupling. Integration of **PDCPD** spectra provided the ratios shown in Table 19. The results show that crosslinking *via* olefin coupling ranges from 21 to 33 %, with W-based catalytic systems showing the highest values. It should be noted that the x values calculated for **PDCPD** dry-gels obtained from W-based systems may be a bit higher, depending on the **PPA** content of the polymeric chain. Those values are given in parentheses (Table 19). However, we believe that the value of x is much closer to the value calculated from eq. 1, because most of linear **PPA** is removed during washes of the wet-gels. In addition, the NMR spectra show symmetrical peaks at 129 ppm and not any peaks apart from the ones expected for **PDCPD**. In any case, the difference in x values for the four catalytic systems is not considered significant.

$$(2-x) / (3+x) = [C_{\text{olefinic}} / C_{\text{aliphatic}}]_{\text{experimental}} \quad (2)$$

Table 19: Calculation of the fraction of **PDCPD** double bonds that participate in crosslinking *via* olefin coupling, based on ¹³C CPMAS spectroscopic data.

| Catalytic system | $C_{\text{olefinic}} / C_{\text{aliphatic}}$ | x^a |
|----------------------|--|---------|
| {W ₂ }/PA | 0.50 | 33 (40) |
| WCl ₆ /PA | 0.52 | 29 (33) |
| Ru-I | 0.56 | 21 |
| Ru-II | 0.54 | 25 |

^a Values in parentheses correspond to x calculated assuming that all **PA** added to the reaction mixture was retained (as **PPA**) on the polymeric chain. However, the actual **PPA** content of the polymeric chain cannot be calculated, because **PPA** is soluble in organic solvents and has been detected in residues of washes, as shown in Figure 32.

8.5 Thermal analysis

Thermogravimetric analysis (TGA) of **W₂-PDCPD** under N₂ showed a small weight loss up to almost 450 °C, which can be divided into two stages (Figure 38, inset). The first stage (7% weight loss), from 100 to 400 °C, corresponds to evaporation and decomposition of unreacted monomers and small polymer chains. Similar behavior has been observed in other polymeric materials.⁹² For **W-PDCPD** the weight loss up to 400 °C is higher (14%) and this stage can be clearly divided into two steps; one from 100-200 °C (3% weight loss) and another one from 200-400 °C (11% weight loss). For **Ru-I-PDCPD** and **Ru-II-PDCPD** the weight loss was very small (3%) during the first stage (up to 400 °C). The second stage, starting after 400 °C, was similar for all dry-gels: all samples showed a sharp weight loss, indicating rapid degradation of the polymeric backbones. It is obvious from these results that the thermal stability practically did not change, and did not seem to depend on the configuration of the polymeric chain.

Differential thermogravimetry (DTG) of **W₂-PDCPD** showed a single decomposition peak at 470 °C (Figure 38), indicating a high degree of crosslinking⁹⁹ and a rather simple decomposition mechanism, involving mainly degradation reactions along the polymeric backbone. For the other three gels the decomposition peaks were bimodal (460 °C and 470 °C; Figure 38), indicating a more complex mechanism of thermal decomposition. For example, isomerization of *cis* to *trans* chains during thermal decomposition is a process that cannot be excluded. This type of reaction has been observed during the thermal decomposition of 1,4-poly(isoprene) and 1,4-poly(butadiene), starting at 300 and 200 °C, respectively.¹¹⁵

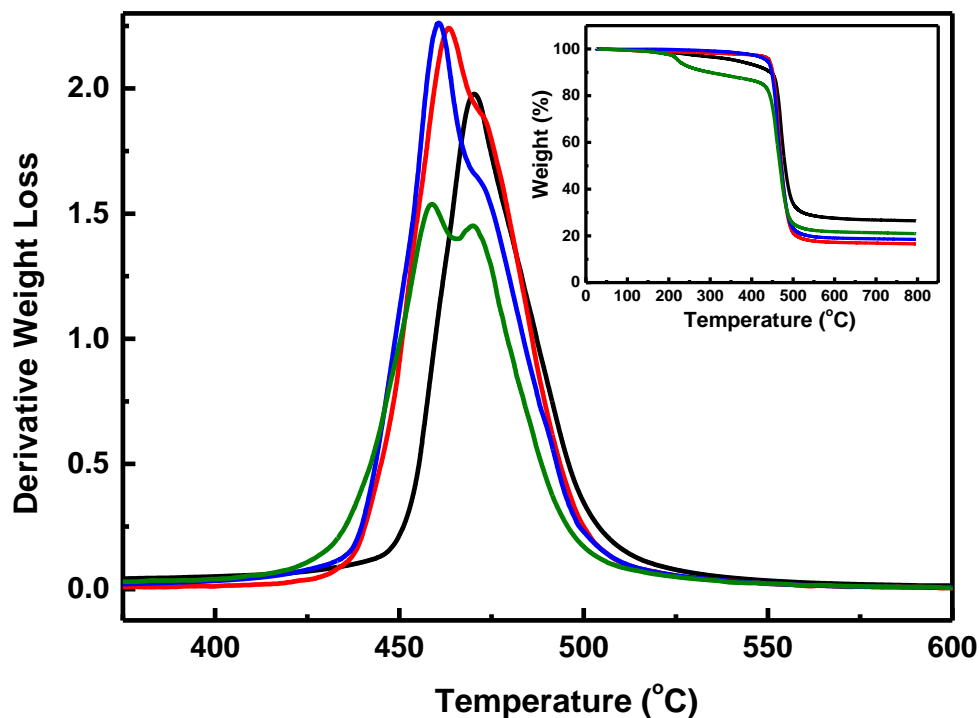


Figure 38: Derivative weight loss with temperature ($^{\circ}\text{C}$) and weight loss ($\%/^{\circ}\text{C}$) with temperature ($^{\circ}\text{C}$; inset) for PDCPD dry-gels obtained from the polymerization of DCPD by the following catalytic systems: $\{\text{W}_2\}/\text{PA}$ (black line), WCl_6/PA (green line), Ru-I (red line) and Ru-II (blue line).

8.6 Swelling of PDCPD gels in toluene

As mentioned above (Section 8.2), **W₂-PDCPD** wet-gels swelled in a number of solvents, with toluene being the most extreme case. That property was further studied with **W₂-PDCPD** dry-gels placed in toluene at room temperature. Those gels showed a linear increase (Figure 39, inset) of their volume by more than 100 \times in 10 days, without loss of their integrity (Figures 39 and 40). Placing the swollen gels in pentane caused rapid shrinkage down to almost to the original volume of the dry-gels. When gels shrunk in pentane, were re-dried and reused, they swelled up to the same volume, with the same rate, for at least three consecutive times. Similar behavior was observed in many other organic solvents (e.g., THF, chlorinated solvents, etc.), although with slower rates and to a different extent. Detailed studies on the extent and

mechanism of swelling of **W₂-PDCPD** gels are presented in Chapter 9. Gels prepared using **WCl₆/PA** and **Ru-II** swelled significantly less, whereas **Ru-I-PDCPD** did not swell at all (Figure 39). A similar trend was observed in the other organic solvents studied. The relationship between the *cis* content of the polymeric chain and the extent of swelling is evident: gels swell more as the *cis* content increases. Detailed data concerning the swelling behavior of **PDCPD** gels are presented in the next Chapter.

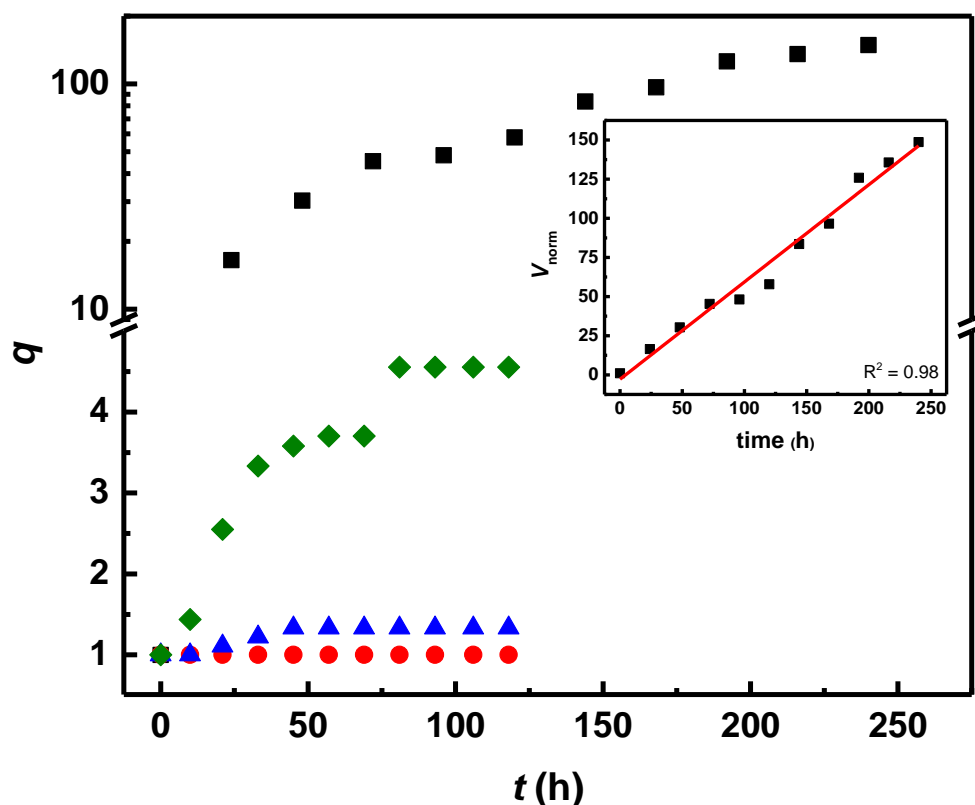


Figure 39: Swelling of PDCPD gels in toluene as a function of the catalytic system: **{W₂}/PA** (black squares), **WCl₆/PA** (green diamonds), **Ru-II** (blue triangles) and **Ru-I** (red dots). Inset: Swelling of a **W₂-PDCPD** dry-gel in toluene with time.



Figure 40: Swelling of a W_2 -PDCPD gel in toluene.

8.7 Conclusions

Poly(dicyclopentadiene) (**PDCPD**) gels were prepared via **ROMP** of dicyclopentadiene (**DCPD**) using two W-based catalytic systems; the first one was based on the ditungsten complex $Na[W_2(\mu-Cl)_3Cl_4(THF)_2] \cdot (THF)_3$ (**{W₂}/PA**), and the second one on the mononuclear WCl_6 complex (**W/PA**). Dry-gels were highly crosslinked, as corroborated by their high thermal stability. Solid-state ^{13}C CPMAS NMR spectroscopy revealed the operation of two mechanisms for crosslinking (one metathetic and one radical), with metathesis being the major pathway (~ 70-80%) in all cases. Most importantly, solid-state ^{13}C NMR along with vibrational spectroscopy (FTIR-ATR and FT-Raman) revealed differences in the *cis/trans* ratio of the double bonds of the polymeric chains. Results were compared also with aerogels **Ru-I-PDCPD** and **Ru-II-PDCPD**, which were synthesized using the first (**Ru-I**) and the second (**Ru-II**) generation Grubbs' catalysts, respectively. Spectroscopic data showed that the configuration of the polymeric chain was predominantly *cis* for W-catalyzed systems and predominantly *trans* for Ru-catalyzed systems. The most extreme cases were **Ru-I-PDCPD**, which consisted of high-*trans* **PDCPD**, and **W₂-PDCPD** dry-gels, which consisted of high-*cis* **PDCPD**. The different *cis* content played a major role in the swelling behavior of the corresponding dry-gels in toluene. In toluene, **W₂-PDCPD** dry-gels swelled and increased their volume by more than 100 times. Such extreme swelling phenomena are rare and may be useful in environmental

remediation, shape memory applications, actuators, chemical delivery systems etc. and are further discussed in Chapter 9. By comparison of **W₂-PDCPD** with **W-PDCPD** dry-gels, as well as with **Ru-II-PDCPD** and **Ru-I-PDCPD** aerogels, it is evident that swelling strongly depends on the configuration of the polymeric chain and increases together with the content of the *cis* configuration. Similar behavior was observed in many other organic solvents (e.g., THF, chlorinated hydrocarbons, etc.), although with slower rates and to a different extent. Therefore, it is concluded that the ditungsten catalytic system considered in this study shows unique advantages in terms of stereochemistry and properties of **PDCPD** gels over the mononuclear W- and Ru-based catalytic systems.

CHAPTER 9

HANSEN SOLUBILITY PARAMETERS AND POTENTIAL APPLICATIONS OF MOSTLY-*CIS* POLYDICYCLOPENTADIENE GELS

9.1 General

As discussed in the previous Chapter, **W₂-PDCPD** dry gels, consisting mostly of *cis* polymer and synthesized using the catalytic system Na[W₂(μ-Cl)₃Cl₄(THF)₂](THF)₃/PA (**{W₂}/PA**), exhibited a remarkable swelling behavior in toluene. Their swelling ability was better not only than the one observed for **PDCPD** gels synthesized using other catalytic systems (WCl₆/PA, 1st and 2nd generation Grubbs' catalysts), but also than that of **PDCPD** films reported in the literature.¹¹⁶ This property was further investigated, by studying the swelling behavior of those gels in a wide range of organic solvents. From a fundamental perspective, the most important outcome of this study was the direct experimental estimation of the Hansen Solubility Parameters (HSP) of **W₂-PDCPD**. From a practical perspective, that study has shown the potential to employ **W₂-PDCPD** for separation of organic solvents from water.

9.2 Swelling of W₂-PDCPD gels in organic solvents

W₂-PDCPD dry-gels swelled in toluene, benzene, chlorobenzene, 1,2- and 1,3-dichlorobenzene, benzyl chloride, CH₂Cl₂, CHCl₃, CCl₄, THF and CS₂. Gels did not swell in pentane, acetone, CH₃CN, CH₃OH, DMF, DMSO, water and oil. The highest degree of swelling was observed in toluene, whereas gels expanded to more than 100× their original volume, before disintegrating (Figures 39 and 41). Significant swelling was also observed in THF (66×) and CHCl₃ (50×). Swelling data for all solvents are summarized in Table 20. The volume degree of swelling (*q*) was calculated by dividing the volume of the swollen gels by the volume of the corresponding dry-gels. Representative plots of *q* as a function of time are shown in Figures 41-43 and 45-55 and photographs of representative samples along different stages of swelling are shown in Figures 44 and 56. In most cases, after being kept in "good"

solvents for extended periods of time, gels disintegrated while they were still expanding (i.e., before they reached the equilibrium volume). During the swelling process the volume of the gels increased either linearly, or stepwise until gels either reached a maximum volume, or disintegrated. Interestingly, even in the “stepwise” volume increase, the overall trend was linear.

According to Prof. Charles Hansen, if a solvent swells a polymer then the diffusivity of the solvent in the swollen polymer is much higher (by several orders of magnitude) than diffusivity in the pure polymer.¹¹⁷ According to Hansen, again, a significant entry resistance may be found within the surface of a polymeric block and is due to the morphology of the polymer at the interface, wherein the mass transfer coefficient can be very low. Different surface morphology can be the result of rapid cooling after, for example, processing by injection molding, or be just a natural state of a given polymer, whereas larger and bulkier molecules have difficulty finding suitable absorption sites to anchor, hop and move into the bulk of the polymeric block. Surface/entry resistance has been described as a boundary condition for the diffusion equation.

In an obvious deviation from Fickian diffusion, Case II diffusion is generally defined as a linear uptake of solvent using a plot of amount absorbed vs. time (not the square root of time as in typical diffusion). This behavior is described by appropriate solutions to the diffusion equation, and is encountered when the diffusion coefficient depends strongly on the solvent concentration. The diffusion coefficient in rigid polymers increases by a factor of about 10 for each additional 3 percent by volume of solvent that is locally present. (By comparison, in elastomers the diffusion coefficient increases by a factor of approximately 10 for each additional 15 percent by volume of solvent.) There is a limit to this rule-of-thumb when the solvent concentration approaches 100% and the diffusion coefficient approaches the self-diffusion value.

In summary, the final element in understanding solvent diffusion in **W₂-PDCPD** is the surface effect that was described above. That is, if for any reason solvent molecules cannot penetrate quickly enough through the boundary of the polymer and the surrounding solvent, the rate of diffusion will

be limited not by diffusion coefficients, but by the surface resistance that is applied in series to regular diffusion.

Table 20: Swelling of W₂-PDCPD gels in various organic solvents.

| Solvent | t_{\max} (h)^a | q_{\max} |
|-------------------------------|--|------------------------------|
| toluene | 240 ^c | 115 |
| tetrahydrofuran | 288 | 66 |
| chloroform | 65 ^c | 50 |
| carbon disulfide | 70 ^c | 21 |
| 1,3-dichlorobenzene | 72 | 19 |
| carbon tetrachloride | 82 ^c | 16 |
| chlorobenzene | 76 ^c | 14 |
| benzene | 82 | 12 |
| methylene chloride | 90 ^c | 10 |
| 1,3,5-trimethylbenzene | 336 ^c | 10 |
| 1,4-dimethylbenzene | 96 ^c | 7 |
| 1,3- dimethylbenzene | 144 ^c | 7 |
| 1,2-dichlorobenzene | 120 | 7 |
| cyclohexane | 144 | 5 |
| benzyl chloride | 119 | 5 |
| 1,4-dioxane | 216 | 4 |
| cyclohexanone | 336 | 4 |
| water | - ^d | 1 |
| pentane | - ^d | 1 |
| <i>N,N</i> -dimethylformamide | - ^d | 1 |
| methanol | - ^d | 1 |
| dimethylsulfoxide | - ^d | 1 |
| diethyl ether | - ^d | 1 |
| acetonitrile | - ^d | 1 |
| acetone | - ^d | 1 |

^a Time in which gels reach maximum volume.

^b Volume degree of swelling at t_{\max} . Mean values of at least three measurements.

^c Last measurement before gels disintegrated.

^d Gels remained unaffected for an infinite amount of time.

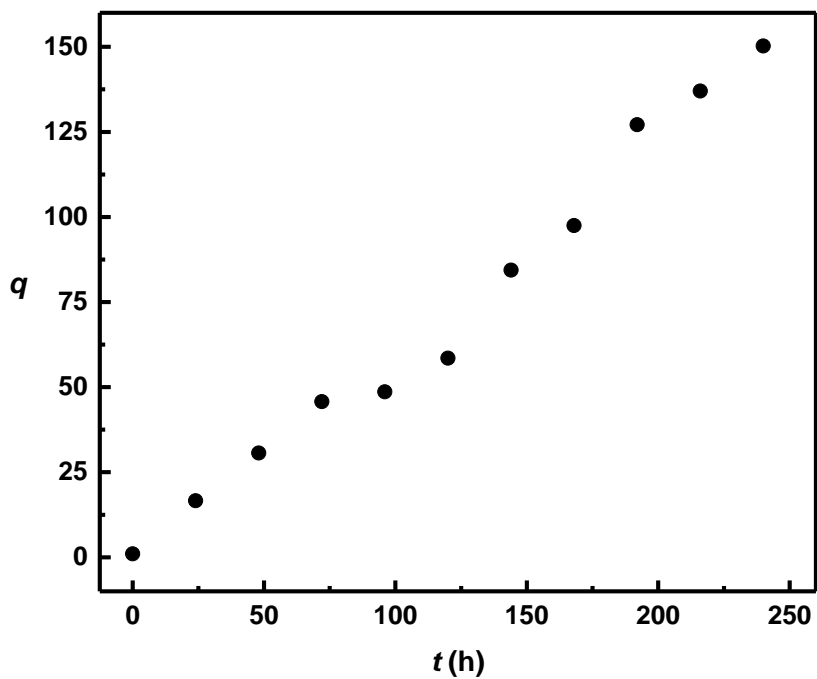


Figure 41: Swelling of a W_2 -PDCPD gel in toluene with time.

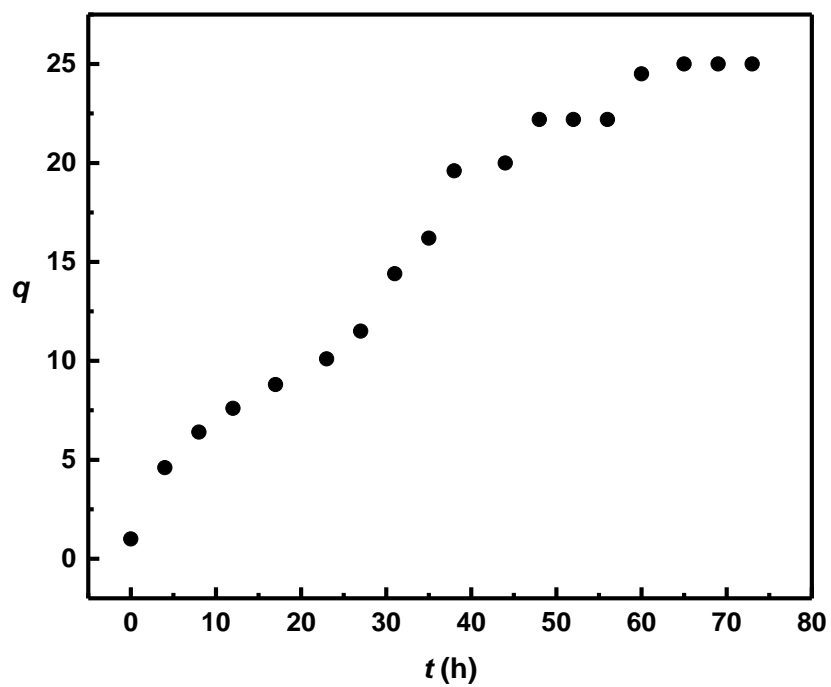


Figure 42: Swelling of a W_2 -PDCPD gel in $CHCl_3$ with time.

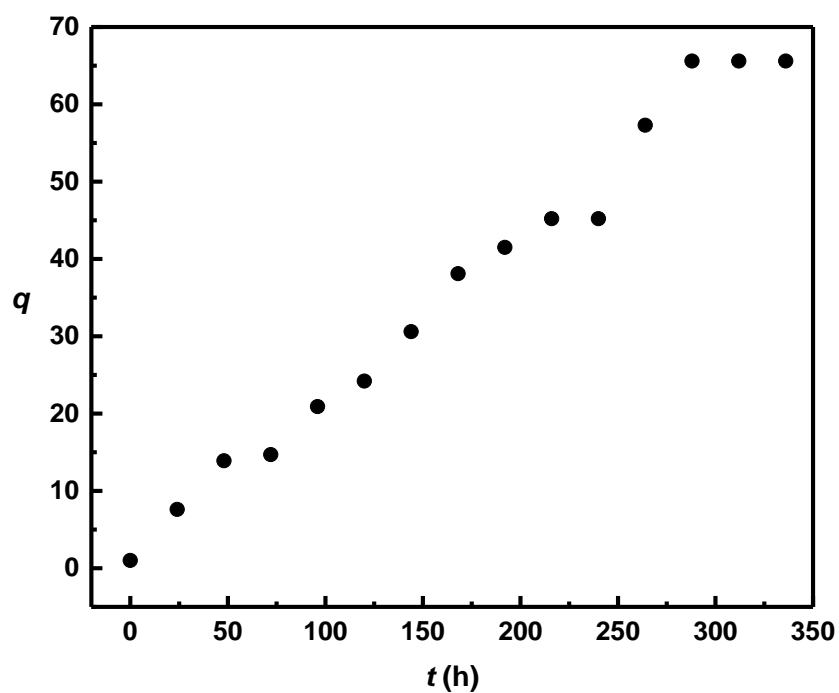


Figure 43: Swelling of a W_2 -PDCPD gel in THF with time.

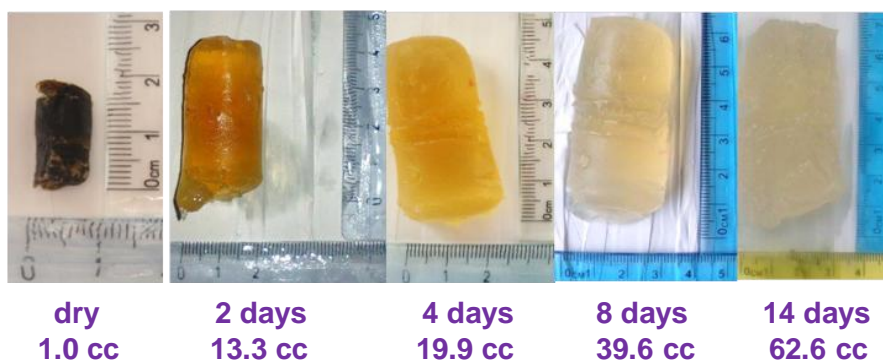


Figure 44: Swelling of a W_2 -DCPD gel in THF.

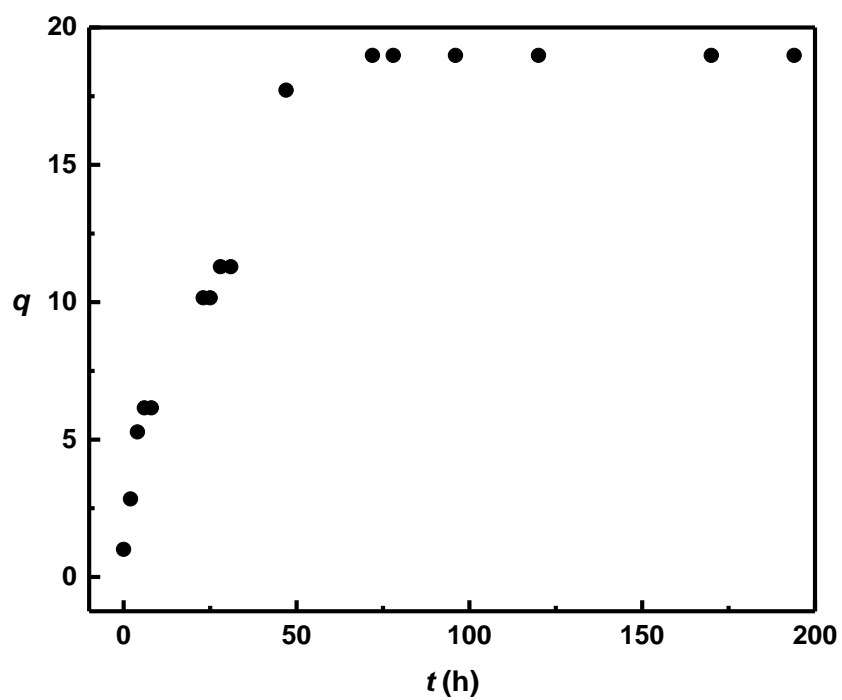


Figure 45: Swelling of a W_2 -PDCPD gel in 1,3-dichlorobenzene with time.

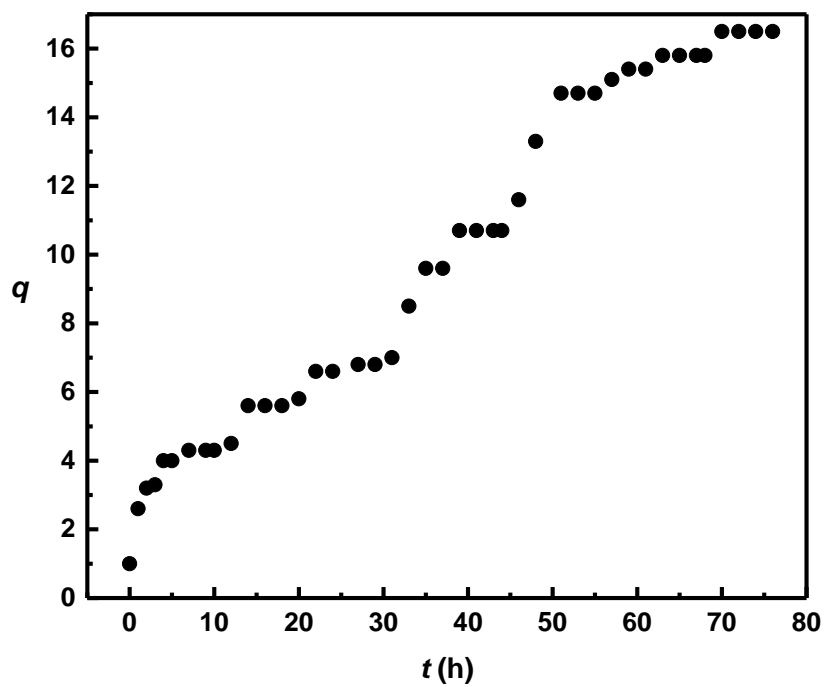


Figure 46: Swelling of a W_2 -PDCPD gel in CS_2 with time.

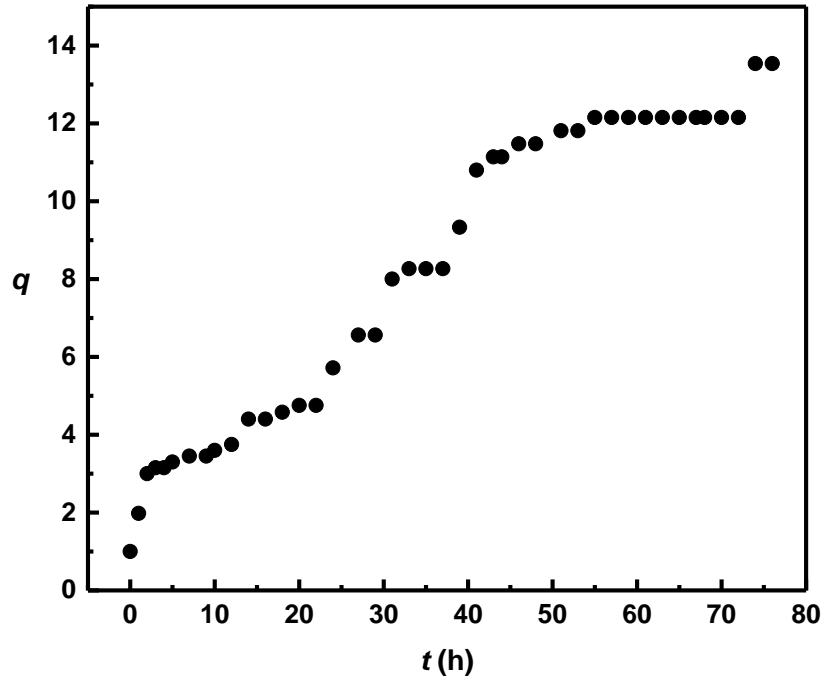


Figure 47: Swelling of a W_2 -PDCPD gel in chlorobenzene with time.

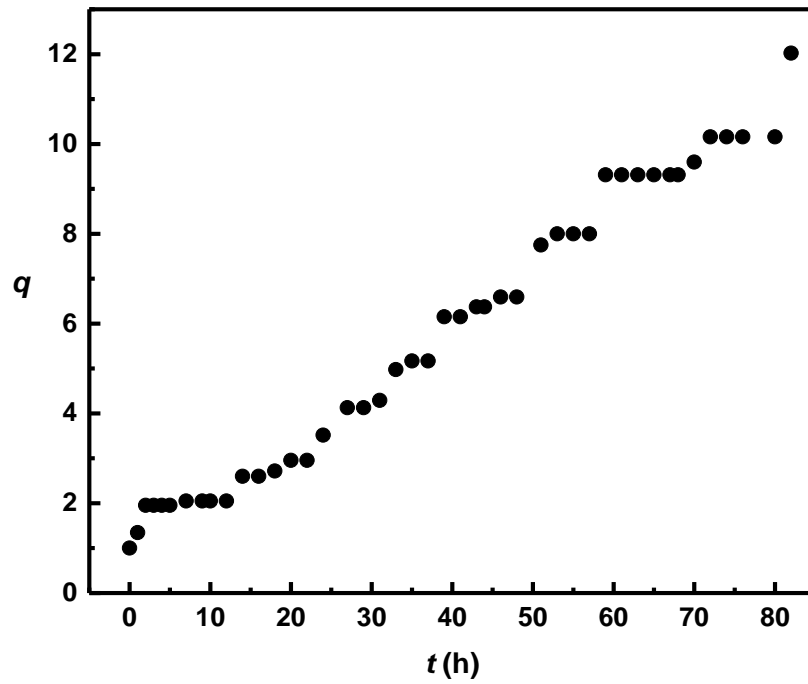


Figure 48: Swelling of a W_2 -PDCPD gel in CCl_4 with time.

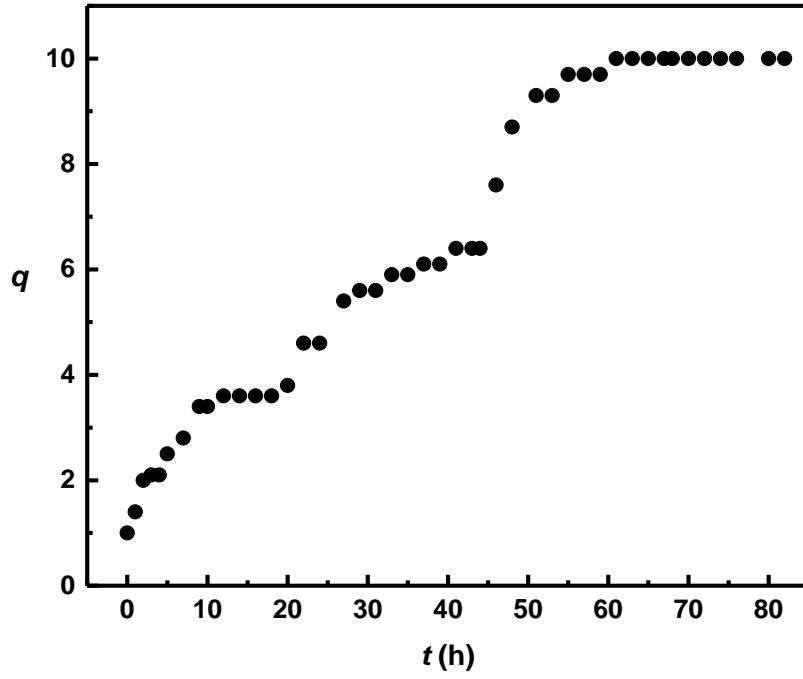


Figure 49: Swelling of a W_2 -PDCPD gel in benzene with time.

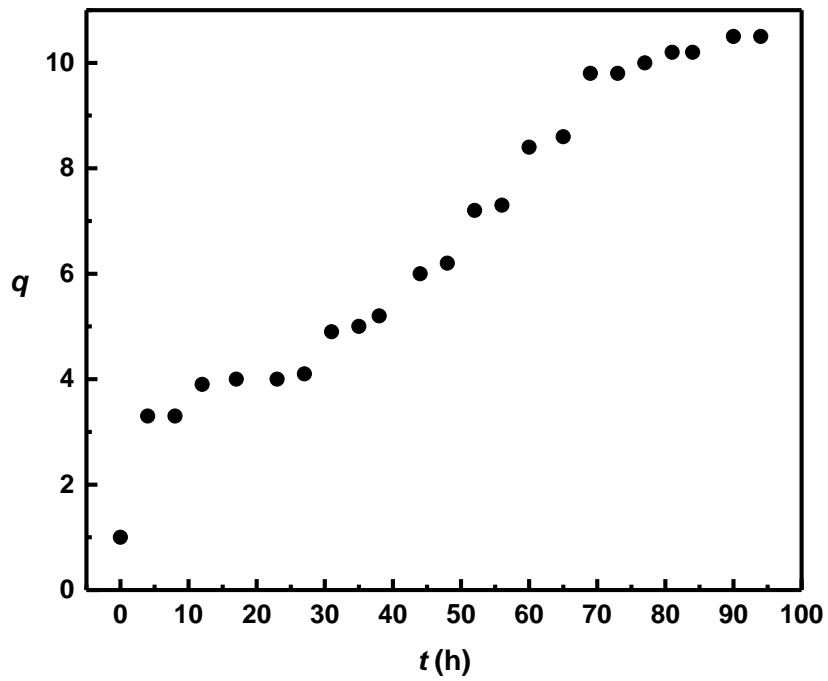


Figure 50: Swelling of a W_2 -PDCPD gel in CH_2Cl_2 with time.

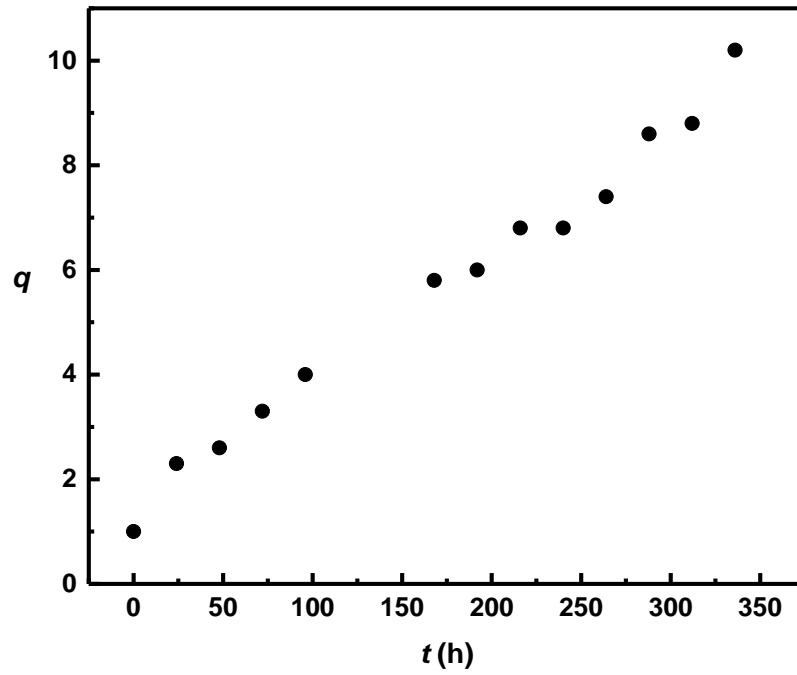


Figure 51: Swelling of a W_2 -PDCPD gel in 1,3,5-trimethylbenzene with time.

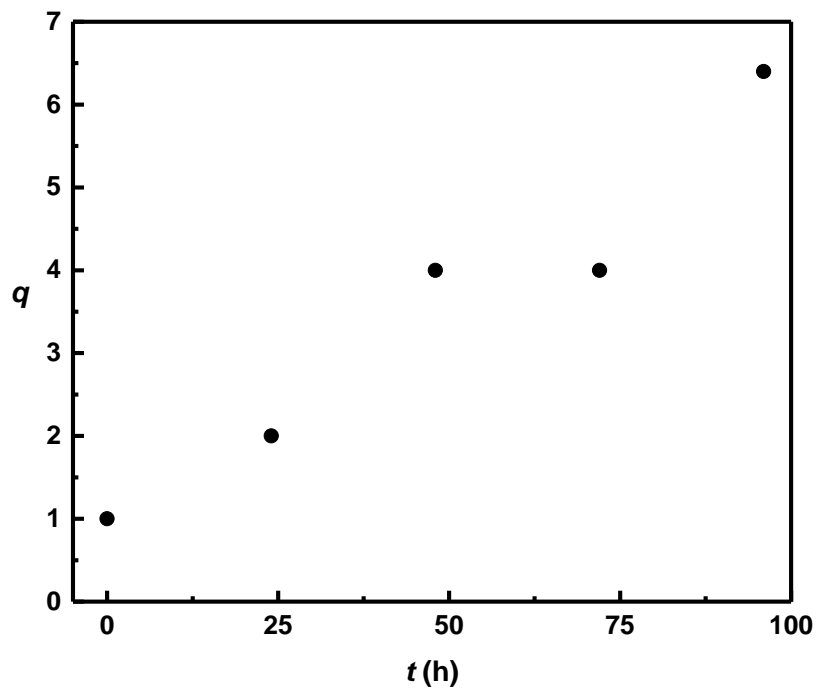


Figure 52: Swelling of a W_2 -PDCPD gel in 1,4-dimethylbenzene with time.

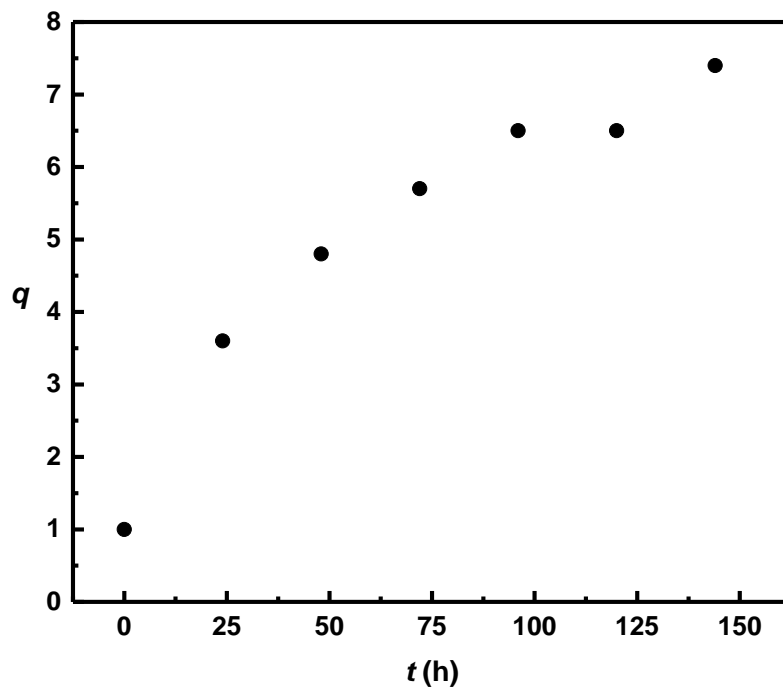


Figure 53: Swelling of a W_2 -PDCPD gel in 1,3-dimethylbenzene with time.

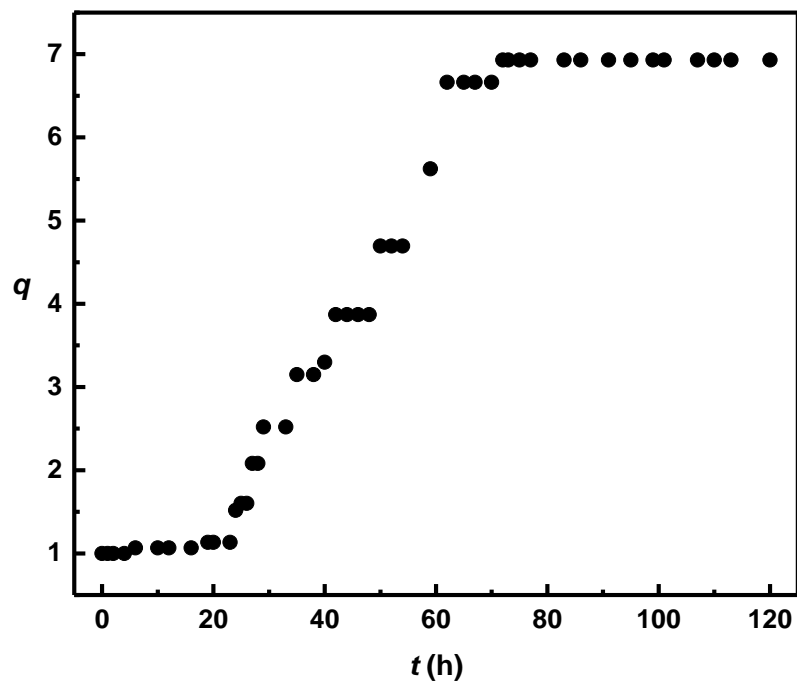


Figure 54: Swelling of a W_2 -PDCPD dry-gel in 1,2-dichlorobenzene with time.

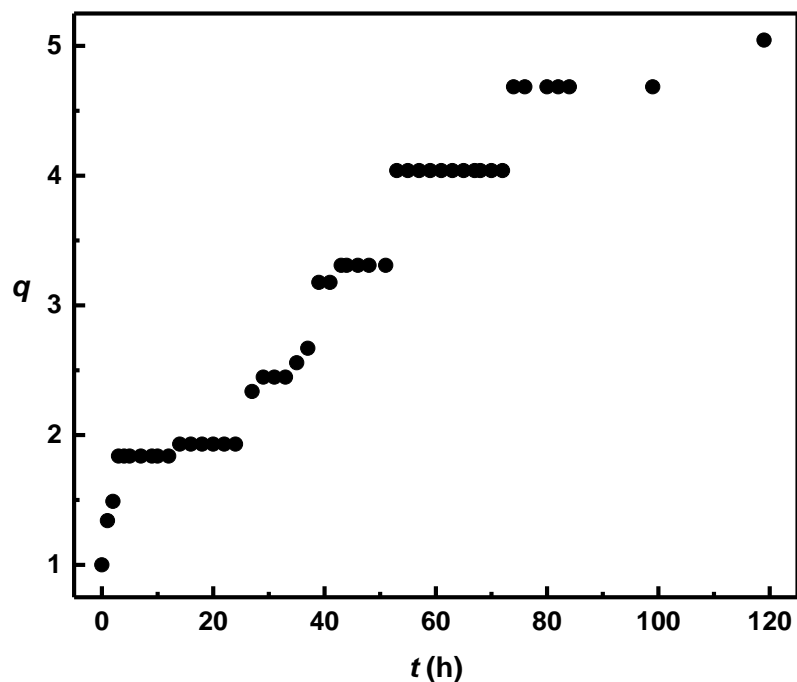


Figure 55: Swelling of a W_2 -PDCPD dry-gel in benzyl chloride with time.

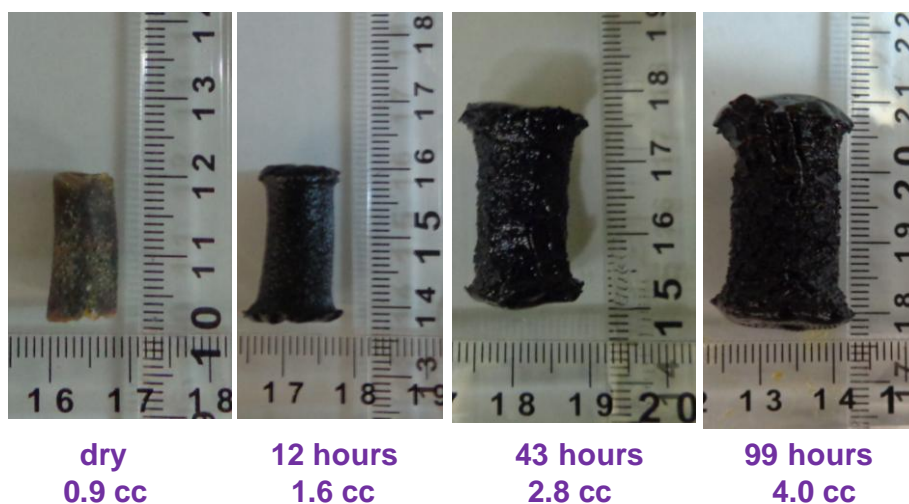


Figure 56: Swelling of a W_2 -DCPD gel in benzyl chloride.

9.3 Hansen Solubility Parameters

The swelling of insoluble polymers in various solvents can be related to the Hansen Solubility Parameters (HSP) of the solvents.^{117,118} The HSP theory takes into consideration three major types of interaction between molecules:

dispersion (D), dipole-dipole (P) and hydrogen bonding (H). The total solubility parameter (δ_T) can be calculated by equation (3), where δ_D , δ_P and δ_H are the parameters representing dispersion (Van der Waals), dipole-dipole and hydrogen bonding interactions, respectively. HSP for all solvents used in this study were taken from ref. 118 and are shown in Table 21 along with the respective maximum volume degree of swelling (q_{max}) of swollen **W₂-PDCPD** gels. Plots of q_{max} vs. δ_T , δ_D , δ_P and δ_H are shown in Figures 57-60. It is noted that q_{max} represents the maximum volume degree of swelling (i.e., the maximum volume) measured experimentally and may be different from the maximum volume degree of swelling that **W₂-PDCPD** gels could reach if they did not disintegrate. That means that q_{max} does not necessarily describe an equilibrium state. Nevertheless, considering that HSP provide only a direction for solvent selection, rather than a precise determination of the relative ability of solvents to dissolve or swell a polymer, the plots of q_{max} vs. HSP can be useful as a general guide in solvent selection.

$$\delta_T^2 = \delta_D^2 + \delta_P^2 + \delta_H^2 \quad (3)$$

Table 21: Hansen Solubility Parameters (HSP) of solvents used in this study and experimentally measured maximum degree of swelling (q_{\max}) of swollen W_2 -PDCPD gels.

| Solvent | δ_D (MPa ^{1/2}) | δ_P (MPa ^{1/2}) | δ_H (MPa ^{1/2}) | δ_T (MPa ^{1/2}) | q_{\max} |
|-------------------------------|-------------------------------------|-------------------------------------|-------------------------------------|-------------------------------------|------------|
| toluene | 18.0 | 1.4 | 2.0 | 18.2 | 115 |
| tetrahydrofuran | 16.8 | 5.7 | 8.0 | 19.5 | 66 |
| chloroform | 17.8 | 3.1 | 5.7 | 18.9 | 50 |
| carbon disulfide | 20.2 | 0.0 | 0.6 | 20.2 | 21 |
| 1,3-dichlorobenzene | 19.2 | 5.1 | 2.7 | 20.0 | 19 |
| chlorobenzene | 19.0 | 4.3 | 2.0 | 19.6 | 14 |
| carbon tetrachloride | 17.8 | 0.0 | 0.6 | 17.8 | 16 |
| methylene chloride | 17.0 | 7.3 | 7.1 | 19.8 | 10 |
| benzene | 18.4 | 0.0 | 2.0 | 18.5 | 12 |
| 1,3,5-trimethylbenzene | 18.0 | 0.6 | 0.6 | 18.0 | 9 |
| 1,4-dimethylbenzene | 17.8 | 1.0 | 3.1 | 18.1 | 7 |
| 1,3-dimethylbenzene | 18.0 | 2.3 | 2.3 | 18.3 | 7 |
| 1,2-dichlorobenzene | 19.2 | 6.3 | 3.3 | 20.5 | 7 |
| cyclohexane | 16.8 | 0.0 | 0.2 | 16.8 | 5 |
| benzyl chloride | 18.8 | 7.1 | 2.6 | 20.3 | 5 |
| 1,4-dioxane | 17.5 | 1.8 | 9.0 | 19.8 | 4 |
| cyclohexanone | 17.8 | 8.4 | 5.1 | 20.3 | 4 |
| water | 15.5 | 16.0 | 42.3 | 47.8 | 1 |
| pentane | 14.5 | 0.0 | 0.0 | 14.5 | 1 |
| <i>N,N</i> -dimethylformamide | 17.4 | 13.7 | 11.3 | 24.9 | 1 |
| methanol | 14.7 | 12.3 | 22.3 | 29.4 | 1 |
| dimethylsulfoxide | 18.4 | 16.4 | 10.2 | 26.7 | 1 |
| diethyl ether | 14.5 | 2.9 | 4.6 | 15.5 | 1 |
| acetonitrile | 15.3 | 18.0 | 6.1 | 24.4 | 1 |
| acetone | 15.5 | 10.4 | 7.0 | 19.9 | 1 |

From Table 20 along with the plot of q_{\max} vs. the total solubility parameter (δ_T ; Figure 57) two conclusions can be drawn: (a) **W_2 -PDCPD** gels did not swell in solvents with $\delta_T > 24$ MPa^{1/2} and (b) **W_2 -PDCPD** gels swelled (to a very

different extent) in solvents with δ_T in the range of 14-24 MPa^{1/2} - although they did not swell in pentane ($\delta_T = 14.5$ MPa^{1/2}), diethyl ether ($\delta_T = 15.5$ MPa^{1/2}) and acetone ($\delta_T = 19.9$ MPa^{1/2}). Since δ_T is composed of three individual components, the dependence of swelling on each one of the three components (δ_D , δ_P and δ_H) was also examined by plotting q_{max} vs. δ_D , δ_P and δ_H (Figures 58-60). No clear trend was identified for δ_H (Figure 58); data points are quite scattered. For δ_P (Figure 59) a trend similar to the trend between q_{max} and δ_T was observed; **W₂-PDCPD** gels did not swell in solvents with $\delta_P > 10$ MPa^{1/2}. There are two exceptions among the solvents in which gels did swell ($\delta_P < 10$ MPa^{1/2}): pentane ($\delta_P = 0.0$ MPa^{1/2}) and diethyl ether ($\delta_P = 2.9$ MPa^{1/2}). For δ_D (Figure 60) an analogous trend was observed; **W₂-PDCPD** gels did not swell in solvents with $\delta_D < 16$ MPa^{1/2}. There are again two solvents that did not follow that trend: DMF ($\delta_D = 17.4$ MPa^{1/2}) and DMSO ($\delta_D = 18.4$ MPa^{1/2}); in those solvents, gels did not swell.

Those results indicate that the P- and D-components, that is dispersion and dipole-dipole interactions, are the most important parameters that affect the swelling behavior of **W₂-PDCPD** gels. This conclusion is in agreement with the chemical composition and structure of **PDCPD**, which excludes hydrogen bonding. The fact that in all cases there are two or three solvents that do not follow the trend reveals the complexity of this matter, and suggests that more than one parameter have to be taken into account in order to understand the swelling behavior of **W₂-PDCPD** gels.

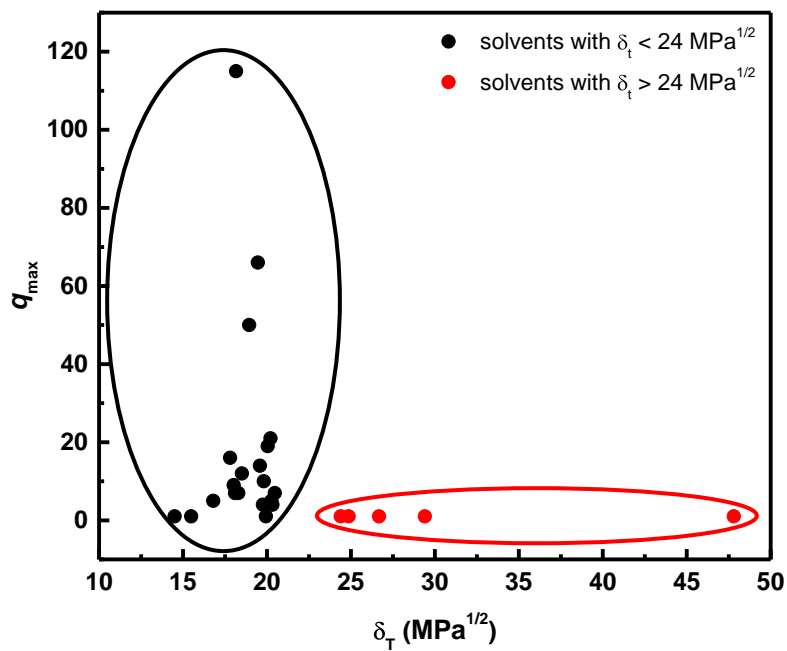


Figure 57: Relation between the maximum volume degree of swelling (q_{\max}) of W_2 -PDCPD gels and the total solubility parameter (δ_T) of the respective solvents.

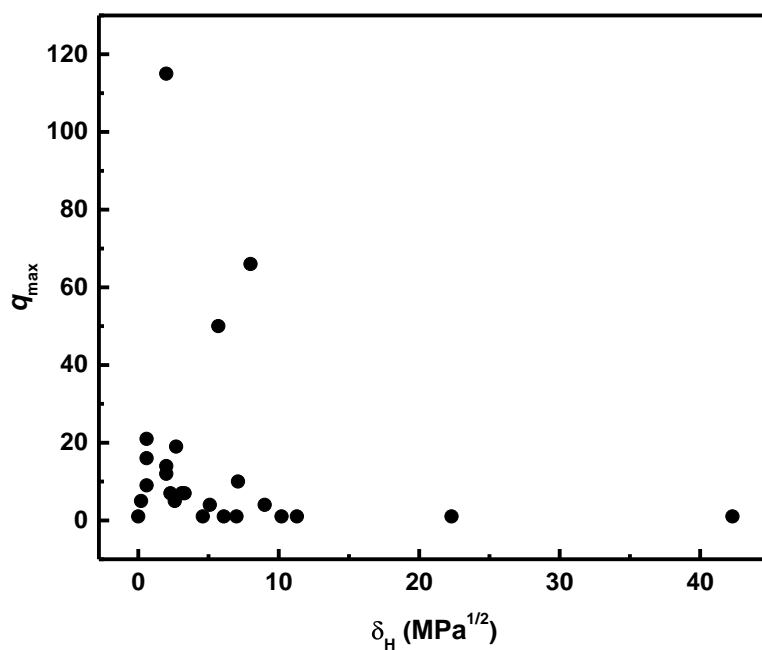


Figure 58: Relation between the maximum volume degree of swelling (q_{\max}) of W_2 -PDCPD gels and the Hansen H-component (δ_H) of the respective solvents.

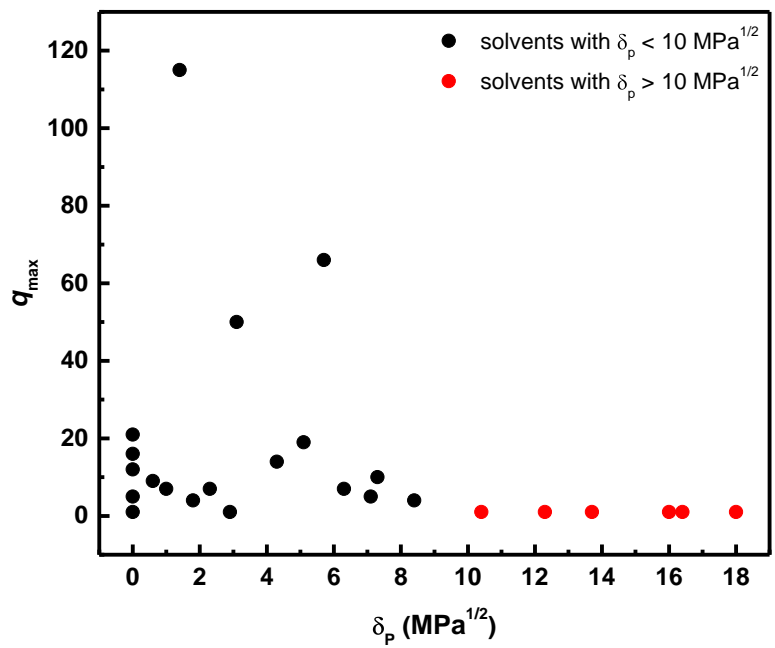


Figure 59: Relation between the maximum volume degree of swelling (q_{max}) of W_2 -PDCPD gels and the Hansen P-component (δ_p) of the respective solvents.

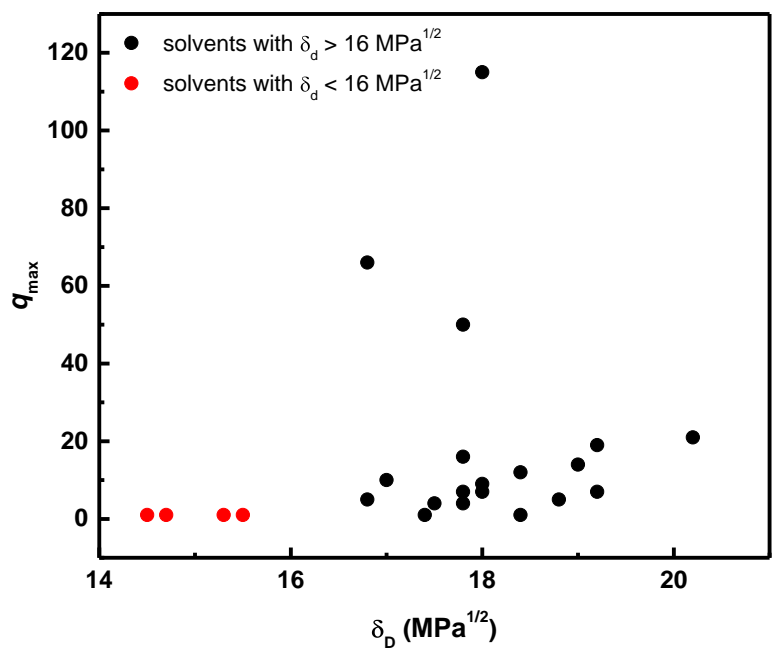


Figure 60: Relation between the maximum volume degree of swelling (q_{max}) of W_2 -PDCPD gels and the Hansen D-component (δ_D) of the respective solvents.

The HSP theory can be used to estimate the HSP of a polymer from the experimental swelling data of that polymer (i.e., **W₂-PDCPD**). To that end, a 3D plot of the individual solubility parameters for each solvent tested was drawn using the HSPiP software 5.0.04. A sphere was constructed with all “good” solvents (in our case “good” solvents are those in which **W₂-PDCPD** gels swelled) inside the sphere and all “bad” solvents (in our case “bad” solvents are those in which no swelling was observed) outside the sphere. There are 2 methods to construct that sphere. According to the 1st method solvents are categorized as “good” or “bad”. According to the 2nd method solvents are given scores in the range of 1 to 6: “1” is given to the “best” solvents and “6” is given to the “worst” solvents. With either method the center of the sphere represents the HSP of **W₂-PDCPD**. Solvents located closer to the center of the sphere would be expected to cause more extensive swelling. The radius of the sphere (R) defines the limits of “happiness”, as stated in the software website. In the case of crosslinked polymers, such as **W₂-PDCPD**, “happiness” is defined as “swells significantly”.

1st Method: Inside-Out Solvents

Table 22 shows the HSP of all solvents used in this study, their empirical classification as score 1 solvents (gels swelled) or score 0 solvents (gels did not swell) and the corresponding RED (Relative Energy Difference) values. RED values were calculated using the formula: RED = (distance of solvent from the center of the sphere) / (radius of the sphere). RED values close to 0 indicate higher, and RED values close to 1 indicate lower affinity of the solvent with the molecule under study (located at the center of the sphere).

Figure 61 shows the generated sphere (R = 5.9) and the HSP (in MPa^{1/2}) for **W₂-PDCPD**: $\delta_D = 18.4$, $\delta_P = 3.3$, $\delta_H = 3.8$ and $\delta_T = 19.1$. The 2D plots (Figure 62) display the boundaries in PDH space and help visualize whether the solvents tested cover sufficiently the entire range of each solubility parameter (δ_P , δ_D , and δ_H). It is evident from the data of Figure 62, that the range of δ_P and δ_D is mostly covered. More solvents should have been tested to cover sufficiently the δ_H range, although that seems to be less important for our

system, because **PDCPD** is essentially a hydrocarbon, and therefore lacks the ability to form hydrogen bonds.

Table 22: Hansen Solubility Parameters (HSP) of the solvents used in this study, scoring according to whether they are good solvents (1) or non-solvents (0), and calculated Relative Energy Differences (RED).

| Solvents | δP | δD | δH | score | RED |
|---------------------------|------------------------------|------------------------------|------------------------------|--------------|------------|
| m-Xylene | 18.0 | 2.3 | 2.3 | 1 | 0.335 |
| Chloroform | 17.8 | 3.1 | 5.7 | 1 | 0.384 |
| Chlorobenzene | 19.0 | 4.3 | 2.0 | 1 | 0.402 |
| m-Dichlorobenzene | 19.2 | 5.1 | 2.7 | 1 | 0.446 |
| p-Xylene | 17.8 | 1.0 | 3.1 | 1 | 0.458 |
| Toluene | 18.0 | 1.4 | 2.0 | 1 | 0.465 |
| o-Dichlorobenzene | 19.2 | 6.3 | 3.3 | 1 | 0.580 |
| Benzene | 18.4 | 0.0 | 2.0 | 1 | 0.640 |
| Benzyl Chloride | 18.8 | 7.1 | 2.6 | 1 | 0.685 |
| Mesitylene | 18.0 | 0.6 | 0.6 | 1 | 0.723 |
| Carbon Tetrachloride | 17.8 | 0.0 | 0.6 | 1 | 0.806 |
| Cyclohexanone | 17.8 | 8.4 | 5.1 | 1 | 0.912 |
| 1,4-Dioxane | 17.5 | 1.8 | 9.0 | 1 | 0.969 |
| Tetrahydrofuran (THF) | 16.8 | 5.7 | 8.0 | 1 | 0.982 |
| Cyclohexane | 16.8 | 0.0 | 0.2 | 1 | 0.990 |
| Carbon Disulfide | 20.2 | 0.0 | 0.6 | 1 | 0.991 |
| Methylene Dichloride | 1.7 | 7.3 | 7.1 | 1 | 0.997 |
| Diethyl Ether | 14.5 | 2.9 | 4.6 | 0 | 1.330 |
| Pentane | 14.5 | 0.0 | 0.0 | 0 | 1.573 |
| Acetone | 15.5 | 10.4 | 7.0 | 0 | 1.643 |
| Dimethyl Formamide (DMF) | 17.4 | 13.7 | 11.3 | 0 | 2.197 |
| Dimethyl Sulfoxide (DMSO) | 18.4 | 16.4 | 10.2 | 0 | 2.469 |
| Acetonitrile | 15.3 | 18.0 | 6.1 | 0 | 2.728 |
| Methanol | 14.7 | 12.3 | 22.3 | 0 | 3.705 |
| Water | 15.5 | 16.0 | 42.3 | 0 | 6.941 |

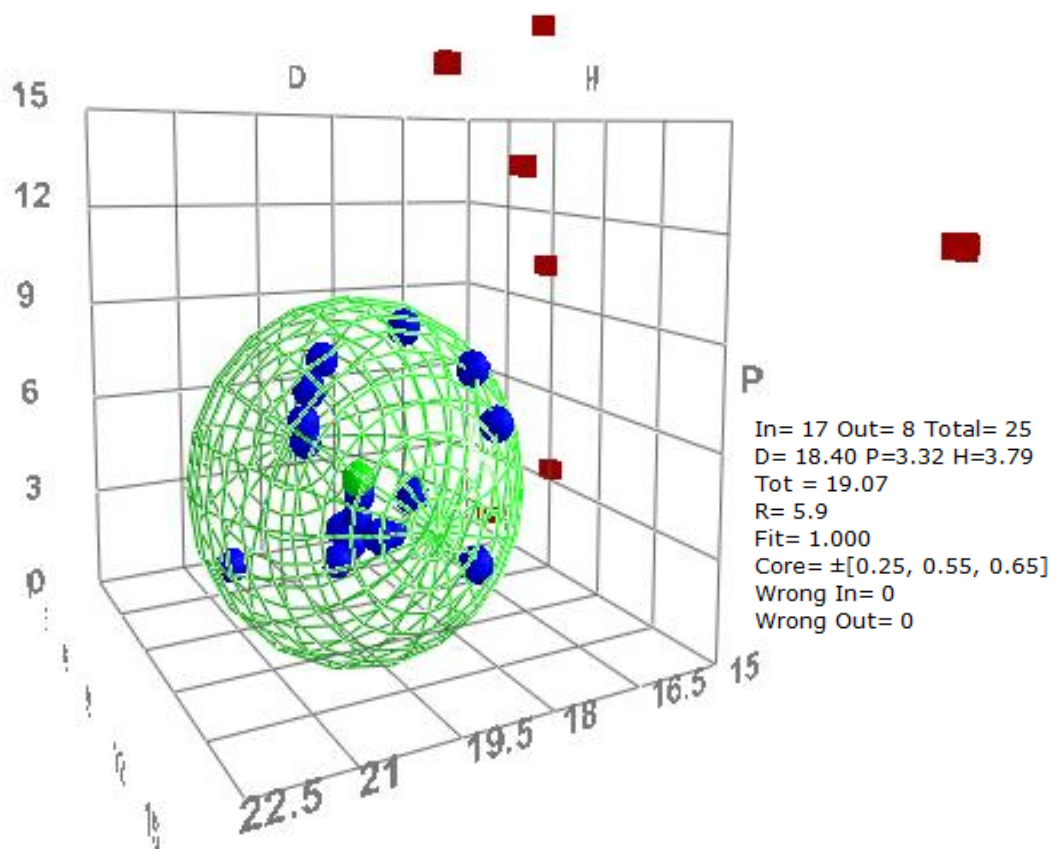


Figure 61: 3D plot of the individual Hansen Solubility Parameters (HSP) for each solvent tested. Blue dots represent solvents in which W_2 -PDCPD gels swelled (“good” solvents). Red squares represent solvents in which no swelling was observed (“bad” solvents). The green dot represents W_2 -PDCPD. The green sphere contains all “good” solvents; the center of the sphere is a reasonable estimate of the HSP of W_2 -PDCPD.

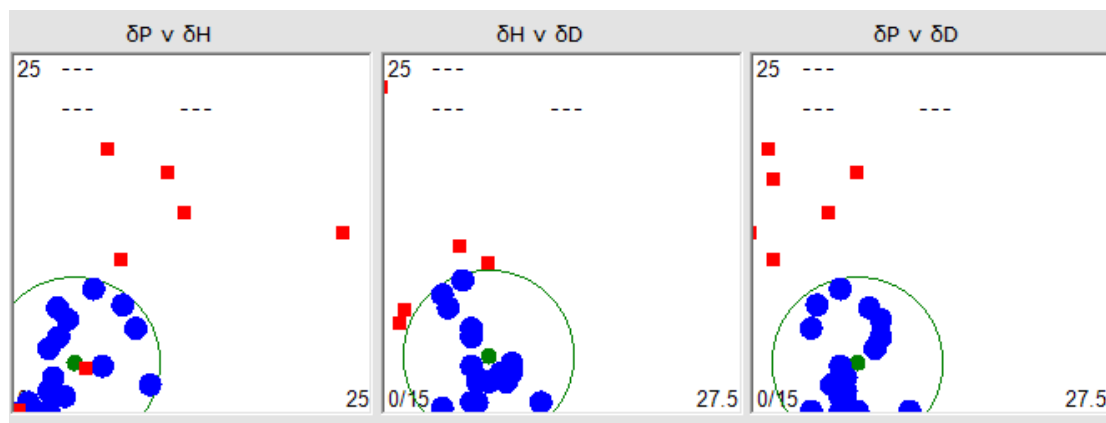


Figure 62: 2D plots of the individual Hansen Solubility Parameters (HSP) for each solvent tested, as indicated. Blue dots represent solvents in which W_2 -PDCPD gels swelled (“good” solvents). Red squares represent solvents in which no swelling was observed (“bad” solvents). The green dot represents W_2 -PDCPD. The green circle contains all “good” solvents.

2nd Method: Score 1-6 Solvents

Table 23 shows the HSP and the molar volume of all solvents used in this study, their classification as “gels swelled extremely” (score 1), to “gels did not swell” (score 6) and the calculated RED values. Solvents have been classified according to the experimental q_{\max} values as follows: “1” for $q_{\max} > 100$, “2” for $q_{\max} \geq 50$, “3” for $q_{\max} > 10$, “4” for $q_{\max} = 5-10$, “5” for $q_{\max} < 5$ and “6” for $q_{\max} = 1$.

Figure 63 shows the generated sphere ($R = 5.9$) and the HSP (in $\text{MPa}^{1/2}$) for **W₂-PDCPD**: $\delta_D = 18.4$, $\delta_P = 3.3$, $\delta_H = 3.8$ and $\delta_T = 19.1$. Those values are identical with the values calculated *via* the 1st method. The 2D plots (Figure 64) are also identical with those generated *via* the 1st method.

The HSP of **W₂-PDCPD** have also been estimated using a theoretical method that relies on the structure of the repeating unit. Those values, $\delta_D = 16.7$, $\delta_P = 0.5$, $\delta_H = 3.4$ and $\delta_T = 17.0 \text{ MPa}^{1/2}$, were significantly different from those calculated from the sphere. The HSP calculated *via* the previous methods are considered more reliable for two reasons: (a) those methods use experimental data, while the theoretical method relies heavily on assumptions about the structure of the polymer; and, (b) **W₂-PDCPD** is not a linear polymer; its structure is complicated by random crosslinking *via* metathesis as well as *via* radical coupling (Scheme 14), thereby neither the repeat unit nor the molecular mass can be estimated with any measure of confidence.

HSP for **DCPD** monomer have been calculated using the same software: $\delta_D = 17.2$, $\delta_P = 2.4$, $\delta_H = 3.0$ and $\delta_T = 17.7 \text{ MPa}^{1/2}$. **DCPD** is located inside the sphere ($\text{RED} = 0.438$, Figure 65). We note that the polymer and the monomer do not change functionality (both are hydrocarbons). Therefore, it is not surprising that the HSP for those two compounds are very similar.

Table 23: Hansen Solubility Parameters (HSP) of the solvents used in this study, scoring according to their swelling capacity from 1 (maximum swelling observed) to 6 (no swelling observed), and calculated Relative Energy Differences (RED).

| Solvents | δ_P | δ_D | δ_H | score | RED |
|---------------------------|------------|------------|------------|--------------|------------|
| m-Xylene | 18.0 | 2.3 | 2.3 | 4 | 0.335 |
| Chloroform | 17.8 | 3.1 | 5.7 | 2 | 0.384 |
| Chlorobenzene | 19.0 | 4.3 | 2.0 | 3 | 0.402 |
| m-Dichlorobenzene | 19.2 | 5.1 | 2.7 | 3 | 0.446 |
| p-Xylene | 17.8 | 1.0 | 3.1 | 4 | 0.458 |
| Toluene | 18.0 | 1.4 | 2.0 | 1 | 0.465 |
| o-Dichlorobenzene | 19.2 | 6.3 | 3.3 | 4 | 0.580 |
| Benzene | 18.4 | 0.0 | 2.0 | 3 | 0.640 |
| Benzyl Chloride | 18.8 | 7.1 | 2.6 | 4 | 0.685 |
| Mesitylene | 18.0 | 0.6 | 0.6 | 4 | 0.723 |
| Carbon Tetrachloride | 17.8 | 0.0 | 0.6 | 3 | 0.806 |
| Cyclohexanone | 17.8 | 8.4 | 5.1 | 5 | 0.912 |
| 1,4-Dioxane | 17.5 | 1.8 | 9.0 | 5 | 0.969 |
| Tetrahydrofuran (THF) | 16.8 | 5.7 | 8.0 | 2 | 0.982 |
| Cyclohexane | 16.8 | 0.0 | 0.2 | 5 | 0.990 |
| Carbon Disulfide | 20.2 | 0.0 | 0.6 | 3 | 0.991 |
| Methylene Dichloride | 1.7 | 7.3 | 7.1 | 4 | 0.997 |
| Diethyl Ether | 14.5 | 2.9 | 4.6 | 6 | 1.330 |
| Pentane | 14.5 | 0.0 | 0.0 | 6 | 1.573 |
| Acetone | 15.5 | 10.4 | 7.0 | 6 | 1.643 |
| Dimethyl Formamide (DMF) | 17.4 | 13.7 | 11.3 | 6 | 2.197 |
| Dimethyl Sulfoxide (DMSO) | 18.4 | 16.4 | 10.2 | 6 | 2.469 |
| Acetonitrile | 15.3 | 18.0 | 6.1 | 6 | 2.728 |
| Methanol | 14.7 | 12.3 | 22.3 | 6 | 3.705 |
| Water | 15.5 | 16.0 | 42.3 | 6 | 6.941 |

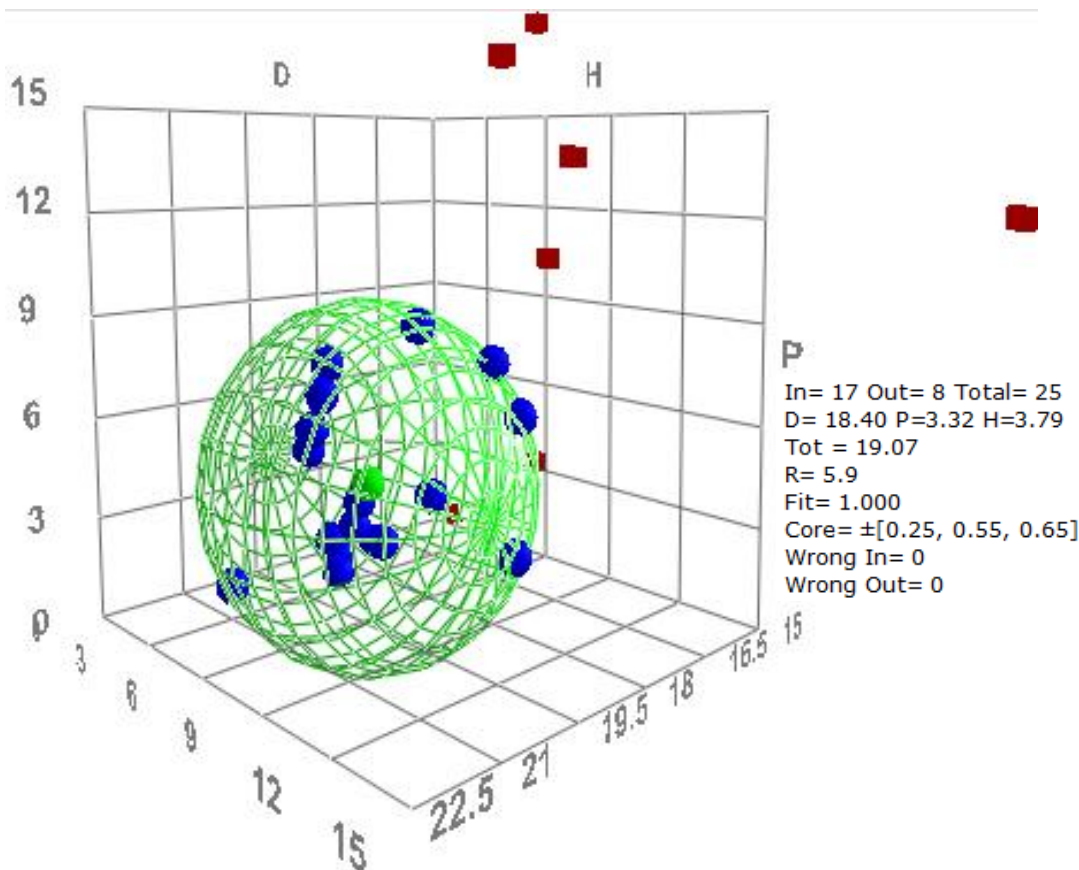


Figure 63: 3D plot of the individual Hansen Solubility Parameters (HSP) for each solvent tested. Blue dots represent solvents in which W_2 -PDCPD gels swelled (“good” solvents). Red squares represent solvents in which no swelling was observed (“bad” solvents). The green dot represents W_2 -PDCPD. The green sphere contains all “good” solvents; the center of the sphere is a reasonable estimate the HSP of W_2 -PDCPD.

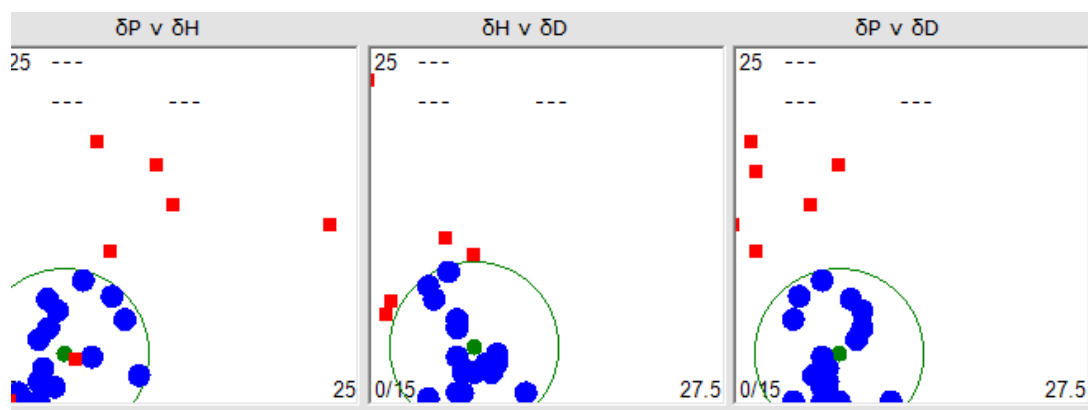


Figure 64: 2D plots of the individual Hansen Solubility Parameters (HSP) for each solvent tested, as indicated. Blue dots represent solvents in which W_2 -PDCPD gels swelled (“good” solvents). Red squares represent solvents in which no swelling was observed (“bad” solvents). The green dot represents W_2 -PDCPD. The green circle contains all “good” solvents.

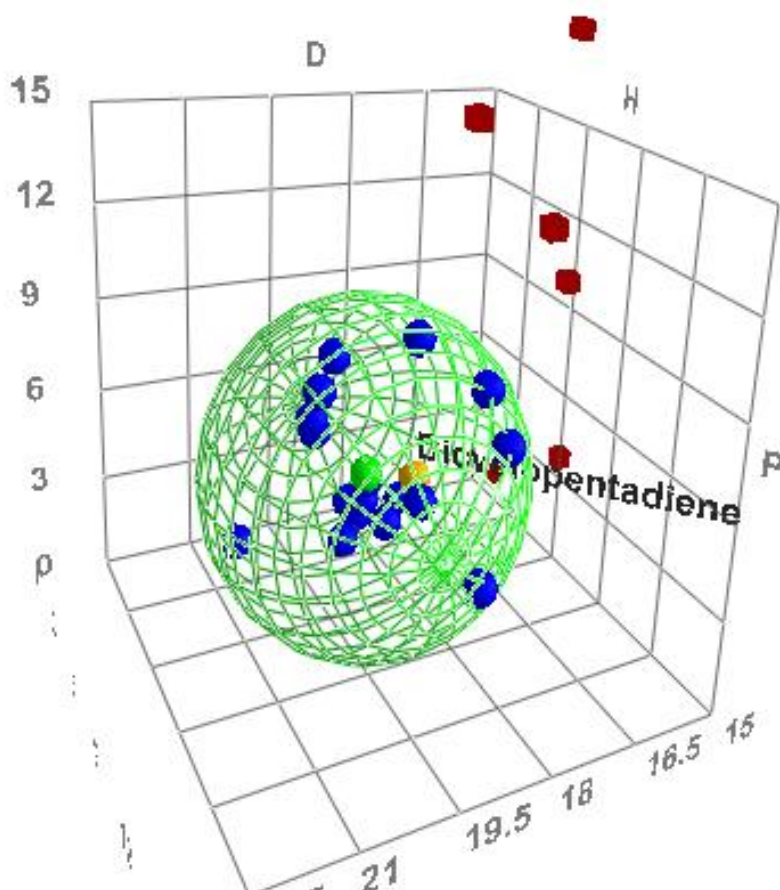


Figure 65: Same as Figure 63 showing also the location of DCPD (orange dot).

According to those results, toluene, for which we have observed the highest volume degree of swelling ($q_{\max} = 115$), is not the solvent closest to the center of the sphere (RED = 0.465); *m*- and *p*-xylenes, chlorobenzene, *m*-dichlorobenzene ($q_{\max} = 7-19$; Table 20) and chloroform ($q_{\max} = 50$) are closer to the center of the sphere than toluene, thereby are predicted to be “better” solvents than toluene, i.e., **W₂-PDCPD** gels would have been expected to swell more in those solvents than in toluene. That inconsistency between the HSP theory and experiment may be attributed to the fact that in all the “better” solvents gels disintegrated while they were still swelling, and therefore they did not reach maximum (equilibrium) volumes. Another notable inconsistency is THF. The RED value for THF is equal to 0.982, meaning that THF is located close to the surface of the sphere, while from the experimental q_{\max} value (66) we would expect that THF would be located close to the center of the sphere. At the moment we cannot account for this result. After all, as was stated above, this method is only a guideline for solvent selection.

Another useful parameter than can be calculated is the HSP distance between a solvent and the polymer, conventionally referred to as R_a . R_a is a measure of how alike the two molecules are and can be calculated using equation (4), where in our case 1 refers to the **W₂-PDCPD** and 2 refers to the solvent. The smaller the R_a value the more likely for the two molecules to be compatible. R_a values for **W₂-PDCPD** gels are shown on Table 24. The results are in general agreement with our previous findings; however, with this method a new clear trend can be observed: **W₂-PDCPD** gels swell in solvents with $R_a < 6$, and do not swell at all in solvents with $R_a > 8$ (7.9). Nevertheless, a quantitative correlation of swelling to the R_a values is risky and was not attempted, because in most solvents gels did not reach equilibrium-swelling.

$$Ra^2 = 4(\delta_{D1} - \delta_{D2})^2 + (\delta_{P1} - \delta_{P2})^2 + (\delta_{H1} - \delta_{H2})^2 \quad (4)$$

Table 24: Hansen Solubility Parameters (HSP) of solvents used in this study, experimentally measured maximum normalized volumes ($V_{\text{norm,max}}$) of swollen W_2 -PDCPD gels and calculated Ra values.

| Solvent | δ_D (MPa ^{1/2}) | δ_P (MPa ^{1/2}) | δ_H (MPa ^{1/2}) | q_{max} | Ra ^a |
|-------------------------------|-------------------------------------|-------------------------------------|-------------------------------------|------------------|-----------------|
| toluene | 18.0 | 1.4 | 2.0 | 115 | 2.7 |
| tetrahydrofuran | 16.8 | 5.7 | 8.0 | 66 | 5.8 |
| chloroform | 17.8 | 3.1 | 5.7 | 50 | 2.3 |
| carbon disulfide | 20.2 | 0.0 | 0.6 | 21 | 5.8 |
| 1,3-dichlorobenzene | 19.2 | 5.1 | 2.7 | 19 | 2.6 |
| chlorobenzene | 19.0 | 4.3 | 2.0 | 14 | 2.4 |
| carbon tetrachloride | 17.8 | 0.0 | 0.6 | 16 | 4.8 |
| methylene chloride | 17.0 | 7.3 | 7.1 | 10 | 5.9 |
| benzene | 18.4 | 0.0 | 2.0 | 12 | 3.8 |
| 1,3,5-trimethylbenzene | 18.0 | 0.6 | 0.6 | 9 | 4.3 |
| 1,4-dimethylbenzene | 17.8 | 1.0 | 3.1 | 7 | 2.7 |
| 1,3-dimethylbenzene | 18.0 | 2.3 | 2.3 | 7 | 2.0 |
| 1,2-dichlorobenzene | 19.2 | 6.3 | 3.3 | 7 | 3.4 |
| cyclohexane | 16.8 | 0.0 | 0.2 | 5 | 5.8 |
| benzyl chloride | 18.8 | 7.1 | 2.6 | 5 | 4.1 |
| 1,4-dioxane | 17.5 | 1.8 | 9.0 | 4 | 5.7 |
| cyclohexanone | 17.8 | 8.4 | 5.1 | 4 | 5.4 |
| water | 15.5 | 16.0 | 42.3 | 1 | 41.0 |
| pentane | 14.5 | 0.0 | 0.0 | 1 | 9.3 |
| <i>N,N</i> -dimethylformamide | 17.4 | 13.7 | 11.3 | 1 | 13.0 |
| methanol | 14.7 | 12.3 | 22.3 | 1 | 21.9 |
| dimethylsulfoxide | 18.4 | 16.4 | 10.2 | 1 | 14.6 |
| diethyl ether | 14.5 | 2.9 | 4.6 | 1 | 7.9 |
| acetonitrile | 15.3 | 18.0 | 6.1 | 1 | 16.1 |
| acetone | 15.5 | 10.4 | 7.0 | 1 | 9.7 |

^a Calculated from equation (4) using HSP for W_2 -PDCPD: $\delta_D = 18.4$, $\delta_P = 3.3$, $\delta_H = 3.8$.

9.4 Separation of organic solvents from water

With an eye on environmental remediation, the swelling studies above suggest that **W₂-PDCPD** gels should be evaluated for their ability to uptake and separate chlorinated solvents from water.

The presence of organic pollutants in water is a serious threat for human health. Chlorinated solvents, in particular, can cause various problems in humans, with dichloromethane having been found toxic for the liver and kidneys as well as harmful to the nervous and reproductive system,^{119,120} chloroform being carcinogenic¹²¹ and responsible for liver damage¹²² and carbon tetrachloride causing damage to several tissues.^{123–125} Furthermore, when chlorinated solvents reach groundwater, their low solubility can give them a long life span, while they can still increase their concentration above the regulatory levels for drinking water.¹²⁶ Given the above, the importance of removing said pollutants from water becomes evident. Although in recent years the focus is mainly given on destructive ways of chlorinated solvents removal, non-destructive physicochemical methods are still employed because they are reliable and give the possibility to recycle the pollutants.¹²⁷ Activated carbons,¹²⁸ carbon nanotubes,¹²⁹ graphene¹³⁰ and sol-gel silica substrates¹³¹ are some of the materials that have been used to absorb solvents.

Figures 66-70 show the relevant experiments and Table 25 summarizes the results of that study. **W₂-PDCPD** gels showed the highest absorption capability for CHCl₃ (14 g of solvent/g of gel), followed by 1,3-dichlorobenzene (12 g of solvent per g of dry-gel), CH₂Cl₂ (10 g of solvent per g of dry-gel), chlorobenzene (8 g of solvent per g of dry-gel) and benzyl chloride (7 g of solvent per g of dry-gel).

The uptake of CHCl₃ by **W₂-PDCPD** gels is almost equal to the uptake by conjugated microporous (co)polymers synthesized from 1,3,5-triethynylbenzene or 1,3,5-triethynylbenzene and 1,4-diethynylbenzene.¹³² **W₂-PDCPD** gels exhibited remarkably higher uptakes (~ 12× higher for CHCl₃, and ~ 4× higher for CH₂Cl₂) than those reported for disulfide-linked polymeric

networks based on trimethylolpropane tris(3-mercaptopropionate), or on pentaerythritol tetrakis(3-mercaptopropionate).¹³³

Although a number of synthetic organic polymers have been used to absorb organic solvents^{132–136} or separate oil from water,^{134,137–141} there have been no reported examples regarding separations of chlorinated solvents from water with those materials.

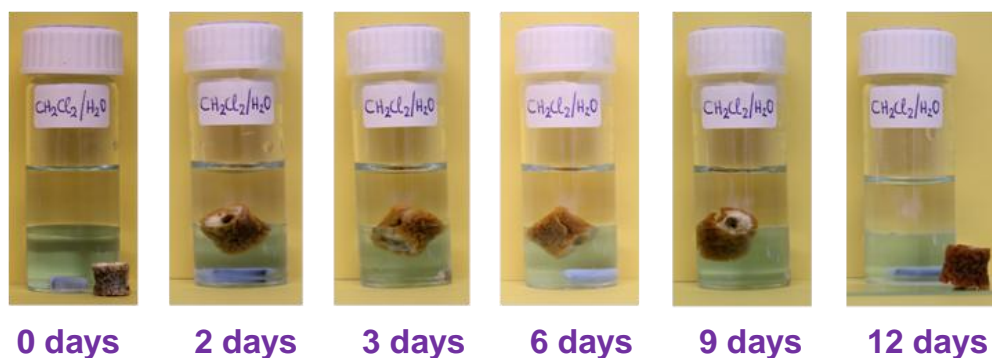


Figure 66: Separation of CH_2Cl_2 (dyed with Sudan blue) from water.

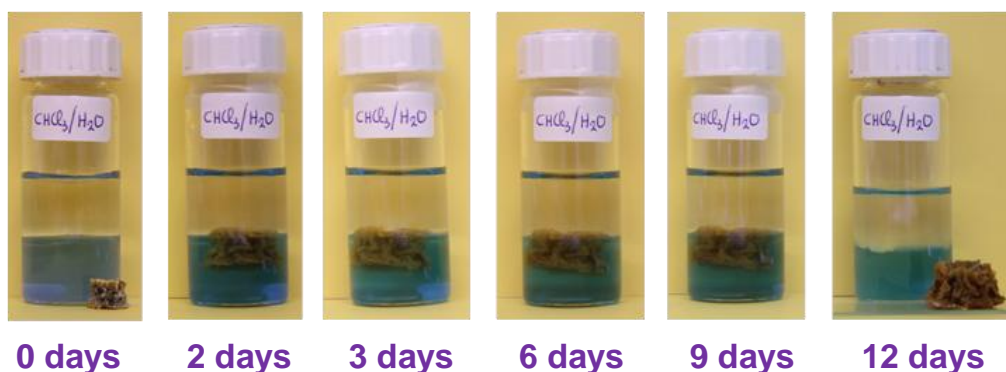


Figure 67: Separation of CHCl_3 (dyed with Sudan blue) from water.

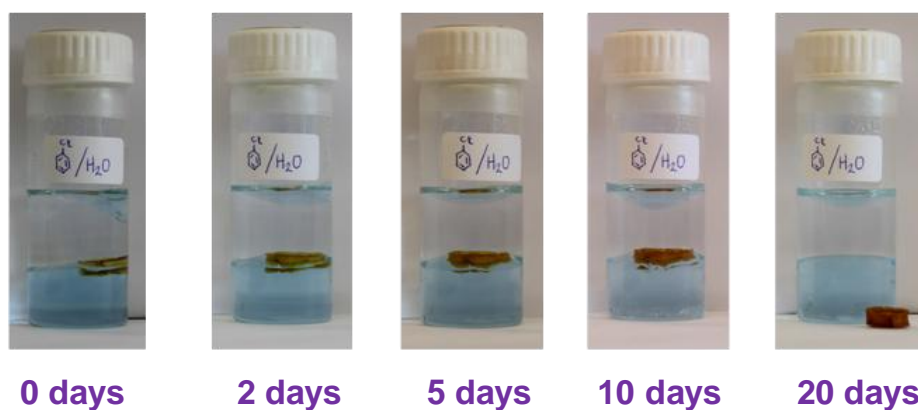


Figure 68: Separation of chlorobenzene (dyed with Sudan blue) from water.

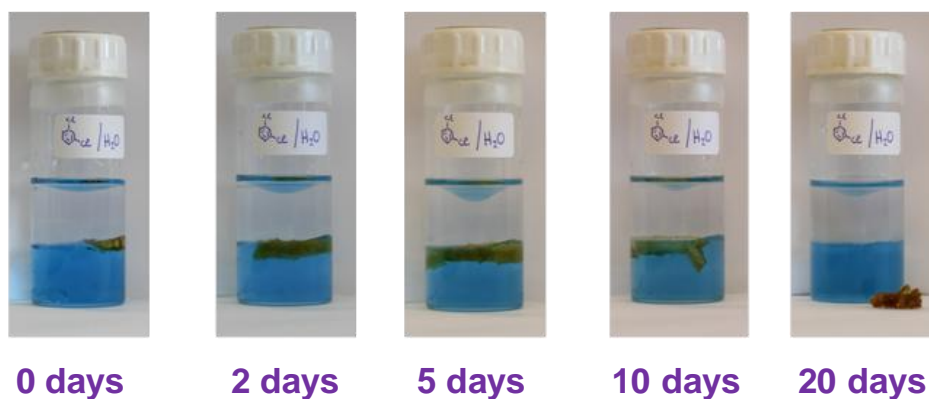


Figure 69: Separation of 1,3-dichlorobenzene (dyed with Sudan blue) from water.

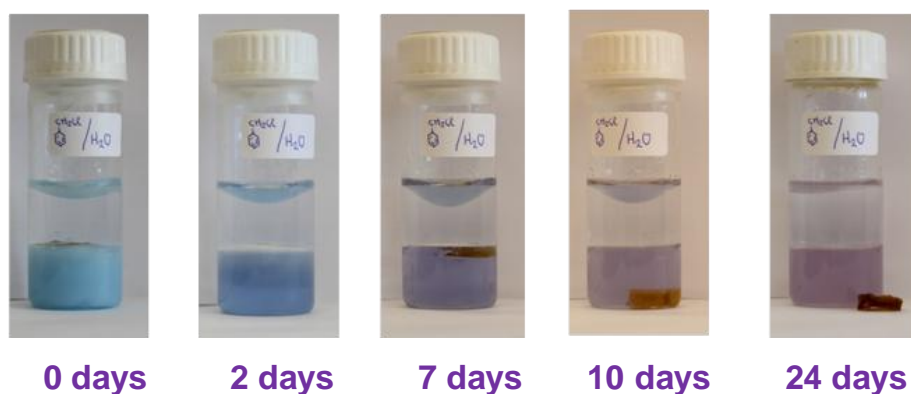


Figure 70: Separation of benzyl chloride (dyed with Sudan blue) from water.

Table 25: Uptake for each solvent when separated from a 1:1 v/v mixture with water.

| Mixture (50 % v/v in H ₂ O) | Solvent uptake (g of solvent / g of gel) |
|---|---|
| methylene chloride | 10 |
| chloroform | 14 |
| chlorobenzene | 8 |
| 1,3-dichlorobenzene | 12 |
| benzyl chloride | 7 |

9.5 Conclusions

W₂-PDCPD gels, synthesized using the catalytic system **{W₂}/PA**, swelled in various organic solvents, mainly aromatic and chlorinated ones. A correlation can be made between the swelling behavior of the gels in each solvent and

the solvents' Hansen Solubility Parameters (HSP), leading to an estimation of the HSP of mostly *cis* **PDCPD**. Based on those findings, these gels were used to separate organic solvents from water, exhibiting remarkably higher solvent uptakes than other polymers reported in literature.

CONCLUSIONS

Controlled Radical Polymerization (CRP) reactions: The catalytic activity of a number Co^{II} and Mn^{II} triphenylamido-amine complexes has been studied. Our results show that $[\text{K}(\text{THF})_6][(\text{L}^5)\text{Co}^{\text{II}}] \cdot 1.5\text{THF}$ (**Co-2**), $[\text{K}(\text{THF})_2(\text{L}^8)\text{Co}^{\text{II}}]_n$ (**Co-3**), $[\text{K}_2(\text{L}^9)_2\text{Co}^{\text{II}}]_n$ (**Co-4**), $\{[\text{K}_2(\text{DMA})_3(\text{L}^{10})_2\text{Co}^{\text{II}}] \cdot 0.5\text{Et}_2\text{O}\}_n$ (**Co-5**) and $[\text{K}(\text{NCMe})_3(\text{L}^{13})\text{Co}^{\text{II}}-\text{NCMe}]$ (**Co-6**) can induce the **CRP** of styrene (**St**) and methyl methacrylate (**MMA**). Some compounds (**Co-3-5**) provided good yields (60-90%; **Co-3** was active only in **St** polymerization), whereas others (**Co-2** and **Co-6**) had better control over the polymerization reactions, albeit with lower yields (12-16% for poly(styrene) (**PS**) and 30-45% for poly(methyl methacrylate) (**PMMA**)). Although a firm correlation between the reactivity and the structure or the redox potential cannot be made at this point, the steric factor seems to play an essential role, since compounds that feature a less hindered fifth coordination site showed the highest reactivity and better control over the polymerization reaction.

The polymers obtained were predominately syndiotactic, consistent with radical polymerization, with two exceptions that exhibited unusually high ratios of isotactic triads. In many cases bimodal distributions were observed, although the molecular weight distributions were not very broad (1.40-2.00), and this strongly indicates that two parallel mechanisms are in operation. Among the three predominant mechanisms (Atom Transfer Radical Polymerization (**ATRP**); Organometallic Mediated Radical Polymerization, (**OMRP**) and Catalytic Chain Transfer polymerization (**CCTP**)) that have been established for cobalt-mediated **CRP** reactions, the first two seem to be more likely for our systems. A detailed mechanistic study is under way.

The Mn^{II} complexes $[\text{K}_2(\text{DMA})_3(\text{L}^4)_2\text{Mn}^{\text{II}}]_2$ (**Mn-1**), $[\text{K}(\text{THF})_4][(\text{L}^5)\text{Mn}^{\text{II}}-\text{THF}]$ (**Mn-2**), $[\text{K}(\text{NCMe})][(\text{L}^6)\text{Mn}^{\text{II}}-\text{NCMe}] \cdot \text{MeCN}$ (**Mn-3**), $[\text{K}(\text{DMA})][(\text{L}^8)\text{Mn}^{\text{II}}-\text{DMA}]$ (**Mn-4**), $[\text{K}(\text{L}^9)\text{Mn}^{\text{II}}]_n$ (**Mn-5**), $[\text{K}_2(\text{THF})_3\{(\text{L}^{10})\text{Mn}^{\text{II}}\}_2] \cdot 2\text{THF}$ (**Mn-6**) and $[\text{K}(\text{THF})_3][(\text{L}^{13})\text{Mn}^{\text{II}}-\text{THF}]$ (**Mn-7**) were far less reactive towards the **CRP** of **St** and **MMA** and the control over the polymerization was not good. Polymers with broad molecular weight distributions were obtained in low yields.

Molecular weight distributions were bimodal, indicating two mechanisms operating in parallel. Because of the low yields and the bad control over the polymerization the reactions were not further investigated.

Copolymerization of norbornene (NBE) and norbornadiene (NBD) via Ring Opening Metathesis Polymerization (ROMP): Statistical poly(norbornene)/poly(norbornadiene) (**PNBE/PNBD**) copolymers have been synthesized *via ROMP* of norbornene (**NBE**) and norbornadiene (**NBD**) using the ditungsten compound $\text{Na}[\text{W}_2(\mu\text{-Cl})_3\text{Cl}_4(\text{THF})_2]\cdot(\text{THF})_3$ (**{W₂}**) as initiator. The composition of the polymeric chain was estimated, although not quantitatively, by solid state NMR data and it was found that the ratio of **NBE/NBD** units was relative to the monomer molar ratio in the reaction mixture. The morphology of the copolymers differed, according to the composition of the polymeric chain. Solid-state ¹³C CPMAS NMR spectroscopy of **PNBD** homopolymer revealed that the only crosslinking mechanism in operation was the metathetic one (no radical coupling). The thermal properties of all copolymers were similar, resembled the properties of **PNBD** homopolymer and indicated a high degree of crosslinking for both **PNBD** homopolymer and the copolymers. Glass transition (T_g) temperatures were lower for the copolymers than for the homopolymers, which is a strong indication that those materials are star-copolymers.

Expanding and improving the catalytic activity of $\text{Na}[\text{W}_2(\mu\text{-Cl})_3\text{Cl}_4(\text{THF})_2]\cdot(\text{THF})_3$: In order to improve the catalytic activity of $\text{Na}[\text{W}_2(\mu\text{-Cl})_3\text{Cl}_4(\text{THF})_2]\cdot(\text{THF})_3$ (**{W₂}**), we have utilized phenylacetylene (**PA**) as co-initiator and examined the reactivity of **{W₂}/PA** towards a number of cycloolefins. **{W₂}/PA** promoted the **ROMP** of **NBE** and 5-vinyl-2-norbornene (**VNBE**) efficiently, providing high molecular weight polymers in high yields and with high stereoselectivity (86% *cis* for **PNBE**). It should be noted that less strained double bonds ($-\text{CH}=\text{CH}_2$) remained unaffected. **NBD** and dicyclopentadiene (**DCPD**) were also activated fast and quantitatively giving insoluble, highly crosslinked polymers.

Compared to **{W₂}**, **{W₂}/PA** was in general more active towards the **ROMP** of all monomers studied, in all solvents, as well as in bulk. The molecular

weights of the polymers obtained were higher (with very few exceptions), while the molecular weight distributions were either retained or improved. The *cis*-specificity of **PNBE** was the same (86% *cis*) with either system.

In situ monitoring of the reaction (**{W₂}/PA/NBE**) by ¹H NMR spectroscopy revealed the formation of active alkylidenes of the propagating chains, in agreement with previous studies on the **W₂**-based catalytic system, but a detailed mechanistic study of the catalytic system is underway.

Synthesis and structural characterization of poly(dicyclopentadiene) (PDCPD) gels: **PDCPD** gels were prepared via **ROMP** of **DCPD** using two **W**-based catalytic systems; the first one was based on the ditungsten complex **{W₂}** (**{W₂}/PA**), and the second one on the mononuclear **WCl₆** complex (**W/PA**). Dry-gels were highly crosslinked, as corroborated by their high thermal stability. Solid-state ¹³C CPMAS NMR spectroscopy revealed the operation of two mechanisms for crosslinking (one metathetic and one radical), with metathesis being the major pathway (~ 70-80%) in all cases. Most importantly, solid-state ¹³C NMR along with vibrational spectroscopy (FTIR-ATR and FT-Raman) revealed differences in the *cis/trans* ratio of the double bonds of the polymeric chains. Results were compared also with aerogels **Ru-I-PDCPD** and **Ru-II-PDCPD**, which were synthesized using the 1st and 2nd generation Grubbs' catalysts (**Ru-I** and **Ru-II**, respectively). Spectroscopic data showed that the configuration of the polymeric chain was predominantly *cis* for **W**-catalyzed systems and predominantly *trans* for **Ru**-catalyzed systems. The most extreme cases were **Ru-I-PDCPD**, which consisted of high-*trans* **PDCPD**, and **W₂-PDCPD** dry-gels, which consisted of high-*cis* **PDCPD**. The different *cis* content played a major role in the swelling behavior of the corresponding dry-gels in toluene. In toluene, **W₂-PDCPD** dry-gels swelled and increased their volume by more than 100 times. Such extreme swelling phenomena are rare and may be useful in environmental remediation, shape memory applications, actuators, chemical delivery systems etc. By comparison of **W₂-PDCPD** with **W-PDCPD** dry-gels, as well as with **Ru-II-PDCPD** and **Ru-I-PDCPD** aerogels, it is evident that swelling strongly depends on the configuration of the polymeric chain and increases

together with the content of the *cis* configuration. Similar behavior was observed in many other organic solvents (e.g., THF, chlorinated hydrocarbons, etc.), although with slower rates and to a different extent. Therefore, it is concluded that the ditungsten catalytic system considered in this study shows unique advantages in terms of stereochemistry and properties of **PDCPD** gels over the mononuclear W- and Ru-based catalytic systems.

Hansen Solubility Parameters (HSP) and potential applications of poly(dicyclopentadiene) (PDCPD) gels: **W₂-PDCPD** gels synthesized by using the **{W₂}/PA** catalytic system swelled in various organic solvents, mainly aromatic and chlorinated ones. A correlation can be made between the swelling behavior of the gels in each solvent and the Hansen Solubility Parameters (HSP) of the solvents, leading to an estimation of the HSP of mostly-*cis* **PDCPD**. Based on those findings, **W₂-PDCPD** gels were used to separate organic solvents from water, exhibiting remarkably higher solvent uptakes than other synthetic organic polymers reported in literature.

ΣΥΜΠΕΡΑΣΜΑΤΑ

Αντιδράσεις Ελεγχόμενου Ριζικού Πολυμερισμού (CRP): Μελετήθηκε η καταλυτική δραστηριότητα μιας σειράς τριφαινυλομιδο-αμινικών συμπλόκων του Co^{II} και του Mn^{II} . Τα αποτελέσματά μας δείχνουν ότι τα σύμπλοκα $[\text{K}(\text{THF})_6][(\text{L}^5)\text{Co}^{\text{II}}] \cdot 1.5\text{THF}$ (**Co-2**), $[\text{K}(\text{THF})_2(\text{L}^8)\text{Co}^{\text{II}}]_n$ (**Co-3**), $[\text{K}_2(\text{L}^9)_2\text{Co}^{\text{II}}]_n$ (**Co-4**), $\{[\text{K}_2(\text{DMA})_3(\text{L}^{10})_2\text{Co}^{\text{II}}] \cdot 0.5\text{Et}_2\text{O}\}_n$ (**Co-5**) και $[\text{K}(\text{NCMe})_3(\text{L}^{13})\text{Co}^{\text{II}}-\text{NCMe}]$ (**Co-6**) προωθούν τον ελεγχόμενο ριζικό πολυμερισμό (**CRP**) του στυρενίου (**St**) και του μεθακρυλικού μεθυλεστέρα (**MMA**). Ορισμένα σύμπλοκα (**Co-3-5**) παρείχαν καλές αποδόσεις (60-90%, το **Co-3** ήταν ενεργό μόνο στον πολυμερισμό του **St**), ενώ άλλα (**Co-2** και **Co-6**) είχαν καλύτερο έλεγχο πάνω στον πολυμερισμό, αν και με χαμηλότερες αποδόσεις (12-16% για **PS** και 30-45% για **PMMA**). Αν και δεν μπορεί να γίνει συσχέτιση ανάμεσα στη δραστηριότητα και τη δομή ή το δυναμικό οξειδωαναγωγής, ο στερεοχημικός παράγοντας δείχνει να παίζει ουσιαστικό ρόλο, καθώς τα σύμπλοκα που είχαν λιγότερο παρεμποδισμένη την πέμπτη θέση σύμπλεξης είχαν τη μεγαλύτερη δραστηριότητα και καλύτερο έλεγχο πάνω στον πολυμερισμό.

Τα πολυμερή που ελήφθησαν ήταν κυρίως συνδιοτακτικά, όπως συνήθως συμβαίνει στο ριζικό πολυμερισμό, με δύο εξαιρέσεις που επέδειξαν ασυνήθιστα υψηλές αναλογίες ισοτακτικών τριάδων. Σε πολλές περιπτώσεις παρατηρήθηκαν διμοριακές κατανομές μοριακών βαρών, αν και αυτές δεν ήταν πολύ ευρείες (1.40-2.00), κάτι που αποτελεί ισχυρή ένδειξη ότι λειτούργησαν δύο παράλληλοι μηχανισμοί. Ανάμεσα στους τρεις κυρίαρχους μηχανισμούς (**ATRP**, **OMRP** και **CCTP**) για καταλυόμενες μέσω συμπλόκων του κοβαλτίου αντιδράσεις **CRP**, οι δύο πρώτοι είναι πιο πιθανοί για τα συστήματά μας.

Τα σύμπλοκα του Mn^{II} $[\text{K}_2(\text{DMA})_3(\text{L}^4)_2\text{Mn}^{\text{II}}]_2$ (**Mn-1**), $[\text{K}(\text{THF})_4][(\text{L}^5)\text{Mn}^{\text{II}}-\text{THF}]$ (**Mn-2**), $[\text{K}(\text{NCMe})][(\text{L}^6)\text{Mn}^{\text{II}}-\text{NCMe}] \cdot \text{MeCN}$ (**Mn-3**), $[\text{K}(\text{DMA})][(\text{L}^8)\text{Mn}^{\text{II}}-\text{DMA}]$ (**Mn-4**), $[\text{K}(\text{L}^9)\text{Mn}^{\text{II}}]_n$ (**Mn-5**), $[\text{K}_2(\text{THF})_3\{(\text{L}^{10})\text{Mn}^{\text{II}}\}_2] \cdot 2\text{THF}$ (**Mn-6**) και $[\text{K}(\text{THF})_3][(\text{L}^{13})\text{Mn}^{\text{II}}-\text{THF}]$ (**Mn-7**) ήταν πολύ λιγότερο δραστικά στη **CRP** του **St** και του **MMA** και ο έλεγχος του πολυμερισμού δεν ήταν καλός. Ελήφθησαν

σε χαμηλές αποδόσεις πολυμερή με ευρείες ατανομές μοριακών βαρών. Οι κατανομές μοριακών βαρών ήταν διμοριακές, υποδεικνύοντας τη λειτουργία δύο παράλληλων μηχανισμών. Λόγω των χαμηλών αποδόσεων και του κακού ελέγχου στον πολυμερισμό, οι αντιδράσεις δε μελετήθηκαν περαιτέρω.

Συμπολυμερισμός νορβορνείου (NBE) και νορβορναδιενίου (NBD) μέσω Μεταθετικού Πολυμερισμού με Διάνοιξη Δακτυλίου (ROMP): Στατιστικά συμπολυμερή πολυνορβορνείου/πολυνορβορναδιενίου (**PNBE/PNBD**) συνετέθησαν μέσω **ROMP** με χρήση του διπυρηνικού συμπλόκου $\text{Na}[\text{W}_2(\mu\text{-Cl})_3\text{Cl}_4(\text{THF})_2] \cdot (\text{THF})_3$ (**{W₂}**) ως ενεργοποιητή. Η σύσταση της πολυμερικής αλυσίδας εκτιμήθηκε, αν και όχι με ακρίβεια, με φασματοσκοπία NMR στερεάς κατάστασης και βρέθηκε ότι η αναλογία των μονάδων **NBE/NBD** ήταν ανάλογη της αναλογίας mol των μονομερών στο μίγμα της αντίδρασης. Η μορφολογία των συμπολυμερών διαφοροποιείται, ανάλογα με τη σύσταση της πολυμερικής αλυσίδας. Η φασματοσκοπία ¹³C CPMAS NMR στερεάς κατάστασης έδειξε ότι ο μόνος μηχανισμός δικτύωσης ήταν ο μεταθετικός (δεν λαμβάνει χώρα ολεφινική σύζευξη). Οι θερμικές ιδιότητες των συμπολυμερών είναι παρόμοιες, και προσομοιάζουν εκείνες του ομοπολυμερούς **PNBD**. Οι θερμοκρασίες υαλώδους μετάπτωσης (T_g) βρέθηκαν να είναι χαμηλότερες για τα συμπολυμερή από ότι για τα ομοπολυμερή και αυτό αποτελεί ισχυρή ένδειξη ότι τα υλικά αυτά είναι αστεροειδή συμπολυμερή.

Επεκτείνοντας και βελτιώνοντας την καταλυτική δραστικότητα του $\text{Na}[\text{W}_2(\mu\text{-Cl})_3\text{Cl}_4(\text{THF})_2] \cdot (\text{THF})_3$: Με σκοπό τη βελτίωση της καταλυτικής δραστικότητας του $\text{Na}[\text{W}_2(\mu\text{-Cl})_3\text{Cl}_4(\text{THF})_2] \cdot (\text{THF})_3$ (**{W₂}**) χρησιμοποιήθηκε φαινυλακετυλένιο (**PA**) ως συγκαταλύτης και μελετήθηκε η δραστικότητα του **{W₂}/PA** ως προς διάφορες κυκλολεφίνες. Το καταλυτικό σύστημα **{W₂}/PA** βρέθηκε ότι καταλύει αποτελεσματικά τη **ROMP** του νορβορνείου (**NBE**) και του 5-βινυλο-2-νορβορνείου (**VNBE**), δίνοντας πολυμερή υψηλού μοριακού βάρους σε υψηλές αποδόσεις και με υψηλή στερεοεκλεκτικότητα (86% *cis* για το **PNBE**). Αξίζει να σημειωθεί ότι οι βινυλικοί διπλοί δεσμοί ($-\text{CH}=\text{CH}_2$) παρέμειναν ανεπηρέαστοι. Το νορβορναδιένιο (**NBD**) και το δικυκλοπενταδιένιο (**DCPD**) επίσης ενεργοποιήθηκαν γρήγορα και ποσοτικά δίνοντας αδιάλυτα πολυμερή με υψηλό βαθμό διακλάδωσης.

Σε σχέση με το $\{W_2\}$, το καταλυτικό σύστημα $\{W_2\}/PA$ ήταν γενικά πιο δραστικό ως προς τη **ROMP** όλων των μονομερών που μελετήθηκαν, σε όλους τους διαλύτες καθώς και απουσία διαλύτη. Τα μοριακά βέρη των πολυμερών που ελήφθησαν ήταν υψηλότερα (με λίγες εξαιρέσεις), ενώ οι κατανομές των μοριακών βαρών διατηρήθηκαν ή βελτιώθηκαν. Η *cis*-εκλεκτικότητα του **PNBE** ήταν ίδια (86% *cis*) και με τα δύο συστήματα.

In situ παρακολούθηση της αντίδρασης ($\{W_2\}/PA/NBE$) με φασματοσκοπία 1H NMR έδειξε το σχηματισμό ενεργών αλκυλιδενίων των επεκτεινόμενων αλυσίδων, σε συμφωνία με προηγούμενες μελέτες, αλλά λεπτομερής μηχανιστική μελέτη του καταλυτικού συστήματος είναι σε εξέλιξη.

Σύνθεση και δομικός χαρακτηρισμός πηκτωμάτων πολυδικυκλοπενταδιενίου (PDCPD): Πηκτώματα **PDCPD** παρασκευάστηκαν μέσω **ROMP** του δικυκλοπενταδιενίου (**DCPD**) χρησιμοποιώντας δύο καταλυτικά συστήματα βασισμένα στο βολφράμιο. Το πρώτο βασίστηκε στο διπυρηνικό σύμπλοκο $Na[W_2(\mu-Cl)_3Cl_4(THF)_2] \cdot (THF)_3$ ($\{W_2\}/PA$), και το δεύτερο στο μονοπυρηνικό σύμπλοκο WCl_6 (**WCl₆/PA**). Τα πηκτώματα είχαν υψηλό βαθμό διακλάδωσης, όπως φάνηκε από την υψηλή θερμική τους σταθερότητα. Η φασματοσκοπία ^{13}C CPMAS NMR στερεάς κατάστασης φανέρωσε τη λειτουργία δύο μηχανισμών δικτύωσης (ενός μεταθετικού και ενός ριζικού), με τη μετάθεση να είναι η κύρια οδός (~ 70-80%) σε όλες τις περιπτώσεις. Επίσης, η φασματοσκοπία ^{13}C NMR στερεάς κατάστασης καθώς και η δονητική φασματοσκοπία (FTIR-ATR και FT-Raman) φανέρωσαν διαφορές στην αναλογία *cis/trans* των διπλών δεσμών της πολυμερικής αλυσίδας. Τα αποτελέσματα συγκρίθηκαν με τα αεροπηκτώματα **Ru-I-PDCPD** και **Ru-II-PDCPD**, που συνετέθησαν με χρήση των καταλυτών Grubbs' πρώτης και δεύτερης γενιάς, αντίστοιχα. Φασματοσκοπικά δεδομένα έδειξαν ότι η διαμόρφωση της πολυμερικής αλυσίδας ήταν κυρίως *cis* για τα συστήματα του W και κυρίως *trans* για συστήματα του Ru. Η διαφορά στο *cis* περιεχόμενο έπαιξε κύριο ρόλο στη διόγκωση των αντιστοιχών πηκτωμάτων στο τολουόλιο. Τα πηκτώματα **W₂-PDCPD** αύξησαν τον όγκο τους περισσότερο από 100 φορές. Τόσο ακραία φαινόμενα διόγκωσης είναι σπάνια και μπορούν να είναι χρήσιμα σε περιβαλλοντικές εφαρμογές κ.α. Συγκρίνοντας τα

πηκτώματα **W₂-PDCPD** με τα **W-PDCPD**, καθώς και με τα αεροπηκτώματα **Ru-II-PDCPD** και **Ru-I-PDCPD**, είναι εμφανές ότι η διόγκωση εξαρτάται ισχυρά από τη διαμόρφωση της πολυμερικής αλυσίδας και αυξάνεται με το ποσοστό της *cis* διαμόρφωσης. Παρόμοια συμπεριφορά παρατηρήθηκε σε πολλούς άλλους οργανικούς διαλύτες (π.χ., THF, χλωριωμένοι υδρογονάνθρακες, κτλ.), αν και με πιο αργούς ρυθμούς και σε διαφορετική έκταση. Επομένως, συμπεραίνεται ότι το καταλυτικό σύστημα **{W₂}/PA** που μελετήθηκε επιδεικνύει μοναδικά πλεονεκτήματα στη στερεοχημεία και τις ιδιότητες των πηκτωμάτων **PDCPD** σε σχέση με μονοπηρυνικά καταλυτικά συστήματα βασισμένα στο W και το Ru.

Παράμετροι διαλυτότητας Hansen (HSP) και πιθανές εφαρμογές πηκτωμάτων πολυδικυκλοπενταδιενίου (PDCPD): Τα πηκτώματα **W₂-PDCPD** που συνετέθησαν με χρήση του καταλυτικού συστήματος **{W₂}/PA** και έχουν υψηλό ποσοστό *cis* πολυμερούς διογκώνονται σε διάφορους οργανικούς διαλύτες, κυρίως αρωματικούς και χλωριωμένους. Έγινε συσχέτιση μεταξύ της διόγκωσης των πηκτωμάτων σε κάθε διαλύτη και των παραμέτρων διαλυτότητας Hansen (HSP) των διαλυτών και μέσω αυτής κατέστη δυνατή η εκτίμηση των παραμέτρων διαλυτότητας του δικτυωμένου **W₂-PDCPD**. Λόγω της ιδιότητάς τους να διογκώνονται σε οργανικούς διαλύτες, τα συγκεκριμένα πηκτώματα χρησιμοποιήθηκαν για το διαχωρισμό χλωριωμένων οργανικών διαλυτών από νερό, επιδεικνύοντας αξιοσημείωτα μεγαλύτερη πρόσληψη διαλύτη από άλλα συνθετικά οργανικά πολυμερή που αναφέρονται στη βιβλιογραφία.

ABBREVIATIONS-ACRONYMS

| | |
|--------|--|
| ATRA | Atom Transfer Radical Addition |
| ATRP | Atom Transfer Radical Polymerization |
| CCTP | Catalytic Chain Transfer Polymerization |
| CMRP | Cobalt Mediated Radical Polymerization |
| CPMAS | Cross Polarization Magic Angle Spinning |
| CRP | Controlled Radical Polymerization |
| DCPD | Dicyclopentadiene |
| DSC | Differential Scanning Calorimetry |
| HETCOR | Heteronuclear Correlation |
| HSP | Hansen Solubility Parameters |
| MMA | Methyl Methacrylate |
| NBD | Norbornadiene |
| NBE | Norbornene |
| NMR | Nuclear Magnetic Resonance |
| OMRP | Organometallic Mediated Radical Polymerization |
| PA | Phenylacetylene |
| PDCPD | Poly(dicyclopentadiene) |
| PMMA | Poly(methyl methacrylate) |
| PNBD | Poly(norbornadiene) |
| PNBE | Poly(norbornene) |
| PS | Poly(styrene) |
| PVNBE | Poly(5-vinyl-2-norbornene) |
| ROMP | Ring Opening Metathesis Polymerization |
| SEC | Size Exclusion Chromatography |
| SEM | Scanning Electron Microscope |
| St | Styrene |
| TGA | Thermogravimetric Analysis |
| VNBE | 5-Vinyl-2-norbornene |

REFERENCES

- (1) M. Ouchi, T. Terashima and M. Sawamoto, Transition Metal-Catalyzed Living Radical Polymerization: Toward Perfection in Catalysis and Precision Polymer Synthesis, *Chem. Rev.*, 109 (11), 2009, pp. 4963–5050.
- (2) K. Matyjaszewski and J. Xia, Atom Transfer Radical Polymerization, *Chem. Rev.*, 101 (9), 2001, pp. 2921–2990.
- (3) M. Hurtgen, C. Detrembleur, C. Jerome and A. Debuigne, Insight into Organometallic-Mediated Radical Polymerization, *Polym. Rev.*, 51 (2), 2011, pp. 188–213.
- (4) A. Debuigne, R. Poli, C. Jérôme, R. Jérôme and C. Detrembleur, Overview of Cobalt-Mediated Radical Polymerization: Roots, State of the Art and Future Prospects, *Prog. Polym. Sci.*, 34 (3), 2009, pp. 211–239.
- (5) B.B. Wayland, G. Poszmik, S.L. Mukerjee and M. Fryd, Living Radical Polymerization of Acrylates by Organocobalt Porphyrin Complexes. *J. Am. Chem. Soc.*, 116 (17), 1994, pp. 7943–7944.
- (6) L.D. Arvanitopoulos, M.P. Gruel and H.J. Harwood, “Living” Free Radical Polymerization Using Alkyl Cobaloximes as Photoinitiators, *Polym. Prep.*, 35, 1994, pp. 549-550.
- (7) T. Pintauer and K. Matyjaszewski, Atom Transfer Radical Addition and Polymerization Reactions Catalyzed by Ppm Amounts of Copper Complexes, *Chem. Soc. Rev.*, 37 (6), 2008, pp. 1087–1097.
- (8) M.A. Fernández-Zúmel, K. Thommes, G. Kiefer, A. Sienkiewicz, K. Pierzchala and K. Severin, Atom-Transfer Radical Addition Reactions Catalyzed by RuCp* Complexes: A Mechanistic Study, *Chem. – Eur. J.*, 15 (43), 2009, pp. 11601–11607.
- (9) C. Ricardo and T. Pintauer, Copper Catalyzed Atom Transfer Radical Cascade Reactions in the Presence of Free-Radical Diazo Initiators as Reducing Agents, *Chem. Commun.*, 21, 2009, pp. 3029–3031.
- (10) W. Tang, Y. Kwak, W. Braunecker, N.V. Tsarevsky, M.L. Coote and K. Matyjaszewski, Understanding Atom Transfer Radical Polymerization: Effect of Ligand and Initiator Structures on the Equilibrium Constants, *J. Am. Chem. Soc.*, 130 (32), 2008, pp. 10702–10713.
- (11) X. Luo, X. Zhao, S. Xu and B. Wang, The Exo-Substituted η^4 -Cyclopentadiene CpCo(I) Complexes: A New Kind of ATRP Catalysts and the Actual Catalyst for the Cobaltocene-Catalyzed ATRP, *Polymer*, 50 (3), 2009, pp. 796–801.
- (12) Z.X. Huang, Y.M. Zhang, H. Li and Y.G. Liu, Controlled/“Living” Radical Polymerization of Methyl Methacrylate Catalyzed by Cobalt Acetate, *Macromol. Chem. Phys.*, 209 (8), 2008, pp. 825–831.
- (13) M.S. Weiser and R. Mülhaupt, Cobalt(II) Octanoate and Cobalt(II) Perfluorooctanoate Catalyzed Atom Transfer Radical Polymerization of

- Styrene in Toluene and Fluorous media—A Versatile Route to Catalyst Recycling and Oligomer Formation, *J. Polym. Sci. Part A: Polym. Chem.*, 43 (17), 2005, pp. 3804–3813.
- (14) Z. Zhang, W. Zhang, X. Zhu, Z. Cheng and J. Zhu, “Living”/controlled Free Radical Polymerization of MMA in the Presence of Cobalt(II) 2-Ethylhexanoate: A Switch from RAFT to ATRP Mechanism, *J. Polym. Sci. Part A: Polym. Chem.*, 45 (24), 2007, pp. 5722–5730.
- (15) Z.H. Li, Y.M. Zhang, M.Z. Xue, L. Zhou and Y.G. Liu, Atom Transfer Radical Polymerization of Methyl Methacrylate Catalyzed by Cobalt Catalyst System, *J. Polym. Sci. Part A: Polym. Chem.*, 43 (21), 2005, pp. 5207–5216.
- (16) Z. Huang, Y. Zhang, H. Li and Y. Liu, A Novel Immobilized Cobalt(II)/Copper(II) Bimetallic Catalyst for Atom Transfer Radical Polymerization (ATRP) of Methyl Methacrylate, *Appl. Catal. Gen.*, 332 (2), 2007, pp. 192–199.
- (17) Z.X. Huang, Y.M. Zhang, H. Li, Y.H. Luan and Y.G. Liu., Atom Transfer Radical Polymerization of Methyl Methacrylate Catalyzed by Ion Exchange Resin Immobilized Co(II) Hybrid Catalyst, *J. Polym. Sci. Part A: Polym. Chem.*, 46 (4), 2008, pp. 1416–1426.
- (18) K. Matsubara and M. Matsumoto, Cobalt(I)-Mediated Living Radical Polymerization of Methyl Methacrylate, *J. Polym. Sci. Part A: Polym. Chem.*, 44 (13), 2006, pp. 4222–4228.
- (19) H. Kaneyoshi and K. Matyjaszewski, Synthesis of Poly(vinyl Acetate)-Graft-Polystyrene by a Combination of Cobalt-Mediated Radical Polymerization and Atom Transfer Radical Polymerization, *J. Polym. Sci. Part A: Polym. Chem.*, 45 (3), 2007, pp. 447–459.
- (20) A. Debuigne, J.R. Caille, C. Detrembleur and R. Jérôme, Effective Cobalt Mediation of the Radical Polymerization of Vinyl Acetate in Suspension, *Angew. Chem. Int. Ed.*, 44 (22), 2005, pp. 3439–3442.
- (21) A. Debuigne, J.R. Caille, N. Willet and R. Jérôme, Synthesis of Poly(vinyl Acetate) and Poly(vinyl Alcohol) Containing Block Copolymers by Combination of Cobalt-Mediated Radical Polymerization and ATRP, *Macromolecules*, 38 (23), 2005, pp. 9488–9496.
- (22) H. Kaneyoshi and K. Matyjaszewski, Radical (Co)polymerization of Vinyl Chloroacetate and N-Vinylpyrrolidone Mediated by Bis(acetylacetonate)cobalt Derivatives, *Macromolecules*, 39 (8), 2006, pp. 2757–2763.
- (23) A. Debuigne, J.R. Caille and R. Jérôme, Highly Efficient Cobalt-Mediated Radical Polymerization of Vinyl Acetate, *Angew. Chem. Int. Ed.*, 44 (7), 2005, pp. 1101–1104.
- (24) B.B. Wayland, L. Basickes, S. Mukerjee, M. Wei and M. Fryd, Living Radical Polymerization of Acrylates Initiated and Controlled by Organocobalt Porphyrin Complexes, *Macromolecules*, 30 (26), 1997, pp. 8109–8112.

- (25) Z. Lu, M. Fryd, B.B. Wayland, New Life for Living Radical Polymerization Mediated by Cobalt(II) Metalloradicals, *Macromolecules*, 37 (8), 2004, pp. 2686–2687.
- (26) S.C.J. Pierik and A.M. van Herk, Catalytic Chain Transfer Copolymerization of Methyl Methacrylate and Butyl Acrylate, *Macromol. Chem. Phys.*, 204 (11), 2003, pp. 1406–1418.
- (27) A.A. Gridnev and S.D. Ittel, Catalytic Chain Transfer in Free-Radical Polymerizations, *Chem. Rev.*, 101 (12), 2001, pp. 3611–3660.
- (28) D.M. Haddleton, E. Depaquis, E.J. Kelly, D. Kukulj, S.R. Morsley, S.A.F. Bon, M.D. Eason and A.G. Steward, Cobalt-Mediated Catalytic Chain-Transfer Polymerization (CCTP) in Water and Water/alcohol Solution, *J. Polym. Sci. Part A: Polym. Chem.*, 39 (14), 2001, pp. 2378–2384.
- (29) D. Kukulj, J.P.A. Heuts and T.P. Davis, Copolymerization of Styrene and α -Methylstyrene in the Presence of a Catalytic Chain Transfer Agent, *Macromolecules*, 31 (18), 1998, pp. 6034–6041.
- (30) J.P.A. Heuts, D. Kukulj, D.J. Forster and T.P. Davis, Copolymerization of Styrene and Methyl Methacrylate in the Presence of a Catalytic Chain Transfer Agent, *Macromolecules*, 31 (9), 1998, pp. 2894–2905.
- (31) D. Kukulj, T.P. Davis, K.G. Suddaby, D.M. Haddleton and R.G. Gilbert, Catalytic Chain Transfer for Molecular Weight Control in the Emulsion Homo- and Copolymerizations of Methyl Methacrylate and Butyl Methacrylate, *J. Polym. Sci. Part A: Polym. Chem.*, 35 (5), 1997, pp. 859–878.
- (32) K. Endo and A. Yachi, Molecular-Weight-Controlled Polymerization of Styrene with $Mn(acac)_3$ in Combination with Organic Halides, *Polym. Bull.*, 46 (5), 2001, pp. 363–369.
- (33) K. Koumura, K. Satoh and M. Kamigaito, Manganese-Based Controlled/Living Radical Polymerization of Vinyl Acetate, Methyl Acrylate, and Styrene: Highly Active, Versatile, and Photoresponsive Systems, *Macromolecules*, 41 (20), 2008, pp. 7359–7367.
- (34) K.J. Ivin and J.C. Mol, *Olefin Metathesis and Metathesis Polymerization*, Academic Press, 1997.
- (35) V. Dragutan and R. Streck, *Catalytic Polymerization of Cycloolefins: Ionic, Ziegler-Natta and Ring-Opening Metathesis Polymerization*, Elsevier, 2000.
- (36) R.H. Grubbs, A.G. Wenzel, D.J. O’Leary and E. Khosravi, *Handbook of Metathesis, 3 Volume Set*, John Wiley & Sons, 2015.
- (37) H.R. Kricheldorf, O. Nuyken and G. Swift, *Handbook of Polymer Synthesis: Second Edition*, CRC Press, 2004.
- (38) M.R. Buchmeiser, Homogeneous Metathesis Polymerization by Well-Defined Group VI and Group VIII Transition-Metal Alkylidenes: Fundamentals and Applications in the Preparation of Advanced Materials, *Chem. Rev.*, 100 (4), 2000, pp. 1565–1604.

- (39) A.D. Schlüter, A. D. *Synthesis of Polymers: New Structures and Methods*, John Wiley & Sons, 2012.
- (40) T. Szymańska-Buzar, Structure and Reactivity of Tungsten(II) and Molybdenum(II) Compounds Containing an MM' Bond, *Coord. Chem. Rev.*, 249 (21–22), 2005, pp. 2195–2202.
- (41) Y. Yamaguchi, A. Fujita, N. Suzuki and T. Ito, Metathesis Polymerization of Norbornene and Terminal Acetylenes Catalyzed by Bis(acetonitrile) Complexes of Molybdenum and Tungsten, *J. Mol. Catal. Chem.*, 240 (1–2), 2005, pp. 226–232.
- (42) V.A. Kormer, I.A. Poletayeva and T.L. Yufa, Cycloolefin Polymerization Initiated by Transition Metal– π -Allylic Complexes, *J. Polym. Sci. [A1]*, 10 (1), 1972, pp. 251–258.
- (43) A. Mutch, M. Leconte, F. Lefebvre and J.M. Basset, Effect of Alcohols and Epoxides on the Rate of ROMP of Norbornene by a Ruthenium Trichloride Catalyst, *J. Mol. Catal. Chem.*, 133 (1–2), 1998, pp. 191–199.
- (44) R.H. Grubbs, Olefin-Metathesis Catalysts for the Preparation of Molecules and Materials (Nobel Lecture), *Angew. Chem. Int. Ed.*, 45 (23), 2006, pp. 3760–3765.
- (45) R.R. Schrock, Multiple Metal–Carbon Bonds for Catalytic Metathesis Reactions (Nobel Lecture), *Angew. Chem. Int. Ed.*, 45 (23), 2006, pp. 3748–3759.
- (46) G. Raptopoulos, A. Grigoropoulos, K. Mertis, P. Paraskevopoulou and M. Pitsikalis, Multinuclear Transition Metal Catalysts for Metathesis Polymerization. Current Developments and Future Perspectives, *Recent Research Developments in Polymer Science*, Transworld Research Network, 2014.
- (47) R.D. Adams and F.A. Cotton, *Catalysis by Di- and Polynuclear Metal Cluster Complexes*, Wiley, 1998.
- (48) E. Whelan, M. Devereux, M. McCann and V. McKee, Non-Polymeric Molybdenum(II) Complexes of Dicarboxylic Acids: synthesis, Structure and Catalytic Properties, *Chem. Commun.*, 5, 1997, pp. 427–428.
- (49) J.G. Hamilton, K.J. Ivin, G.M. McCann and J.J. Rooney, Mechanism of Ring-Opening Polymerization of 1-methylbicyclo[2.2.1]hept-2-Ene Using Metathesis Catalysts, *Makromol. Chem.*, 186 (7), 1985, pp. 1477–1494.
- (50) E.P. Bokaris and M.M. Kosmas, All Cis-poly(NBE) Derived by the ROMP Catalysts Based on WCl_6 , *J. Mol. Catal. Chem.*, 192 (1–2), 2003, pp. 263–273.
- (51) V.P. Günther, F. Haas, G. Marwede, K. Nützel, W. Oberkirch, G. Pampus, N. Schön and J. Witte, Ringöffnende Polymerisation Des Cyclopentens (Katalysatoren, Polymerisation, Produkteigenschaften). *Angew. Makromol. Chem.* **1970**, 14 (1), 87–109.

- (52) G. Floros, *Catalytic Polymerization of Unsaturated Organic Compounds with Transition Metal Complexes*, PhD Thesis, Department of Chemistry, National and Kapodistrian University of Athens, 2009.
- (53) G. Floros, N. Saragas, P. Paraskevopoulou, N. Psaroudakis, S. Koinis, M. Pitsikalis, N. Hadjichristidis and K. Mertis, Ring Opening Metathesis Polymerization of Norbornene and Derivatives by the Triply Bonded Tungsten Complex $\text{Na}[\text{W}_2(\mu\text{-Cl})_3\text{Cl}_4(\text{THF})_2]\cdot(\text{THF})_3$, *Polymers*, 4 (4), 2012, pp. 1657–1673.
- (54) D. Chriti, A. Grigoropoulos, G. Raptopoulos, G. Charalambidis, V. Nikolaou, A.G. Coutsolelos, M. Pitsikalis, K. Mertis and P. Paraskevopoulou, Metathesis Polymerization Reactions Induced by the Bimetallic Complex $(\text{Ph}_4\text{P})_2[\text{W}_2(\mu\text{-Br})_3\text{Br}_6]$, *Polymers*, 7 (12), 2015, pp. 2611–2624.
- (55) A. Demonceau, A.F. Noels, E. Saive and A.J. Hubert, Ruthenium-Catalysed Ring-Opening Metathesis Polymerization of Cycloolefins Initiated by Diazoesters, *J. Mol. Catal.*, 76 (1), 1992, pp. 123–132.
- (56) N. Oshima, H. Suzuki and Y. Moro-Oka, Synthesis and Some Reactions of Dichloro(pentamethylcyclopentadienyl)ruthenium(III) Oligomer, *Chem. Lett.*, 13 (7), 1984, pp. 1161–1164.
- (57) J.L. Brumaghim and G.S. Girolami, Ring-Opening Metathesis Polymerization of Norbornene by $\text{Cp}^*\text{Os}_2\text{Br}_4$ and Related Compounds, *Organometallics*, 18 (10), 1999, pp. 1923–1929.
- (58) F.W. Michelotti and W.P. Keaveney, Coordinated Polymerization of the Bicyclo-[2.2.1]-Heptene-2 Ring System (Norbornene) in Polar Media, *J. Polym. Sci. A*, 3 (3), 1965, pp. 895–905.
- (59) I. Czełuśniak and T. Szymańska-Buzar, Ring-Opening Metathesis Polymerization of Norbornene and Norbornadiene by Tungsten(II) and Molybdenum(II) Complexes, *J. Mol. Catal. Chem.*, 190 (1–2), 2002, pp. 131–143.
- (60) T. Szymańska-Buzar, T. Głowiak and I. Czełuśniak, The Initiation of Ring-Opening Metathesis Polymerisation of Norbornadiene by Seven-Coordinate Molybdenum(II) Compounds. X-Ray Crystal Structure of $[\text{Mo}(\mu\text{-Cl})(\text{SnCl}_3)(\text{CO})_3(\eta^4\text{-NBD})]$, *J. Organomet. Chem.*, 640 (1–2), 2001, pp. 72–78.
- (61) T. Szymańska-Buzar, T. Głowiak and I. Czełuśniak, Reactivity of $[\text{Mo}(\mu\text{-Cl})(\text{SnCl}_3)(\text{CO})_3(\text{NCMe})_2]$ towards Norbornadiene.: X-Ray Crystal Structure of $[\text{Mo}(\mu\text{-Cl})(\text{SnCl}_3)(\text{CO})_2(\eta^4\text{-C}_7\text{H}_8)(\text{NCMe})]$, *Polyhedron*, 21 (24), 2002, pp. 2505–2513.
- (62) I. Czełuśniak, T. Szymańska-Buzar, A. Kenwright and E. Khosravi, Ring-Opening Metathesis Polymerization of 5,6-Bis(Chloromethyl)-Norbornene by Tungsten(II) and Molybdenum(II) Complexes, *Catal. Lett.*, 81 (3–4), 2002, pp. 157–161.

- (63) M. Górski and T. Szymańska-Buzar, Tungsten(II)-Initiated Ring-Opening Metathesis Polymerization and Other C–C Bond Forming Reactions of 5-Vinyl-2-Norbornene, *J. Mol. Catal. Chem.*, 257 (1–2), 2006, pp. 41–47.
- (64) M. Zyder, A. Kochel and T. Szymańska-Buzar, A New Versatile Binuclear Seven-Coordinate Complex of Molybdenum(II), $[(\mu\text{-Cl})_2\{\text{Mo}(\mu\text{-Cl})(\text{SnCl}_3)(\text{CO})_3\}_2]_2^-$, *J. Organomet. Chem.*, 694 (26), 2009, pp. 4196–4203.
- (65) T.J. Malosh, J.R. Shapley, R.J. Lawson, D.N.T. Hay and T.N. Rohrabough Jr., Diene–iridium–tin Complexes. Comparison of Conjugated versus Non-Conjugated Dienes and Trimethyltin versus Trichlorotin as Ligands. Ring Opening Metathesis Polymerization of Norbornene by $\text{Ir}(\text{1,5-Cycloocta-diene})_2\text{SnCl}_3$, *J. Organomet. Chem.*, 745–746, 2013, pp. 98–105.
- (66) R. Çelenligil-Çetin, P. Paraskevopoulou, R. Dinda, R.J. Staples, E. Sinn, N.P. Rath and P. Stavropoulos, Synthesis, Characterization, and Reactivity of Iron Trisamidoamine Complexes That Undergo Both Metal- and Ligand-Centered Oxidative Transformations, *Inorg. Chem.*, 47 (3), 2008, pp. 1165–1172.
- (67) R. Çelenligil-Çetin, P. Paraskevopoulou, N. Lalioti, Y. Sanakis, R.J. Staples, N.P. Rath and P. Stavropoulos, Metalloradical Complexes of Manganese and Chromium Featuring an Oxidatively Rearranged Ligand, *Inorg. Chem.*, 47 (23), 2008, pp. 10998–11009.
- (68) R. Çelenligil-Çetin, P. Paraskevopoulou, R. Dinda, N. Lalioti, Y. Sanakis, A.M. Rawashdeh, R.J. Staples, E. Sinn and P. Stavropoulos, Oxidative Ligand Rearrangement Due to Incipient Aminyl Radicals in the Oxidation of Iron(II) Species with Dioxygen, *Eur. J. Inorg. Chem.*, 2008 (5), 2008, pp. 673–677.
- (69) P. Paraskevopoulou, L. Ai, Q. Wang, D. Pinnapareddy, R. Acharyya, R. Dinda, P. Das, R. Çelenligil-Çetin, G. Floros, Y. Sanakis, A. Choudhury, N.P. Rath and P. Stavropoulos, Synthesis and Characterization of a Series of Structurally and Electronically Diverse Fe(II) Complexes Featuring a Family of Triphenylamido-Amine Ligands, *Inorg. Chem.*, 49 (1), 2010, pp. 108–122.
- (70) M.B. Jones and C.E. MacBeth, Tripodal Phenylamine-Based Ligands and Their Co^{II} Complexes, *Inorg. Chem.*, 46 (20), 2007, pp. 8117–8119.
- (71) M.B. Jones, B.S. Newell, W.A. Hoffert, K.I. Hardcastle, M.P. Shores and C.E. MacBeth, Chelating Tris(amidate) Ligands: Versatile Scaffolds for Nickel(II), *Dalton Trans.*, 39 (2), 2009, pp. 401–410.
- (72) L. Chu, K.I. Hardcastle and C.E. MacBeth, Transition Metal Complexes Supported by a Neutral Tetraamine Ligand Containing N,N-Dimethylaniline Units, *Inorg. Chem.*, 49 (16), 2010, pp. 7521–7529.
- (73) M.B. Jones, K.I. Hardcastle and C.E. MacBeth, Synthetic, Spectral and Structural Studies of Mononuclear $\text{tris}(\kappa^2\text{-Amidate})$ Aluminium Complexes Supported by Tripodal Ligands, *Polyhedron*, 29 (1), 2010, pp. 116–119.

- (74) M.B. Jones, K.I. Hardcastle, K.S. Hagen and C.E. MacBeth, Oxygen Activation and Intramolecular C–H Bond Activation by an Amidate-Bridged Diiron(II) Complex, *Inorg. Chem.*, 50 (14), 2011, pp. 6402–6404.
- (75) S.K. Sharma, P.S. May, M.B. Jones, S. Lense, K.I. Hardcastle, C.E. MacBeth, Catalytic Dioxygen Activation by Co(II) Complexes Employing a Coordinatively Versatile Ligand Scaffold, *Chem. Commun.*, 47 (6), 2011, pp. 1827–1829.
- (76) M.H. Chisholm, B.W. Eichhorn, K. Folting, J.C. Huffman, C.D. Ontiveros, W.E. Streib and W.G. Van der Sluys, Preparation and Characterization of Sodium heptachloropentakis(THF)ditungstate(1-). A Synthetically Useful Precursor for X₃W.tplbond.WX₃ Compounds Where X = CH₂-Tert-Bu, NMe₂ and O-Tert-Bu, *Inorg. Chem.*, 26 (19), 1987, pp. 3182–3186.
- (77) A. Bang, D. Mohite, A.M. Saeed, N. Leventis and C. Sotiriou-Leventis, Polycyclopentadiene Aerogels from First- versus Second-Generation Grubbs' Catalysts: A Molecular versus a Nanoscopic Perspective, *J. Sol-Gel Sci. Technol.*, 75 (2), 2015, pp. 460–474.
- (78) V. Bagchi, G. Raptopoulos, P. Das, S. Christodoulou, Q. Wang, L. Ai, A. Choudhury, M. Pitsikalis, P. Paraskevopoulou and P. Stavropoulos, Synthesis and Characterization of a Family of Co(II) Triphenylamido-Amine Complexes and Catalytic Activity in Controlled Radical Polymerization of Olefins, *Polyhedron*, 52, 2013, pp. 78–90.
- (79) F. di Lena and K. Matyjaszewski, Transition Metal Catalysts for Controlled Radical Polymerization, *Prog. Polym. Sci.*, 35 (8), 2010, pp. 959–1021.
- (80) K. Matyjaszewski and T.P. Davis, *Handbook of Radical Polymerization*, John Wiley & Sons, 2003.
- (81) G. Moineau, C. Granel, P. Dubois, R. Jérôme and P. Teyssié, Controlled Radical Polymerization of Methyl Methacrylate Initiated by an Alkyl Halide in the Presence of the Wilkinson Catalyst, *Macromolecules*, 31 (2), 1998, pp. 542–544.
- (82) T. Ando, M. Kamigaito and M. Sawamoto, Iron(II) Chloride Complex for Living Radical Polymerization of Methyl Methacrylate, *Macromolecules*, 30 (16), 1997, pp. 4507–4510.
- (83) K. Matyjaszewski, M. Wei, J. Xia and N.E. McDermott, Controlled/"Living" Radical Polymerization of Styrene and Methyl Methacrylate Catalyzed by Iron Complexes, *Macromolecules*, 30 (26), 1997, pp.8161–8164.
- (84) G. Moineau, M. Minet, P. Dubois, P. Teyssié, T. Senninger and R. Jérôme, Controlled Radical Polymerization of (Meth)acrylates by ATRP with NiBr₂(PPh₃)₂ as Catalyst, *Macromolecules*, 32 (1), 1999, pp. 27–35.
- (85) C. Granel, P. Dubois, R. Jérôme and P. Teyssié, Controlled Radical Polymerization of Methacrylic Monomers in the Presence of a Bis(ortho-Chelated) Arylnickel(II) Complex and Different Activated Alkyl Halides, *Macromolecules*, 29 (27), 1996, pp. 8576–8582.

- (86) D.M. Haddleton, C.B. Jasieczek, M.J. Hannon and A.J. Shooter, Atom Transfer Radical Polymerization of Methyl Methacrylate Initiated by Alkyl Bromide and 2-Pyridinecarbaldehyde Imine Copper(I) Complexes, *Macromolecules*, 30 (7), 1997, pp. 2190–2193.
- (87) M. Kato, M. Kamigaito, M. Sawamoto and T. Higashimura, Polymerization of Methyl Methacrylate with the Carbon Tetrachloride/Dichlorotris-(triphenylphosphine)ruthenium(II)/Methylaluminum Bis(2,6-Di-Tert-Butylphenoxide) Initiating System: Possibility of Living Radical Polymerization, *Macromolecules*, 28 (5), 1995, pp. 1721–1723.
- (88) T. Nakano and Y. Okamoto, Helix-Sense-Selective Free-Radical Polymerization of 1-Phenyldibenzosuberonyl Methacrylate Using a Cobalt(II) Complex, *Macromolecules*, 32 (7), 1999, pp. 2391–2393.
- (89) A. Gridnev, The 25th Anniversary of Catalytic Chain Transfer, *J. Polym. Sci. Part A: Polym. Chem.*, 38 (10), 2000, pp. 1753–1766.
- (90) N. Saragas, G. Floros, P. Paraskevopoulou, N. Psaroudakis, S. Koinis, M. Pitsikalis and K. Mertis, Polymerization of Terminal Alkynes with a Triply Bonded Tungsten Halo-Complex, *J. Mol. Catal. Chem.*, 303 (1–2), 2009, pp. 124–131.
- (91) F.A. Cotton, C.A. Murillo and R.A. Walton, *Multiple Bonds between Metal Atoms*, Springer Science & Business Media, 2005.
- (92) V.P. Carvalho Jr., C.P. Ferraz and B.S. Lima-Neto, Tailored Norbornene-Based Copolymer with Systematic Variation of Norbornadiene as a Crosslinker Obtained via ROMP with Alternative Amine Ru Catalysts, *Eur. Polym. J.*, 48 (2), 2012, pp. 341–349.
- (93) B. Düz, C.K. Elbistan, A. Ece and F. Sevin, Application of Carbon Arc-Generated Mo- and W-Based Catalyst Systems to the ROMP of Norbornene, *Appl. Organomet. Chem.*, 23 (9), 2009, pp. 359–364.
- (94) B. Bell, J.G. Hamilton, O.N.D. Mackey and J.J. Rooney, Microstructure of Ring-Opened Polymers and Copolymers of Norbornadiene, *J. Mol. Catal.*, 77 (1), 1992, pp. 61–73.
- (95) N. Saragas, G. Floros, G. Raptopoulos, M. Pitsikalis, P. Paraskevopoulou and K. Mertis, Exploring the Reactivity of $\text{Na}[\text{W}_2(\mu\text{-Cl})_3\text{Cl}_4(\text{THF})_2]\cdot(\text{THF})_3$ towards the Polymerization of Selected Cycloolefins, *Molecules*, 20 (12), 2015, pp. 21896–21908.
- (96) T.C. Mauldin and M.R. Kessler, Enhanced Bulk Catalyst Dissolution for Self-Healing Materials, *J. Mater. Chem.*, 20 (20), 2010, pp. 4198–4206.
- (97) J. Hakala, M.M. Hänninen and A. Lehtonen, Imido-tungsten(VI) Complexes with Chelating Phenols as ROMP Catalysts, *Inorg. Chem. Commun.*, 14 (9), 2011, pp. 1362–1364.
- (98) K. Nomura, K. Suzuki, S. Katao and Y. Matsumoto, Ring-Opening Polymerization of THF by Aryloxo-Modified (Imido)vanadium(V)-Alkyl Complexes and Ring-Opening Metathesis Polymerization by Highly

- Active $V(\text{CHSiMe}_3)(\text{NAd})(\text{OC}_6\text{F}_5)(\text{PMe}_3)_2$, *Organometallics*, 31 (14), 2012, pp. 5114–5120.
- (99) E. Khosravi and T. Szymanska-Buzar, *Ring Opening Metathesis Polymerisation and Related Chemistry: State of the Art and Visions for the New Century*, Springer Science & Business Media, 2012.
- (100) T.A. Davidson, K.B. Wagener and D.B. Priddy, Polymerization of Dicyclopentadiene: A Tale of Two Mechanisms, *Macromolecules*, 29 (2), 1996, pp. 786–788.
- (101) L. Bencze, A. Kraut-Vass and L. Prókai, Mechanism of Initiation of the Metathesis of Norbornene Using $W(\text{CO})_3\text{Cl}_2(\text{AsPh}_3)_2$ as Catalyst, *J. Chem. Soc. Chem. Commun.*, 13, 1985, pp. 911–912.
- (102) L. Bencze, G. Szalai and T.L. Overton, Investigation of the Catalytic Properties of the Thermally Activated Dichloro-Tetracarbonyl-Tungsten in Olefin Metathesis Reaction, *Inorganica Chim. Acta*, 254 (1), 1997, pp. 5–7.
- (103) L. Bencze, N. Bíró, B. Szabó-Ravasz and L. Mihichuk, Chemical Transformations of $cis\text{-}W(\text{CO})_4(\text{C}_5\text{H}_5\text{N})_2$ in the Ring-Opening Metathesis Polymerization of Norbornene, *Can. J. Chem.*, 82 (4), 2004, pp. 499–503.
- (104) M.F. Faroni and R.L. Tucker, Studies on the Mechanism of Olefin Metathesis Promoted by a Heterogeneous Catalyst, *J. Mol. Catal.*, 8 (1), 1980, pp. 85–90.
- (105) A.S. Veige, P.T. Wolczanski and E.B. Lobkovsky, Dehydrogenation of $[\{(\text{silox})_3\text{Nb}\}_2(\eta\text{-}1,2;\eta\text{-}5,6\text{-C}_8\text{H}_8)]$ ($\text{silox}=\text{tBu}_3\text{SiO}$) to $[\{(\text{silox})_3\text{Nb}\}_2(\eta\text{-}1,2;\eta\text{-}5,6\text{-C}_8\text{H}_6)]$ and Its Subsequent Alkene-to-Alkylidene Rearrangement, *Angew. Chem. Int. Ed.*, 40 (19), 2001, pp. 3629–3632.
- (106) T. Oshika and H. Tabuchi, Ring-Opening Polymerization of Norbornene and Its Derivatives by MoCl_5 , WCl_6 and ReCl_5 Catalysts, *Bull. Chem. Soc. Jpn.*, 41 (1), 1968, pp. 211–217.
- (107) D.T. Lavery, M.A. McKervey, J.J. Rooney and A. Stewart, Mechanism of Initiation of Ring-Opening Polymerization of Norbornene Catalysed by Transition-Metal Halides, *J. Chem. Soc. Chem. Commun.*, 6, 1976, pp. 193–194.
- (108) H. Balcar, A. Dosedlová and L. Petrusová, Ring-Opening Metathesis Polymerization of Dicyclopentadiene by Unicomponent Catalysts Derived from WCl_6 , *J. Mol. Catal.*, 77 (3), 1992, pp. 289–295.
- (109) J.M. Kamphaus, J.D. Rule, J.S. Moore, N.R. Sottos and S.R. White, A New Self-Healing Epoxy with Tungsten (VI) Chloride Catalyst, *J. R. Soc. Interface*, 5 (18), 2008, pp. 95–103.
- (110) D.P. Mohite, S. Mahadik-Khanolkar, H. Luo, H. Lu, C. Sotiriou-Leventis and N. Leventis, Polydicyclopentadiene Aerogels Grafted with PMMA: I. Molecular and interparticle Crosslinking, *Soft Matter*, 9 (5), 2013, pp. 1516–1530.

- (111) D.P. Mohite, S. Mahadik-Khanolkar, H. Luo, H. Lu, C. Sotiriou-Leventis and N. Leventis, Polydicyclopentadiene Aerogels Grafted with PMMA: II. Nanoscopic Characterization and Origin of Macroscopic Deformation, *Soft Matter*, 9 (5), 2013, pp. 1531–1539.
- (112) M.J. Abadie, M. Dimonie, C. Couve and V. Dragutan, New Catalysts for Linear Polydicyclopentadiene Synthesis, *Eur. Polym. J.*, 36 (6), 2000, pp. 1213–1219.
- (113) N. Saragas, *Selective Polymerization of Alkynes and Cycloolefins with Bimetallic Complexes of the Transition Metals*, PhD Thesis, Department of Chemistry, National and Kapodistrian University of Athens, 2009.
- (114) D. Schaubroeck, S. Brughmans, C. Vercaemst, J. Schaubroeck and F. Verpoort, Qualitative FT-Raman Investigation of the Ring Opening Metathesis Polymerization of Dicyclopentadiene, *J. Mol. Catal. Chem.*, 254 (1–2), 2006, pp. 180–185.
- (115) M.A. Golub and R.J. Gargiulo, Thermal Degradation of 1,4-Polyisoprene and 1,4-Polybutadiene, *J. Polym. Sci. [B]*, 10 (1), 1972, pp. 41–49.
- (116) T.R. Long, A. Gupta, A.L.M. Li, D.G. Rethwisch and N.B. Bowden, Selective Flux of Organic Liquids and Solids Using Nanoporous Membranes of Polydicyclopentadiene, *J. Mater. Chem.*, 21 (37), 2011, pp. 14265–14276.
- (117) C.M. Hansen, *Hansen Solubility Parameters: A User's Handbook, Second Edition*, CRC Press, 2007.
- (118) S. Abbott, C.M. Hansen and H. Yamamoto, *Hansen Solubility Parameters in Practice*, 5th edition, 2015.
- (119) T.B. Starr, G. Matanoski, M.W. Anders and M.E. Andersen, Workshop Overview: Reassessment of the Cancer Risk of Dichloromethane in Humans, *Toxicol. Sci.*, 91 (1), 2006, pp. 20–28.
- (120) A.E. Olvera-Bello, E. Estrada-Muñiz, G. Elizondo and L. Vega, Susceptibility to the Cytogenetic Effects of Dichloromethane Is Related to the Glutathione S-Transferase Theta Phenotype, *Toxicol. Lett.*, 199 (3), 2010, pp. 218–224.
- (121) National Toxicology Program. Report on the Carcinogenesis Bioassay of Chloroform, *Natl. Cancer Inst. Carcinog. Tech. Rep. Ser.*, 1976, 1976, pp. 1–60.
- (122) M. Cappelletti, D. Frascari, D. Zannoni and S. Fedi, Microbial Degradation of Chloroform, *Appl. Microbiol. Biotechnol.*, 96 (6), 2012, pp. 1395–1409.
- (123) A. Hermenean, A. Ardelean, M. Stan, H. Herman, C.V. Mihali, M. Costache and A. Dinischiotu, Protective Effects of Naringenin on Carbon Tetrachloride-Induced Acute Nephrotoxicity in Mouse Kidney, *Chem. Biol. Interact.*, 205 (2), 2013, pp. 138–147.

- (124) L.W.D. Weber, M. Boll and A. Stampfl, Hepatotoxicity and Mechanism of Action of Haloalkanes: Carbon Tetrachloride as a Toxicological Model, *Crit. Rev. Toxicol.*, 33 (2), 2003, pp. 105–136.
- (125) K.V. Anand, R. Anandhi, M. Pakkiyaraj and P. Geraldine, Protective Effect of Chrysin on Carbon Tetrachloride (CCl₄)—induced Tissue Injury in Male Wistar Rats, *Toxicol. Ind. Health*, 27 (10), 2011, pp. 923–933.
- (126) J.F. Pankow and J.A. Cherry *Dense Chlorinated Solvents and Other DNAPLs in Groundwater: History, Behavior, and Remediation*, Waterloo Press, 1996.
- (127) B. Huang, C. Lei, C. Wei and G. Zeng, Chlorinated Volatile Organic Compounds (Cl-VOCs) in Environment — Sources, Potential Human Health Impacts, and Current Remediation Technologies, *Environ. Int.*, 71, 2014, pp. 118–138.
- (128) L. Alwary, M. Gafar and A. Rumie, Liquid Phase Adsorption of Phenol and Chloroform by Activated Charcoal, *Chem. Eng. Technol.*, 34 (11), 2011, pp. 1883–1890.
- (129) X. Gui, J. Wei, K. Wang, A. Cao, J. Zhu, Y. Jia, Q. Shu and D. Wu, Carbon Nanotube Sponges, *Adv. Mater.*, 22 (5), 2010, pp. 617–621.
- (130) J. Åkesson, O. Sundborg, O. Wahlström and E. Schröder, A van Der Waals Density Functional Study of Chloroform and Other Trihalomethanes on Graphene, *J. Chem. Phys.*, 137 (17), 2012, 174702.
- (131) M.A. Hernández, A.I. González, L. Corona, F. Hernández, F. Rojas, M. Asomoza, S. Solís, R. Portillo and M.A. Salgado, Chlorobenzene, Chloroform, and Carbon Tetrachloride Adsorption on Undoped and Metal-Doped Sol–gel Substrates (SiO₂, Ag/SiO₂, Cu/SiO₂ and Fe/SiO₂), *J. Hazard. Mater.*, 162 (1), 2009, pp. 254–263.
- (132) A. Li, H.-X. Sun, D.-Z. Tan, W.-J. Fan, S.-H. Wen, X.-J. Qing, G.-X. Li, S.-Y. Li and W.Q. Deng, Superhydrophobic Conjugated Microporous Polymers for Separation and Adsorption, *Energy Environ. Sci.*, 4 (6), 2011, pp. 2062–2065.
- (133) H.A. Patel, M.S. Yavuz and C.T. Yavuz, Exceptional Organic Solvent Uptake by Disulfide-Linked Polymeric Networks, *RSC Adv.*, 4 (46), 2014, pp. 24320–24323.
- (134) E.U. Kulawardana and D.C. Neckers, Photoresponsive Oil Sorbers, *J. Polym. Sci. Part Polym. Chem.*, 48 (1), 2010, pp. 55–62.
- (135) A.M. Atta, R.A.M. El-Ghazawy, R.K. Farag and A.-A. A. Abdel-Azim, Crosslinked Reactive Macromonomers Based on Polyisobutylene and Octadecyl Acrylate Copolymers as Crude Oil Sorbers, *React. Funct. Polym.*, 66 (9), 2006, pp. 931–943.
- (136) Y. Zhang, S. Wei, F. Liu, Y. Du, S. Liu, Y. Ji, T. Yokoi, T. Tatsumi and F.-S. Xiao, Superhydrophobic Nanoporous Polymers as Efficient Adsorbents for Organic Compounds, *Nano Today*, 4 (2), 2009, pp. 135–142.

- (137) R.K. Farag and S.M. El-Saeed, Synthesis and Characterization of Oil Sorbers Based on Docosanyl Acrylate and Methacrylates Copolymers, *J. Appl. Polym. Sci.*, 109 (6), 2008, pp. 3704–3713.
- (138) G.-R. Shan, P.-Y. Xu, Z.-X. Weng and Z.-M. Huang, Oil-Absorption Function of Physical Crosslinking in the High-Oil-Absorption Resins, *J. Appl. Polym. Sci.*, 90 (14), 2003, pp. 3945–3950.
- (139) X.-M. Zhou and C.-Z. Chuai, Synthesis and Characterization of a Novel High-Oil-Absorbing Resin, *J. Appl. Polym. Sci.*, 115 (6), 2010, pp. 3321–3325.
- (140) J. Yuan, X. Liu, O. Akbulut, J. Hu, S.L. Suib, J. Kong and F. Stellacci, Superwetting Nanowire Membranes for Selective Absorption, *Nat. Nanotechnol.*, 3 (6), 2008, pp. 332–336.
- (141) F.J. Ortega, M. Ventre and P.A. Netti, Biodegradable Material for the Absorption of Organic Compounds and Nanoparticles, *Biomacromolecules*, 15 (9), 2014, pp. 3321–3327.